Molecular and Mechanical Regulators of Lymphatic Biology

THÈSE N^{O} 4096 (2008)

PRÉSENTÉE LE 2 JUILLET 2008

À LA FACULTE SCIENCES DE LA VIE
LABORATOIRE DE MÉCANOBIOLOGIE ET DE MORPHOGENÈSE (SV/SB/STI)
PROGRAMME DOCTORAL EN BIOTECHNOLOGIE ET GÉNIE BIOLOGIQUE

ÉCOLE POLYTECHNIQUE FÉDÉRALE DE LAUSANNE

POUR L'OBTENTION DU GRADE DE DOCTEUR ÈS SCIENCES

PAR

Joseph Michael RUTKOWSKI

M.Sc. in Chemical Engineering, Northwestern University, Evanston, Illinois, Etats-Unis
et de nationalité américaine

acceptée sur proposition du jury:

Prof. N. Stergiopulos, président du jury
Prof. M. Swartz, directrice de thèse
Prof. Y. Barrandon, rapporteur
Prof. D. Negrini, rapporteur
Prof. D. Zawieja, rapporteur

ÉCOLE POLYTECHNIQUE
FÉDÉRALE DE LAUSANNE

Suisse
2008

TABLE OF CONTENTS

This page is intentionally left blank.

ABSTRACT

Lymphatic vessels exist in nearly all tissues, yet, despite their omnipresence, there remains a large knowledge gap between the described fundamental roles of lymphatic capillaries and our understanding of their functional biology, adaptive ability, and pathological response. This thesis addressed these shortcomings by utilizing an integrative biomedical engineering approach to examine molecular and mechanical regulators of lymphatic capillaries using *in vivo* models of lymphatic capillary biology, function, and adaptation.

Using a model of skin regeneration in the mouse tail, we demonstrated that slow interstitial flow created by lymphatic drainage was necessary for lymphatic capillary organization. This novel model permitted the identification of spatial, temporal and chemical factors governing lymphangiogenesis. In contrast to the sprouting mechanism of blood angiogenesis, lymphatic endothelial cells (LECs) were demonstrated to organize in a vasculogenesis-like manner, migrating in the direction of interstitial flow and then organizing into functional lymphatic capillaries. Lymphangiogenesis was inhibited by blocking vascular endothelial growth factor (VEGF)-C signaling from day 0, but initiation of receptor blockade once LECs had already migrated did not prevent vessel organization. This uniquely demonstrated the need for a biochemical mediator (VEGF-C) to initiate lymphangiogenesis, but that an important biomechanical force, interstitial flow, was necessary for functional capillary organization.

Further insight into the necessity of interstitial flow in LEC biology was found in the response of lymphatic capillary to induced lymphedema, wherein lymphatic drainage is significantly reduced. In a mouse tail model of secondary lymphedema, we demonstrated that the edematous environment – characterized by extracellular matrix breakdown, lipid accumulation, and reduced interstitial flow – resulted in hyperplasia of LECs but concurrent poor function due to the lack of interstitial flow as an organizational guiding cue. Similar dermal matrix adaptations to dysfunctional lymphatic drainage were also noted in two mouse models of congenital lymphedema, the Chy and VEGFR-3-Ig mice, further demonstrating the intimate connection of lymphatic capillary function with tissue maintenance and remodeling.

To quantitatively demonstrate the changes in lymphatic capillary uptake and tissue hydraulic conductivity found in these and other transgenic mouse models, we developed a poroelastic model of interstitial transport. Tissue hydraulic conductivity was also calculated in tissues

lacking lymphatics using an unsteady-state solution, demonstrating that lymphedema causes a significant increase in tissue conductivity. This model was then utilized to assess the effects of a high fat diet, metabolic disorders, and lymphatic dysfunction on the tissue and on lymphatic capillary function. We discovered that lymphatic capillary uptake function was significantly reduced with dyslipidemia, suggesting a novel interplay between lymphatic function and lipid metabolism.

Additionally, we uncovered a new and critical role for lymphangiogenesis and lymphatic transport in reproduction. We demonstrated that lymphangiogenesis is a regular, non-pathological event during folliculogenesis in the ovary. These new lymphatic capillaries are seemingly necessary for hormone transport from the ovary – an essential feedback mechanism during pregnancy. Blockade of lymphangiogenesis resulted in decreased systemic progesterone and estradiol levels and resulted in failed fetal development.

In conclusion, this work highlights the critical roles of the lymphatic circulation and demonstrates the interplay between lymphatic biology and the biochemical and biophysical environment in which lymphatic capillaries reside. Interstitial flow and the interstitium modulate lymphatic behavior, and lymphatic function, in turn, controls the tissue microenvironment.

Keywords: lymphatic, interstitial flow, extracellular matrix, VEGF-C, VEGFR-3, lymphangiogenesis, lymphedema, folliculogenesis

RÉSUMÉ

Les vaisseaux lymphatiques se trouvent dans pratiquement tous les tissus. Pourtant, malgré leur présence importante, il y a encore une grande différence de connaissance entre les rôles fondamentaux des capillaires lymphatiques déjà décrits et les connaissances que nous avons de leur fonction biologique, leur capacité adaptative et la réponse pathologique. Cette thèse vise à combler ces lacunes en utilisant l'ingénierie biomédicale pour examiner les régulateurs mécaniques et moléculaires des capillaires lymphatiques grâce à des modèles *in vivo* de la biologie, des fonctions et de l'adaptation des capillaires lymphatiques.

En utilisant un modèle de régénération de la peau sur la queue des souris, nous avons démontré que le flux interstitiel lent créé par le drainage lymphatique était nécessaire pour l'organisation des capillaires lymphatiques. Ce nouveau modèle a permis l'identification de facteurs spatiaux, temporaux et chimiques gérant la lymphangiogénèse. Contrairement au mécanisme de croissance pour l'angiogénèse du sang, les cellules endothéliales lymphatiques (LECs) ont démontré une organisation semblable à la vasculogénèse, migrant en direction du flux interstitiel, puis en s'organisant en capillaires lymphatiques fonctionnels. La lymphangiogénèse est inhibée en bloquant la signalisation des facteurs de croissance endothéliale vasculaire (VEGF-C) à partir du jour 0, mais l'initiation du blocus de récepteur une fois que les LECs ont déjà migré, n'empêche pas l'organisation des vaisseaux. Cette nouvelle approche a démontré le besoin de médiateur biochimique (VEGF-C) pour initier la lymphangiogénèse, mais qu'une force biomécanique importante, un flux interstitiel, était nécessaire pour l'organisation des capillaires fonctionnels.

De plus, la nécessité du flux interstitiel dans la biologie des LECs a été démontrée dans la réponse des capillaires lymphatiques à un lymphœdème induit, où le drainage lymphatique est significativement réduit. Dans le modèle de lymphœdème secondaire dans la queue de souris, nous avons démontré que l'environnement œdémateux – caractérisé par une défaillance de la matrice extracellulaire, une accumulation des lipides et une réduction du flux interstitiel – a pour conséquence une hyperplasie des LECs, mais conduit à une fonction diminuée due au manque de flux interstitiel comme signal organisationnel. Des adaptations similaires de la matrice dermale au dysfonctionnement du drainage lymphatique ont aussi été remarquées dans deux modèles de souris de lymphœdème congénital, les souris Chy et VEGFR-3-Ig, de

plus elles démontrent la connexion intime de la fonction des capillaires lymphatiques avec la maintenance du tissu et son remodelage.

Pour démontrer quantitativement les changements dans l'absorption des capillaires lymphatiques et la conductivité hydraulique du tissu trouvé dans ces modèles de souris transgéniques, nous avons développé un modèle poro-élastique de transport interstitiel. La conductivité hydraulique du tissu a aussi été calculée dans les tissus manquants de lymphatiques en utilisant une solution non-stationnaire, démontrant que le lymphœdème provoque une augmentation significative de la conductivité du tissu. Ce modèle a été utilisé ensuite pour tester les effets d'un régime enrichi en graisses, des troubles métaboliques et des dysfonctions des lymphatiques sur le tissu et la fonction des capillaires lymphatiques. Nous avons découvert que l'absorption des capillaires lymphatiques a été fortement réduite avec une dyslipidémie, mettant en évidence une nouvelle interaction entre la fonction lymphatique et le métabolisme des lipides.

De plus, nous avons découvert un nouveau rôle critique pour la lymphangiogénèse et le transport lymphatique dans la reproduction. Nous avons démontré que la lymphangiogénèse est un événement régulier et non pathologique lors de la folliculogénèse dans l'ovaire. Ces nouveaux capillaires lymphatiques sont apparemment nécessaires pour le transport des hormones à partir de l'ovaire – un mécanisme essentiel durant la grossesse. Bloquer la lymphangiogénèse résulte en une diminution importante du niveau de progestérone et d'oestrdiol et conduit à un défaut du développement du fœtus.

En conclusion, ce travail met en évidence les rôles critiques de la circulation lymphatique et démontre les interactions entre la biologie lymphatique et l'environnement biochimique et biophysique dans lequel se trouvent les capillaires lymphatiques. Le flux interstitiel et l'interstitium modulent le comportement et la fonction des lymphatiques, qui eux-mêmes, contrôlent le microenvironnement du tissu adjacent.

Mots-clés : lymphatiques, flux interstitiel, matrice extracellulaire, VEGF-C, VEGFR-3, lymphangiogénèse, lymphœdème, folliculogénèse.

ACKNOWLEDGEMENTS

Deciding to pursue this thesis research is an undertaking that has evolved throughout my entire lifetime. It is, unfortunately, impossible to acknowledge everyone individually that has assisted me down this path, from those that initially motivated me in this pursuit to those that have emotionally, academically, and financially supported me in this endeavor, I immediately thank you all collectively: my personal growth, life, and career have been enriched by your contributions. The following individuals have, as my aging memory recollects, offered substantial and critical support in this accomplishment worthy of me specifically offering their praises:

I would first and foremost like to specifically thank my advisor, boss, mentor, and friend, Professor Melody Swartz, for providing me the opportunity to work under her, to learn from her, and to gain the appreciation from her of just how considerable an accomplishment this thesis is. Without her continued, positive reinforcement throughout what has been an incredibly complex several years, this thesis would certainly not have been possible and I would not be as pleased with the outcome today as I can truly admit. Thank you for your consistent praise and support beyond what I ever thought as necessary from an advisor; you have truly provided cause for a lifetime of thanks.

Even though the names and faces within, and even the geographic coordinates of, the laboratory have changed through the years, each person and place has left an indelible mark on my work, my growth as a scientist, and my extra-laboratory life and viewpoints. Coming to work each day would have been impossible if not for the pleasure of working with you all. I can only hope that in the future I have the opportunity to work with a group as intellectually stimulating and personably enjoyable as you. More specifically, I would like to thank Mark Fleury for his help and friendship though a trans-continental move, Jacqueline Shields and Adrian Shieh for their constant wisdom and assistance in science and life, and Sai Reddy for his constant motivation and drive, excellent scientific discussion, and, most importantly, unending friendship and support.

I would also like to thank all of my friends and family, especially my family, for offering their continued love, support, and praise through the years. Both through the highs and through the lows – as well as my constant griping about something – you have never wavered in your care and encouragement, and for that I am eternally grateful.

To Carolyn, the love of my life, my shoulder to cry on, my ear to listen, best friend and biggest supporter, I thank you for everything. Not one single day of progress would have been made towards this thesis without you by my side. Indeed, having to put up with all of the trials and tribulations of my thesis endeavor while simultaneously completing your own is not a task that I would wish on anyone, but you have shined through commendably. I love you, thank you, and dedicate this work to you.

"The time has come…"

CHAPTER 1:
OVERVIEW OF THE THESIS

1.1: Aims

The overall goals of this thesis are to identify and explore interactions between molecular and mechanical regulators of lymphatic capillary biology with respect to both quiescent tissue homeostasis and the pathological tissue states of skin regeneration (lymphangiogenesis) and lymphedema, and to quantitatively demonstrate alterations in lymphatic capillary function.

The specific aims addressed in this thesis are to:

(1) Identify the relative importance and interplay of contributing factors – molecular, mechanical, and cellular – to lymphangiogenesis in adult skin regeneration.

(2) Determine the tissue pathology of both primary (congenital) and secondary (induced) lymphedema and how lymphatic capillary biology and function are affected.

(3) Quantify changes in lymphatic capillary drainage function in response to potential molecular effectors.

(4) Define a role for lymphatic capillaries and ovarian lymphangiogenesis in female reproduction.

1.2: Motivation & Approach

Lymphatic vessels and lymphatic circulation is found throughout the body and forms an integral part of the body's circulatory system. Despite the critical roles that lymphatic capillaries plays in modulating interstitial fluid balance, maintaining immune surveillance, and transporting lipids, knowledge of the lymphatic system and the biology of lymphatic endothelial cells (LECs), particularly with regard to their function, remains lacking. To date, the bulk of research focused on lymphatic capillaries has been aimed at (a) developmental biology and (b) lymphangiogenesis in tumor progression. This research has elucidated an array of LEC-specific molecular markers, growth factors, and signaling molecules, and by comparing and contrasting lymphangiogenesis – both developmental and pathological – with the more widely studied blood angiogenesis, has lent a great deal of understanding and brought attention to the importance of lymphatic biology in the scientific community. By taking this approach, however, it leaves a significant opportunity to explore what we still do

not know about lymphatic capillary biology: How do adult lymphatic capillaries in the skin actually function and what factors may modulate this? Do LECs adapt to their environment and consequently modulate lymphatic capillary function? And what is the pathobiology of lymphatic capillaries in lymphedema and inflammatory conditions?

To approach these questions, an integrative biomedical engineering approach was taken. The complex biochemical and biomechanical environment in which dermal lymphatic capillaries reside would normally lead to the simplified, *in vitro* methods to directly determine outcomes of various experimental questions. For example: adding growth factors to LECs growing on 2-D plastic surfaces may help to identify the molecular response to the growth factor, but tells us little of the actual mechanism of lymphangiogenesis in a 3-D tissue environment. Well-designed engineered systems and experiments can, however, be applied *in vivo* so as to more relevantly tackle the problem of lymphatic capillary function. In this way, the environment remains wholly coupled to the biology, and vice versa. One of the principle examples in this work is in models utilizing the mouse tail. All lymphatic flow in the tail must move from the tip of the tail back towards the body. Because of the simple, cylindrical geometry of the tail, this flow is macroscopically unidirectional. This allowed not only the application of a quantitative model of lymphatic uptake and interstitial transport (Chapter 6), but also permits the mouse-tail model of lymphangiogenesis (Chapter 3) to have a well-understood direction of interstitial transport. Thus, by approaching and developing models integrating the anatomy, biology, physiology, and mechanics of the adult lymphatic environment, we can confidently address the adaptive responses of the lymphatic endothelium *in vivo* and gain keen insight into controlling factors of lymphatic capillary biology.

1.3: Thesis Overview

The contents of the subsequent chapters of this thesis, and the studies that they represent, are summarized here so as to frame them directly within the overall objective and specific aims. Chapter 2 provides a general overview of background information on lymphatic capillaries and the environment in which they reside so that the subsequent research manuscripts may be held in better context.

The first manuscript chapter, Chapter 3, defines the mechanism of lymphangiogenesis in regenerating mouse skin and characterizes – spatially and temporally – lymphatic organization and potentially contributing factors. The mode of vessel regrowth was not sprouting from existing capillaries, but rather a process akin to embryonic vasculogenesis.

Single LECs, or groups of LECs, first migrate in to the regenerating tissue, in the direction of interstitial fluid flow, and then coalesce to form organized, functional vessels.

As the mechanism of lymphangiogenesis detailed in Chapter 3 was very step-wise and pseudo-independent of VEGF-C signaling (the paramount lymphatic growth factor), Chapter 4 then discusses work on cooperative and redundant signaling of the receptors to VEGF-C, VEGFR-2 and VEGFR-3, in proliferation, migration, and organization of LECs during lymphangiogenesis. As the prevalent pathway of lymphangiogenesis, we found that VEGFR-3 signaling was, indeed, important to initiate lymphangiogenesis – through LEC proliferation and migration – but was not required for the later LEC organization into new vessels. Rather, VEGFR-3 signaling initiates lymphangiogenesis, but functional capillary organization is VEGF-C-independent: interstitial flow is the organizing guidance cue. Chapters 3 and 4, completing Specific Aim 1, thus present the balance and interplay between molecular signaling and the mechanical, organizational force of fluid flow.

Chapter 5 then presents what happens to lymphatic capillaries and their environment when interstitial flow stops in secondary lymphedema induced in the mouse tail. The chapter describes the model and the temporal characterization with respect to matrix degradation, lipid accumulation, and lymphatic vessel hyperplasia. What is truly interesting is that despite LEC proliferation, the lack of flow as an organizational guidance cue results in grossly hyperplastic, poorly functioning lymphatic capillaries. The model also successfully recapitulated the initial breakdown of the extracellular matrix and the subsequent dermal remodeling and subcutaneous lipid accumulation observed in the human condition. Lack of a normal matrix further hinders the ability of lymphatic capillaries to function normally.

In Chapter 7, two models of congenital primary lymphedema, the Chy and K14-VEGFR-3-Ig mice, are described and used to further demonstrate the adaptive tissue response to lymphedema and serve as an excellent basis of studying fluid transport in the interstitium. Chapter 6 presents the development of methods to quantify lymphatic capillary uptake and tissue hydraulic conductivity. The mouse models of primary lymphedema present the unsteady-state solution to the developed equations, as there is insignificant fluid flux to the lymphatic capillaries (because there are no lymphatics to take up interstitial fluid). Further discussion on quantifying lymphatic function in normal and edematous mice, a necessary step in determining the actual success of potential treatments for pathologies resulting from lymphatic dysfunction, is also presented in Chapter 6. For example, we found that dyslipidemia in the tissue reduced lymphatic function and that targeting lipids may improve functional drainage. Specific Aims 2 and 3 were therefore accomplished in Chapters 5, 6, and

7. More specifically: Chapters 5 and 6 explore both induced and congenital lymphedema with respect to their tissue morphology and changes to lymphatic capillary morphology and function; Chapter 6 quantifies lymphatic capillary functional uptake of interstitial fluid in these models; and Chapter 6 also identifies dyslipidemia in the tissue as a negative effector of lymphatic capillary function.

Lymphatic vessels are known to modulate fluid balance, immune cell transport, and lipid metabolism, but in Chapter 8, a novel role for lymphatics and lymphangiogenesis in reproduction is presented. Blood angiogenesis has been established as an essential process in the ovaries both during folliculogenesis and sustained pregnancy, but lymphatics, lymphangiogenesis, and their potential roles have been sorely ignored. We found that lymphatic vessels function in the murine ovary for hormone transport during pregnancy, and that a lack of lymphatic capillaries during reproduction resulted in significantly reduced systemic progesterone and estrogen levels. Without these new lymphatic capillaries, fetal development was impaired and pregnancies failed. By discovering this novel role for lymphatics in reproduction, Specific Aim 4 was completed.

The findings of the thesis study are then summarized in the concluding chapter, Chapter 9. Key results are placed within the context of the field and a brief discussion of the current and future directions that these results might lead are also included.

CHAPTER 2:
BACKGROUND ON THE LYMPHATICS AND INTERSTITIAL FLOW

2.1: The Lymphatic System

Fluid transport through the lymphatic vasculature forms an integral part of the body's circulation. Throughout nearly all tissues of the body, lymphatic capillaries drain interstitial fluid, macromolecules, and cells and transport them, through larger conducting lymphatic vessels and the lymph nodes (Figure 2.1), back to systemic blood circulation. As interstitial fluid is sourced from fluid extravasted from the blood vasculature, the lymphatics maintain tissue homeostasis and complete the body's circulatory loop (1).

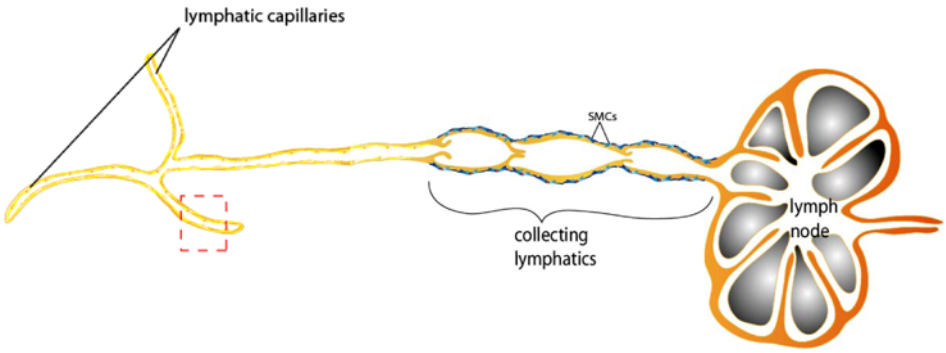

Figure 2.1: Schematic of the lymphatic vessels encompassing lymphatic circulation. The focus of this thesis is the initial lymphatic capillaries, here shown in respect to the greater downstream lymphatics and lymph nodes. Artwork courtesy Carolyn Yong.

While often neglected as nothing more than a passive tissue drainage system, in reality the roles of the lymphatic circulation are more active, diverse, and important. By serving as the low pressure reservoir in vascularized tissues, the lymphatic vessels promote interstitial flow – the subtle fluid flow through the extracellular matrix from blood capillaries and into initial lymphatic vessels (2). Interstitial flow has been demonstrated to be a key morphoregulator of cells in the interstitium (2, 3), so the lymphatic vessels actually have the potential to control the morphogenesis and migration of other cell types such as tumor and immune cells (4). Lymphatic vessels, by connecting the periphery to the lymph nodes, allow not only active immune cell trafficking for antigen presentation within the lymph node, but may also permit the nodes to sample incoming fluid for inflammatory mediators or antigens (5). Dietary lipid uptake from the intestinal lumen is, surprisingly, first through the lymphatic capillaries located within the villi of the intestinal wall (6). The lymphatic circulation is thus potentially important in regulating lipid metabolism as well.

2.1.1: Lymphatic Endothelial Cells (LECs)

While in standard *in vitro* culture conditions blood endothelial cells and LECs are phenotypically quite similar, LECs *in vivo* form vessels that function very differently from the blood vasculature. Research on the embryonic development of the lymphatic vasculature has identified several genes and molecules specific to LECs that drive their differentiation, may modulate their function, and permit their identification both in culture and in tissues (Table 2.1)(7). In total, LECs differ from blood endothelial cells not only in molecular expression, but also in their molecular responses and adaptive morphoregulation, likely due to their different roles *in vivo*. Once formed into capillaries, the differences between the blood and lymphatic endothelium, and how these differences impact their respective functions, becomes more striking.

Gene	Function	Lymphatic phenotype	Lethality
Ang2 gene targeted [65]	Growth factor, ligand of Tie-2	Hypoplasia, chylous ascites ($^{-/-}$)	$^{-/-}$: perinatal or normal, $^{+/-}$: normal
Efnb2, PDZ-binding mutant [54]	Ligand of EphB receptors	Retrograde lymph flow, chylothorax, ectopic mural cells, absent valves ($^{-/-}$)	$^{-/-}$: perinatal, $^{+/-}$: normal
Foxc2 gene targeted [86]	Transcription factor	Abnormal lymphatic patterning, presence of mural cells, absent valves ($^{-/-}$) [49], Lymphatic vessel and lymph node hyperplasia ($^{+/-}$) [87]	$^{-/-}$: E12.5-perinatal, $^{+/-}$: normal
Integrin α9, gene targeted [68]	Adhesion receptor	Lymphoedema, chylothorax ($^{-/-}$)	$^{-/-}$: perinatal, $^{+/-}$: normal
Elk3 (Net) gene targeted [67]	Transcription factor	Lymphangiectasis, chylotorax ($^{-/-}$)	$^{-/-}$: perinatal, $^{+/-}$: normal
Nrp2 gene targeted [57]	Receptor for VEGF-C, some VEGF isoforms and semaphorins	Transient hypoplasia of lymphatic capillaries ($^{-/-}$)	$^{-/-}$: perinatal, $^{+/-}$: normal
Podoplanin (*Gp38*) gene targeted [55]	Membrane glycoprotein	Lymphangiectasis, abnormal lymph transport ($^{-/-}$)	$^{-/-}$: perinatal, $^{+/-}$: normal
Prox1 gene targeted [27]	Transcription factor	No lymphatic vessels ($^{-/-}$), Chylous ascites $^{+/-}$	$^{-/-}$: E14.5, $^{+/-}$: perinatal in most backgrounds
Slp76 and *Syk*, gene targeted [45]	Tyrosine kinase (Syk); adaptor protein (Slp76)	Failure of separation of blood and lymphatic vasculature, chylous ascites ($^{-/-}$)	Slp76$^{-/-}$: perinatal, Slp76$^{+/-}$: normal, Syk$^{-/-}$: perinatal, Syk$^{+/-}$: normal
Sox18 (ragged, spontaneous missense mutations) [88]	Transcription factor	Edema and chylous ascites ($^{-/-}$)	$^{-/-}$: perinatal, $^{+/-}$: normal
Trisomy 16 (Ts16) [89]	Many	Nuchal edema, abnormal size and structure of jugular lymph sacs from E14	E16–E20
Vegfc, gene targeted [29]	Growth factor, ligand of VEGFR-3	No lymphatic vessels ($^{-/-}$) hypoplasia, chylous ascites ($^{+/-}$)	$^{-/-}$: E17–19, $^{+/-}$:perinatal or normal
Vegfr3 (*Chy*, ethylnitrosourea-induced mutation) [72]	Receptor tyrosine kinase, kinase inactivating mutation I1053F	Hypoplasia, chylous ascites ($^{+/-}$)	$^{-/-}$: E10, $^{+/-}$:perinatal or normal

Table 2.1: Genes attributed to the lymphatic endothelium and the transgenic consequence in mouse models (table taken from Tammela, 2005 (7))

2.1.2: Lymphatic capillaries

Initial lymphatic vessel morphology varies strikingly from that of their blood counterparts (Table 2.2) due to their functional differences (7). Lymphatic vessels exist in the tissue as a collapsed network of overlapping LECs, are not surrounded by pericytes, possess minimal interrupted basement membrane, and are directly anchored to the extracellular matrix

(ECM) by anchoring filaments (8, 9) where basement membrane is lacking. These physical vessel characteristics permit open fluid flow into the vessel from the interstitial space. While it may be contrary to initial intuition, because of the anchoring filaments that tightly tie LECs to the extracellular matrix, when interstitial fluid pressure (IFP) increases – and therefore, a demand for lymphatic drainage – the vessels are not crushed, but, rather are pulled open as the ECM expands (Figure 2.2) to increase flux into the capillary (10). In tissues with low compliance, (i.e., a stiffer matrix) the capillaries are thereby more sensitive to changes in IFP and fluid uptake is readily increased, as in the healthy lung (11).

Lymphatic capillary uptake of fluid proceeds between the overlapping LECs through unique cell-cell junctions (9, 12). These junctions – recently described to be analogous in appearance to overlapping oak leaves (13) – are incredibly dynamic, with LECs actively responding to changes in interstitial flows, inflammatory molecules, and migrating cells by altering their molecular expression to open or close these cell-cell connections (13, 14), resulting in accordingly increased or decreased drainage. Fluid entry into lymphatic capillaries is further described in section 2.2.1 and quantified *in vivo* in Chapter 6.

	Blood vessel capillaries	Lymphatic capillaries	Collecting lymphatic vessels
Lumena	Regular, narrow	Irregular, wide	Circular, wide
Endothelial cells	Abundant cytoplasm	Scant cytoplasm	Not known
Bileaflet valves	Absent	Absent	Present
Cell–cell junctions	Adherens, tight	Loose, valve-like overlaps	Not known
Cell membrane invaginations and cytoplasmic vesicles	Scant	Abundant	Not known
Basement membrane	Present	Mostly absent	Thinner than in blood vessels of same size
Encircling pericytes	Present	None	Present, coverage increases with increasing luminal size
Anchoring filaments	Absent	Present	Absent
Blood	Present	Usually absent	Usually absent

Table 2.2: Morphological differences between blood capillaries, lymphatic capillaries and collecting lymphatic vessels (table taken from Tammela, 2005 (7))

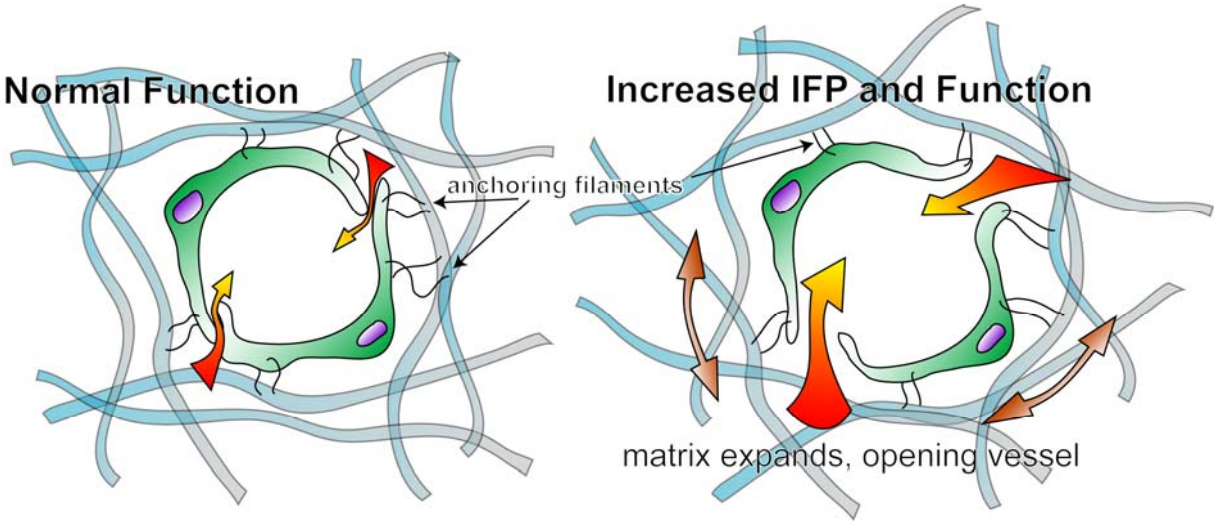

Figure 2.2: Flow enters lymphatic capillaries between cells; increased interstitial pressure (IFP) expands the matrix, pulling on the LECs and their anchoring filaments, opening the cell-cell junctions; pulling the cell-cell junctions open permits increased drainage into the capillary (original artwork).

2.1.3: Greater Lymphatics

Initial lymphatics lead to larger collecting lymphatic vessels that further connect lymph nodes and downstream collecting vessels before returning lymph flow to the blood circulation (Figure 2.2). Unlike the initial lymphatic capillaries, collecting vessels possess bileaflet valves to limit backflow and smooth muscle that intrinsically pumps to maintain lymph flow (10). Indeed, this pumping is necessary for the low pressure lymphatic network to actually propel lymph throughout the body. This thesis does not focus on transport within these vessels, but they play a vital role in maintaining lymphatic drainage from upstream tissues.

Lymph nodes are lymphoid organs located throughout the lymphatic network that provide the primary specific immune sampling from peripheral tissues and permit the development of an antigen specific lymphocyte response (5). Lymph node anatomy and physiology is a detailed field in of itself, primarily focused on the organs' roles in immunity and as cancer metastasis sites. This thesis does not focus on transport within collecting lymphatic vessels, nor lymph node function, but acknowledges the vital role they play in maintaining lymphatic drainage from upstream tissues.

2.2: Roles of Lymphatic Capillaries

2.2.1: Interstitial Flow Driven by Lymphatic Capillary Function

From a physical perspective, the primary role of the lymphatic capillaries is to drain interstitial fluid, thus maintaining tissue homeostasis and driving interstitial flow. Fluid entry into lymphatic capillaries is quite different, however, than fluid extravasation from the blood vasculature. Extravasation is governed by Starling's law of capillary filtration:

$$J_v = Lp\left(\left(P_{capillary} - P_{\text{int}erstitium}\right) + \sigma\left(\pi_{capillary} - \pi_{\text{int}erstitium}\right)\right),$$

which demonstrates the balance between hydrostatic pressure, ΔP, and osmotic pressure, $\Delta\pi$, across the capillary wall governed by the reflection coefficient, σ, and the overall vessel filtration coefficient, Lp. The equation can be applied to lymphatic drainage – reversing the pressure differences, of course – when adapted properly taking into account the unique morphology of the lymphatic capillary. As interstitial fluid flow directly into the lymphatic capillary, and not through the vessel wall, the osmotic pressure driving force, $\Delta\pi$, is zero. Similarly, because σ (which ranges from 0.0-1.0 for zero to complete reflection) refers to the vessel's ability to prevent the extravasation/intravasation of molecules (e.g., proteins), in lymphatics capillaries this term is also zero (15). What remains is merely the hydrostatic pressure driving force and the filtration coefficient, Lp, which is governed by the overall vessel permeability and vessel wall area (both of which increase when the vessel is opened by interstitial pressure increases). Further use of Starling's law of capillary filtration and in calculating fluid flux into lymphatic capillaries is given in Chapter 6.

Fluid entry into lymphatic capillaries thus provides for interstitial flow as fluid is transported across the interstitium from blood to lymphatic capillary. While these flow rates are very small (0.1-10 μm/s) (3), a new appreciation for subtle flow effects on cell behavior is increasingly emerging. The morphogenetic potential of interstitial flow, along with further explanations of its sources and importance are found in the original review manuscript entitled, "A Driving Force for Change: Interstitial Flow as a Morphoregulator", included as an Appendix to this chapter.

2.2.2: Lymphatic Capillaries in Immunity

Antigen-presenting immune cells (APCs), dendritic cells and macrophages, after encountering antigens in the periphery, migrate to a lymphatic capillary and traffic to the sentinel lymph node. Lymphatic vessels secrete the cytokine CCL21, which serves as a chemoattractant for APCs via binding to the APC receptor CCR7 (5). How interstitial flow affects this process and whether or not LECs can actively regulate APC attraction and entry is the topic of current research in the laboratory; it is believed that these cells behave similarly to metastatic tumor cells (4). According to the theory of autologous chemotaxis, proper lymphatic capillary drainage function may be necessary for APC trafficking and entry into lymphatic circulation. More comprehensive reading on the role of the lymphatic system in immunity can be found in the excellent reviews: (5, 16, 17).

2.2.3: Lymphatic Capillaries in Lipid Transport

Lymphatic vessels are the primary route of lipid absorption from the small intestine. Enterocytes, specialized cells of the intestinal epithelium, package lipids into chylomicrons, which then enter the lymphatic capillaries (also called lacteals) found within the intestinal villi (6). In this way, lipids first pass through the lymphatic circulation before entering the blood circulation and subsequent metabolism in the liver (18). As this thesis is focused on lymphatic capillaries in the dermis, intestinal lymphatics and their potential role in lipid metabolism are not directly discussed. However, dermal lymphatic capillaries, by taking up extravasated molecules from the interstitium, provide the route of reverse lipid transport from the skin. Indeed, when capillary function is compromised, lipid accumulates in the dermal tissue space (19). Thus, dermal lipid accumulation and adipogenesis can be utilized as a marker of lymphatic dysfunction and a potential exists for further cross-talk between lymphatic function and adiposity – an area currently under intense exploration. The impact of dyslipidemia on dermal lymphatic capillary uptake is quantified in Chapter 6.

2.3: Lymphangiogenesis

Lymphangiogenesis, the growth of new lymphatic vessels, is modulated by many of the lymphatic molecules ascribed above (Table 2.1). The molecules important in

developmental lymphangiogenesis, however, are different from those considered to be paramount in the adult during lymphangiogenesis associated with wound healing or tumor growth and metastasis (20). The principal, and most widely studied, growth factors driving lymphangiogenesis are members of the vascular endothelial growth factor (VEGF) family. VEGF-C and -D were identified and characterized following much work on the role of lymphatics in tumor progression and the search for potential lymphangiogenic therapies in lymphedema (21) as the growth factors essential for the proliferation and migration of LECs (22). Blocking the primary receptor to these ligands, VEGFR-3, inhibits lymphangiogenesis in healing wounds (22, 23), inflammation (24, 25), and prevents tumor metastasis (26). In this thesis, the mechanism of lymphangiogenesis in adult skin regeneration is explored more in depth in Chapter 3 and the role of VEGFR-3 signaling in this process is more clearly defined in Chapter 4. The role of lymphangiogenesis during reproductive cycles in the ovary is newly described in Chapter 9.

2.4: Lymphedema

Lymphedema is the most common pathology directly linked to lymphatic fluid transport. Lymphedema is classified generally into two forms: primary (congenital) and secondary (induced). Primary lymphedema has been linked to mutations in LEC genes essential for proper lymphatic vessel development; improper development of lymphatic valve structures or insufficient organization of dermal lymphatic capillaries leads to failed interstitial fluid and lymph clearance (27-30). Secondary lymphedema is caused when pre-existing, normal lymphatic vessels are ligated by surgery (e.g., lymph node removal as a treatment to prevent breast cancer metastasis), inflammation, or radiation, among others (31). As a chronic pathology, dysfunctional lymphatic transport leads to remodeling of the skin and subcutaneous extracellular matrix, accumulation of lipids, and failures in immune response in the tissue or limb upstream from the ligation (19). These morphological adaptations can worsen the condition and prevent successful resolution – indeed while compression cuffs, massage, and surgical removal of tissue have demonstrated success in minimizing the condition, unfortunately, there is no complete “cure” for lymphedema (31). The pathology of secondary lymphedema is characterized in Chapter 4, while the tissue adaptation to primary lymphedema, and the resultant fluid transport implications, are demonstrated in Chapters 5 and 6.

Chapter 2 Bibliography

1. Swartz, M.A. 2001. The physiology of the lymphatic system. *Adv Drug Deliv Rev* 50:3-20.
2. Rutkowski, J.M., and Swartz, M.A. 2007. A driving force for change: interstitial flow as a morphoregulator. *Trends Cell Biol* 17:44-50.
3. Swartz, M.A., and Fleury, M.E. 2007. Interstitial flow and its effects in soft tissues. *Annu Rev Biomed Eng* 9:229-256.
4. Shields, J.D., Fleury, M.E., Yong, C., Tomei, A.A., Randolph, G.J., and Swartz, M.A. 2007. Autologous chemotaxis as a mechanism of tumor cell homing to lymphatics via interstitial flow and autocrine CCR7 signaling. *Cancer Cell* 11:526-538.
5. Randolph, G.J., Angeli, V., and Swartz, M.A. 2005. Dendritic-cell trafficking to lymph nodes through lymphatic vessels. *Nat Rev Immunol* 5:617-628.
6. Phan, C.T., and Tso, P. 2001. Intestinal lipid absorption and transport. *Front Biosci* 6:D299-319.
7. Tammela, T., Petrova, T.V., and Alitalo, K. 2005. Molecular lymphangiogenesis: new players. *Trends Cell Biol* 15:434-441.
8. Grimaldi, A., Moriondo, A., Sciacca, L., Guidali, M.L., Tettamanti, G., and Negrini, D. 2006. Functional arrangement of rat diaphragmatic initial lymphatic network. *Am J Physiol Heart Circ Physiol* 291:H876-885.
9. Schmid-Schonbein, G.W. 1990. Microlymphatics and lymph flow. *Physiol Rev* 70:987-1028.
10. Zawieja, D. 2005. Lymphatic biology and the microcirculation: past, present and future. *Microcirculation* 12:141-150.
11. Moriondo, A., Pelosi, P., Passi, A., Viola, M., Marcozzi, C., Severgnini, P., Ottani, V., Quaranta, M., and Negrini, D. 2007. Proteoglycan fragmentation and respiratory mechanics in mechanically ventilated healthy rats. *J Appl Physiol* 103:747-756.
12. Lynch, P.M., Delano, F.A., and Schmid-Schonbein, G.W. 2007. The primary valves in the initial lymphatics during inflammation. *Lymphat Res Biol* 5:3-10.
13. Baluk, P., Fuxe, J., Hashizume, H., Romano, T., Lashnits, E., Butz, S., Vestweber, D., Corada, M., Molendini, C., Dejana, E., et al. 2007. Functionally specialized junctions between endothelial cells of lymphatic vessels. *J Exp Med* 204:2349-2362.
14. Johnson, L.A., Clasper, S., Holt, A.P., Lalor, P.F., Baban, D., and Jackson, D.G. 2006. An inflammation-induced mechanism for leukocyte transmigration across lymphatic vessel endothelium. *J Exp Med* 203:2763-2777.
15. Swartz, M.A., Kaipainen, A., Netti, P.A., Brekken, C., Boucher, Y., Grodzinsky, A.J., and Jain, R.K. 1999. Mechanics of interstitial-lymphatic fluid transport: theoretical foundation and experimental validation. *J Biomech* 32:1297-1307.
16. Angeli, V., and Randolph, G.J. 2006. Inflammation, lymphatic function, and dendritic cell migration. *Lymphat Res Biol* 4:217-228.
17. Randolph, G.J. 2001. Dendritic cell migration to lymph nodes: cytokines, chemokines, and lipid mediators. *Semin Immunol* 13:267-274.
18. Reddy, L.H., and Murthy, R.S. 2002. Lymphatic transport of orally administered drugs. *Indian J Exp Biol* 40:1097-1109.
19. Rutkowski, J.M., Moya, M., Johannes, J., Goldman, J., and Swartz, M.A. 2006. Secondary lymphedema in the mouse tail: Lymphatic hyperplasia, VEGF-C upregulation, and the protective role of MMP-9. *Microvasc Res* 72:161-171.
20. Adams, R.H., and Alitalo, K. 2007. Molecular regulation of angiogenesis and lymphangiogenesis. *Nat Rev Mol Cell Biol* 8:464-478.

21. Oliver, G., and Alitalo, K. 2005. The lymphatic vasculature: recent progress and paradigms. *Annu Rev Cell Dev Biol* 21:457-483.
22. Goldman, J., Rutkowski, J.M., Shields, J.D., Pasquier, M.C., Cui, Y., Schmokel, H.G., Willey, S., Hicklin, D.J., Pytowski, B., and Swartz, M.A. 2007. Cooperative and redundant roles of VEGFR-2 and VEGFR-3 signaling in adult lymphangiogenesis. *Faseb J* 21:1003-1012.
23. Pytowski, B., Goldman, J., Persaud, K., Wu, Y., Witte, L., Hicklin, D.J., Skobe, M., Boardman, K.C., and Swartz, M.A. 2005. Complete and specific inhibition of adult lymphatic regeneration by a novel VEGFR-3 neutralizing antibody. *J Natl Cancer Inst* 97:14-21.
24. Baluk, P., Tammela, T., Ator, E., Lyubynska, N., Achen, M.G., Hicklin, D.J., Jeltsch, M., Petrova, T.V., Pytowski, B., Stacker, S.A., et al. 2005. Pathogenesis of persistent lymphatic vessel hyperplasia in chronic airway inflammation. *J Clin Invest* 115:247-257.
25. Bock, F., Onderka, J., Dietrich, T., Bachmann, B., Pytowski, B., and Cursiefen, C. 2008. Blockade of VEGFR3-signalling specifically inhibits lymphangiogenesis in inflammatory corneal neovascularisation. *Graefes Arch Clin Exp Ophthalmol* 246:115-119.
26. Roberts, N., Kloos, B., Cassella, M., Podgrabinska, S., Persaud, K., Wu, Y., Pytowski, B., and Skobe, M. 2006. Inhibition of VEGFR-3 activation with the antagonistic antibody more potently suppresses lymph node and distant metastases than inactivation of VEGFR-2. *Cancer Res* 66:2650-2657.
27. Harvey, N.L., Srinivasan, R.S., Dillard, M.E., Johnson, N.C., Witte, M.H., Boyd, K., Sleeman, M.W., and Oliver, G. 2005. Lymphatic vascular defects promoted by Prox1 haploinsufficiency cause adult-onset obesity. *Nat Genet* 37:1072-1081.
28. Karkkainen, M.J., Saaristo, A., Jussila, L., Karila, K.A., Lawrence, E.C., Pajusola, K., Bueler, H., Eichmann, A., Kauppinen, R., Kettunen, M.I., et al. 2001. A model for gene therapy of human hereditary lymphedema. *Proc Natl Acad Sci U S A* 98:12677-12682.
29. Makinen, T., Jussila, L., Veikkola, T., Karpanen, T., Kettunen, M.I., Pulkkanen, K.J., Kauppinen, R., Jackson, D.G., Kubo, H., Nishikawa, S., et al. 2001. Inhibition of lymphangiogenesis with resulting lymphedema in transgenic mice expressing soluble VEGF receptor-3. *Nat Med* 7:199-205.
30. Petrova, T.V., Karpanen, T., Norrmen, C., Mellor, R., Tamakoshi, T., Finegold, D., Ferrell, R., Kerjaschki, D., Mortimer, P., Yla-Herttuala, S., et al. 2004. Defective valves and abnormal mural cell recruitment underlie lymphatic vascular failure in lymphedema distichiasis. *Nat Med* 10:974-981.
31. Rockson, S.G. 2001. Lymphedema. *Am J Med* 110:288-295.

This page is intentionally left blank.

APPENDIX to Chapter 2:

ORIGINAL MANUSCRIPT 1

A driving force for change: Interstitial flow as a morphoregulator

Joseph M. Rutkowski and Melody A. Swartz

Institute of Bioengineering, École Polytechnique Fédérale de Lausanne (EPFL), Switzerland

Submitted 12 September 2006; accepted in final form 16 November 2006

TRENDS in Cell Biology

2007 Jan;17(1):44-50. First published December 1, 2006.

ABSTRACT

Dynamic stresses that are present in all living tissues drive small fluid flows, called interstitial flows, through the extracellular matrix. Interstitial flow not only helps to transport nutrients throughout the tissue, but also has important roles in tissue maintenance and pathobiology that have been, until recently, largely overlooked. Here, we present evidence for the various effects of interstitial flow on cell biology, including its roles in embryonic development, tissue morphogenesis and remodeling, inflammation and lymphedema, tumor biology and immune cell trafficking. We also discuss possible mechanisms by which interstitial flow can induce morphoregulation, including direct shear stress, matrix–cell transduction (as has been proposed in the endothelial glycocalyx) and the newly emerging concept of autologous gradient formation.

INTRODUCTION

The importance of dynamic mechanical stress (see Glossary) in tissue development, maintenance, function and pathogenesis has been well established for several decades. The field of biomechanics originated to characterize the mechanical behavior of tissues that serve obvious mechanical functions (e.g. bone, muscle, arteries and lung tissue) and how these mechanical properties change in pathological states. This research evolved and branched into the field of mechanobiology, which focuses on understanding the cell biology that controls tissue mechanics, in other words, the response of cells to mechanical stress and the way they adapt to and control their mechanical environment [1 and 2]. Mechanobiology research today remains largely devoted to understanding the control of mechanically important tissues for tissue engineering applications and other areas of therapeutic design.

However, even in tissues that do not serve primarily mechanical functions or undergo obvious strains, mechanical stress is an important regulator of tissue development, health and pathology. Dynamic stresses and pressure gradients exist in all living tissues. These tissue stresses can impart forces on the cell, including fluid shear stress, pressure forces and forces on integrins, and they can also affect cell behavior by transporting solutes and shaping the extracellular distribution of key signaling proteins. For example, small fluid flows within the interstitial space are needed to drive protein transport from the blood to interstitial cells, because proteins are too large to readily diffuse the distances between blood capillaries, distances optimized for the transport of oxygen and other small molecules to cells. Dynamic stresses are therefore not only present in all living tissues, but are also required for physiological functions and tissue homeostasis. A clear example of the necessity of activity is seen in the atrophy of muscle and bone when movement is limited.

Here, we focus on the importance of a subtle but essential dynamic force: interstitial fluid flow. We argue not only that interstitial flow is an important morphoregulator in tissue development, maintenance and remodeling, but also that it is used by interstitial cells to signal the state of their surroundings, help establish extracellular microenvironments, and guide lymphocytes and tumor cells towards draining lymphatic vessels (also referred to generally herein as lymphatics).

What is interstitial flow?

Interstitial flow is fluid flow through a 3D matrix, around interstitial cells such as fibroblasts, tumor cells, tissue immune cells and adipocytes. It differs from open-channel flow, such as blood flow within vessels, in several ways (Figure 1): for example, it generally flows with a much slower velocity because of the high flow resistance of the extracellular matrix, it moves around the cell–matrix interface in all directions rather than only on the apical side, and it can have important effects on pericellular protein gradients, particularly those that are matrix binding. Interstitial flow also occurs across the blood vessel wall (called transvascular flow) (e.g. in arteries, this flow is two orders of magnitude slower than that of the blood) and the glycocalyx on the luminal surface of blood endothelium can impart some features of interstitial flow on the endothelium.

Interstitial flow is driven primarily by plasma leaving a blood capillary through its wall and draining into the initial lymphatics (Figure 2). Even when lymphatics are not functional or are blocked, some interstitial flow can occur by plasma reabsorption in post-capillary venules (although not all can be removed this way). In healthy adult tissues, the pressure difference between the two capillary networks maintains fluid pressure gradients that are altered by skeletal motion and also by subtle movements, such as those arising from arterial pulsation, respiration and organ movement. One noted exception to the intervascular pressure driving force is in cartilage and bone, where dynamic compression drives flow through the matrix.

There are only a few direct measurements of interstitial flow velocities *in vivo* in the literature; these velocities are difficult to measure and interpret because they are so slow and heterogeneous, they depend on the tracer moving with the same velocity as the fluid (which is difficult to confirm in the dense interstitial space, and the tracer can also cause artifacts when introduced into the tissue), and they have only been measured close to the surface by fluorescence recovery after photobleaching (FRAP) or nuclear magnetic resonance (NMR). Furthermore, these measurements are typically performed in anesthetized animals, in which interstitial fluid velocities are likely to be substantially different from those in awake animals because of changes in blood pressure and lymphatic pumping [3 and 4]. Reported measured velocities vary between 0.1 and 4.0 $\mu m\, s^{-1}$ [5 and 6]. Interstitial flow velocity can also be estimated using Darcy's law, which relates velocity to the pressure gradient and the hydraulic conductivity, K (Box 1). This is sometimes more convenient, because interstitial pressures can

be measured more reliably using micropipettes or wick-in-needle techniques [7] and K can be measured in tissues *ex vivo* using confined compression tests [8 and 9].

Even though it can be extremely slow, interstitial flow can have important effects on tissue morphogenesis and function, cell migration and differentiation and matrix remodeling, among other processes. The mechanisms by which such flows can drive cell response might be purely mechanical, such as shear stress on the cell surface, pressure force 'pushing' on the cell or tethering forces on cell–matrix connections (Figure 3). Importantly, it can also have non-mechanical affects on the cells, such as shifting the pericellular distribution of secreted proteins (e.g. morphogens, proteases and chemokines). These transport effects are likely to be more important than mechanical stress in tissues that do not serve primarily mechanical functions, because of the small magnitudes of stresses and flows found there. In these tissues, interstitial flow-induced protein redistribution might help to direct cell migration and guide the cell–cell interactions that lead to pattern formation during morphogenesis. Thus, interstitial flow affects both the mechanical microenvironment of the cell and the biochemical environment to which it is so acutely tuned.

Biological flows in development

In embryos that have not yet developed a vascular system or heart, flow that is driven through the differentiating cell mass is necessary for proper development. In the embryonic node (an embryonic structure located at the anterior tip of the primitive centerline) ciliary movement generates the leftward movement of fluid that leads to the left–right asymmetry of the organs (in which the heart is on the left, the liver on the right, etc.) [10], and when this cilia-driven flow within the node is reversed experimentally, the left–right asymmetry becomes reversed [11]. It has been suggested through mathematical modeling that nodal flow directs morphogen transport and mixing, thus driving asymmetric development [12]. This is indeed likely, because the actions of morphogens (to give cells directional and positional information) are achieved through their transcellular concentration gradients rather than their absolute amounts. In developing embryos, such spatial information guides cell differentiation [13]. Morphogen transport and gradient patterning are also believed to regulate the branching of developing lungs in the embryo [14], and it is expected that interstitial flows, caused by embryonic lung movements that simulate breathing, would influence morphogen distributions. Interstitial flow can also impart shear stress on the cell surface, which, as a

mechanical stimulus, can itself drive embryonic cell differentiation and determine lineage fate [15 and 16] and could be responsible for shaping organs [17 and 18].

Interstitial flow has also been implicated in lymphatic development. Using a skin regeneration model in which interstitial fluid flow could be traced and correlated with lymphatic proliferation, migration and reorganization over time, it has been shown that lymphatic cells migrate in the direction of interstitial flow and organize around fluid channels, and that they cannot organize into functional capillaries when interstitial flow is severely reduced [19 and 20]. Thus, interstitial flow can act as an important morphogenic cue, by mechanisms we discuss later.

Interstitial flow in tissue function and pathology

Much evidence has emerged to indicate that interstitial flow has an important regulatory role in tissue function. Transvascular flow across the arterial wall provides nutrient transport to the metabolically active cells there, and seemingly has a crucial role in maintaining arterial smooth muscle tone [21, 22 and 23]. In cartilage, where lymphatics are absent and intercellular distances are large, interstitial fluid flow is driven by mechanical loading and is necessary for nutrient transport and cell–cell communication when diffusion is inadequate [24, 25 and 26]. Also, interstitial flow rather than solid stress is responsible for at least some of the mechanical stress-induced matrix production in cartilage [27], because dynamic rather than static compression was found to promote proteoglycan and collagen synthesis [28] and increase chondrocyte metabolism [29] (interstitial flow is always present in tissues undergoing dynamic compression). Dynamic compression stimulates directional deposition of proteoglycans and matrix fiber compaction in the direction of flow [26] and directs remodeling by enhancing the transport of tissue inhibitor of metalloproteinase-1 (TIMP-1) [30]. In bone, physical activity causes oscillatory compression that has been estimated to increase the convective transport of macromolecules up to 100 times more than what is possible with diffusion [31]. Finally, in tissue repair, the migration of endothelial and epithelial cells is crucial for wound healing, which (at least on 2D surfaces) can be activated by shear stress [32 and 33], suggesting that interstitial flow also promotes wound healing in 3D tissues by shear stress. *In vitro*, interstitial flow enhances blood and lymphatic capillary formation [34] and acts synergistically with matrix-bound VEGF to induce capillarogenesis, probably by enhancing and directing the liberation of VEGF from the matrix to guide organization in the direction of flow [35, 36 and 37].

Physiological evidence that interstitial flow is crucial in normal tissue function can be seen in pathologies in which interstitial flow is reduced or enhanced. Lymphedema is a condition in which interstitial fluid flow is severely reduced due to either malformations in the lymphatic system (primary lymphedema) or blockage downstream, such as that which occurs after lymph node resection (secondary lymphedema). The accumulation, rather than clearance, of fluid from the interstitial space results in inflammation and extensive tissue remodeling, lymphatic hyperplasia, and adipocyte growth and lipid accumulation [38 and 39]. Fluid stagnation in lymphedema also prevents normal immune cell trafficking in the affected tissue, which can exacerbate the pathology. These resultant chronic pathological conditions in lymphedema highlight the importance of interstitial fluid convection in maintaining healthy tissue.

Abnormally increased interstitial flow rates can occur during inflammation (when blood capillaries become leaky) and can also trigger fibroblasts to differentiate or remodel the extracellular matrix. Although this can be due to increased transport of differentiation factors from inflammatory cells to fibroblasts, increased interstitial flow itself could be an important contributing factor to the development of tissue fibrosis: *in vitro* studies have shown that 4–10 $\mu m\ s^{-1}$ interstitial flow through a 3D collagen matrix seeded with human lung or dermal fibroblasts causes autocrine upregulation of transforming growth factor (TGF)-β1, differentiation into myofibroblasts (Figure 4a), increased collagen production and collagen alignment [40, 41 and 42]. In this way, high interstitial flow could be an early signaling cue of inflammation that triggers fibroblasts to begin rapid matrix repair. It could also help explain why tissue fibrosis often follows inflammation in many tissues, including the lung, skin and surrounding tumors, and why fibrosis can occur in the apparent absence of inflammatory cells, such as in idiopathic pulmonary fibrosis [43 and 44].

Interstitial flow in cancer

Interstitial flow in and around tumor tissue has particular importance in delivering anticancer agents to tumor tissue. Given that growing tumors induce angiogenesis and angiogenic tumor vessels are more permeable to proteins and large molecules than mature vessels [45], there has been substantial interest in exploiting tumor vessel permeability to selectively accumulate drug carriers by size in tumor tissue. However, interstitial transport is driven by pressure differences between the blood and interstitium, and in tumors interstitial fluid pressure is higher, ranging from 10 mmHg to 20 mmHg (with measurements as high as

90 mmHg), than in normal tissues, which have pressures that are typically <10 mmHg (Table 1) [46]. Thus, the driving force for fluid movement from the blood into the tumor stroma is lower than that in normal tissues. These high interstitial pressures are due in part to the lack of functional lymphatics within the tumor [47] and result in a net convective flow out from the tumor mass into the surrounding tissue as a result of the lower interstitial pressure found there. (The conclusion that tumors lack functional lymphatics is controversial, however; several reports have suggested that metastatic tumors can induce lymphatic growth into the tumor mass [48].)

Although the challenges to therapeutic delivery to solid tumors have been researched extensively, the impact of the extratumoral interstitial flow environment on tumor biology has not been much explored. Slow interstitial flow from the tumor mass into the surrounding tissue and draining lymphatics might, for example, help the tumor invade tissue and lymphatics by directing proteolytic enzymes and autocrine chemokines away from the tumor and towards the draining lymphatics. Alternatively, it might promote the formation of a fibrotic capsule around the tumor (as flow itself can drive fibroblast differentiation, as mentioned earlier [41]), which might inhibit tumor spread. Also, it is likely to affect the recruitment and function of tumor-associated macrophages that are found around highly invasive tumors [49] by further distributing chemotactic factors.

New insights into how interstitial flow can affect tumor biology and invasion are just beginning to emerge. For example, it was recently shown that tumor cell proliferation can be influenced by intratumoral pressure [50]. In tumors overexpressing lymphangiogenic growth factors, peritumoral lymphatics (those surrounding and draining the tumor) were found to drain fluid at an increased rate, and tumor cells were directly observed homing to those lymphatics [51]. Finally, recent *in vitro* studies suggest that interstitial flow from tumor cells directed towards lymphatic endothelial cells greatly enhances the migration of tumor cells towards the lymphatics, through a combination of autocrine and paracrine signaling mechanisms [Shields, J.D, unpublished data]. We explore this possibility further when discussing autologous chemotaxis.

Mechanisms of flow-induced cell response

Evidence that interstitial flow can direct mechanotransduction events on the cell surface comes from recent studies on the endothelial glycocalyx. Originally, the shear stress

effects seen on endothelial cells were presumed to be due directly to fluid shear stress acting on the cell surface, but there is increasing appreciation for the role of the glycocalyx in moderating or amplifying fluid stresses to the cell surface. The primary constituents of the glycocalyx are heparan sulfate, chondroitin sulfate and hyaluronan [52], anchored to the cell by proteoglycan core proteins. The role of the glycocalyx in transducing shear stress to the cell has been demonstrated by selectively degrading these components and exposing the cells to shear: for example, when either heparinase or hyaluronidase were applied to an endothelial cell monolayer, well established responses to shear stress, such as the release of nitric oxide, were eliminated [53 and 54]. Although such stresses are not identical to those in true interstitial flow, as mentioned earlier, the fact that cells might sense flow only when the glycocalyx is intact gives strong support to the importance of cell–ECM connections in transducing mechanical stress by slow interstitial flow. In 3D *in vitro* matrices, cell surface shear stresses for flow rates of $1\ \mu m\ s^{-1}$ were estimated to average 5×10^{-3} to 7×10^{-3} dyne cm^{-2} and peak at 1.5×10^{-2} dyne cm^{-2}, although the precise architecture of matrix fibers strongly affected these stresses [55]. It is unknown to what limit cells might sense shear stress, but with such low levels, it is likely that the glycocalyx and/or surrounding ECM helps amplify the signals to transduce mechanical stress to the cell.

Another mechanism by which interstitial flow can affect cellular responses is by changing pericellular diffusion gradients of morphogens that are redistributed by the flow according to how they are transported: by diffusive and/or convective transport (see Glossary). Given that morphogens act by directing cellular responses spatially according to transcellular gradients, subtle changes in their pericellular distributions (e.g. the introduction of asymmetry) can have important effects on directed cell processes. In addition, many chemokines and growth factors that are both secreted by and act upon the same cell bind strongly to the matrix (usually to sulfated proteoglycan components of the matrix), including members of the vascular endothelial growth factor (VEGF), fibroblast growth factor (FGF), Wnt and TGF families and many immunoresponsive chemokines, such as CCL21, that direct leukocyte migration [56]. The binding of these factors to the matrix gives the cell more control of its microenvironment and enables solid-phase gradients to form. In addition, some of these proteins can signal to cells in both their liberated and their matrix-bound forms.

Interstitial flow in cell homing: the concept of autologous chemotaxis

Chemokine gradients act as directional signals for cell chemotaxis or morphogenesis. Because migrating cells move up a chemokine concentration gradient, it is generally assumed that the chemokine is secreted by an upstream cell or tissue. An alternative mechanism, however, has recently been described whereby a cell can receive directional cues while simultaneously being the source of such cues, using interstitial flow. In this mechanism, even extremely subtle flows can affect the pericellular distribution of self-secreted proteins that interact with the matrix and thus cause autologous transcellular gradients, increasing in the direction of flow, to form (Figure 4c) [57]. Flow only slightly biases the distributions of a secreted matrix-binding morphogen and proteases that can liberate the morphogen, but those effects multiply and combine with the fact that, once the morphogen is liberated, it is further biased by flow. In this way, the ability of the secreted morphogen to bind the matrix serves as an amplification mechanism for autocrine gradient formation only in the presence of subtle interstitial flow. This has been demonstrated experimentally using a 3D culture of endothelial cells suspended in a VEGF-containing matrix, in which VEGF was covalently bound and liberated only upon proteolytic release by the cells [35]; capillary organization occurred only in the presence of both VEGF and interstitial flow (Figure 4b). This was presumably due to directed liberation of VEGF.

This putative phenomenon of autocrine morphogen gradient formation by interstitial flow and matrix binding of morphogens suggests that leukocytes and tumor cells might use interstitial flow to home to draining lymphatics. This is possible when the cell expresses the homing chemokine receptor and also secretes the chemokine ligand. These cells include tumor cells [expressing the chemokine receptor CCR7 and the ligand CCL21 (Shields, J.D., unpublished data)], dendritic cells (expressing the chemokine receptor CCR7 and the ligand CCL19 [58]) and macrophages (expressing VEGF receptor-3 and its ligand VEGF-C [49]). As all of these ligands can bind to the matrix, and as all are important cues for migration, there is potential for each to direct migration by this mechanism. Mathematical modeling shows that even the smallest flows can create autologous gradients in such systems [57]. Not only might this help to explain why certain cell types have receptors for ligands that they themselves secrete, but this mechanism of self-directed cell migration might also be fundamental to the movement of tumor and immune cells in the direction of interstitial transport, that is, towards functional lymphatic vessels and on to the nearest lymph node.

Flow-induced autologous chemotaxis has recently been demonstrated *in vitro,* using human invasive and noninvasive breast cancer cells, to take place through the chemokine CCR7 and its receptor CCL21: whereas flow strongly enhanced the migration of tumor cells through 3D matrices in the direction of flow, blocking CCR7 signaling eliminated this effect (Shields, J.D., unpublished data). Thus, it is possible that autologous chemotaxis is a powerful mechanism that cells use to find and home to functional draining lymphatics.

CONCLUDING REMARKS

In summary, interstitial flow is an important component of normal tissue function and homeostasis and of many pathologies, from development through to adulthood. It might also be a key morphoregulator, acting by giving directional cues to cells. As prime examples, dendritic cell trafficking to lymph nodes and tumor invasion and dissemination through lymphatics can use interstitial flow to home towards lymphatic capillaries. Future research that incorporates and examines interstitial flow as a key microenvironmental component will be necessary to elucidate such mechanisms fully and exploit its potential in therapy and tissue engineering.

GLOSSARY

Autologous chemotaxis
: a migratory mechanism whereby a cell can respond to a chemotactic gradient while at the same time being the source of the chemokine, when interstitial flow is present, to create the transcellular gradient.

Convection
: transport driven by fluid movement.

Diffusion
: transport driven by random thermal molecular motion (from high to low concentration).

Fluid shear stress
: the tangential stress exerted on a surface (e.g. of a cell) due to fluid viscosity and flow.

Glycocalyx
: a layer of heparan sulfate proteoglycans and hyaluronan secreted by and coating endothelial cells.

Matrix binding
: the ability of a morphogen to be chemically bound to the matrix, typically through interactions with sulfated proteoglycans.

Pressure gradient
: the difference in pressure divided by a unit length.

Stress
: force per unit area.

Box 1: Darcy's law

$$v = -K\frac{\Delta P}{l}$$

where v is the bulk fluid velocity, K is the hydraulic conductivity, and ΔP is the pressure difference over length l of the tissue.

Darcy's law provides the fundamental equation for low Reynolds number flows through porous media. Originally developed in 1856 to describe flow through a gravel bed, Darcy's law (here in simplified form) can be applied to biological tissues to calculate interstitial flow velocities because the physical parameters of pressure and K can be measured more readily.

REFERENCES

1. Pedersen, J.A., and Swartz, M.A. (2005) Mechanobiology in the third dimension. *Ann Biomed Eng* 33, 1469-1490
2. Wang, J.H., and Thampatty, B.P. (2006) An introductory review of cell mechanobiology. *Biomech Model Mechanobiol* 5, 1-16
3. Bruegger, D.*, et al.* (2002) Microvascular changes during anesthesia: sevoflurane compared with propofol. *Acta Anaesthesiol Scand* 46, 481-487
4. McHale, N.G., and Thornbury, K. (1986) A method for studying lymphatic pumping activity in conscious and anaesthetized sheep. *J Physiol* 378, 109-118
5. Chary, S.R., and Jain, R.K. (1989) Direct measurement of interstitial convection and diffusion of albumin in normal and neoplastic tissues by fluorescence photobleaching. *Proc Natl Acad Sci U S A* 86, 5385-5389
6. Dafni, H.*, et al.* (2002) Overexpression of vascular endothelial growth factor 165 drives peritumor interstitial convection and induces lymphatic drain: magnetic resonance imaging, confocal microscopy, and histological tracking of triple-labeled albumin. *Cancer Res* 62, 6731-6739
7. Wiig, H. (1990) Evaluation of methodologies for measurement of interstitial fluid pressure (Pi): physiological implications of recent Pi data. *Crit Rev Biomed Eng* 18, 27-54
8. Anand, S.*, et al.* (1995) Enzyme-Mediated Proteolysis of Fibrous Biopolymers - Dissolution Front Movement in Fibrin or Collagen under Conditions of Diffusive or Convective-Transport. *Biotechnology and Bioengineering* 48, 89-107
9. Levick, J.R. (1987) Flow through interstitium and other fibrous matrices. *Q J Exp Physiol* 72, 409-437
10. Mercola, M. (2003) Left-right asymmetry: nodal points. *J Cell Sci* 116, 3251-3257
11. Nonaka, S.*, et al.* (2002) Determination of left-right patterning of the mouse embryo by artificial nodal flow. *Nature* 418, 96-99
12. Cartwright, J.H.*, et al.* (2004) Fluid-dynamical basis of the embryonic development of left-right asymmetry in vertebrates. *Proc Natl Acad Sci U S A* 101, 7234-7239
13. Gurdon, J.B., and Bourillot, P.Y. (2001) Morphogen gradient interpretation. *Nature* 413, 797-803
14. Warburton, D.*, et al.* (2005) Molecular mechanisms of early lung specification and branching morphogenesis. *Pediatr Res* 57, 26R-37R
15. Estes, B.T.*, et al.* (2004) Mechanical signals as regulators of stem cell fate. *Curr Top Dev Biol* 60, 91-126
16. Hosseinkhani, H.*, et al.* (2005) Perfusion culture enhances osteogenic differentiation of rat mesenchymal stem cells in collagen sponge reinforced with poly(glycolic Acid) fiber. *Tissue Eng* 11, 1476-1488
17. Blatnik, J.S.*, et al.* (2005) The influence of fluid shear stress on the remodeling of the embryonic primary capillary plexus. *Biomech Model Mechanobiol* 4, 211-220
18. DeGroff, C.G.*, et al.* (2003) Flow in the early embryonic human heart: a numerical study. *Pediatr Cardiol* 24, 375-380
19. Boardman, K.C., and Swartz, M.A. (2003) Interstitial flow as a guide for lymphangiogenesis. *Circ Res* 92, 801-808
20. Rutkowski, J.M.*, et al.* (2006) Characterization of lymphangiogenesis in a model of adult skin regeneration. *Am J Physiol Heart Circ Physiol*
21. Wang, S., and Tarbell, J.M. (2000) Effect of fluid flow on smooth muscle cells in a 3-dimensional collagen gel model. *Arterioscler Thromb Vasc Biol* 20, 2220-2225

22. Tada, S., and Tarbell, J.M. (2000) Interstitial flow through the internal elastic lamina affects shear stress on arterial smooth muscle cells. *Am J Physiol Heart Circ Physiol* 278, H1589-1597
23. Kim, M.H.*, et al.* (2004) Control of the arteriolar myogenic response by transvascular fluid filtration. *Microvasc Res* 68, 30-37
24. Grodzinsky, A.J.*, et al.* (2000) Cartilage tissue remodeling in response to mechanical forces. *Annu Rev Biomed Eng* 2, 691-713
25. Chandran, P.L., and Barocas, V.H. (2004) Microstructural mechanics of collagen gels in confined compression: poroelasticity, viscoelasticity, and collapse. *J Biomech Eng* 126, 152-166
26. Quinn, T.M.*, et al.* (1998) Mechanical compression alters proteoglycan deposition and matrix deformation around individual cells in cartilage explants. *J Cell Sci* 111 (Pt 5), 573-583
27. Fitzgerald, J.B.*, et al.* (2006) Shear and compression differentially regulate clusters of functionally-related temporal transcription patterns in cartilage tissue. *J Biol Chem*
28. Kerin, A.*, et al.* (2002) Molecular basis of osteoarthritis: biomechanical aspects. *Cell Mol Life Sci* 59, 27-35
29. Evans, R.C., and Quinn, T.M. (2006) Dynamic compression augments interstitial transport of a glucose-like solute in articular cartilage. *Biophys J*
30. Garcia, A.M.*, et al.* (1998) Transport of tissue inhibitor of metalloproteinases-1 through cartilage: contributions of fluid flow and electrical migration. *J Orthop Res* 16, 734-742
31. Knothe Tate, M.L. (2003) "Whither flows the fluid in bone?" An osteocyte's perspective. *J Biomech* 36, 1409-1424
32. Albuquerque, M.L.*, et al.* (2000) Shear stress enhances human endothelial cell wound closure in vitro. *Am J Physiol Heart Circ Physiol* 279, H293-302
33. Li, S.*, et al.* (2005) Mechanotransduction in endothelial cell migration. *J Cell Biochem* 96, 1110-1126
34. Ng, C.P.*, et al.* (2004) Interstitial flow differentially stimulates blood and lymphatic endothelial cell morphogenesis in vitro. *Microvasc Res* 68, 258-264
35. Helm, C.L.*, et al.* (2005) Synergy between interstitial flow and VEGF directs capillary morphogenesis in vitro through a gradient amplification mechanism. *Proc Natl Acad Sci U S A* 102, 15779-15784
36. Helm, C.L.*, et al.* (2006) Engineered Blood and Lymphatic Capillaries in 3D VEGF-Fibrin-Collagen Matrices with Interstitial Flow. *Biotechnology and Bioengineering*
37. Semino, C.E.*, et al.* (2006) Autocrine EGF receptor activation mediates endothelial cell migration and vascular morphogenesis induced by VEGF under interstitial flow. *Exp Cell Res* 312, 289-298
38. Olszewski, W.L. (2003) The lymphatic system in body homeostasis: physiological conditions. *Lymphat Res Biol* 1, 11-21; discussion 21-14
39. Rutkowski, J.M.*, et al.* (2006) Secondary lymphedema in the mouse tail: Lymphatic hyperplasia, VEGF-C upregulation, and the protective role of MMP-9. *Microvasc Res*
40. Ng, C.P., and Swartz, M.A. (2003) Fibroblast alignment under interstitial fluid flow using a novel 3-D tissue culture model. *Am J Physiol Heart Circ Physiol* 284, H1771-1777
41. Ng, C.P.*, et al.* (2005) Interstitial fluid flow induces myofibroblast differentiation and collagen alignment in vitro. *J Cell Sci* 118, 4731-4739
42. Ng, C.P., and Swartz, M.A. (2006) Mechanisms of interstitial flow-induced remodeling of fibroblast-collagen cultures. *Ann Biomed Eng* 34, 446-454
43. Pardo, A., and Selman, M. (2002) Idiopathic pulmonary fibrosis: new insights in its pathogenesis. *Int J Biochem Cell Biol* 34, 1534-1538

44. Thannickal, V.J., *et al.* (2004) Mechanisms of pulmonary fibrosis. *Annu Rev Med* 55, 395-417
45. Jain, R.K. (2005) Antiangiogenic therapy for cancer: current and emerging concepts. *Oncology (Williston Park)* 19, 7-16
46. Jain, R.K. (1999) Transport of molecules, particles, and cells in solid tumors. *Annu Rev Biomed Eng* 1, 241-263
47. Padera, T.P., *et al.* (2002) Lymphatic metastasis in the absence of functional intratumor lymphatics. *Science* 296, 1883-1886
48. Achen, M.G., *et al.* (2006) Targeting lymphangiogenesis to prevent tumour metastasis. *Br J Cancer* 94, 1355-1360
49. Skobe, M., *et al.* (2001) Concurrent induction of lymphangiogenesis, angiogenesis, and macrophage recruitment by vascular endothelial growth factor-C in melanoma. *Am J Pathol* 159, 893-903
50. Hofmann, M., *et al.* (2006) Lowering of Tumor Interstitial Fluid Pressure Reduces Tumor Cell Proliferation in a Xenograft Tumor Model. *Neoplasia* 8, 89-95
51. Hoshida, T., *et al.* (2006) Imaging steps of lymphatic metastasis reveals that vascular endothelial growth factor-C increases metastasis by increasing delivery of cancer cells to lymph nodes: therapeutic implications. *Cancer Res* 66, 8065-8075
52. Shields, J.D., *et al.* (2006) Autologous chemotaxis as a mechanism of tumor cell homing to lymphatics via interstitial flow and autocrine CCR7 signaling. *Cancer Cell*
53. Tarbell, J.M., and Pahakis, M.Y. (2006) Mechanotransduction and the glycocalyx. *J Intern Med* 259, 339-350
54. Florian, J.A., *et al.* (2003) Heparan sulfate proteoglycan is a mechanosensor on endothelial cells. *Circ Res* 93, e136-142
55. Moon, J.J., *et al.* (2005) Role of cell surface heparan sulfate proteoglycans in endothelial cell migration and mechanotransduction. *J Cell Physiol* 203, 166-176
56. Pedersen, J.A., *et al.* (2006) Effects of extracellular fiber architecture on cell membrane shear stress in a 3D fibrous matrix. *J Biomech* in press
57. Patel, D.D., *et al.* (2001) Chemokines have diverse abilities to form solid phase gradients. *Clin Immunol* 99, 43-52
58. Fleury, M.E., *et al.* (2006) Autologous morphogen gradients by subtle interstitial flow and matrix interactions. *Biophys J* 91, 113-121
59. Randolph, G.J., *et al.* (2005) Dendritic-cell trafficking to lymph nodes through lymphatic vessels. *Nat Rev Immunol* 5, 617-628
60. Netti, P.A., *et al.* (2000) Role of extracellular matrix assembly in interstitial transport in solid tumors. *Cancer Res* 60, 2497-2503
61. Swartz, M.A., *et al.* (1999) Mechanics of interstitial-lymphatic fluid transport: theoretical foundation and experimental validation. *J Biomech* 32, 1297-1307
62. Wiig, H., *et al.* (2003) New and active role of the interstitium in control of interstitial fluid pressure: potential therapeutic consequences. *Acta Anaesthesiol Scand* 47, 111-121
63. Kajimura, M., *et al.* (2001) Interstitial fluid pressure surrounding rat mesenteric venules during changes in fluid filtration. *Exp Physiol* 86, 33-38
64. Wang, D.M., and Tarbell, J.M. (1995) Modeling interstitial flow in an artery wall allows estimation of wall shear stress on smooth muscle cells. *J Biomech Eng* 117, 358-363

FIGURE LEGENDS

Figure 1. Interstitial and intravascular flows and their corresponding microenvironments. A blood vessel is shown, with insets showing the transvascular and glycocalyx regions. Black arrows represent luminal flow, and green arrows represent intra-glycocalyx, transvascular, and interstitial flows. By definition, interstitial flow refers to fluid flow around an interstitial cell: a cell attached to extracellular matrix in three dimensions. For endothelial cells, flow within vessels occurs only on the apical surface. Where there is a glycocalyx, flow might percolate through that network of proteoglycans and cause complex stresses on the cell surface, but fluid flow is still two-dimensional with respect to the cell surface. However, the intimate cell–matrix–flow interactions at the glycocalyx–cell interface might lead to effects similar to those in three dimensions. Intravascular pressure can drive flow through the vascular wall, but endothelial cells and smooth muscle cells will experience flow stresses through cell–cell connections and through cell–matrix connections as in true interstitial flow.

Figure 2. Determinants of interstitial flow velocity. Darcy's law describes fluid flow through a 3D matrix as being driven by a fluid pressure gradient and controlled by a flow resistance. It is analogous to water flow through a mat of hair in a bathtub drain: the more dense the hair mat, the slower the fluid drains. One important source of interstitial convection is fluid movement driven by the pressure gradient between blood and lymphatic capillaries (red and green, respectively), determined by the pressure difference ($P_{blood} - P_{lymphatic}$) divided by the intercapillary distance. The pressure gradient yields a resultant velocity, $\underline{v}$ (green arrows), controlled by the interstitial hydraulic conductivity, K, which varies depending on the density and composition of each tissue (Box 1, Table 1).

Figure 3. The direct effects that interstitial flow has on cells. Interstitial flow can induce **(a)** fluid shear stress, σ, on the cell surface; **(b)** forces normal to the cell surface (F); **(c)** shear and normal forces to the pericellular matrix that is mechanically coupled to the cytoskeleton; and **(d)** redistribution of pericellular proteins (autocrine and paracrine signals) that bind cell receptors.

Figure 4. Examples of cellular responses to interstitial flow. **(a)** Interstitial flow at 4 μm/s levels (right) cause human dermal fibroblasts seeded in type I collagen to differentiate into myofibroblasts by upregulation of TGF-β and align themselves and the matrix fibers perpendicular to the flow. Reproduced with permission from Ref. [41]; the scale bar

represents 20 μm. **(b)** Human blood endothelial cells form branched structures with lumens when cultured under interstitial flow (right). Here, low levels (4 μm/s) of interstitial flow greatly enhanced the effects of matrix-bound VEGF on capillary morphogenesis. Reproduced with permission from Ref. [35]; the scale bar represents 40 μm. **(c)** Computational modeling demonstrates that when morphogens or chemokines are autologously secreted by a cell in matrix-binding form and under low levels of interstitial flow, autologous morphogen gradients develop to guide cell processes in the direction of flow. The concentration profiles of liberated VEGF released by cell-secreted proteases,under the conditions in (b) are shown. Reproduced with permission from Ref. [35].

This page is intentionally left blank.

Figure 1

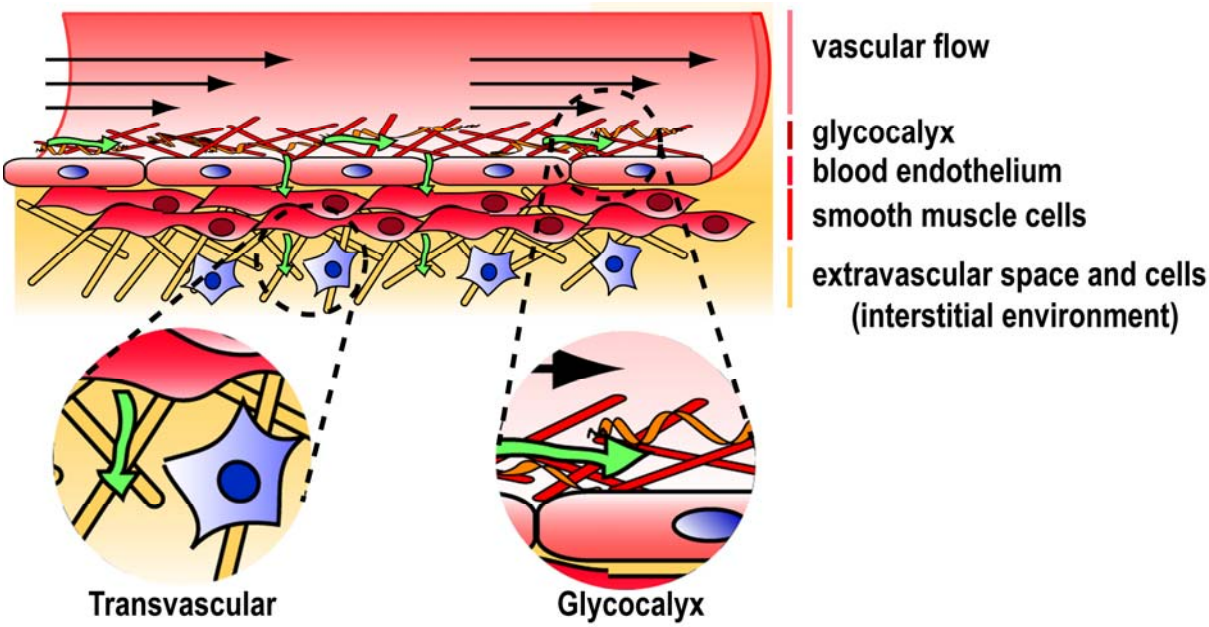
vascular flow
glycocalyx
blood endothelium
smooth muscle cells
extravascular space and cells
(interstitial environment)
Transvascular
Glycocalyx

This page is intentionally left blank.

Figure 2

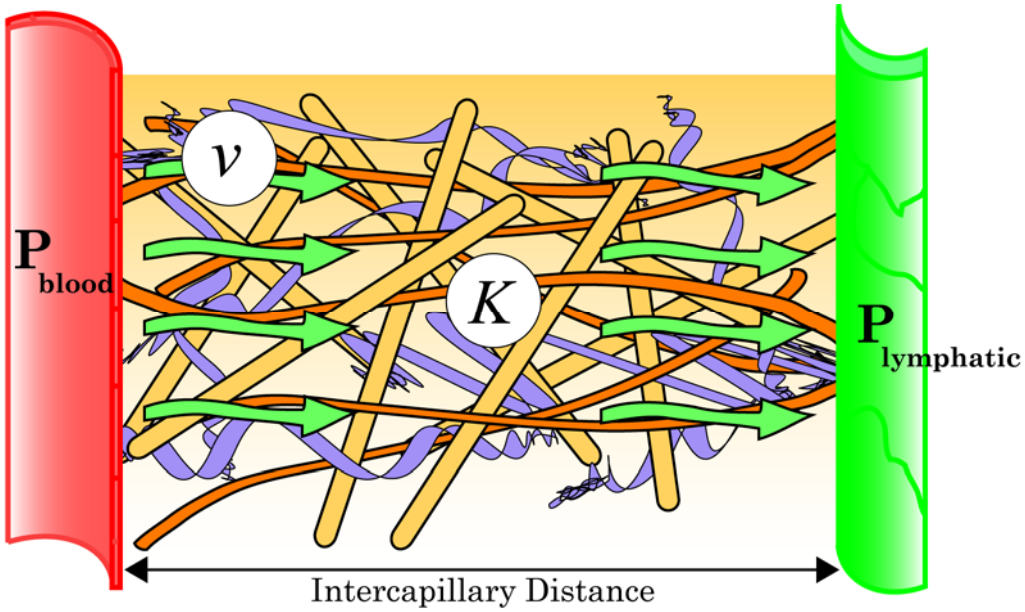

This page is intentionally left blank.

Figure 3

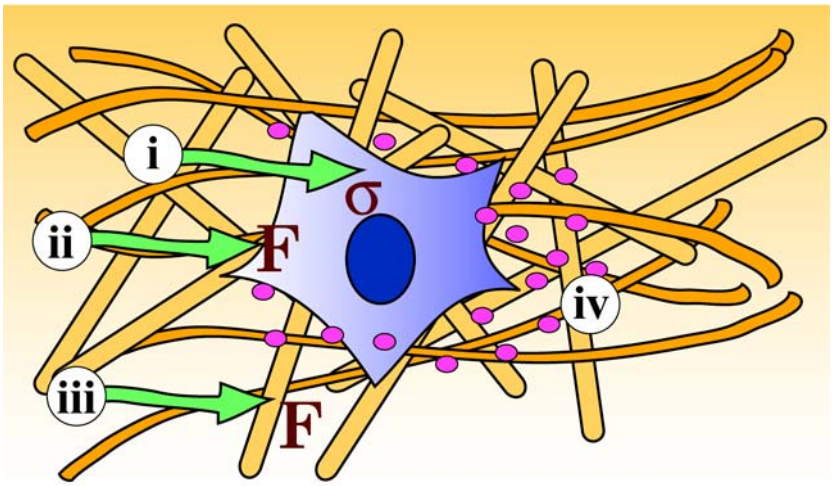

This page is intentionally left blank.

Figure 4

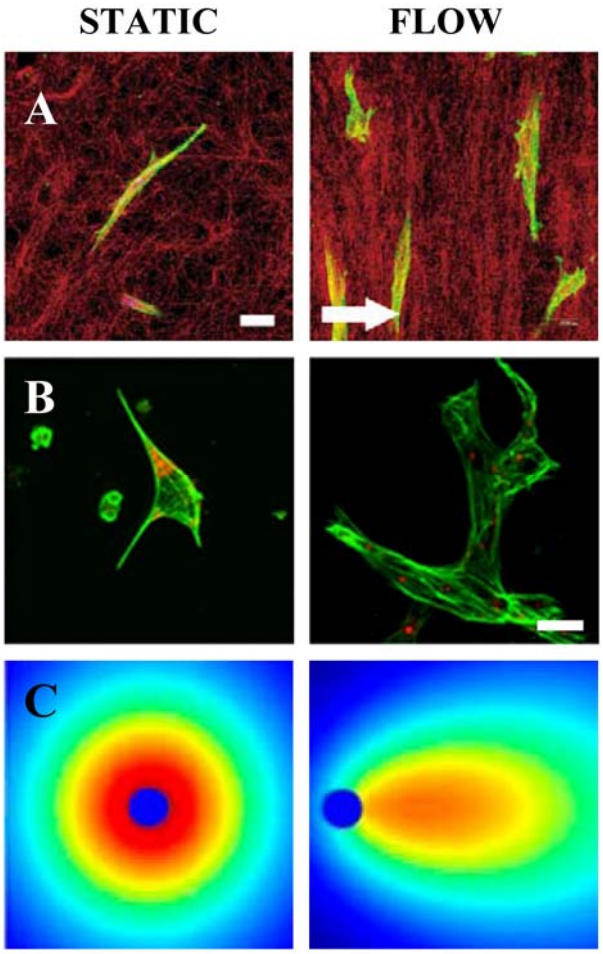

This page is intentionally left blank.

CHAPTER 3:
ORIGINAL MANUSCRIPT 2

Characterization of Lymphangiogenesis in a Model of Adult Skin Regeneration

Joseph M. Rutkowski[1], Kendrick C. Boardman[2], and Melody A. Swartz[1,2]

[1]Institute of Bioengineering, École Polytechnique Fédérale de Lausanne (EPFL), Lausanne, Switzerland
[2]Department of Biomedical Engineering, Northwestern University, Evanston, IL USA

Submitted 9 January 2006; accepted in final form 25 April 2006

American Journal of Physiology – Heart and Circulatory Physiology

291: H1402-H1410, 2006. First published April 28, 2006.

ABSTRACT

To date, adult lymphangiogenesis is not well understood. In this study we describe the evolution of lymphatic capillaries in regenerating skin and correlate lymphatic migration and organization with the expression of matrix metalloproteinases (MMPs), immune cells, the growth factors VEGF-A and VEGF-C, and the heparan sulfate proteogylcan perlecan, a key component of basement membrane. We show that while lymphatic endothelial cells (LECs) migrate and organize unidirectionally, in the direction of interstitial fluid flow, they do not sprout into the region but rather migrate as single cells that later join together into vessels. Furthermore, in a modified "shunted flow" version of the model, infiltrated LECs fail to organize into functional vessels, indicating that interstitial fluid flow is necessary for lymphatic organization. Perlecan expression on new lymphatic vessels was only observed after vessel organization was complete, and also appeared first in the distal region, consistent with the directionality of lymphatic migration and organization. VEGF-C expression peaked at the initiation of lymphangiogenesis but was reduced to lower levels throughout organization and maturation. In mice lacking MMP-9, lymphatics regenerated normally, suggesting that MMP-9 is not required for lymphangiogenesis, at least in mouse skin. This study thus characterizes the process of adult lymphangiogenesis and differentiates it from sprouting blood angiogenesis, verifies its dependence on interstitial fluid flow for vessel organization, and correlates its temporal evolution with those of relevant environmental factors.

Key words: lymphatic, vasculogenesis, interstitial fluid flow, MMP-9, perlecan

INTRODUCTION

Adult lymphangiogenesis is an important process that occurs in wound healing and may play a role in lymphedema and cancer metastasis. Increasingly, the importance of lymphatic biology is being realized and many key advances in the field have recently emerged, particularly in the identification and characterization of key molecular regulators of lymphangiogenesis (1, 2). Through the analysis of gene expression in embryonic development, for example, the control of the lymphatic endothelial cell (LEC) phenotype by Prox1 (3) and the requirement of neuropilin-2 (4) and podoplanin (5) expression by LECs in embryonic lymphatic vessel formation have been established. Vascular endothelial growth factor (VEGF) receptor-3 (VEGFR-3) (6) and its ligands VEGF-C (7-9) and VEGF-D (10) have been well-established as critical for both embryonic and adult lymphangiogenesis, although VEGFR-3 ligation may not be required for lymphatic vessel maintenance (11). Developmental and mechanistic studies of these factors and others, including angiopoietin-1 (12) and -2 (13), are continuing to elucidate the molecular underpinnings of lymphangiogenesis.

Despite this emerging knowledge, lymphangiogenesis in adult tissues is not adequately understood. Regulators of developmental lymphangiogenesis may not necessarily have the same relevance in adult lymphangiogenesis or lymphatic regeneration, particularly considering that many of these factors play multiple roles in early development of both blood and lymphatic vessels before becoming specific to one type of endothelial cell in adulthood (2). Furthermore, many studies of adult lymphangiogenesis utilize models in which lymphatic growth is induced by orthotopic human tumor xenografts in mice (1) or by exogenous stimulation in alymphatic tissues (14, 15), which may not accurately reflect physiologically relevant situations.

We recently developed a mouse model of adult lymphangiogenesis in regenerating skin and used it to demonstrate the role of interstitial flow in lymphangiogenesis (16, 17). In this model, a small circumferential band of skin is removed from the middle of the tail, fitted with a gas-permeable silicone sleeve, and filled with collagen. The collagen provides a scaffold for tissue regeneration that is initially cell-free, allowing the infiltration of immune cells and ingrowth of blood and lymphatic vessels to be tracked both spatially and temporally as the tissue regenerates. Furthermore, the silicone sleeve keeps the wound moist and intact and prevents granulation; indeed, the regenerated skin is virtually identical to native skin except for the absence of hair follicles that do not regenerate. Importantly, the collagen

scaffold serves as a fluid bridge for the one-way interstitial convection of lymph fluid between the distal and proximal halves of the tail. In other words, since lymph always flows from the tip of the mouse tail towards the body, interstitial fluid flow through the regenerating region will always be unidirectional.

We previously used this model to demonstrate that interstitial flow plays an organizational role in lymphangiogenesis, specifically showing that lymphatic capillaries develop in the direction of lymph flow. We had hypothesized that flow was necessary to create fluid channels in the regenerating region into which LECs migrate and organize into lymphatic vessels. This model was also used to demonstrate that although complete inhibition of lymphangiogenesis in regenerating skin could be achieved by systemic delivery of mF431C1, a VEGFR-3 blocking antibody (11), excess VEGF-C in the regenerating region could not enhance physiological lymphangiogenesis (18). This model has thus proven useful for studying the effects of established biochemical cues on lymphatic regeneration.

Here we characterize the process of lymphangiogenesis in the regenerating skin model to assess relative timing, distribution, and importance of some potential key regulating factors relative to lymphatic growth. Specifically, we examine lymphatic growth and morphology at early (1, 3, 5, 7, and 10 days) and later (17, 25, and 60 days) timepoints in the regeneration process and correlate temporally the presence of VEGF-C, VEGF-A, the heparan sulfate proteoglycan (HSPG) perlecan (a key component of basement membrane), MMPs, and immune cells to lymphatic growth and morphology. We demonstrate that lymphatic regeneration occurs via single LECs migrating with interstitial fluid flow and later, after populating the region, coalescing into vessels. We also provide further evidence that interstitial fluid flow is necessary for LEC organization using a shunted flow modification of our model. We show that VEGF-C expression is decreased as the lymphatic vessels become connected and functional, at which time a discontinuous perlecan expression pattern begins to become present on the lymphatics. Also, our data suggests that MMP-9 may not be important in adult dermal lymphangiogenesis, and support previous observations that macrophages may play a critical role (15).

MATERIALS & METHODS

Animal and sample preparation

All studies utilized 6–8 week old female BALB/c mice (Charles River Laboratories, France); 3-5 mice were used at each timepoint. Mice were anesthetized with an intraperitoneal injection of ketamine (65 mg/kg), xylazine (13 mg/kg), and acepromazine (2mg/kg). An analgesic, butorphanol (0.05 mg/kg), was administered subcutaneously twice daily for three days following the procedure. All protocols were approved by the Veterinary Authorities of the Canton Vaud according to Swiss law (protocol number # 1687).

Mice were prepared as described previously (17). Briefly, a 2 mm wide circumferential band of dermal tissue was excised midway up the tail. The area was then covered with a gas-permeable silicone sleeve and filled with type I rat tail collagen (BD Pharmingen, San Jose, CA). The sleeve was secured with Nexaband adhesive (Abbott Labs, Abbott Park, IL) at the proximal edge. Mice were sacrificed at specified times from 1-60 days post-procedure. Additionally, to test the hypothesis that interstitial fluid flow is necessary for lymphatic organization, a modified "shunted flow" model was prepared in three mice. In this modified model, a 2 mm square excision was made instead of a circumferential excision, allowing for lymph to circumvent around the regenerating region through existing lymphatics in the intact tissue (Fig. 1).

After sacrificing the animals, a section of tail 8 mm long (containing the regenerating region along with some native distal and proximal tissue) was removed and flash frozen in liquid N_2. Tissue samples were transversely cryosectioned into 12 and 60 μm-thick sections and stored at -80˚C until immunostaining.

To further examine the role of MMP-9 in this model, MMP-9 deficient on an FVB/NJ background, along with wild-type controls, were obtained (FVB.Cg-*Mmp9*^{tm1Tvu}/J; The Jackson Laboratory, Bar Harbor, ME). Nine female mice at 6 weeks of age from the MMP-9 deficient strain and 9 female FVB/NJ controls were prepared as described. Three mice from each group were sacrificed at 17, 25, and 60 days.

Microlymphangiography

Mice were anesthetized as above and the regeneration of the lymphatic vasculature was examined by fluorescence microlymphangiography (17, 19). A fluorescently labeled macromolecule (2000 kDa fluorescein-conjugated dextran, 2 mg/ml; Molecular Probes, Carlsbad, CA) was injected intradermally at a constant pressure of 45 cm of water into the tip

of the tail. As the fluorescent tracer was picked up and transported by the lymphatic vessels, it was clearly visible within dermal lymphatic capillaries, thus providing a clear visualization of lymphatic functionality. The lymphatic vasculature was monitored with a Zeiss Axiovert 200M fluorescence microscope and Zeiss MRm camera.

Immunofluorescence and immunohistochemistry

To visualize blood endothelial cells (BECs) and LECs, both thin (12 μm) and thick (60 μm) sections were co-stained with primary antibodies to the lymphatic-specific marker LYVE-1 (1:500; rabbit polyclonal; Upstate, Charlottesville, VA), and endothelial cell marker CD31 (1:200; rat polyclonal; BD Pharmingen). Although CD31 has an affinity for lymphatics, co-staining eliminated any discrepancy in identifying BECs from LECs. For immune cells and MMPs, thin (12 μm) sections were labeled using the following anti-mouse antibodies: the leukocyte-common CD45 (1:100; rat monoclonal; BD Pharmingen), the macrophage-specific surface marker F4/80 (1:50; rat monoclonal; Serotec, Raleigh, NC), the Langerhans dendritic cell protein langerin (1:50; goat polyclonal; Santa Cruz Biotechnology, Santa Cruz, CA), MMP-2 (1:25; goat polyclonal; R&D Systems, Minneapolis, MN), MMP-8 (1:100; goat polyclonal; Santa Cruz Biotechnology), MMP-9 (1:400; rabbit polyclonal; Chemicon, Temecula, CA) or MMP-13 (1:500; goat polyclonal; Chemicon). The heparan sulfate proteoglycan perlecan was also stained (1:500; rat monoclonal; U.S. Biological, Swampscott, MA) together with LYVE-1. These antibodies were detected with Alexafluor 488 or 594-conjugated donkey, rabbit, and goat IgG secondary antibodies (1:200, Molecular Probes, Carlsbad, CA), counterstained with DAPI (Vector Labs, Burlingame, CA). Thin sections were observed and imaged under a Zeiss Axiovert 200M fluorescence microscope with an Axiocam MRm camera. Confocal stacks of thick (60 μm) sections were scanned using a Zeiss LSM 510 Meta confocal microscope and maximum projections were generated for presentation.

VEGF-A and VEGF-C were labeled immunohistochemically. Sections were first fixed in 4% PFA, blocked against endogenous biotin and avidin (Biotin Blocking System, Dako, Carpenteria, CA), then labeled with VEGF-A (1:50; rabbit polyclonal; Santa Cruz) or VEGF-C (1:50; goat polyclonal; Santa Cruz) and biotinylated secondary antibodies (1:200; AffiniPure donkey and rabbit, respectively; Jackson ImmunoResearch, West Grove, PA). These were then visualized using the ABC-AP kit and VectaRed (Vector Labs). Sections were counterstained with hematoxylin, dehydrated, and mounted with Eukitt (Fluka Chemie AG,

Buchs, Switzerland). Images were captured with an Olympus AX70 Microscope and DP70 Camera.

Image analysis

Images of the regenerating region were assembled into complete montages in Photoshop (Adobe Systems, San Jose, CA). LECs were defined as cells with a blue (DAPI-stained) nuclei surrounded by green (LYVE-1 with AlexaFluor 488) labeling. After defining the borders of the region, the number of LECs within each half of the regenerating region were counted and summed across three random 12 μm sections from each animal. Similarly, Langerhans dendritic cells were counted by identifying nuclei of langerin-labeled cells in the regenerating regions of three 12 μm sections at each time point.

Metamorph 6.3 image analysis software (Molecular Devices Corp., Sunnyvale, CA) was used for quantifying MMPs, growth factors, and other immune cells. For immune cells and MMPs, three regenerating region montages from like groups of images were analyzed to identify positive fluorescent labeling using intensity thresholding. The region was then clearly identified with a freehand tool (with care taken to exclude pockets or defects in the tissue sections) and the percentage of stained area within each regenerating region was obtained. Values for three regions were averaged. For growth factor quantification, the color range of Vector Red (Vector Labs) staining, indicating positive labeling of either VEGF-A or VEGF-C, was identified and the percent coverage of each regenerating region was similarly measured. The data was normalized for each factor to the maximum expression.

Statistics

ANOVA and two-tailed t-tests were performed to determine statistical significance. Data are reported as average ± standard deviation. For MMPs, immune cells, and growth factors, the total expression during regeneration was compared to that of normal (control) tissue to determine significance in upregulation during regeneration. Additionally, single-factor ANOVA was performed on expression during regeneration to determine if there were significant differences among all of the time points.

RESULTS AND DISCUSSION

Unidirectional regeneration with interstitial fluid flow

First, we confirmed our earlier findings (17) that in regenerating mouse tail skin, lymphangiogenesis occurred in the direction of lymphatic flow – distal to proximal – which was also the direction of interstitial flow in the regenerating skin where lymph flow was interrupted. We further quantified this directionality in migration to demonstrate statistical significance (Fig. 2*F*). This was in contrast to blood angiogenesis, which occurred from all directions in the regenerating skin. Quantification of LECs in 12 μm sections revealed that the regenerating region was initially free of LECs and remained so through day 10 (Fig. 2*E*). While very few LECs were seen in the region at day 10 (Fig. 2*B*), those present were confined to the distal half (P=0.007) (Fig 2*F*). At day 17 (Fig. 2*C*), some LECs were present in the proximal half, but the distal population was much greater (P<0.001). Even at later timepoints of 25 and 40 days, LECs populated the upstream (distal) region significantly more than the downstream region (P=0.04 and P=0.006 for 25 and 40 days, respectively), indicating that proliferation and migration were occurring primarily from the distal region. Even though the total number of LECs in the region did not significantly change after day 17 (Fig. 2*E*), it was not until day 60 (Fig. 2*D*), when functional and continuous lymphatic capillaries appeared normal, that the distribution of LECs equalized between both halves of the regenerating region (P=0.4).

To further explore whether interstitial flow is necessary for lymphatic organization, mice were prepared with a square regenerating region (as opposed to the circumferential model), which allows lymph flow to be circumvented around the implanted collagen gel in the intact lymphatic vessels. Unlike the circumferential collagen implant, where distal lymph must flow interstitially through the regenerating region to be picked up by functional lymphatics on the proximal side, lymph need not flow through the high resistance regeneration zone in the square model since the intact surrounding lymphatic vessels provide a lower resistance to flow. While this relative lack of directional interstitial flow did not inhibit re-epithelialization or blood angiogenesis, we found that LECs failed to organize into a connected, functional lymphatic network in this shunted flow region (Fig. 1), demonstrating that interstitial fluid flow is necessary for functional lymphatic capillary organization.

Conversely, blood vessel regeneration was independent of the interstitial flow direction. Blood vessels initially appeared to sprout from the deeper, larger blood vessels underneath the regenerating region (near the bone) at day 7, and at day 10, sprouts were seen

equally from distal and proximal edges as well (Fig. 2*B*). By day 17, blood vessels were present throughout the region. In the square shunted flow model, blood vessel regeneration was indistinguishable from that seen in the circumferential model (data not shown), as was re-epithelialization of the collagen gel.

Lymphatic morphogenesis: coalescing rather than sprouting

Confocal microscopy of 60 μm sections revealed that in contrast to sprouting, LECs migrated as single cells (sometimes coalescing into small groups of cells) in the direction of interstitial flow, and, after sufficiently populating the region, later organized into vessels. LECs were generally absent from the regenerating region until day 10 when individual LECs or small groups were seen migrating into the distal half of the region (Fig. 3*A*). By day 17, multicellular groups or ducts were present (Fig. 3*B*), but were not connected to other groups. LECs predominantly began to organize in a fashion reminiscent of vasculogenesis by day 25. At this time, LECs in both the distal and proximal halves were already organized into vessel structures (Fig. 3*C*). At day 60, the regenerated region had a complete lymphatic vasculature whose morphology appeared similar to that of native vessels. In contrast, during concurrent blood angiogenesis, new blood vessels sprout directly from the existing native vasculature. Thus, by migrating as single cells in the direction of interstitial flow and then later coalescing into individual short vessel fragments and eventually into an interconnected capillary network, LEC organization into vessels was more reminiscent of vasculogenesis than of sprouting angiogenesis.

Development of basement membrane following lymphatic organization

Past analysis of endothelial cell basement membrane composition has shown that the predominant HSPG in the basement membrane of mature blood vessels is perlecan (20). This HSPG, produced in varying degrees by all endothelial cells (21), is essential for developmental vasculogenesis in mice (22), and is expressed during angiogenesis (23) and following vessel injury (24). Although lymphatic capillaries have a discontinuous basement membrane (25), it is not known at what stage during lymphangiogenesis it appears. Using confocal microscopy on 60 μm sections, we observed perlecan co-localization with lymphatic vessels in regenerating skin only after organization had occurred, at day 25 and day 60 (Fig. 3). Furthermore, its expression followed the spatial pattern of vessel formation and organization. At early times, before vessel organization was seen (day 10 and day 17), perlecan expression was limited to new blood vessels. At day 25 (Fig. 3*C*), when significant

organization of LECs into vessels was underway, some lymphatic structures in the distal half were perlecan positive while those in the proximal half were not. By day 60 (Fig. 3*D*), nearly all lymphatic vessels in the distal half were co-localized with perlecan, but in the proximal half where some vessels were still forming, perlecan expression appeared more sporadically. In normal intact skin, the lymphatic capillaries strongly expressed perlecan (Fig. 3*E*). Thus, since the HSPG perlecan identifies basement membrane on regenerating lymphatic vessels and appears only after vessel organization has occurred, it may be indicative of lymphatic vessel maturation. Additionally, its initial appearance only on distal vessels further demonstrates the directionality of both LEC migration and lymphatic organization in this model.

Early VEGF-A and -C upregulation

Expression of VEGF-A and VEGF-C were highest during the initiation of both blood and lymph angiogenesis. VEGF-A expression (Fig. 4) appeared to be highest at day 5, slightly preceding observable blood angiogenesis. These differences in expression, however, were not statistically significant. VEGF-C expression (Fig. 4) was highest prior to, and during the initiation of, lymphangiogenesis (days 3-10). This expression was significantly higher at days 3-10 than at days 17 and 25 ($P=0.033$). These expression profiles suggest that heightened expression of both VEGF-A and VEGF-C signaling might be most important in early (i.e. initiation) rather than later (i.e. organization and maturation) stages of vasculogenesis and lymphangiogenesis, consistent with their known functional roles (2, 26).

MMP expression

MMPs known to be upregulated in murine wound healing, specifically MMP-2, -8, -9, and -13 (27-29), were examined to determine their transient relationship to lymphatic regeneration. Our results suggest that only MMP-9 and MMP-13 were significantly elevated in the regenerating region compared to normal control skin ($P=0.006$ and 0.001, respectively), although the expression of MMP-2 was almost significantly higher during regeneration than in control tissue ($P=0.056$) and appeared to peak at day 17 (Fig. 4). MMP-2 and -9 play important roles in extracellular matrix remodeling (30, 31), endothelial cell migration (32-34), and vasculogenesis (34, 35); we found that MMP-2 expression (Fig. 4) increased after day 10, concurrent with blood angiogenesis and at the initiation of lymphangiogenesis. Surprisingly, MMP-9 expression was very low after day 7, so its link to endothelial cell migration might be more important for blood angiogenesis but not critical to lymphangiogenesis. MMP-13 has

been demonstrated to play a critical role in blood neovascularization (36) in conjunction with macrophages, which help induce angiogenic sprouting by using MMPs to extravasate from blood vessels (37). MMP-13 expression appeared to peak early, by day 7, thus preceding elevated macrophage numbers in the regenerating region (below). Although a role in blood neovascularization has been established (36), it is therefore possible that MMP-13 activity is only critical for revascularization by mechanisms dependent on sprouting from the existing vasculature. MMP-8 expression was very low at all times in the regenerating tissue, despite other observations that it is upregulated in dermal wounds by neutrophils (38).

To examine the hypothesis that MMP-9 is not necessary for adult dermal lymphangiogenesis, we examined lymphatic regeneration in transgenic mice lacking MMP-9. The regenerating regions of these MMP-9 deficient mice were stained for LECs and BECs at day 17 and day 60. There were no observable differences in the extent or morphology of either lymphatic or blood vessels in the regenerating region of these mice compared to matched wild-type control mice (Fig. 5*A*). Additionally, the number of LECs identified in the regenerating region at day 17, a critical timepoint in regeneration, was the same between the MMP-deficient mice and matched wild type controls (P=0.48) (Fig. 5*B*). This is not inconsistent with other reports that showed minimal differences in blood angiogenesis in MMP-9 deficient mice (39, 40). It has been suggested that MMP-2 might have a more crucial role than MMP-9 in retinal angiogenesis (40) and that synergy between MMP-2 and -9 is essential for tumor vascularization (39); our data suggests that MMP-2 might be more important in lymphangiogenesis, at least in regenerating mouse skin, than MMP-9.

The temporal expression patterns of each of the MMPs surveyed correlated with the results other wound healing studies (27, 28, 38, 41). While it was not possible to define the exact role of each MMP due to their release by many cell types, including infiltrating immune cells, keratinocytes, and endothelial cells, as well as potentially overlapping and/or redundant roles in many different components of the skin regeneration process, our data demonstrate that in terms of timing, MMP-2 was the most closely correlated to the onset of lymphangiogenesis, and that lymphangiogenesis appeared normal in MMP-9 null mice.

Immune cell infiltration

Macrophages and dendritic cells, as antigen-presenting immune cells, utilize lymphatic vessels in adaptive immunity and may be involved in lymphangiogenesis (15); furthermore, macrophages both secrete VEGF-C (42) and chemotact up a VEGF-C gradient (43) and may thus help direct LEC migration as well. We found that macrophage numbers

were much higher during regeneration (P=0.001) and peaked during LEC migration and organization at days 17-25 (P=0.058), hinting that macrophages may contribute to pre-lymphatic fluid channeling, a role already demonstrated in blood angiogenesis (44) and consistent with recent findings that macrophages are necessary in inflammation-induced corneal lymphangiogenesis (15). Total immune cell numbers peaked at day 3 (P<0.001)(Fig. 4). These early infiltrating immune cells at day 3 were typically neutrophils, as evidenced by polymorphonuclear Giemsa staining (data not shown). Very few Langerhans dendritic cells, normally present in the epidermis, were seen in the regenerating region until day 17 or 25, presumably when the regenerated epidermis is sufficiently integrated (P=0.028). Due to intense immune cell infiltration during inflammation and in the wound healing response, exact roles for immune cells were difficult to discern, however, the correlation of macrophage infiltration with lymphangiogenesis at later times supports the prospective role of macrophages in pre-lymphatic tunneling.

CONCLUSIONS

This study of lymphangiogenesis in regenerating skin provides new insight into adult lymphatic regeneration in a physiologically relevant environment and correlates potential contributing factors, such as MMPs and immune cells, to this process. We showed that migrating LECs populate the regenerating region in the direction of interstitial fluid flow, and then grow together in a vasculogenesis-like fashion to form a new interconnected network of lymphatic vessels. Also, we demonstrated that interstitial flow is necessary for the organization of LECs into a functional network while MMP-9 was not. Among the factors examined, the timing of MMP-2 and macrophages were more closely correlated to the late infiltration of LECs in the regenerating region, while basement membrane begins to develop only after the lymphatic structures have organized into functional vessels.

ACKNOWLEDGEMENTS

The authors are grateful to Dr. Hugo Schmökel, Veronique Garea, Sai T. Reddy, and Jeffrey Blatnik for invaluable assistance with the animals and Miriella Pasquier for sectioning and other assistance. The authors thank the NIH (RO1-HL075217-01), NSF (BES-0134551), and The Swiss National Science Foundation for funding.

REFERENCES

1. Achen, M.G., McColl, B.K., and Stacker, S.A. 2005. Focus on lymphangiogenesis in tumor metastasis. *Cancer Cell* 7:121-127.
2. Oliver, G., and Alitalo, K. 2005. THE LYMPHATIC VASCULATURE: Recent Progress and Paradigms. *Annu Rev Cell Dev Biol* 21:457-483.
3. Wigle, J.T., and Oliver, G. 1999. Prox1 function is required for the development of the murine lymphatic system. *Cell* 98:769-778.
4. Yuan, L., Moyon, D., Pardanaud, L., Breant, C., Karkkainen, M.J., Alitalo, K., and Eichmann, A. 2002. Abnormal lymphatic vessel development in neuropilin 2 mutant mice. *Development* 129:4797-4806.
5. Schacht, V., Ramirez, M.I., Hong, Y.K., Hirakawa, S., Feng, D., Harvey, N., Williams, M., Dvorak, A.M., Dvorak, H.F., Oliver, G., et al. 2003. T1alpha/podoplanin deficiency disrupts normal lymphatic vasculature formation and causes lymphedema. *Embo J* 22:3546-3556.
6. Kukk, E., Lymboussaki, A., Taira, S., Kaipainen, A., Jeltsch, M., Joukov, V., and Alitalo, K. 1996. VEGF-C receptor binding and pattern of expression with VEGFR-3 suggests a role in lymphatic vascular development. *Development* 122:3829-3837.
7. Jeltsch, M., Kaipainen, A., Joukov, V., Meng, X., Lakso, M., Rauvala, H., Swartz, M., Fukumura, D., Jain, R.K., and Alitalo, K. 1997. Hyperplasia of lymphatic vessels in VEGF-C transgenic mice. *Science* 276:1423-1425.
8. Joukov, V., Pajusola, K., Kaipainen, A., Chilov, D., Lahtinen, I., Kukk, E., Saksela, O., Kalkkinen, N., and Alitalo, K. 1996. A novel vascular endothelial growth factor, VEGF-C, is a ligand for the Flt4 (VEGFR-3) and KDR (VEGFR-2) receptor tyrosine kinases. *Embo J* 15:290-298.
9. Oh, S.J., Jeltsch, M.M., Birkenhager, R., McCarthy, J.E., Weich, H.A., Christ, B., Alitalo, K., and Wilting, J. 1997. VEGF and VEGF-C: specific induction of angiogenesis and lymphangiogenesis in the differentiated avian chorioallantoic membrane. *Dev Biol* 188:96-109.
10. Achen, M.G., Jeltsch, M., Kukk, E., Makinen, T., Vitali, A., Wilks, A.F., Alitalo, K., and Stacker, S.A. 1998. Vascular endothelial growth factor D (VEGF-D) is a ligand for the tyrosine kinases VEGF receptor 2 (Flk1) and VEGF receptor 3 (Flt4). *Proc Natl Acad Sci U S A* 95:548-553.
11. Pytowski, B., Goldman, J., Persaud, K., Wu, Y., Witte, L., Hicklin, D.J., Skobe, M., Boardman, K.C., and Swartz, M.A. 2005. Complete and specific inhibition of adult lymphatic regeneration by a novel VEGFR-3 neutralizing antibody. *J Natl Cancer Inst* 97:14-21.
12. Tammela, T., Saaristo, A., Lohela, M., Morisada, T., Tornberg, J., Norrmen, C., Oike, Y., Pajusola, K., Thurston, G., Suda, T., et al. 2005. Angiopoietin-1 promotes lymphatic sprouting and hyperplasia. *Blood* 105:4642-4648.
13. Gale, N.W., Thurston, G., Hackett, S.F., Renard, R., Wang, Q., McClain, J., Martin, C., Witte, C., Witte, M.H., Jackson, D., et al. 2002. Angiopoietin-2 is required for postnatal angiogenesis and lymphatic patterning, and only the latter role is rescued by Angiopoietin-1. *Dev Cell* 3:411-423.
14. Cao, Y., Linden, P., Farnebo, J., Cao, R., Eriksson, A., Kumar, V., Qi, J.H., Claesson-Welsh, L., and Alitalo, K. 1998. Vascular endothelial growth factor C induces angiogenesis in vivo. *Proc Natl Acad Sci U S A* 95:14389-14394.
15. Maruyama, K., Ii, M., Cursiefen, C., Jackson, D.G., Keino, H., Tomita, M., Van Rooijen, N., Takenaka, H., D'Amore, P.A., Stein-Streilein, J., et al. 2005.

Inflammation-induced lymphangiogenesis in the cornea arises from CD11b-positive macrophages. *J Clin Invest* 115:2363-2372.
16. Swartz, M.A., and Boardman, K.C., Jr. 2002. The role of interstitial stress in lymphatic function and lymphangiogenesis. *Ann N Y Acad Sci* 979:197-210; discussion 229-134.
17. Boardman, K.C., and Swartz, M.A. 2003. Interstitial flow as a guide for lymphangiogenesis. *Circ Res* 92:801-808.
18. Goldman, J., Le, T.X., Skobe, M., and Swartz, M.A. 2005. Overexpression of VEGF-C causes transient lymphatic hyperplasia but not increased lymphangiogenesis in regenerating skin. *Circ Res* 96:1193-1199.
19. Swartz, M.A., Berk, D.A., and Jain, R.K. 1996. Transport in lymphatic capillaries. I. Macroscopic measurements using residence time distribution theory. *Am J Physiol* 270:H324-329.
20. Segev, A., Nili, N., and Strauss, B.H. 2004. The role of perlecan in arterial injury and angiogenesis. *Cardiovasc Res* 63:603-610.
21. Whitelock, J.M., Graham, L.D., Melrose, J., Murdoch, A.D., Iozzo, R.V., and Underwood, P.A. 1999. Human perlecan immunopurified from different endothelial cell sources has different adhesive properties for vascular cells. *Matrix Biol* 18:163-178.
22. Jiang, X., and Couchman, J.R. 2003. Perlecan and tumor angiogenesis. *J Histochem Cytochem* 51:1393-1410.
23. Sephel, G.C., Kennedy, R., and Kudravi, S. 1996. Expression of capillary basement membrane components during sequential phases of wound angiogenesis. *Matrix Biol* 15:263-279.
24. Kinsella, M.G., Tran, P.K., Weiser-Evans, M.C., Reidy, M., Majack, R.A., and Wight, T.N. 2003. Changes in perlecan expression during vascular injury: role in the inhibition of smooth muscle cell proliferation in the late lesion. *Arterioscler Thromb Vasc Biol* 23:608-614.
25. Swartz, M.A. 2001. The physiology of the lymphatic system. *Adv Drug Deliv Rev* 50:3-20.
26. Carmeliet, P. 2005. VEGF as a key mediator of angiogenesis in cancer. *Oncology* 69:4-10.
27. Madlener, M., Parks, W.C., and Werner, S. 1998. Matrix metalloproteinases (MMPs) and their physiological inhibitors (TIMPs) are differentially expressed during excisional skin wound repair. *Exp Cell Res* 242:201-210.
28. Lijnen, H.R., Lupu, F., Moons, L., Carmeliet, P., Goulding, D., and Collen, D. 1999. Temporal and topographic matrix metalloproteinase expression after vascular injury in mice. *Thromb Haemost* 81:799-807.
29. Balbin, M., Fueyo, A., Knauper, V., Pendas, A.M., Lopez, J.M., Jimenez, M.G., Murphy, G., and Lopez-Otin, C. 1998. Collagenase 2 (MMP-8) expression in murine tissue-remodeling processes. Analysis of its potential role in postpartum involution of the uterus. *J Biol Chem* 273:23959-23968.
30. Stamenkovic, I. 2003. Extracellular matrix remodelling: the role of matrix metalloproteinases. *J Pathol* 200:448-464.
31. Gillard, J.A., Reed, M.W., Buttle, D., Cross, S.S., and Brown, N.J. 2004. Matrix metalloproteinase activity and immunohistochemical profile of matrix metalloproteinase-2 and -9 and tissue inhibitor of metalloproteinase-1 during human dermal wound healing. *Wound Repair Regen* 12:295-304.

32. Haas, T.L., Davis, S.J., and Madri, J.A. 1998. Three-dimensional type I collagen lattices induce coordinate expression of matrix metalloproteinases MT1-MMP and MMP-2 in microvascular endothelial cells. *J Biol Chem* 273:3604-3610.
33. Jadhav, U., Chigurupati, S., Lakka, S.S., and Mohanam, S. 2004. Inhibition of matrix metalloproteinase-9 reduces in vitro invasion and angiogenesis in human microvascular endothelial cells. *Int J Oncol* 25:1407-1414.
34. Nakamura, E.S., Koizumi, K., Kobayashi, M., and Saiki, I. 2004. Inhibition of lymphangiogenesis-related properties of murine lymphatic endothelial cells and lymph node metastasis of lung cancer by the matrix metalloproteinase inhibitor MMI270. *Cancer Sci* 95:25-31.
35. Lambert, V., Wielockx, B., Munaut, C., Galopin, C., Jost, M., Itoh, T., Werb, Z., Baker, A., Libert, C., Krell, H.W., et al. 2003. MMP-2 and MMP-9 synergize in promoting choroidal neovascularization. *Faseb J* 17:2290-2292.
36. Zijlstra, A., Aimes, R.T., Zhu, D., Regazzoni, K., Kupriyanova, T., Seandel, M., Deryugina, E.I., and Quigley, J.P. 2004. Collagenolysis-dependent angiogenesis mediated by matrix metalloproteinase-13 (collagenase-3). *J Biol Chem* 279:27633-27645.
37. Moldovan, N.I., Goldschmidt-Clermont, P.J., Parker-Thornburg, J., Shapiro, S.D., and Kolattukudy, P.E. 2000. Contribution of monocytes/macrophages to compensatory neovascularization - The drilling of metalloelastase-positive tunnels in ischemic myocardium. *Circulation Research* 87:378-384.
38. Nwomeh, B.C., Liang, H.X., Cohen, I.K., and Yager, D.R. 1999. MMP-8 is the predominant collagenase in healing wounds and nonhealing ulcers. *J Surg Res* 81:189-195.
39. Masson, V., de la Ballina, L.R., Munaut, C., Wielockx, B., Jost, M., Maillard, C., Blacher, S., Bajou, K., Itoh, T., Itohara, S., et al. 2005. Contribution of host MMP-2 and MMP-9 to promote tumor vascularization and invasion of malignant keratinocytes. *Faseb J* 19:234-236.
40. Ohno-Matsui, K., Uetama, T., Yoshida, T., Hayano, M., Itoh, T., Morita, I., and Mochizuki, M. 2003. Reduced retinal angiogenesis in MMP-2-deficient mice. *Invest Ophthalmol Vis Sci* 44:5370-5375.
41. Salo, T., Makela, M., Kylmaniemi, M., Autio-Harmainen, H., and Larjava, H. 1994. Expression of matrix metalloproteinase-2 and -9 during early human wound healing. *Lab Invest* 70:176-182.
42. Schoppmann, S.F., Birner, P., Stockl, J., Kalt, R., Ullrich, R., Caucig, C., Kriehuber, E., Nagy, K., Alitalo, K., and Kerjaschki, D. 2002. Tumor-associated macrophages express lymphatic endothelial growth factors and are related to peritumoral lymphangiogenesis. *Am J Pathol* 161:947-956.
43. Skobe, M., Hamberg, L.M., Hawighorst, T., Schirner, M., Wolf, G.L., Alitalo, K., and Detmar, M. 2001. Concurrent induction of lymphangiogenesis, angiogenesis, and macrophage recruitment by vascular endothelial growth factor-C in melanoma. *Am J Pathol* 159:893-903.
44. Moldovan, N.I. 2002. Role of monocytes and macrophages in adult angiogenesis: a light at the tunnel's end. *J Hematother Stem Cell Res* 11:179-194.

FIGURE LEGENDS

Fig. 1. Interstitial flow and the mouse tail model of skin regeneration. (*A*) In the circumferential model, lymph flow from distal lymphatics (that is traveling in the proximal direction) must move interstitially through the collagen implant in order to continue its flow in the proximal lymphatic capillaries. Functional and organized lymphatic capillaries are seen by microlymphangiography at day 60. (*B*) In the square model, lymph flow is circumvented around the implant in pre-existing lymphatic capillaries, and the entire lymphatic circuit is uninterrupted. Lymph does not become interstitial fluid in the implant as in the circumferential model, and thus interstitial flow through this square implant is much less than that through the circumferential implant. In this shunted flow model, LECs do not organize into a functional network (as evidenced by microlymphangiography), despite the otherwise normal skin regeneration. In all microlymphangiography images, green indicates the lymph fluid tracer (fluorescein-dextran) and thus identifies functional lymphatics and interstitial flow of post-lymph through the regenerating regions. Bar = 1 mm.

Fig. 2. Lymphatic regeneration occurs in the direction of interstitial flow as shown by maximum projections of confocal scans. (*A*) At 7 days, the regenerating region (marked by yellow dashes) is free of LECs, but blood vessels (red) appear to sprout from deeper vessels (open arrows). (*B*) At day 10, very few LECs (arrowheads) are seen, while blood vessel sprouting is present in all directions. (*C*) At day 17, LECs (green) are seen in higher numbers in the distal end of the regenerating region, and more organization (arrows) is also seen in the distal end. LECs in the proximal half mostly remain as single cells. Blood vessels are present throughout the regenerating region. (*D*) At day 60, LECs are present throughout the regenerating region and organized into an interconnected network, similar to that seen in native skin (white arrow). Note the overall contraction of the regenerating region over time. Bar = 300 μm. (*E*) Quantification of total LECs in the regenerating region confirms that LEC infiltration begins around day 10, is drastically increased at day 17, and is mostly complete by day 25. (*F*) Relative distribution of LECs in the distal vs. proximal halves of the regenerating region verifies qualitative observations that migration is primarily occurring from the distal end. Through day 40, the relative number of LECs in the distal half is consistently and significantly greater than that in the proximal half. By day 60, LEC distribution is normalized. (* $P<0.05$)

Fig. 3. Lymphangiogenesis as a process of cell migration and subsequent organization, rather than sprouting, with basement membrane developing after vessels become functional. Shown are maximum projections of confocal scans. (*A*) At day 10, the regenerating region is mostly free of LECs (green) with only a few LECs (arrows heads) present near the distal end. The basement membrane proteoglycan perlecan (red) is readily detected on blood vessels. (*B*) At day 17, LECs are present throughout the entire regenerating region and organized into discrete and separate multi-cellular structures. Perlecan expression is not seen to be co-localized with any of these structures, indicating that basement membrane is absent in these primitive structures. (*C*) At day 25, lymphatic organization is extensive and nearly complete. Perlecan is detected only on lymphatic vessels in the distal half of the regenerating region (arrows). (*D*) By day 60, a discontinuous perlecan staining pattern is present on nearly all lymphatic vessels (arrows), although staining is visibly stronger in the distal half. (*E*) Lymphatic capillaries in native skin show strong perlecan staining. Bar=50 μm.

Fig. 4. Comparison of the relative temporal expression patterns of VEGF-A and VEGF-C, MMPs, and immune cells during regeneration. VEGF-A expression was highest at the initiation of angiogenesis (days 5). VEGF-C expression was highest during the initiation of lymphangiogenesis (days 5-10) and was reduced during the organization phase (days 17+). Expression of MMP-2 peaked during lymphangiogenesis. MMP-8 expression was very low throughout regeneration. MMP-9 was high at early times, but decreased after day 7, while MMP-13 expression was highest before day 10, just preceding macrophage infiltration. Early infiltration of CD45+ immune cells at day 3 primarily reflects neutrophils. Macrophages (F4/80+) were highest after day 10, correlating with the onset of LEC infiltration. Langerhans dendritic cells (langerin+) did not repopulate the region until day 17 and later, when LECs were present and undergoing vessel organization. (* $P<0.05$; over control indicates significant change in regeneration, over bracket indicates temporal significance during regeneration)

Fig. 5. No differences were seen in lymphatic regeneration in MMP-9 null mice *vs.* matched wild type controls. (*A*) The regenerated blood (red) and lymphatic (green) vessels in MMP-9 null mice were morphologically indistinguishable to those in control mice at day 17 and day 60. Bar=150 μm. (*B*) The number of LECs counted in the regenerating region at day 17 was not significantly different between the mouse strains ($P=0.48$).

This page is intentionally left blank.

Figure 1

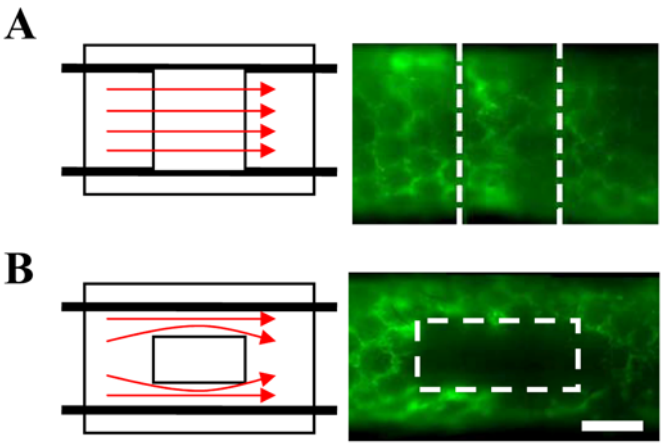

This page is intentionally left blank.

Figure 2

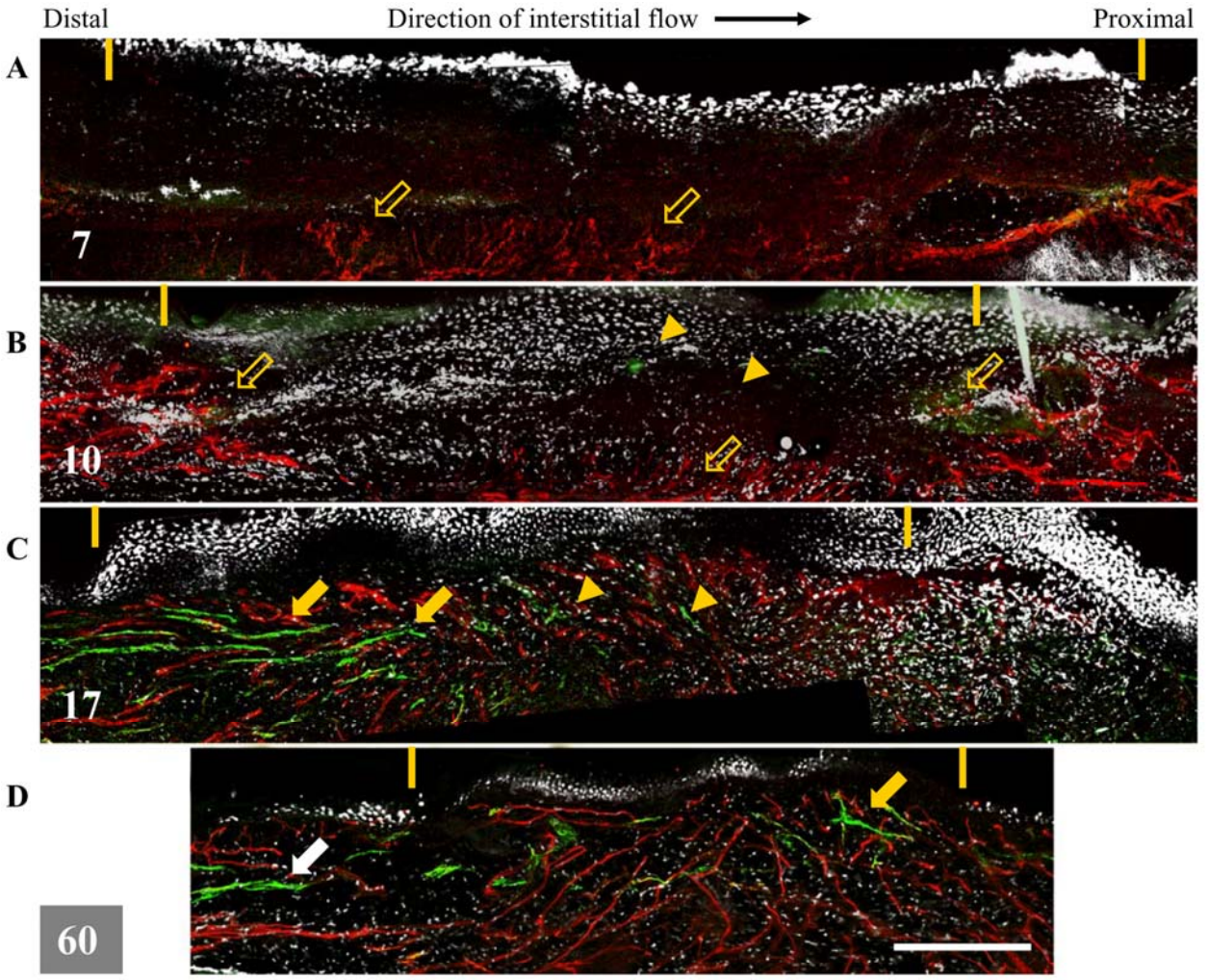
Distal
Direction of interstitial flow
Proximal
A
7
B
10
C
17
D
60

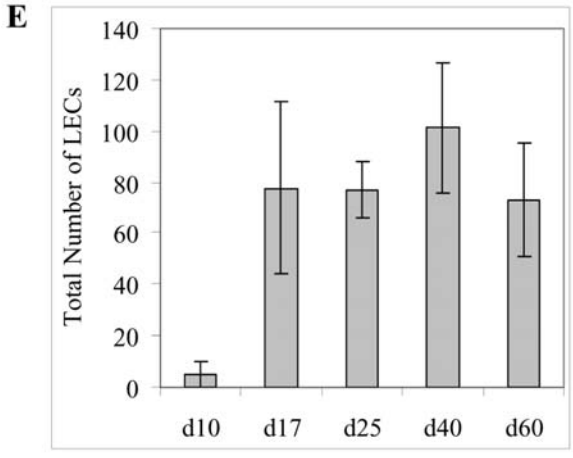
E
Total Number of LECs
140
120
100
80
60
40
20
0
d10
d17
d25
d40
d60

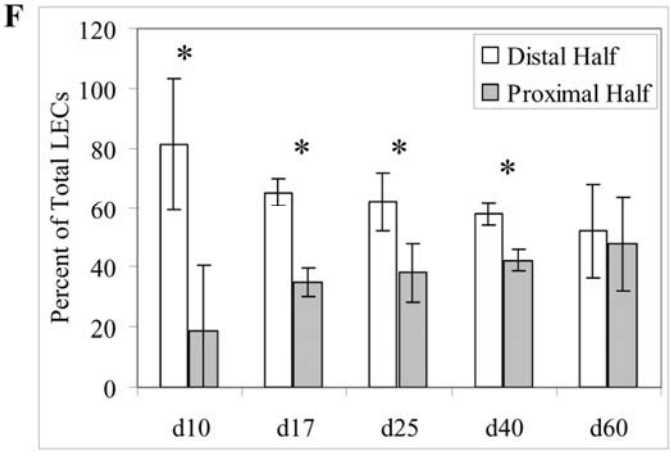
F
Percent of Total LECs
120
100
80
60
40
20
0
Distal Half
Proximal Half
*
*
*
*
d10
d17
d25
d40
d60

This page is intentionally left blank.

Figure 3

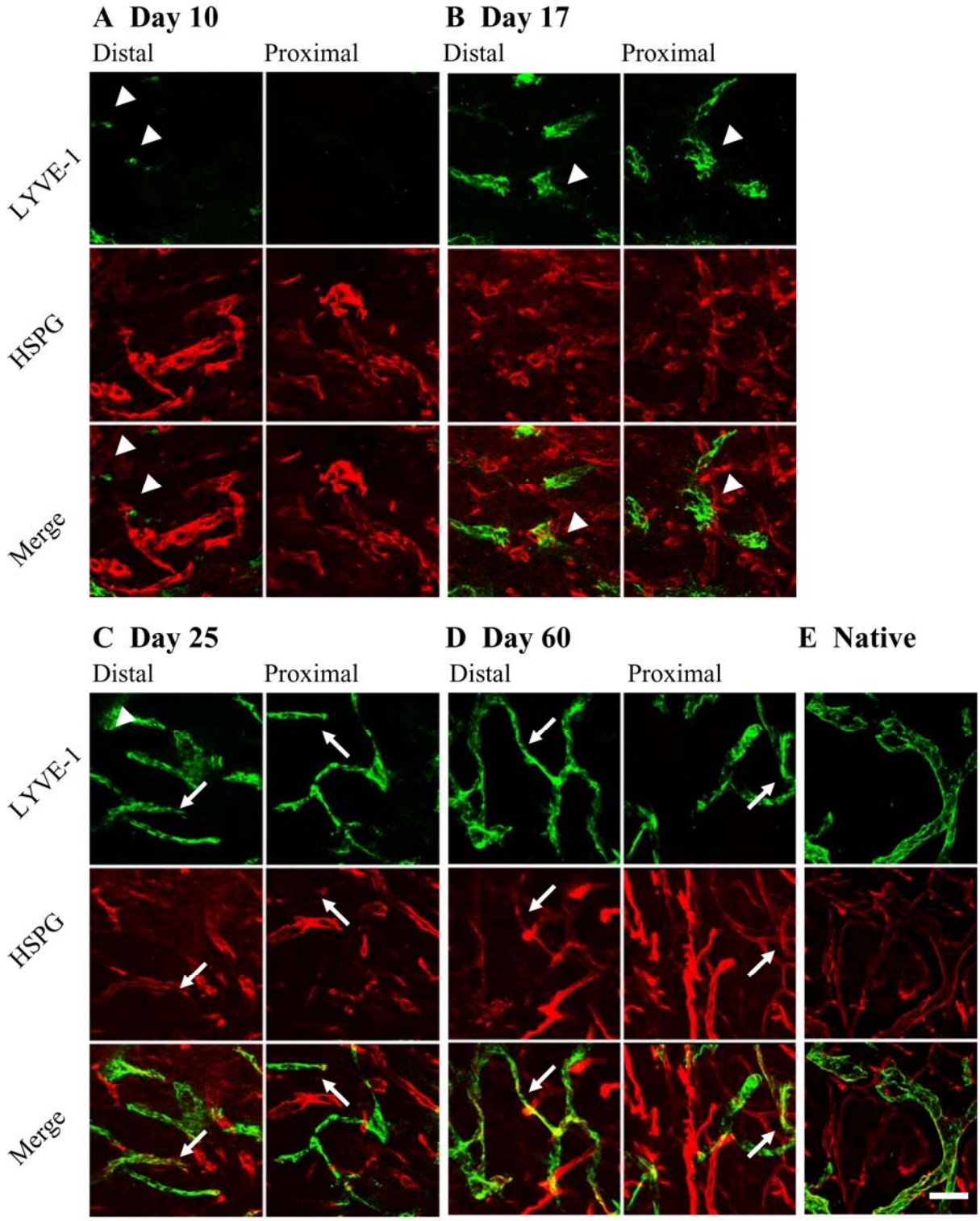
A Day 10
B Day 17
C Day 25
D Day 60
E Native
Distal
Proximal
LYVE-1
HSPG
Merge

This page is intentionally left blank.

Figure 4

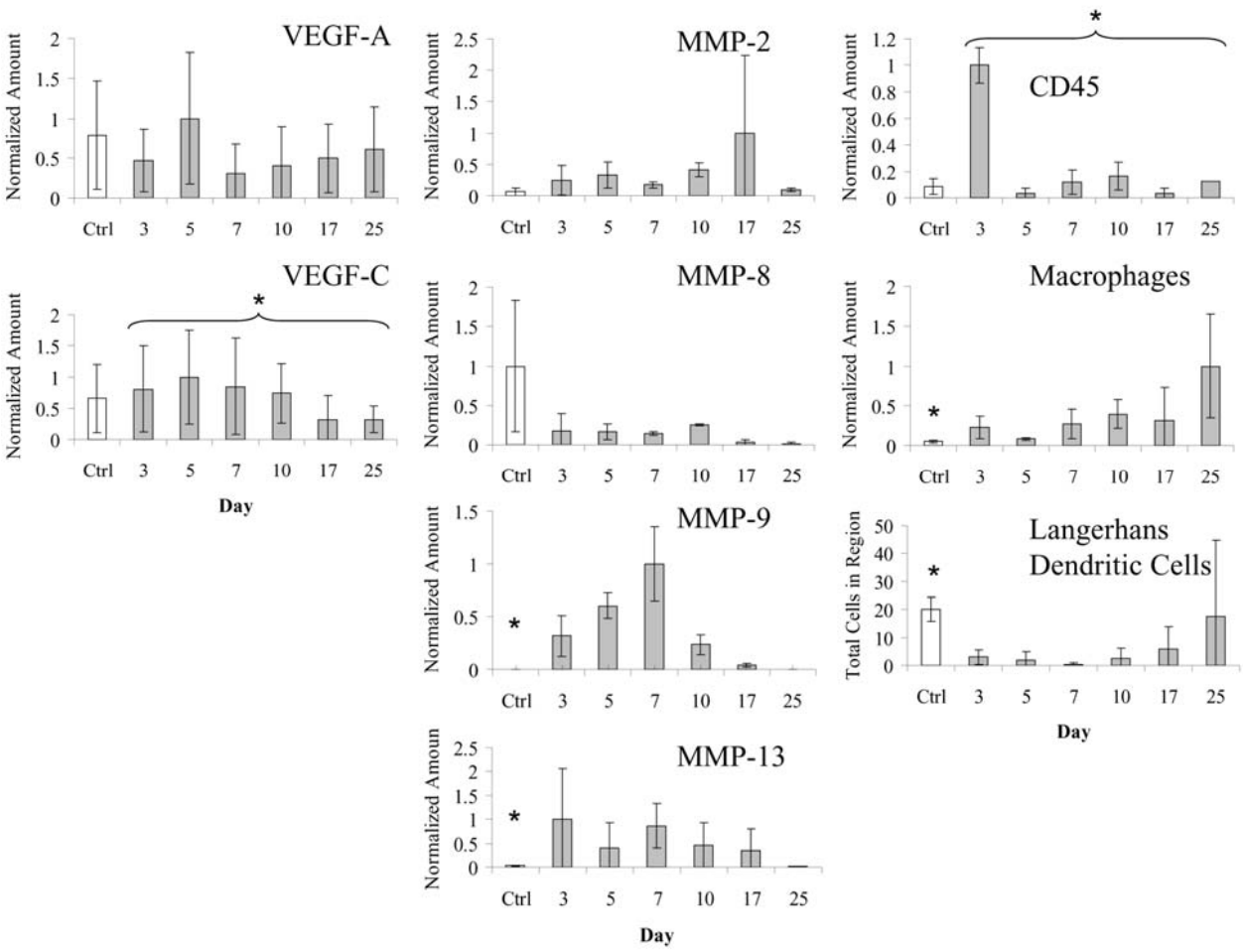
VEGF-A
MMP-2
CD45
VEGF-C
MMP-8
Macrophages
MMP-9
Langerhans
Dendritic Cells
MMP-13
Normalized Amount
Total Cells in Region
Ctrl 3 5 7 10 17 25
Day
*

This page is intentionally left blank.

Figure 5

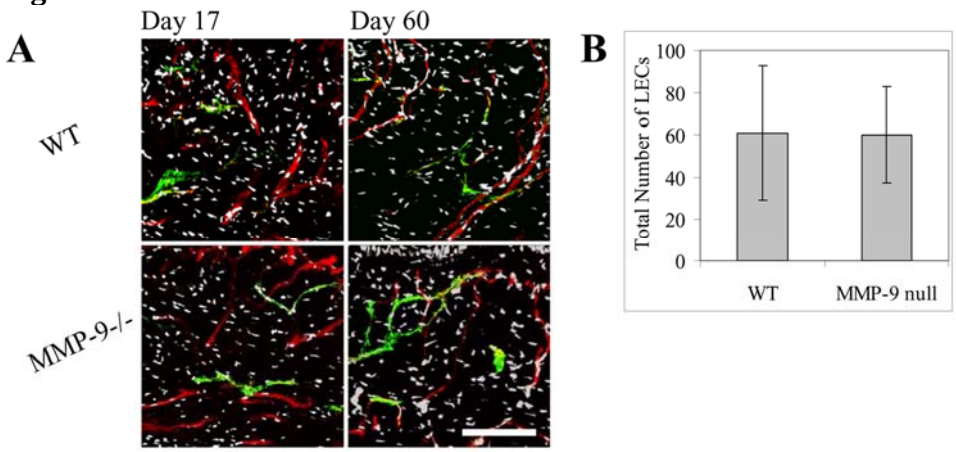
A
Day 17
Day 60
WT
MMP-9-/-
B
Total Number of LECs
100
80
60
40
20
0
WT
MMP-9 null

This page is intentionally left blank.

CHAPTER 4:
ORIGINAL MANUSCRIPT 3

Cooperative and redundant roles of VEGFR-2 and VEGFR-3 signaling in adult lymphangiogenesis

Jeremy Goldman[1]*, Joseph M. Rutkowski[1]*, Jacqueline D. Shields[1]*, Miriella C. Pasquier[1], Yingjie Cui[1], Hugo G. Schmökel[1], Stephen Willey[2], Daniel J. Hicklin[3], Bronislaw Pytowski[2], and Melody A. Swartz[1]

1: Institute of Bioengineering, École Polytechnique Fédérale de Lausanne (EPFL), Switzerland
2: Tumor Biology ImClone Systems, New York, NY
3: Experimental Therapeutics, ImClone Systems, New York, NY
* These authors contributed equal work

Submitted 15 June 2006; accepted in final form 9 November 2006

The FASEB Journal

2007;21:1003-1012. First published January 8, 2007.

ABSTRACT

Activation of vascular endothelial growth factor receptor -3 (VEGFR-3) by VEGF-C initiates lymphangiogenesis by promoting lymphatic proliferation and migration. However, it is unclear whether VEGFR-3 signaling is required beyond these initial stages, namely during the organization of new lymphatic endothelial cells (LECs) into functional capillaries. Furthermore, the role of VEGFR-2, which is also expressed on LECs and binds VEGF-C, is unclear. We addressed these questions by selectively neutralizing VEGFR-3 and/or VEGFR-2 for various time periods in an adult model of lymphangiogenesis in regenerating skin. While blocking either VEGFR-2 or VEGFR-3 with specific antagonist mAbs (DC101 and mF4-31C1, respectively) prior to lymphatic migration prevented lymphangiogenesis, blocking VEGFR-3 subsequent to migration did not affect organization into functional capillaries, and VEGFR-2 blocking had only a small hindrance on organization. These findings were confirmed *in vitro* using human LECs and anti-human antagonist mAbs (IMC-1121a and hF4-3C5): both VEGFR-2 and -3 signaling were required for migration and proliferation, but tubulogenesis in 3D cultures was unaffected by VEGFR-3 blocking and partially hindered by VEGFR-2 blocking. Furthermore, both *in vitro* and *in vivo*, while VEGFR-3 blocking had no effect on LEC organization, co-neutralization of VEGFR-2 and VEGFR-3 completely prevented lymphatic organization. Our findings demonstrate that cooperative signaling of VEGFR-2 and -3 is necessary for lymphatic migration and proliferation, but VEGFR-3 is redundant with VEGFR-2 for LEC organization into functional capillaries.

Key words: VEGF-C, mouse, *in vitro*, wound healing, vasculogenesis

INTRODUCTION

Vascular endothelial growth factor (VEGF) receptor -3 (VEGFR-3) activation by its ligands VEGF-C and VEGF-D is necessary for developmental and adult lymphangiogenesis (1-4). In tumor models, neutralization of VEGF-C with soluble VEGFR-3 reduced lymphangiogenesis and lymphatic function at the periphery of VEGF-C–overexpressing tumors (5). Signaling through VEGFR-3 has therefore been implicated in tumor lymph node metastases (6-8). Indeed, this importance has been demonstrated through the inhibition of VEGFR-3 that prevented prostate and melanoma (9) and breast cancer metastases (10) by suppressing tumor-associated lymphangiogenesis.

However, lymphangiogenesis is a complex process comprised of multiple events including lymphatic endothelial cell (LEC) proliferation, migration, organization, and vessel maturation. Although VEGFR-3 signaling has been shown to be unnecessary for lymphatic maintenance and function of existing lymphatic vessels (5), its roles in each of the various steps of lymphatic development remain unclear. Proteolytically processed (mature) VEGF-C and -D can also bind to VEGFR-2 (11-13), and the activation of VEGFR-2 can also induce or guide lymphangiogenesis (14, 15). Furthermore, it has been reported that VEGFR-2 can form heterodimers with VEGFR-3 (16, 17), but it is unclear whether heterodimer phosphorylation signals different functional responses than homodimer phosphorylation. It is also not known how these receptors interact from a functional perspective and how their different signaling patterns may affect different stages of lymphatic development.

Here we explore the individual and combined roles of VEGFR-2 and VEGFR-3 signaling in three distinct components of adult lymphangiogenesis – LEC proliferation, migration, and vessel organization – using complementary *in vivo* and *in vitro* models. We use a model of adult skin regeneration in the mouse tail that we developed previously to investigate the role of interstitial flow in the organization of lymphangiogenesis during dermal wound healing. In that study, we showed that lymphangiogenesis proceeds by unidirectional migration of LECs in the direction of interstitial fluid flow along fluid channels, followed by subsequent organization into a functional network of lymphatic vessels in a manner reminiscent of vasculogenesis (18, 19). Thus, in this model, adult lymphangiogenesis can be clearly divided temporally into three discrete phases – migration (determined by the distal-to-proximal distribution of cells in the regenerating region), proliferation (determined by total LEC number), and capillary organization (determined by immunostaining thick sections and via

microlymphangiography) - allowing us to investigate the importance of VEGFR-2 and VEGFR-3 signaling at each phase.

Using this model, we previously demonstrated that endogenous VEGF-C expression is increased during lymphatic migration and proliferation but decreased during later stages of lymphatic organization (18, 19), and that delivery of exogenous VEGF-C induced lymphatic hyperplasia without improving lymphatic organization or function beyond control levels (20). Additionally, in this same model, blockage of VEGFR-3 with the mAb mF4-31C1 prevented regeneration of functional lymphatic vessels in the mouse skin without affecting pre-existing vessels (21). These findings suggest that while VEGF-C/VEGFR-3 signaling is necessary for lymphangiogenesis, it may not serve an important role in the functional or organizational evolution of lymphangiogenesis. Based on these results, we hypothesized that VEGFR-2 and VEGFR-3 signaling are important primarily during the early stages of lymphangiogenesis, which require LEC migration and proliferation, but are less important during the subsequent organization of LECs into functional lymphatic capillaries. To this end, antagonist mAbs against mouse VEGFR-2 and -3 were delivered at different stages of physiological lymphatic regeneration in adult mouse skin to determine the specific roles of these receptors in lymphangiogenesis. To support our *in vivo* results we also examined the importance of these receptors using *in vitro* models of human LEC migration, proliferation, and 3-D tubulogenesis in the presence or absence of antagonist mAbs to human VEGFR-2 and VEGFR-3.

MATERIALS AND METHODS

Neutralizing Antibodies

All antagonist antibodies were provided by ImClone Systems, NY, NY. For *in vivo* studies, 0.625 mg of anti-mouse VEGFR-2 (DC101) (22) and/or anti-mouse VEGFR-3 (mF4-31C1) (21) were injected intraperitoneally every two days. For *in vitro* studies, anti-human VEGFR-2 (IMC-1121a, 20 μg/mL) and anti-human VEGFR-3 (hF4-3C5, 10 μg/mL) (23) were used.

In vivo studies

Lymphangiogenesis model

For all studies 6–8 week old, female BALB/c mice (Charles River Laboratories, France) were used; at least three mice were used for each condition at each time point examined. Mice were anesthetized with an intraperitoneal injection of ketamine (65 mg/kg), xylazine (13

mg/kg), and acepromazine (2 mg/kg). An analgesic, butorphanol (0.05 mg/kg), was administered subcutaneously twice daily for three days following the procedure. All protocols were approved by the Veterinary Authorities of the Canton Vaud according to Swiss law (protocol number #1687).

The regenerating region of skin was created as previously described (18). Briefly, a 2-mm wide circumferential band of dermal tissue (in which the lymphatic network in the tail skin is contained) was excised midway up the tail, leaving the underlying bone, muscle, major blood vessels, and tendons intact. The area was then covered with a close–fitting, gas permeable silicone sleeve and filled with type I rat tail collagen (BD Pharmingen, San Diego, CA). The collagen scaffold provides a pre-existing matrix in which epithelial and subepithelial tissues readily regenerate. LECs later observed within this region were thus the result of de novo cell migration, proliferation, and organization.

The neutralizing antibodies were then administered as described above for durations that varied by experimental group (Table 1).

Detection of functional lymphatics via microlymphangiography

To visualize lymph flow patterns *in situ*, a 2 mg/mL solution of fluorescein-conjugated dextran of 70kDa (Molecular Probes, Carlsbad, CA) was injected intradermally into the tail tip at a constant pressure where it was taken up and transported by the lymphatics in the proximal direction, revealing functional lymphatic vessels and fluid channels. Fluorescence images were captured with a Zeiss MRm camera on a Zeiss Axiovert 200M fluorescence microscope.

Immunofluorescence and immunohistochemistry

Tail specimens were cut into either 12 or 60 μm-thick longitudinal cryosections and immunostained. To detect LECs, a rabbit polyclonal antibody against the lymphatic-specific hyaluronan receptor LYVE-1 (Upstate, Charlottesville, VA) was used along with an Alexa Fluor 488 conjugated goat anti-rabbit secondary antibody (Molecular Probes). To detect blood endothelial cells, a rat polyclonal CD31 antibody (BD Pharmingen) was used along with an Alexa Fluor 546 conjugated goat anti-rat secondary antibody (Molecular Probes). Cell nuclei were labeled with DAPI (Vector Labs, Burlingame, CA). Thin-section images of the regenerating region were imaged (as above) and assembled into complete montages in Photoshop (Adobe Systems, San Jose, CA). Thick sections were imaged with confocal microscopy on a Zeiss LSM 510 META confocal microscope; maximum projections are

presented. LECs were defined as cells with a nucleus completely surrounded by LYVE-1 labeling. After defining the borders of the regenerating region, the number of LECs within each half were counted and summed across three random 12 μm sections from each animal.

In vitro studies

Lymphatic endothelial cell (LEC) culture

Human dermal LECs were isolated from neonatal foreskins as previously described (24) and maintained in EBM basal media (Cambrex, Walkersville, MD) supplemented with 20% FBS, 1% penicillin-streptomycin-amphotericin B (both GIBCO, Carlsbad, California), 1 μg/mL hydrocortisone, and 50 μmol/l DBcAMP (both Sigma, St. Louis, MO) in collagen type I coated flasks (50 μg/mL). They were utilized until passage 8.

In vitro proliferation assay

The effects of VEGFR-2 and VEGFR-3 signaling on LEC proliferation were evaluated using a colorimetric BrdU Kit (Calbiochem, San Diego, CA). LECs were serum-starved for 2 h, seeded into a collagen-coated 96 well plate ($3x10^4$ cells/well), and allowed to adhere for an additional 2 h. 100 μl full medium supplemented with 100 ng/mL recombinant human wildtype VEGF-C (rhVEGF-C, 2179-VC-025 , R & D Systems, Minneapolis, MN) along with either (i) 10 μg/mL Hf4-3C5, (ii) 20 μg/mL IMC-1121a, (iii) a combination of both antibodies, or (iv) no antibodies. Proliferation (proportional to BrdU incorporation) was measured after 24, 48 and 72 hours of receptor blockage. Samples were fixed and permeabilized, then BrdU incorporation was detected according to the manufacturer's instructions.

In vitro migration assay

Polycarbonate transwell inserts (8 μm pore, Millipore, Billerica, MA) were coated with 50 μg/mL type I collagen (BD Bioscience). LECs were seeded at a density of 10^5 cells per insert in basal growth medium. The lower chamber consisted of either basal media alone or full growth media supplemented with 100 ng/mL rhVEGF-C and either (i) 10 μg/mL Hf4-3C5, (ii) 20 μg/mL IMC-1121a, (iii) a combination of both antibodies, or (iv) no antibodies. Appropriate neutralizing antibodies were also added to the top chamber for the duration of the experiment. Chambers were incubated at 37ºC for 24 hours before the samples were washed with PBS and fixed in methanol at 4 ºC. Non-migrated cells were removed with a cotton

swab. The membranes were then removed and mounted with Vectashield containing DAPI (Vector). Samples were visualized with a 40x objective and the numbers of migrated cells within 8 random fields of view were counted. Migration per insert was then calculated and expressed as fold increase over control.

***In vitro* tubulogenesis assay**

A gel suspension assay was used to assess LEC organization, independent of proliferation and migration, into capillary tubules within a 3D environment. LECs were seeded within Growth Factor Reduced Matrigel (BD Biosciences) at densities of either $0.5x10^6$ (low density) or $1.5x10^6$ cells per mL (high density). The solution was plated into 8-well coverslip chamberslides (Lab-TEK Nalge Nunc, Naperville,) and the gel was allowed to polymerize for 2 h before treatment. Gels were subsequently maintained at 37ºC/5% CO_2 in either basal media or full media supplemented with 100 ng/mL rhVEGF-C and either (i) 10 µg/mL hF4-3C5, (ii) 20 µg/mL IMC-1121a, (iii) a combination of both antibodies, or (iv) no antibodies. After 6 days, gels were fixed in 2% PFA and cell structures were visualized with Alexafluor 488-conjugated phalloidin (Molecular Probes) and counterstained with DAPI. Samples were visualized using confocal microscopy (as above). Tube length per unit area was calculated using Image J software (NIH, Bethesda, MD)

Immunoprecipitation and immunoblot for receptor phosphorylation

LECs were grown to 95% confluence in 10 cm culture dishes. Cells were washed in PBS and serum starved for 48 hours and then incubated in the presence of either 10 µg/mL hf4-3C5, 10 µg/mL IMC-1121a, a combination of both, or neither for 30 minutes. Samples were then treated with 100 ng/mL wildtype rhVEGF-C for 20 minutes, lysed with modified RIPA buffer supplemented with a protease inhibitor cocktail (Pierce, Rockford, IL; and 1% PMSF) and phosphatase inhibitor cocktails (Sigma). Cleared lysate supernatants were then incubated with either 2 µg/ml anti-human VEGFR-3 (sc-321, Santa Cruz) or 2 µg/ml anti-human VEGFR-2 (AF357, R & D Systems) and 30 µl Protein A/G agarose beads (Pierce) overnight at 4ºC. The pellets were then washed three times in inhibitor-supplemented lysis buffer, washed once in PBS, and boiled in laemmli sample buffer. Protein samples were then separated by SDS polyacrylamide gel electrophoresis, transferred onto nitrocellulose membrane, and phosphorylated VEGFR-2 or VEGFR-3 was detected with mouse anti-human PY20 (1.0 µg/mL, Upstate) and an HRP-conjugated secondary antibody (Amersham

Biosciences, Uppsala, Sweden). Total receptor was detected with either anti-VEGFR-3 (sc-321) or anti-VEGFR-2 (sc-6251, Santa Cruz).

Statistical methods

For determination of LEC numbers in the regenerating region, at least three sections were counted per specimen. Data is presented as mean ± one standard deviation. All *P* values were calculated using a two-sided Student's t-test.

RESULTS

Adult lymphatic regeneration without receptor neutralization

Immunostaining of control mouse 60 μm-thick cryosections from the mouse tail skin regeneration model (Fig. 1*A*) demonstrated that unorganized LECs began to migrate into and proliferate within the distal half of the regenerating region 10 days post surgery (Fig. 1*B*). At day 17, LECs were present in both distal and proximal halves but were largely unorganized. At day 60, LECs in the control mice were highly organized into lymphatic vessels, indicating a regenerated lymphatic capillary network. All LYVE-1 positive cells (and structures) were confirmed to be LECs in this model (Supplemental Fig. 1).

Microlymphangiography, in which a fluorescent tracer is injected intradermally into the tip of the tail and taken up by the functional distal lymphatics, confirmed that the newly formed functional lymphatic vessels in the regenerating region did not sprout from pre-existing vessels but instead organized after migration (Fig. 1*C*). At both days 10 and 17, prior to organization of LECs into regenerating lymphatic capillaries, upstream lymph collected at the distal boundary and slowly diffused across the regenerating region. At day 60, when LECs were organized into vessels, upstream lymph was transported through the region inside regenerated hexagonal lymphatic vessels.

Effects of VEGFR-3 neutralization on lymphatic regeneration *in vivo*

To determine the involvement of VEGFR-3 in different stages of lymphangiogenesis, VEGFR-3 was inhibited during different stages of lymphatic regeneration. Consistent with our previous observations (21), we found that inhibition of VEGFR-3 from day 0 to day 60 completely prevented lymphangiogenesis as demonstrated by both immunohistochemical and functional analyses (Fig. 1*D-E*). When VEGFR-3 blockade was removed subsequent to the initiation of lymphangiogenesis but prior to substantial lymphatic migration (days 10-60 of

regeneration), LECs failed to migrate into the regenerating region and no functional vessels were formed. This finding confirmed that VEGFR-3 signaling is necessary for LEC migration into regenerating tissue.

At day 17 of normal regeneration, we found large numbers of unorganized LEC clusters, but no tubular capillary-like structures (Fig. 1*F*); thus, we also inhibited VEGFR-3 from day 17 to day 60. Surprisingly, LEC clusters efficiently organized into functional vessels despite the absence of VEGFR-3 signaling and were indistinguishable from regenerated lymphatics in control mice (Fig. 1*D-E*). Thus, VEGFR-3 is crucial for the migration and colonization of the wound during regenerative lymphangiogenesis, but not for their organization into functional vessels.

LECs appear inside the regenerating region as a result of their proliferation, migration or both since the regenerating region is initially acellular. Furthermore, it has been established that LECs migrate and organize from the distal end to the proximal end in this model, consistent with the direction of fluid flow (18, 19). Thus, LECs found in the regenerating region result primarily from cell migration from the distal host dermis. The total number of LECs and their distal-to-proximal distribution in the regenerating region are indicative of the degree of LEC migration and proliferation, respectively, over a given period of time. In untreated mice, quantitative measurements of LECs (LYVE-1 labeled cells in thin cryosections) in the distal vs. proximal halves of the regenerating region confirmed their unidirectional migration, with cells initially entering the distal region at day 10 and gradually migrating until, by day 60, the LECs are uniformly distributed throughout the entire region (Fig. 1*F*, 1*G*). Blocking VEGFR-3 activation from day 10 to 60 or from day 17 to 60 significantly decreased the total number of LECs as compared to untreated controls (Fig. 1*F*). Blocking of VEGFR-3 also prevented LEC migration into the proximal portion of the regenerating region (Fig. 1*G*), resulting in the skewing of the LEC distribution towards the distal region. Specifically, we observed a significant difference between the percentage of LECs in the distal vs. proximal portions of the regenerating regions in mice treated with blocking mAbs to VEGFR-3 during days 10-60 and days 17-60. These distributions were remarkably similar to the distributions seen at days 10 and 17 in the wounds of control animals (Fig. 1*G*), lending further credence to arrested migration. Their overall numbers were similar to those when blocking was begun as well, attesting to arrested proliferation.

Blocking VEGFR-3 from day 17 to 60 prevented further LEC migration and proliferation in regenerating tissue, but did not hinder the organization of LECs into functional capillaries within the regenerating region. Therefore, these findings strongly

suggest that VEGFR-3 activation is critical for LEC migration and proliferation but not their functional organization into lymphatic vessels.

Effects of VEGFR-2 neutralization on adult lymphangiogenesis

The effects of blocking VEGFR-2 activation on lymphangiogenesis were similar to those resulting from blocking VEGFR-3 (Fig. 2*A*). First, VEGFR-2 blocking from day 0-60 completely blocked any lymphangiogenic response, consistent with other reports that VEGFR-2 is essential to lymphangiogenesis (14, 25, 26). VEGFR-2 blocking from day 10-60 also resulted in the prevention of lymphatic migration, while blocking from day 17-60 allowed existing LECs in the regenerating region to organize into lymphatic vessels. This data suggest that the activation of VEGFR-2 is also necessary for LEC proliferation and migration but not for LEC organization into functional vessels. However, while analysis of total LEC numbers in the regenerating region (Fig. 2*C*) when VEGFR-3 was blocked between days 17-60 demonstrated that the number of LECs remained constant at the level present at the initiation of treatment (day 17), LEC numbers following VEGFR-2 blocking for the same period were reduced. This may reflect a small role of VEGFR-2 in LEC survival during later stages of lymphangiogenesis.

Effects of combined VEGFR-2 and VEGFR-3 neutralization on adult lymphangiogenesis

Since the neutralization of either VEGFR-2 or VEGFR-3 signaling alone inhibited LEC migration and proliferation but did not prevent their subsequent organization into lymphatic capillaries, we hypothesized that VEGFR-3 may be redundant with VEGFR-2 for lymphatic organization. To explore this possibility, mice were treated with both antagonist antibodies to VEGFR-2 and VEGFR-3 during various periods of skin regeneration (blocking between day 0-60, 10-60, and 17-60). Lymphatic regeneration was completely arrested in all cases (Fig. 2*B-D*), confirming the hypothesis and demonstrating the necessity for signaling of at least one of these receptors for all stages of lymphangiogenesis.

Roles of VEGFR-2 and VEGFR-3 signaling in LEC proliferation *in vitro*

The processes necessary for lymphatic regeneration, LEC proliferation, migration, and capillary organization, can be more readily assessed using *in vitro* studies that allow the roles of VEGFR-2 and VEGFR-3 signaling on each of these processes to be investigated in greater detail. Unlike the multitude of potentially contributing factors in the regeneration region that may cloud the

in vivo assesments, these LEC-only *in vitro* studies permit a transparent examination of the specific impacts receptor blocking has on LEC behavior. To be able assess the roles of VEGFR-2 and VEGFR-3 on proliferation, migration and organization *in vitro*, we first confirmed that our cultured LECs possessed functional receptors by immunoprecipitation (Fig. 3*A*). Stimulation with recombinant human wild type VEGF-C induced receptor signaling via tyrosine phosphorylation of both VEGFR-2 (top two panels) and VEGFR-3 (lower two panels). Furthermore, the efficiency of both human blocking antibodies was clarified. Neutralization of VEGFR-3 specifically prevented VEGFR-3 phosphorylation but showed little to no effect on VEGFR-2 signaling. Likewise, neutralization of VEGFR-2 blocked its phosphorylation down to baseline levels (seen when no VEGF-C was added to the medium), but allowed VEGFR-3 to phosphorylate. We also saw the presence of VEGFR-2/-3 heterodimers, as seen in each of the immunoprecipitation experiments (i.e., a lower MW band (corresponding to VEGFR-3) was phosphorylated along with the 200 kDa band (corresponding to VEGFR-2) that was co-immunoprecipitated, as seen in the top panel.

Complete medium supplemented with 100 ng/mL VEGF-C promoted LEC proliferation (7.2 ± 0.3 fold increase over matching control after 72 h). Blocking the activation of either VEGFR-2 or VEGFR-3 significantly (but not completely) inhibited LEC proliferation (to 5.0 ± 0.3 fold and 3.7 ± 0.4 fold, respectively; Fig. 3*B*). Combined inhibition of both receptors further reduced proliferation (to 2.2 ± 0.3 fold).

Role of VEGFR-2 and VEGFR-3 signaling in LEC migration *in vitro*

The relative importance of VEGFR-2 and VEGFR-3 signaling in LEC migratory responses *in vitro* mirrored those seen *in vivo* (Fig. 3*C*). Full media supplemented with 100 ng/mL recombinant human wild type VEGF-C (untreated) induced a 14 ± 3 fold increase in migration over basal levels. Inhibition of either VEGFR-2 or VEGFR-3 significantly decreased migration by 58% and 75%, respectively. Furthermore, combined inhibition of both receptors completely abolished LEC migration stimulated by VEGF-C. Thus, the activation of both receptors *in vitro* was necessary for LEC migration in an apparently additive manner.

Role of VEGFR-2 and VEGFR-3 signaling in LEC organization *in vitro*

Finally, we examined the roles of VEGFR-2 and VEGFR-3 in capillary organization using *in vitro* tubulogenesis experiments under conditions that do not require LEC proliferation. When seeded at 1.5 x 10^6 cells/mL, LECs readily formed tubular networks with numerous filopodia between cells of neighboring structures (Fig. 4*A*). Similar multicellular structures were also seen in cultures with VEGFR-3 blocking. Organization was also seen when VEGFR-2 was blocked although this was

hindered in comparison to control and VEGFR-3 blockage. When the receptors were blocked together, almost no tubular structures were observed. To quantify these observations, the organizational capacity of LECs within a 3D matrix for each culture condition was measured as total tube length per unit area (Fig. 4*B*). Although capillary structures were clearly visible, VEGFR-2 blockage resulted in reduced tube length compared with full media supplemented with VEGF-C alone. In contrast, blocking VEGFR-3 had no effect on the ability of LECs to form tube-like networks. Low density (0.5×10^6 cells/mL) seeded LECs failed to organize with or without blocking (data not shown), suggesting that LEC organization in 3D gels requires a minimum seeding density or maximum LEC-LEC distance for cell signaling.

These observations corroborate our *in vivo* data and demonstrate that while lymphatic capillary organization does not require VEGFR-3 signaling when VEGFR-2 signaling is functional, one or the other is needed, and VEGFR-2 appears to be more important than VEGFR-3 in LEC organization.

DISCUSSION

Using complimentary *in vivo* and *in vitro* studies designed to clearly delineate the contributing processes of lymphatic regeneration, we demonstrate that VEGFR-3 plays both cooperative and redundant functions with VEGFR-2 in lymphangiogenesis. Signaling through both receptors concurrently is required for LEC migration and proliferation. However, once LECs are present in sufficient numbers, VEGFR-3 signaling is redundant with VEGFR-2 for organization, since blocking VEGFR-3 had no effect on organization. Likewise, VEGFR-2 signaling is partially redundant with VEGFR-3, since organization was hindered but not blocked when VEGFR-2 was blocked. We use the term ‘redundant’ rather than ‘unnecessary’ because at least one receptor is necessary – when both receptors are blocked simultaneously, vessel organization is blocked. These findings support the hypothesis that VEGFR-3 signaling is critical for lymphatic proliferation and migration, but not for functional organization of lymphatic vessels, and represent, to our knowledge, the first demonstration of the individual roles of VEGFR-2 and VEGFR-3 in these three distinct components of lymphangiogenesis.

Although less physiologically relevant, the *in vitro* studies allowed further confirmation of receptor roles specifically in LEC proliferation, migration, and organization in the absence of other cells or confounding cellular events that might also be affected by VEGFR-2 and VEGFR-3. Consistent with our in vivo data, VEGFR-3 was completely redundant with VEGFR-2 signaling for LEC tubulogenesis. In order for tube formation to

show receptor redundancy, high seeding density was necessary to minimize the amount of migration required for vessel formation, since lower seeding densities did not promote tubulogenesis under any blocking condition. Again, this redundancy was consistent with our *in vivo* data, where the VEGFR-3-independent organization of new lymphatic capillaries occurred only if sufficient time was allowed for LECs to proliferate and migrate into the region of regeneration. Likewise, failures in organization, specifically in the proximal half of the regenerating region, are thus likely the result of a sparse LEC population at the start of receptor blocking. Thus, the strong corroboration between our *in vivo* and *in vitro* data indicate that the effects seen *in vivo* are most likely due to receptor activation on LECs and not on other cells that might express VEGFR-3, such as macrophages (27-29).

It has been previously reported that heterodimerization with VEGFR-2 may be required for VEGFR-3 phosphorylation in aortic endothelial cells (16), but LECs are known to express higher levels of VEGFR-3 than blood endothelial cells (12, 24), particulary those from large vessels, and it has also been shown that both VEGFR-3 homodimers and VEGFR-3/-2 heterodimers can form in human LECs (17). Our data support the concept that both homodimer and heterodimer forms play different functional roles, and indeed, we see that both forms are phosphorylated with VEGF-C (Fig. 3A). However, we were not able to conclusively determine which dimer pairs (or combinations thereof) are required for the different stages of LEC proliferation, migration, and capillary organization.

Our findings have important implications for VEGF-C therapies designed to induce lymphangiogenesis and help corroborate seemingly conflicting reports on its effects. If VEGFR-3 activation is largely redundant for lymphatic organization, but necessary for LEC migration and proliferation, as our data show, then VEGF-C therapy would only be potentially useful in augmenting lymphangiogenesis in areas where lymphatics are not present or are present in sub-optimal densities. It may also have the effect of making normally regenerating lymphatics more hyperplastic rather than creating a denser lymphatic capillary network, since VEGF-C overexpression has been reported to lead to increased lymphatic diameter (hyperplasia) without increased lymphatic density (20, 30, 31). Furthermore, reports that VEGF-C delivery results in increased lymphangiogenesis and/or improved lymphatic function come largely from models where lymphatic function was disrupted by wounding (32-34); in this case, VEGF-C could act by restoring lymphatic proliferation and migration into and across the wound, where lymph or interstitial flow would then help drive lymphatic organization. Finally, VEGF-C delivery in tissues that are normally devoid of lymphatics such as the cornea would certainly be required to initiate lymphatic endothelial cell migration and

proliferation (27, 35, 36) without necessarily being required for lymphatic organization. Taken together, these data suggest that VEGF-C therapy may be successful in cases where lymphangiogenesis needs to be initiated (as in the case of congenital lymphedema) but not in cases where lymphatic capillaries are intact but poorly functional (e.g., if the tissue matrix is badly damaged, such as following radiation therapy) or blocked downstream (e.g., following lymph node resection).

In summary, our results demonstrate that VEGFR-3 cooperates with VEGFR-2 in early stages of lymphangiogenesis by inducing LEC migration and proliferation, but serves redundant functions in later stages of lymphatic capillary organization. Importantly, we show that VEGFR-3 signaling is required neither for the organization of lymphatic capillaries nor for establishing or maintaining lymphatic function, which may rely instead on the activation of other lymphatic receptors such as Tie2 (36, 37) and neuropillin-2 (38) as well as on functional cues such as interstitial fluid flow (18, 19). These results also have important implications for anti-lymphangiogenesis therapy and corroborate recent evidence (10) demonstrating that combined inhibition of VEGFR-2 and VEGFR-3 may more effectively reduce tumor lymphangiogenesis and consequent lymphatic metastasis than the inhibition of either receptor alone.

ACKNOWLEDGEMENTS

The authors thank Veronique Garea for assistance with the animal studies and Sai T. Reddy for lymphatic function analysis. The authors are grateful to the National Heart, Lung, and Blood Institute (RO1-HL075217-01), the National Science Foundation (BES-0134551), and the Swiss National Science Foundation for funding.

REFERENCES

1. Aoki, Y., and Tosato, G. 2005. Lymphatic regeneration: new insights from VEGFR-3 blockade. *J Natl Cancer Inst* 97:2-3.
2. Oliver, G., and Alitalo, K. 2005. The lymphatic vasculature: recent progress and paradigms. *Annu Rev Cell Dev Biol* 21:457-483.
3. Olsson, A.K., Dimberg, A., Kreuger, J., and Claesson-Welsh, L. 2006. VEGF receptor signalling - in control of vascular function. *Nat Rev Mol Cell Biol* 7:359-371.
4. Swartz, M.A., and Skobe, M. 2001. Lymphatic function, lymphangiogenesis, and cancer metastasis. *Microsc Res Tech* 55:92-99.
5. Karpanen, T., Egeblad, M., Karkkainen, M.J., Kubo, H., Yla-Herttuala, S., Jaattela, M., and Alitalo, K. 2001. Vascular endothelial growth factor C promotes tumor lymphangiogenesis and intralymphatic tumor growth. *Cancer Res* 61:1786-1790.
6. Su, J.L., Yang, P.C., Shih, J.Y., Yang, C.Y., Wei, L.H., Hsieh, C.Y., Chou, C.H., Jeng, Y.M., Wang, M.Y., Chang, K.J., et al. 2006. The VEGF-C/Flt-4 axis promotes invasion and metastasis of cancer cells. *Cancer Cell* 9:209-223.
7. He, Y., Rajantie, I., Pajusola, K., Jeltsch, M., Holopainen, T., Yla-Herttuala, S., Harding, T., Jooss, K., Takahashi, T., and Alitalo, K. 2005. Vascular endothelial cell growth factor receptor 3-mediated activation of lymphatic endothelium is crucial for tumor cell entry and spread via lymphatic vessels. *Cancer Res* 65:4739-4746.
8. Alitalo, K., and Carmeliet, P. 2002. Molecular mechanisms of lymphangiogenesis in health and disease. *Cancer Cell* 1:219-227.
9. Lin, J., Lalani, A.S., Harding, T.C., Gonzalez, M., Wu, W.W., Luan, B., Tu, G.H., Koprivnikar, K., VanRoey, M.J., He, Y., et al. 2005. Inhibition of lymphogenous metastasis using adeno-associated virus-mediated gene transfer of a soluble VEGFR-3 decoy receptor. *Cancer Res* 65:6901-6909.
10. Roberts, N., Kloos, B., Cassella, M., Podgrabinska, S., Persaud, K., Wu, Y., Pytowski, B., and Skobe, M. 2006. Inhibition of VEGFR-3 activation with the antagonistic antibody more potently suppresses lymph node and distant metastases than inactivation of VEGFR-2. *Cancer Res* 66:2650-2657.
11. Joukov, V., Sorsa, T., Kumar, V., Jeltsch, M., Claesson-Welsh, L., Cao, Y., Saksela, O., Kalkkinen, N., and Alitalo, K. 1997. Proteolytic processing regulates receptor specificity and activity of VEGF-C. *Embo J* 16:3898-3911.
12. Joukov, V., Pajusola, K., Kaipainen, A., Chilov, D., Lahtinen, I., Kukk, E., Saksela, O., Kalkkinen, N., and Alitalo, K. 1996. A novel vascular endothelial growth factor, VEGF-C, is a ligand for the Flt4 (VEGFR-3) and KDR (VEGFR-2) receptor tyrosine kinases. *Embo J* 15:290-298.
13. Achen, M.G., Jeltsch, M., Kukk, E., Makinen, T., Vitali, A., Wilks, A.F., Alitalo, K., and Stacker, S.A. 1998. Vascular endothelial growth factor D (VEGF-D) is a ligand for the tyrosine kinases VEGF receptor 2 (Flk1) and VEGF receptor 3 (Flt4). *Proc Natl Acad Sci U S A* 95:548-553.
14. Hong, Y.K., Lange-Asschenfeldt, B., Velasco, P., Hirakawa, S., Kunstfeld, R., Brown, L.F., Bohlen, P., Senger, D.R., and Detmar, M. 2004. VEGF-A promotes tissue repair-associated lymphatic vessel formation via VEGFR-2 and the alpha1beta1 and alpha2beta1 integrins. *Faseb J* 18:1111-1113.
15. Kunstfeld, R., Hirakawa, S., Hong, Y.K., Schacht, V., Lange-Asschenfeldt, B., Velasco, P., Lin, C., Fiebiger, E., Wei, X., Wu, Y., et al. 2004. Induction of cutaneous delayed-type hypersensitivity reactions in VEGF-A transgenic mice results in chronic

skin inflammation associated with persistent lymphatic hyperplasia. *Blood* 104:1048-1057.
16. Alam, A., Herault, J.P., Barron, P., Favier, B., Fons, P., Delesque-Touchard, N., Senegas, I., Laboudie, P., Bonnin, J., Cassan, C., et al. 2004. Heterodimerization with vascular endothelial growth factor receptor-2 (VEGFR-2) is necessary for VEGFR-3 activity. *Biochem Biophys Res Commun* 324:909-915.
17. Dixelius, J., Makinen, T., Wirzenius, M., Karkkainen, M.J., Wernstedt, C., Alitalo, K., and Claesson-Welsh, L. 2003. Ligand-induced vascular endothelial growth factor receptor-3 (VEGFR-3) heterodimerization with VEGFR-2 in primary lymphatic endothelial cells regulates tyrosine phosphorylation sites. *J Biol Chem* 278:40973-40979.
18. Boardman, K.C., and Swartz, M.A. 2003. Interstitial flow as a guide for lymphangiogenesis. *Circ Res* 92:801-808.
19. Rutkowski, J.M., Boardman, K.C., and Swartz, M.A. 2006. Characterization of lymphangiogenesis in a model of adult skin regeneration. *Am J Physiol Heart Circ Physiol*.
20. Goldman, J., Le, T.X., Skobe, M., and Swartz, M.A. 2005. Overexpression of VEGF-C causes transient lymphatic hyperplasia but not increased lymphangiogenesis in regenerating skin. *Circ Res* 96:1193-1199.
21. Pytowski, B., Goldman, J., Persaud, K., Wu, Y., Witte, L., Hicklin, D.J., Skobe, M., Boardman, K.C., and Swartz, M.A. 2005. Complete and specific inhibition of adult lymphatic regeneration by a novel VEGFR-3 neutralizing antibody. *J Natl Cancer Inst* 97:14-21.
22. Witte, L., Hicklin, D.J., Zhu, Z., Pytowski, B., Kotanides, H., Rockwell, P., and Bohlen, P. 1998. Monoclonal antibodies targeting the VEGF receptor-2 (Flk1/KDR) as an anti-angiogenic therapeutic strategy. *Cancer Metastasis Rev* 17:155-161.
23. Persaud, K., Tille, J.C., Liu, M., Zhu, Z., Jimenez, X., Pereira, D.S., Miao, H.Q., Brennan, L.A., Witte, L., Pepper, M.S., et al. 2004. Involvement of the VEGF receptor 3 in tubular morphogenesis demonstrated with a human anti-human VEGFR-3 monoclonal antibody that antagonizes receptor activation by VEGF-C. *J Cell Sci* 117:2745-2756.
24. Podgrabinska, S., Braun, P., Velasco, P., Kloos, B., Pepper, M.S., and Skobe, M. 2002. Molecular characterization of lymphatic endothelial cells. *Proc Natl Acad Sci U S A* 99:16069-16074.
25. Cursiefen, C., Chen, L., Borges, L.P., Jackson, D., Cao, J., Radziejewski, C., D'Amore, P.A., Dana, M.R., Wiegand, S.J., and Streilein, J.W. 2004. VEGF-A stimulates lymphangiogenesis and hemangiogenesis in inflammatory neovascularization via macrophage recruitment. *J Clin Invest* 113:1040-1050.
26. Shibuya, M., and Claesson-Welsh, L. 2005. Signal transduction by VEGF receptors in regulation of angiogenesis and lymphangiogenesis. *Exp Cell Res*.
27. Maruyama, K., Ii, M., Cursiefen, C., Jackson, D.G., Keino, H., Tomita, M., Van Rooijen, N., Takenaka, H., D'Amore, P.A., Stein-Streilein, J., et al. 2005. Inflammation-induced lymphangiogenesis in the cornea arises from CD11b-positive macrophages. *J Clin Invest* 115:2363-2372.
28. Schoppmann, S.F., Birner, P., Stockl, J., Kalt, R., Ullrich, R., Caucig, C., Kriehuber, E., Nagy, K., Alitalo, K., and Kerjaschki, D. 2002. Tumor-associated macrophages express lymphatic endothelial growth factors and are related to peritumoral lymphangiogenesis. *Am J Pathol* 161:947-956.
29. Skobe, M., Hamberg, L.M., Hawighorst, T., Schirner, M., Wolf, G.L., Alitalo, K., and Detmar, M. 2001. Concurrent induction of lymphangiogenesis, angiogenesis, and

macrophage recruitment by vascular endothelial growth factor-C in melanoma. *Am J Pathol* 159:893-903.
30. Isaka, N., Padera, T.P., Hagendoorn, J., Fukumura, D., and Jain, R.K. 2004. Peritumor lymphatics induced by vascular endothelial growth factor-C exhibit abnormal function. *Cancer Res* 64:4400-4404.
31. Jeltsch, M., Kaipainen, A., Joukov, V., Meng, X., Lakso, M., Rauvala, H., Swartz, M., Fukumura, D., Jain, R.K., and Alitalo, K. 1997. Hyperplasia of lymphatic vessels in VEGF-C transgenic mice. *Science* 276:1423-1425.
32. Saaristo, A., Tammela, T., Timonen, J., Yla-Herttuala, S., Tukiainen, E., Asko-Seljavaara, S., and Alitalo, K. 2004. Vascular endothelial growth factor-C gene therapy restores lymphatic flow across incision wounds. *Faseb J* 18:1707-1709.
33. Szuba, A., Skobe, M., Karkkainen, M.J., Shin, W.S., Beynet, D.P., Rockson, N.B., Dakhil, N., Spilman, S., Goris, M.L., Strauss, H.W., et al. 2002. Therapeutic lymphangiogenesis with human recombinant VEGF-C. *Faseb J* 16:1985-1987.
34. Yoon, Y.S., Murayama, T., Gravereaux, E., Tkebuchava, T., Silver, M., Curry, C., Wecker, A., Kirchmair, R., Hu, C.S., Kearney, M., et al. 2003. VEGF-C gene therapy augments postnatal lymphangiogenesis and ameliorates secondary lymphedema. *J Clin Invest* 111:717-725.
35. Mimura, T., Amano, S., Usui, T., Kaji, Y., Oshika, T., and Ishii, Y. 2001. Expression of vascular endothelial growth factor C and vascular endothelial growth factor receptor 3 in corneal lymphangiogenesis. *Exp Eye Res* 72:71-78.
36. Morisada, T., Oike, Y., Yamada, Y., Urano, T., Akao, M., Kubota, Y., Maekawa, H., Kimura, Y., Ohmura, M., Miyamoto, T., et al. 2005. Angiopoietin-1 promotes LYVE-1-positive lymphatic vessel formation. *Blood* 105:4649-4656.
37. Tammela, T., Saaristo, A., Lohela, M., Morisada, T., Tornberg, J., Norrmen, C., Oike, Y., Pajusola, K., Thurston, G., Suda, T., et al. 2005. Angiopoietin-1 promotes lymphatic sprouting and hyperplasia. *Blood* 105:4642-4648.
38. Yuan, L., Moyon, D., Pardanaud, L., Breant, C., Karkkainen, M.J., Alitalo, K., and Eichmann, A. 2002. Abnormal lymphatic vessel development in neuropilin 2 mutant mice. *Development* 129:4797-4806.

FIGURE LEGENDS

Fig. 1. Effects of VEGFR-3 neutralization in a model of lymphatic regeneration. *A*) Left: *In vivo* model of adult lymphangiogenesis. A circumferential band of skin is removed, covered with a silastic sleeve, and filled with type I collagen that serves as a fluid bridge between the distal and proximal lymphatics and provides a support for tissue regeneration; box indicates area of inset, right. Inset: Approximate location of images in *B*-*E*. The black square indicates the distal region shown in the immunostained thick sections in *B* and *D*, while the white box indicates the region shown in the microlymphangiography analyses of functional regeneration in *C* and *E*. *B*) Immunostaining for BECs (CD31, red) and LECs (LYVE-1, green) at various timepoints shows progression of normal (untreated) regeneration lymphangiogenesis. At day 10, the region is primarily LEC-free. At day 17, many LECs are present, and they appear in unconnected clusters. At day 60, fully connected lymphatic structures are present throughout the regenerating region. *C*) Microlymphangiography reveals the lack of functional lymphatic vessels at days 10 and 17, and functional and architecturally restored lymphatic network at day 60. *D*) Neutralizing VEGFR-3 from the onset of lymphangiogenesis (day 0 or 10) through day 60 completely inhibits any lymphatic growth in the regenerating region. However, blocking from day 17 to 60 does not inhibit the organization of LECs that had migrated into the regenerating region. Bar=150μm. *E*) Analysis for blocking schedules in *D* confirms the functionality of lymphatics that form in the absence of VEGFR-3 between days 17 and 60, where functional lymphatic transport is visible within the distal portion of the regenerating region. Bar=300μm. *F*) Quantification of LEC numbers in the regenerating region under various blocking schedules. In normal regeneration, LEC numbers are low at day 10, medium at day 17, and high at day 60. When VEGFR-3 is blocked, cell numbers are similar to those at the onset of blocking (i.e., those at days 10 and 17 in control mice), indicating that VEGFR-3 blocking prevents cell proliferation but does not affect cell survival. *$P<0.05$ compared with day 10 control, $^{\#}$ $P<0.05$ compared with day 17 control. *G*) Distribution of LECs in the regenerating region indicates the direction of LEC migration. In normal regeneration, the few LECs present at day 10 are present only in the distal edge; at day 17, LECs are present throughout but still more numerous in the distal half; by 60 days, LEC distribution is even throughout the region. When VEGFR-3 is blocked during days 10-60 and 17-60, LEC distributions are statistically similar to those at the onset of blocking, indicating that LEC migration was arrested when VEGFR-3 blocking began. *$P<0.05$ between distal and proximal fraction.

Fig. 2. Effects of VEGFR-2 blocking and combined VEGFR-3 and VEGFR-2 blocking on lymphatic regeneration. *A*) VEGFR-2 blocking alone (top panel) prevented lymphatic regeneration when the mAb was administered during days 0-60. Minimal regeneration was observed when VEGFR-2 was blocked from days 10-60. Organization of LECs into lymphatic capillaries was seen when VEGFR-2 was blocked from days 17-60. Combined blockade of both receptors between days 17-60 (lower panel) drastically inhibited lymphatic organization, with very few vessels present. Bar=150μm. *B*) The number of LECs in the regenerating region at day 60 was somewhat diminished when VEGFR-2 was blocked during days 17-60 and diminished greatly when both receptors were blocked during this time period indicating that VEGFR-2 signaling may affect LEC survival, particularly that of unorganized LECs. *P<0.05 compared with day 10 control, $^{\#}$ P<0.05 compared with day 17 control. *C*) The distribution of LECs in the regenerating region. The effects of individually blocking either VEGFR-2 or VEGFR-3 on LEC distribution resulted in a cell distribution similar to that seen on day 17 of controls, suggesting inhibition of migration and proliferation. Combined blocking of both receptors, however, resulted in LEC distribution similar to that of day 10 controls. *P<0.05 between distal and proximal fraction.

Figure 3. Signaling by both VEGFR-2 and VEGFR-3 is important for LEC proliferation and migration *in vitro*. *A*) Wild-type VEGF-C stimulated receptor activation via tyrosine phosphorylation of both VEGFR-2 and VEGFR-3 in cultured human microvascular LECs, and neutralizing antibodies specifically inhibited phosphorylation of their respective receptors, whilst allowing signaling of the other. The top two panels show immunoblots (performed in parallel) from VEGFR-2 immunoprecipitated samples; top blot shows PY-20 and reveals phosphorylated protein of both a 200 kDa and 110 kDa, while second blot shows VEGFR-2 appearing only as a 200 kDa protein, verifying equal protein loading and demonstrating the presence of co-immunopreciptated VEGFR-3. The bottom two panels show immunoblots (performed in parallel) from VEGFR-3 immunoprecipitated samples; third blot shows PY-20 and again reveals phosphorylation of both approximately 200 kDa and 110 kDa bands, which can be inhibited when VEGFR-3 is neutralized. The second blot shows total VEGFR-3. IC indicates where isotype-matched control IgG was used in place of blocking antibodies in the medium. *B)* After 72 hours of treatment, blockade of either VEGFR-2 or VEGFR-3 reduced VEGF-C-induced LEC proliferation. This was further inhibited when both receptors were blocked simultaneously. *C*) Blocking either VEGFR-2 or VEGFR-3

substantially decreased VEGF-C-induced LEC migration, while combined blockade completely abolished this migratory response. *P<0.05, **P<0.01 vs untreated; $^{\#}$ P<0.05, $^{\#\#}$ P<0.01 vs other conditions as indicated.

Figure 4. VEGFR-3 is redundant with VEGFR-2 for LEC tubulogenesis *in vitro*.
A) VEGF-C stimulated formation of multicellular structures leading to an extensive tubular network. Inhibition of VEGFR-2 permitted LEC organization, although the extent of tubulogenesis was hindered compared with untreated LECs. VEGFR-3 inhibition did not affect LEC tubulogenesis, whilst combined blockade of both receptors completely prevented tubulogenesis. Bar=100μm. *B*) Quantification of organization expressed as total tube length per mm^2 confirmed these observations and demonstrated that VEGFR-3 blocking has no effect on tubulogenesis. $^{\#}$P<0.05, $^{\#\#}$P<0.01 as indicated.

Figure 1

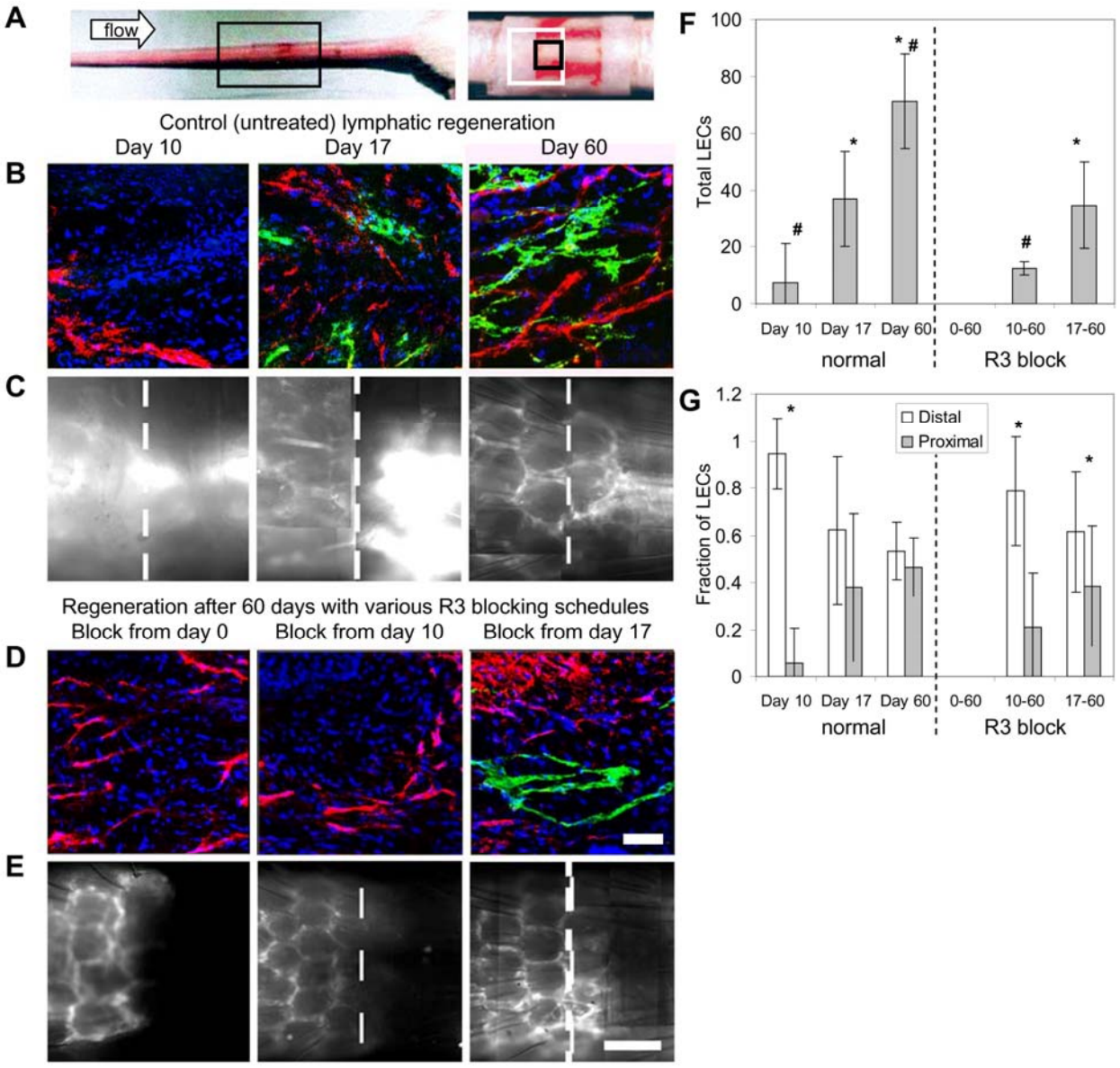
A
flow
Control (untreated) lymphatic regeneration
Day 10
Day 17
Day 60
B
C
Regeneration after 60 days with various R3 blocking schedules
Block from day 0
Block from day 10
Block from day 17
D
E
F
Total LECs
Day 10
Day 17
Day 60
0-60
10-60
17-60
normal
R3 block
G
Distal
Proximal
Fraction of LECs

This page is intentionally left blank.

Figure 2

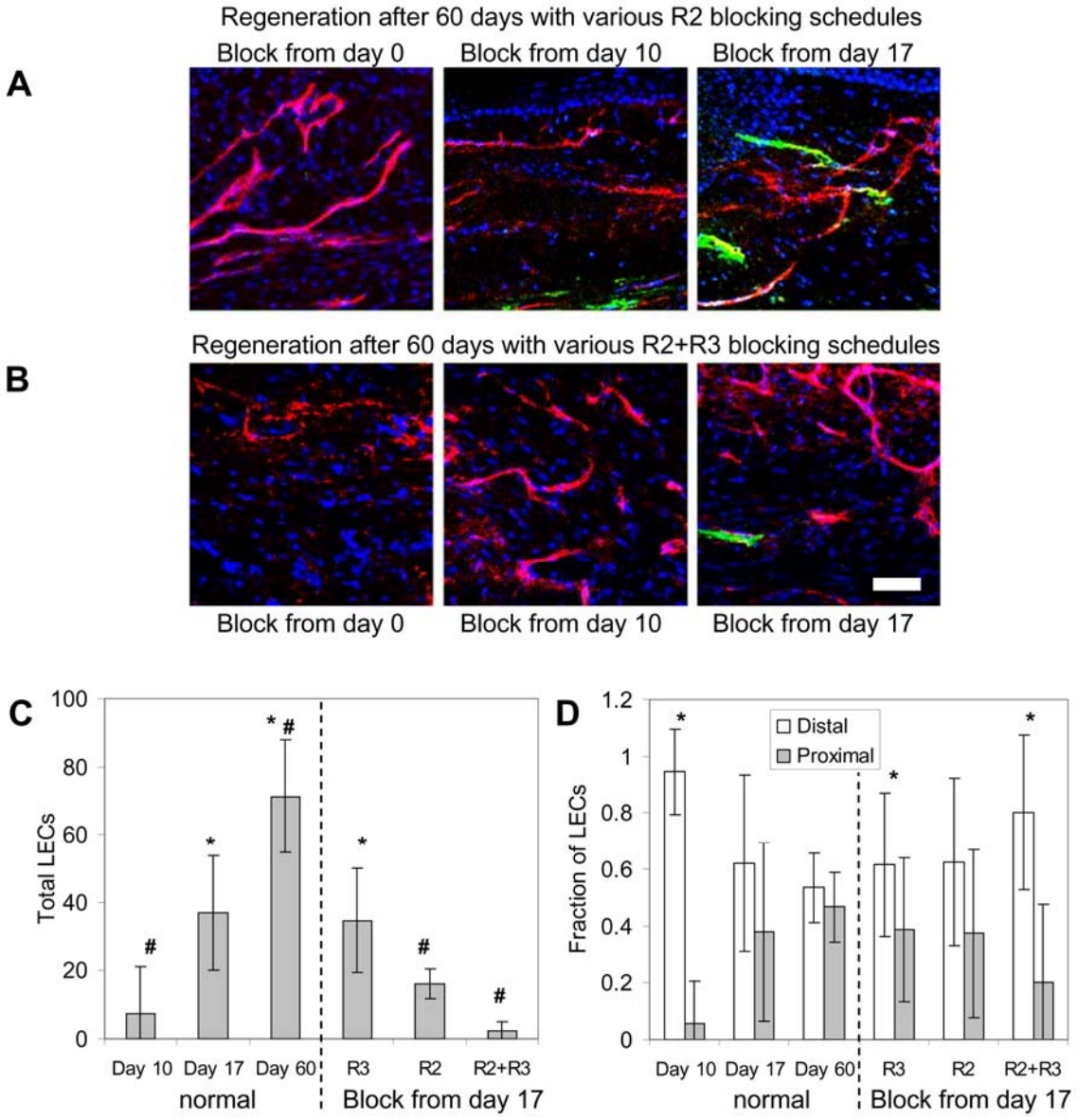
A
Regeneration after 60 days with various R2 blocking schedules
Block from day 0
Block from day 10
Block from day 17
B
Regeneration after 60 days with various R2+R3 blocking schedules
Block from day 0
Block from day 10
Block from day 17
C
Total LECs
100
80
60
40
20
0
Day 10
Day 17
Day 60
R3
R2
R2+R3
normal
Block from day 17
D
Fraction of LECs
1.2
1
0.8
0.6
0.4
0.2
0
Distal
Proximal
Day 10
Day 17
Day 60
R3
R2
R2+R3
normal
Block from day 17

This page is intentionally left blank.

Figure 3

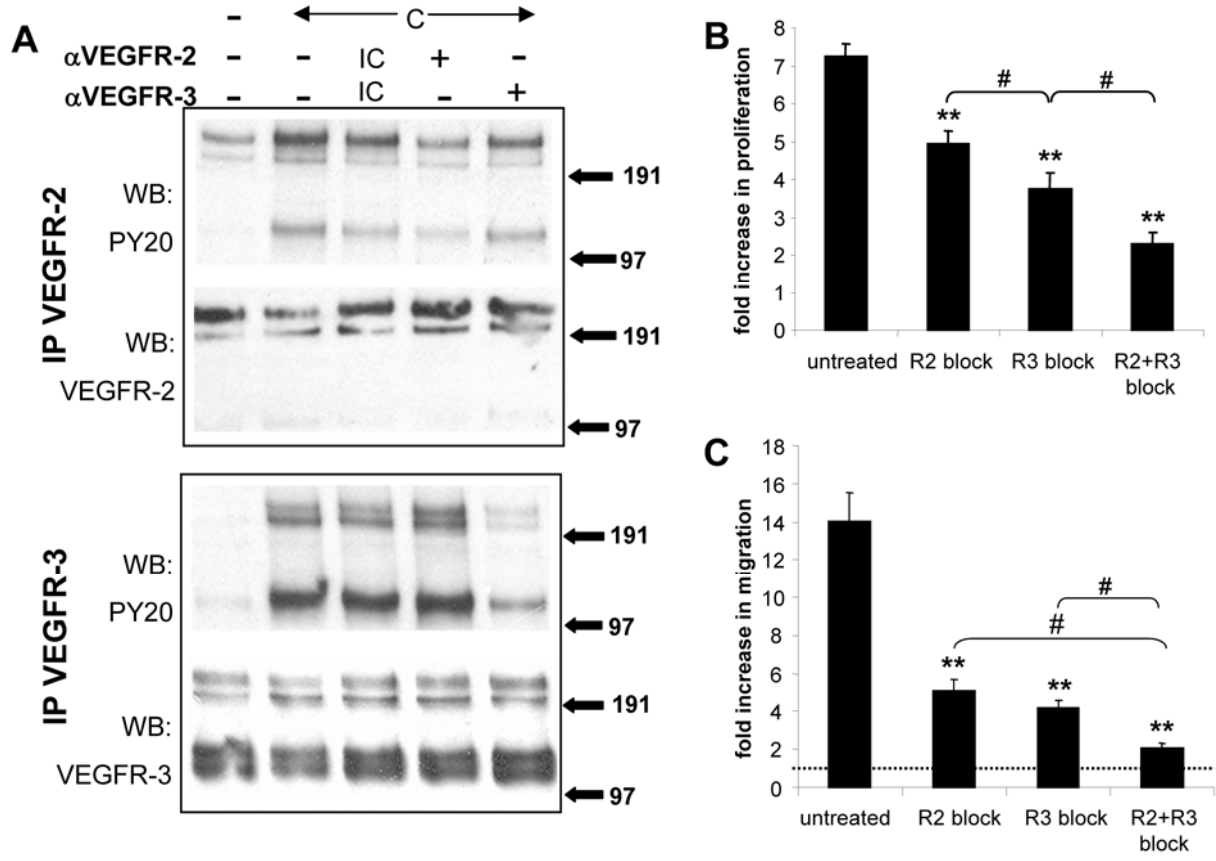
A
C
αVEGFR-2
αVEGFR-3
IC
IC
IP VEGFR-2
WB:
PY20
WB:
VEGFR-2
IP VEGFR-3
WB:
PY20
WB:
VEGFR-3
191
97
191
97
191
97
191
97
B
fold increase in proliferation
untreated
R2 block
R3 block
R2+R3 block
C
fold increase in migration
untreated
R2 block
R3 block
R2+R3 block

This page is intentionally left blank.

Figure 4

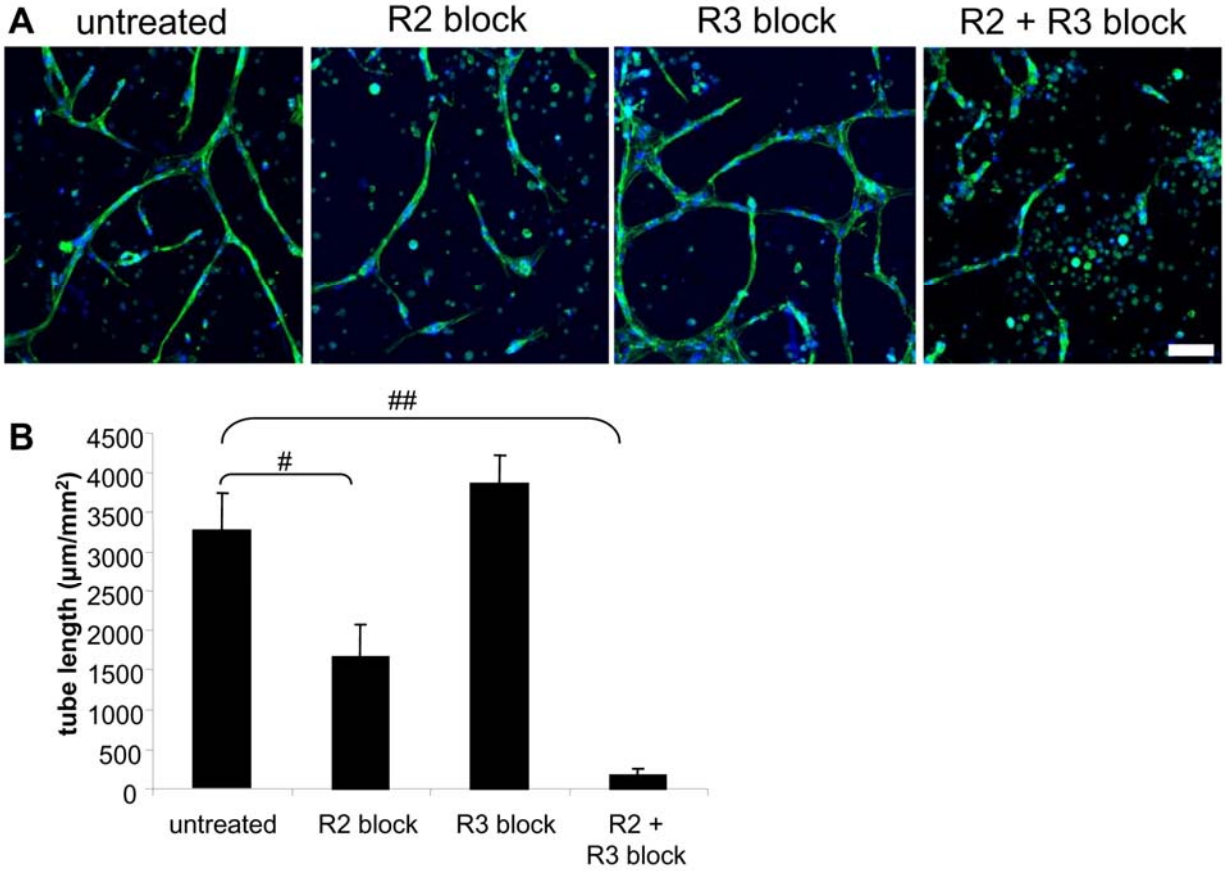
A
untreated
R2 block
R3 block
R2 + R3 block
B
tube length (µm/mm²)
4500
4000
3500
3000
2500
2000
1500
1000
500
0
#
##
untreated
R2 block
R3 block
R2 +
R3 block

This page is intentionally left blank.

Table 1

	Normal Regeneration	R3 Block			R2 Block			R3 + R2 Block		
Day 0	Cell free									
Day 10	LECs proliferate and migrate only at the distal edge									
Day 17	LECs migrating throughout region; primitive and disconnected structures begin to form									
Day 25	Organization continues and some functionality is established but incomplete									
Day 60	Functional, mature lymphatic network									

This page is intentionally left blank.

Supplemental Figure 1

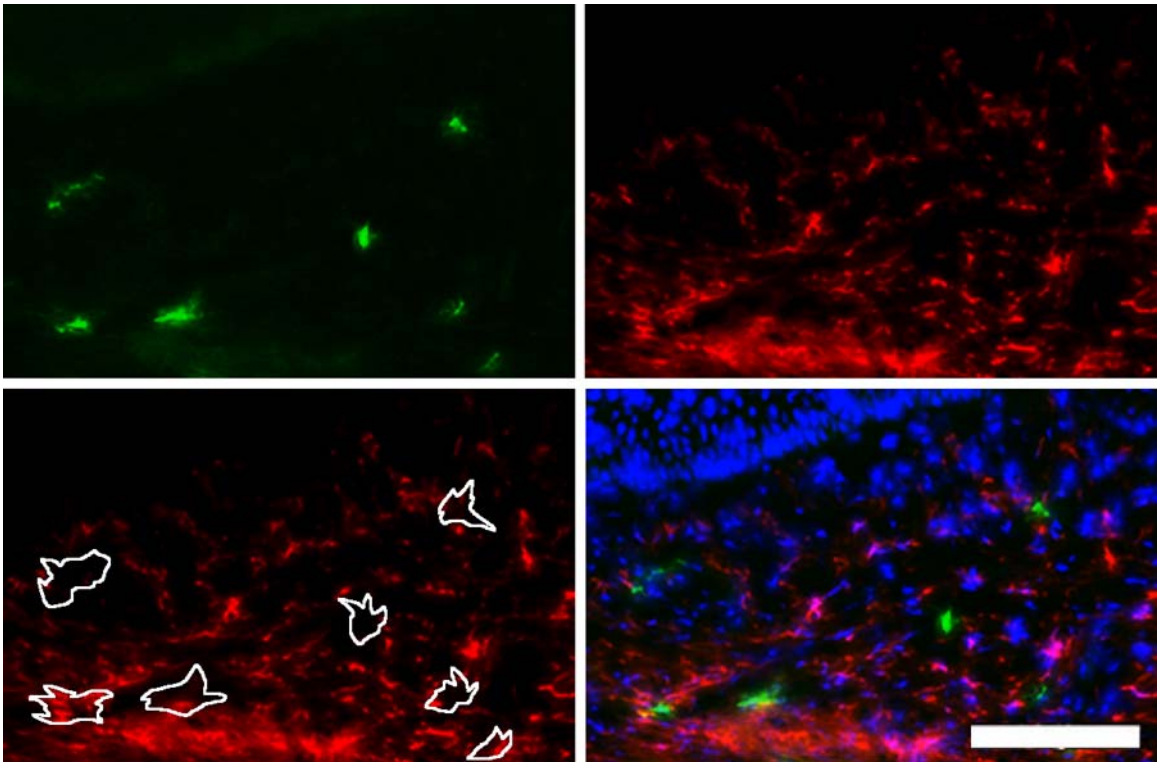

Supplemental Figure 1: Cells identified as lymphatic endothelial cells (LECs) do not express macrophage markers. On 10 μm-thick cryosections, LYVE-1 (green, top panel) labeled unorganized LECs in a normal regenerating region at 25 days. F4/80 (red, top panel. BD Pharmingen; 1:50) labeled the dense macrophage population in the region. Highlighting the LYVE-1 positive cells, there is no overlap (bottom panel). As both markers are found on the cell surface, lack of colocalization demonstrates that the mechanism of lymphatic regeneration in the mouse tail does not intimately involve LYVE-1 expressing macrophages. Bar=100 μm.

This page is intentionally left blank.

CHAPTER 5:
ORIGINAL MANUSCRIPT 4

Secondary lymphedema in the mouse tail: Lymphatic hyperplasia, VEGF-C upregulation, and the protective role of MMP-9

Joseph M. Rutkowski[1], Monica Moya[2], Jimmy Johannes[2], Jeremy Goldman[2,3], and Melody A. Swartz[1,2]

[1]Institute of Bioengineering, École Polytechnique Fédérale de Lausanne (EPFL), Lausanne, Switzerland
[2]Department of Biomedical Engineering, Northwestern University, Evanston, IL
[3]Current address: Department of Biomedical Engineering, Michigan Technological University, Houghton, MI

Submitted 23 February 2006; accepted in final form 26 July 2006

Microvascular Research

2006 Nov;72(3):161-71. First published July 26, 2006.

ABSTRACT

Disturbances in the microcirculation can lead to secondary lymphedema, a common pathological condition that, despite its frequency, still lacks a cure. Lymphedema is well-described clinically, but while the genetic underpinnings that cause lymphatic malformations and primary lymphedema are being discovered, the pathophysiology and pathobiology of secondary lymphedema remains poorly understood, partly due to the lack of well-described experimental models. Here, we provide a detailed characterization of secondary lymphedema in the mouse tail and correlate the evolution of tissue swelling to changes in tissue architecture, infiltration of immune cells, deposition of lipids, and proliferation and morphology of the lymphatic vessels. We show that sustained swelling leads to lymphatic hyperplasia and upregulation of vascular endothelial growth factor (VEGF)-C, which may exacerbate the edema since the hyperplastic vessels leak lymph back into the interstitium. The onset of lymphatic hyperplasia occurred prior to the onset of lipid accumulation and peak VEGF-C expression. Langerhans dendritic cells were seen in the dermis migrating from the epidermis to the lymphatic capillaries in edematous tissue. Furthermore, these results were consistent between two different normal mouse strains, but swelling was significantly greater in a matrix metalloproteinase (MMP)-9 null strain. Thus, by characterizing this highly reproducible model of secondary lymphedema, we conclude that VEGF-C upregulation and lymphatic hyperplasia resulting from dermal lymphatic ligation and lymphedema leads to decreased drainage function and that MMP-9 may be important in counteracting tissue swelling.

Key Words: lymphatic function, extracellular matrix, lipid deposition, MMP-9, VEGF-C

INTRODUCTION

Lymphedema is a common pathology of tissue fluid balance often due to defects in lymphatic uptake and/or transport. Primary lymphedema results from defects of the lymphatic system leading to insufficiencies in transport, while the more common secondary lymphedema arises as a consequence to surgical, malignant, inflammatory, or traumatic disruption of the lymphatics (1, 2). As a chronic disease, lymphedema leads to the remodeling of skin and subcutaneous tissues (3), accumulation of lipids (4), macrophage recruitment (5), and failures in Langerhans dendritic cell migration (6) in the affected tissue. Unfortunately, this potentially debilitating condition lacks a cure and current treatment for chronic lymphedema, which include regular massage treatments and pressure applications or surgical removal of edematous tissue, can only slow its progression but not reverse the condition (2, 7, 8).

Recent studies have identified key regulators of lymphatic development and the genetic underpinnings of primary lymphedema caused by lymphatic malformation in development. However, the pathophysiology of secondary lymphedema – including the interplay between inflammatory events, matrix remodeling, and local lymphatic response – is less understood, and because of this, it is still not clear to what extent therapies aimed at lymphatic regrowth can be used to treat various types of secondary lymphedema. For example, if lymphedema is caused by downstream blockage (e.g., surgical removal of lymph nodes), do the previously healthy lymphatic capillaries respond to the tissue swelling by growing, or by regressing? Do they still facilitate immune cell trafficking? Without an understanding of the tissue-lymphatic pathophysiology of secondary lymphedema, rational treatment options will continue to be elusive.

Key molecular players in lymphatic development have been demonstrated primarily by transgenic models; mutations in these regulators commonly lead to either embryonic mortality or lymphatic irregularities and symptoms of primary edema (9). Prox1, for example, governs the commitment of endothelial cells to a lymphatic lineage in development and Prox1 null embryonic mice die before birth (10) while surviving Prox1 heterozygotes possess discontinuous lymphatic endothelium and exhibit abnormal fluid and lipid accumulation in the interstitium (11). Mice lacking angiopoietin-2, thought to play a role in vascular remodeling and lymphatic patterning, have disorganized, irregular lymphatic vessels and exhibit dermal edema and chylous ascites (12). Mutations in Foxc2, a transcription factor expressed on developing lymphatics, have been identified as the cause of lymphedema-

distichiasis in humans that, unlike other types of congenital lymphedema, is characterized by hyperplastic lymphatic vessels (13, 14). Foxc2-null and -heterozygous mice posses hyperplastic lymphatic vessels and malfunctioning lymphatic valves that result in lymphatic backflow and abnormal lymphatic drainage (15, 16). A mutant allele for vascular endothelial growth factor (VEGF) receptor-3 (VEGFR-3) is responsible for Milroy's disease in humans, a congenital disorder characterized by primary lymphedema in the extremities, as well as the Chy mouse phenotype that exhibits lymphatic defects similar to the human condition (17). VEGFR-3 and its ligand VEGF-C are also critical for both embryonic (18) and adult lymphangiogenesis (19, 20). These findings suggest that targeting lymphatic molecular mechanisms for improving lymphatic function may lead to a successful treatment of lymphedema and, as a result, research has focused on the most well-studied lymphatic molecular pathway to potentially treat conditions of both primary and secondary lymphedema: VEGFR-3 and VEGF-C (17, 21, 22). However, VEGF-C overexpressing mice display hyperplastic lymphatics (23) and we recently showed that excess VEGF-C delivered to otherwise normally regenerating skin led to hyperplastic lymphatic vessels without any increase in function (24). The proper resolution of lymphedema is likely dependent on the initial cause of the pathology, and effective treatments for primary and secondary lymphedema are therefore likely to differ. While the causes of primary lymphedema are increasingly appreciated, there remain gaps in our understanding of the pathophysiology and pathobiology of secondary lymphedema. These gaps are largely due to the absence of well-characterized models of secondary lymphedema.

Existing models of secondary lymphedema in the dog hindlimb (25, 26), rat hindlimb (27, 28), or rabbit ear (21) disrupt lymphatic transport through the excision of a circumferential band of skin and subcutaneous tissue. These models can sustain significant lymphedema for 3-4 weeks and result in a chronic increase in limb or ear volume. We earlier described a model of secondary lymphedema in the mouse tail skin (29, 30). Here, we characterize this model of secondary lymphedema to not only determine the reproducibility across several strains of mice, but moreover, to also describe the relative timing of the appearance of chronic symptoms, such as changes in extracellular matrix structure, accumulation of lipids, and recruitment of macrophages with the overall degree of swelling of the tail skin. We then correlate the timing of the lymphatic response and expression of VEGF-C to these pathological outcomes and show that sustained tissue swelling leads to hyperplasia and subsequent decrease in function of the lymphatic capillaries, closely followed by a drastic increase in local VEGF-C expression. Additionally, to ascertain the importance of matrix

metalloprotenases (MMP)s in the inevitable matrix changes during tail swelling, mice lacking MMP-9, a key MMP in tissue remodeling (31), were also examined and found to experience a much higher increase in tail volume during secondary lymphedema. Thus, this characterization of the mouse tail model and correlation of molecular, cellular, and physiological changes over time lends new insight into the pathophysiology of secondary lymphedema, including the observation that lymphatic hyperplasia and VEGF-C overexpression may be key responses to chronic swelling.

MATERIALS AND METHODS

Mouse tail model of lymphedema

These studies used 6-8 week old female mice, 10 per group, of the following strains: BALB/c (Charles River Laboratories, Wilmington, MA), FVB/NJ (Charles River Laboratories, France) and MMP-9 null on an FVB background (FVB.Cg-Mmp9^{tm1Tvu}/J; The Jackson Laboratory, Bar Harbor, ME). Mice were anesthetized with a subcutaneous injection of ketamine (65 mg/kg), xylazine (13 mg/kg), and acepromazine (2mg/kg). An analgesic, butorphanol (0.05 mg/kg), was administered subcutaneously twice daily for three days following the procedure. All protocols were approved by the ACUC of Northwestern University and the Veterinary Authorities of the Canton Vaud according to Swiss law.

To create lymphedema, a circumferential incision was made through the dermis close to the tail base to sever the dermal lymphatic vessels. The edges of this incision were then pushed apart with a cauterizing iron, thereby disturbing the deeper lymphatics, preventing superficial bleeding, and creating a 2-3 mm gap to delay wound closure. Care was taken to maintain the integrity of the major underlying blood vessels and tendons so that the tail distal to the incision did not become necrotic. An age-matched control group of mice was maintained without this procedure to measure the baseline tail volume during the time course of the analysis.

Daily volume measurements of the tails, from the tip to the distal edge of the wound, were made by volume displacement. For untreated mice, a circumferential mark was made on the tail 10 mm from the tail base to mimic the incision site for reproducibility in measuring.

Sample preparation

Mice were sacrificed at various times up to 30 days post-procedure. The tail was excised at the site of the edema procedure and the distal tissue was flash frozen in liquid N_2. Tissue samples were transversely cryosectioned into 12 and 60 μm-thick sections and stored at -80˚C until immunostaining.

Microlymphangiography

Mice were anesthetized as above and the integrity of the lymphatic vasculature of the tail was examined by fluorescence microlymphangiography (30, 32, 33). A fluorescently labeled macromolecule (2000 kDa tetramethylrhodamine-conjugated dextran, 2 mg/ml; Molecular Probes, Carlsbad, CA) was injected intradermally at a constant pressure of 45 cm of water into the tip of the tail. Because of its large size, the tracer was taken up by the lymphatics but was excluded from the blood vasculature. As the fluorescent tracer was transported by the lymphatic vessels, it was clearly visible within dermal lymphatic capillaries, thus providing a clear visualization of lymphatic functionality. The filling of the lymphatic vasculature was monitored for 90 minutes with a Zeiss Axiovert 200M fluorescence microscope and Zeiss MRm camera set at equal exposure time for each mouse.

Immunohistochemistry and histology

To visualize lymphatic vessels, thin (12 μm) and thick (60 μm) sections were co-stained with a primary antibody to the lymphatic-specific marker LYVE-1 (1:500; rabbit polyclonal; Upstate, Charlottesville, VA). Thin sections were also labeled using anti-mouse antibodies for the macrophage-specific surface marker F4/80 (1:50; rat monoclonal; Serotec, Raleigh, NC) and the Langerhans dendritic cell protein langerin (1:50; goat polyclonal; Santa Cruz Biotechnology, Santa Cruz, CA). These antibodies were detected with Alexafluor 488 or 594-conjugated donkey, rabbit, and goat IgG secondary antibodies (1:200, Molecular Probes), counterstained with DAPI (Vector Labs, Burlingame, CA), and observed and imaged as above. Thick sections were scanned using a Zeiss LSM 510 Meta confocal microscope. PCNA staining was achieved on thin sections with a monoclonal biotinylated mouse anti-PCNA primary antibody (prediluted; Zymed Laboratories, South San Francisco, CA) and detected with Texas Red-conjugated avidin (Vector Labs).

VEGF-C was labeled immunohistochemically on thin sections. Sections were first fixed in 4% PFA, blocked against endogenous biotin and avidin activity (Biotin Blocking System, Dako, Carpenteria, CA), then labeled with anti-mouse VEGF-C (1:50; goat polyclonal; Santa

Cruz) and biotinylated secondary antibody (1:500; AffiniPure rabbit; Jackson ImmunoResearch, West Grove, PA). This was then visualized using the ABC-AP kit and Vector Black (Vector Labs). Sections were counterstained with Orange G (Merck KGaA, Darmstadt, Germany), dehydrated, and mounted with Eukitt (Fluka Chemie AG, Buchs, Switzerland). Images were captured with an Olympus AX70 Microscope and DP70 Camera.

Masson's trichrome was used to stain collagen and oil red O (Sigma-Aldrich, Buchs, Switzerland) to stain lipids on thin sections. Sections were mounted and imaged as above, except oil red O stained sections were counterstained with hematoxylin and not dehydrated but immediately mounted with Glycergel mounting medium (Dako).

Image Analysis

Images of each tail section were first assembled into complete montages in Photoshop (Adobe Systems, San Jose, CA). To quantify LEC hyperplasia, LECs were defined as cells with a blue (DAPI-stained) nucleus surrounded by green LYVE-1 staining, and lymphatic structures were defined as continuous groups of LYVE-1 labeled cells. The numbers of LECs within each structure were counted in three random 12 μm sections from each animal.

To quantify VEGF-C expression, Metamorph 6.3 image analysis software (Molecular Devices Corp., Sunnyvale, CA) was used. Three labeled sections from each timepoint were analyzed. In each, the region between the epidermis and underlying tendon was clearly identified with a freehand tool, and the total intensity within this region was integrated.

Statistics

For quantified data, ANOVA followed by two-tailed Student's t-tests were performed to determine statistical significance between two groups or among different timepoints. Data are reported as average ± standard deviations. Tail volumes are presented as a change over normal, LEC counts as total cells, and VEGF-C as normalized to the maximum.

RESULTS

Degree and sustainability of swelling

All three strains of mice tested (BALB/c, FVB/NJ, and MMP-9 null) sustained reproducible edema for a period of at least 30 days. In the wild-type strains examined, FVB/NJ and BALB/c, tail volume measurements consistently peaked at 15 days following the ligation procedure with a volume increase of 55-75% (Fig. 1). Resolution of edema in these

mice also consistently occurred to within 20% of control volume by 30 days. Two FVB/NJ mice were kept for 60 days and their increased tail volumes were sustained (both 17% larger than baseline at day 60) in agreement with past work (29). MMP-9 null mice experienced significantly more tissue swelling than wild-type controls both with a higher peak volume change at 15 days of 115% (P=0.0287) and higher 30 day volume change of 75%.

Matrix changes and lipid accumulation

In normal tail skin, the dermis possesses a much higher density of collagen than the underlying hypodermis. One day after of lymphatic disruption, we observed an immediate reduction in collagen density throughout the dermis, while the subcutaneous tissue layer of the hypodermis was drastically swollen (Fig. 2A). Within the first week, however, the density of collagen in the dermis increased, and by day 14 the collagen architecture in the dermis appeared similar to that of normal tissue. The change in tail volume was thus mainly due to hypodermal swelling. The hypodermis remained swollen with decreased collagen density until day 30, when collagen density again appeared normal, although total tissue volume was significantly increased.

In addition to its propensity to accumulate fluid and swell, the hypodermis also exhibited a striking increase in lipid deposition (Fig. 2B). Lipid accumulation in the hypodermis, visualized through oil red O staining, became visible after 7 days, peaked at 14 days, and was maintained through 30 days. Macrophages were also present throughout the dermis and hypodermis in edematous skin at all time points examined (Fig. 2C).

Lymphatic function in edematous tail skin

The lymphatic network of the mouse tail skin consists of a regular, hexagonal network of dermal lymphatic capillaries that are easily visualized by fluorescence microlymphangiography (20, 32, 33). Furthermore, measures of how much volume is infused into the tail at fixed pressure is indicative of hydraulic conductivity and lymphatic function (30). Microlymphangiography in normal vs. edematous tails revealed functional insufficiencies in the lymphatics and increased hydraulic conductivity (Fig. 3). In normal mice, the lymphatic capillaries took up ~8 μl in 90 min of fluorescent dextran infused into the tail tip at 45 cm water; while in contrast, day 10 edematous tails took up ~30 μl of dextran in 90 min at the same pressure. Despite the increase in hydraulic conductivity and dramatic increase in injected fluid flow rate for a given injection pressure, the lymphatic capillaries in edematous tails remained functional in taking up the injected fluid tracer; however,

fluorescent tracer was visible in the interstitial space around the capillary network, suggesting that the lymphatics in edematous skin were leaky and prone to backflow. After 60 days, the edema was reduced and the lymphatic leakiness was decreased but not entirely resolved.

Lymphatic hyperplasia

Lymphatic ligation and subsequent tissue swelling led to marked morphological changes in the dermal lymphatics caused by the proliferation of LECs and subsequent enlargement of the lymphatic vessels. PCNA-positive LECs were seen in hyperplastic lymphatic vessels at day 10 (Fig. 4A). A reduced number of PCNA-positive cells were seen in lymphatic vessels at 20 days, and none were visible at 30 days. Confocal microscopy of the lymphatic vessels in the tail during edema (Fig. 4B) revealed that the morphology of the vessels was clearly altered, with striking hyperplasia during the period when overall swelling was the greatest (7 to 21 days). The number of LECs counted in each lymphatic structure was significantly higher than in normal vessels, peaking at 7 days ($P<0.001$). After this, the number of LECs per structure decreased, but still remained significantly higher than normal throughout the resolution of edema ($P<0.001$) (Fig. 4C).

Heightened VEGF-C expression

VEGF-C expression in normal tail skin was low, consistent with earlier findings (24, 34). In the first days after lymphatic ligation, tail swelling and lymphatic vessel hyperplasia were already significant but VEGF-C expression remained low (Fig. 5). VEGF-C began to increase throughout the edematous tissue at day 7 ($P=0.037$) and peaked at day 14 ($P=0.022$). Expression remained high as the swelling began to resolve at day 21 ($P=0.014$), and was decreased to normal levels at day 30. VEGF-C was mostly concentrated in the hypodermis, where the swelling was maximal but few lymphatic vessels were present. Thus, while VEGF-C was upregulated in edematous tissue, its expression patterns did not necessarily correlate with lymphatic hyperplasia.

Dendritic cell migration

Langerhans dendritic cells reside in the epidermis and migrate to the lymphatics in response to immune challenges (35). In normal tissue, Langerin+ cells were seen both in the epidermis and in the dermis near lymphatic vessels (Fig. 6). However, these cells were confined to the epidermis after lymphatic ligation until day 14, where they appeared to be migrating towards the lymphatics despite the hyperplastic appearance and transport

insufficiencies of the lymphatic vessels (Fig. 6). Therefore, at days 14, 21, and 30, correlating with the peak and resolution phase of edema, these cells were present in the dermis near the hyperplastic lymphatic vessels, suggesting a return to normal function.

Increased fluid uptake and propensity for edema in MMP-9 null mice

In untreated (non-edematous) mice, the lymphatic capillary architecture was similar in MMP-9 null vs. wildtype control tails as visualized by microlymphangiography (Fig. 7A, B), although the lymphatic networks in MMP-9 null mice appeared much brighter than in control mice and took up 50% more fluid in 90 min at a fixed infusion pressure of 45 cm water than did the controls (12 vs. 8 μl). While there appeared to be minor indications of fluorescent tracer outside of the well-defined lymphatic vessels (Fig. 7B), there was little evidence of actual lymph leakage from the capillaries into the interstitium, as was clearly seen in edematous tails. This minor defects were likely the result of the increased brightness of the tail images resulting from increased tracer uptake (images were taken at the same exposure). Confocal imaging of the lymphatic vessels revealed no obvious differences in lymphatic vessel morphology from normal mice, suggesting that the increased fluid tracer uptake in untreated MMP-9 null mice was the result of either more efficient lymphatic transport or a higher hydraulic conductivity of extracellular matrix.

Surprisingly, despite the apparently normal or above normal functionality of the lymphatics, MMP-9 null mice with lymphatic ligation exhibited a far greater degree of swelling than did wild-type mice, particularly between 7 and 21 days ($P< 0.001$; Fig. 1), and took longer to resolve ($P<0.001$; Fig. 1). This swelling was so rapid and so extensive that it actually led to necrosis of the tail in a two of the seven mice tested. Examination of the extracellular matrix of the tail skin revealed that the collagen density of MMP-9 null mice was, in fact, less than that of the wild-type controls. This was the case both in untreated tails and those after 14 days of edema. Therefore, the increased tracer fluid uptake into the tail seen in untreated MMP-9 null mice was probably due to an increase in hydraulic conductivity. This difference in the matrix architecture, in conjunction with the inability to maintain tail volume during swelling, suggests that MMP-9 plays an important role in the maintenance of extracellular tissue fluid.

DISCUSSION

To help elucidate the pathophysiology of secondary lymphedema, we characterized and correlated key molecular-, cellular-, and tissue-level changes over time in the mouse tail edema model and demonstrated its reproducibility and sustainability. We found that in otherwise healthy tissue, sustained swelling induced by lymphatic ligation leads to lymphatic hyperplasia and VEGF-C upregulation. Interestingly, LEC proliferation began before VEGF-C upregulation, suggesting that lymphatic hyperplasia may be supported by VEGF-C only later, from day 14 (the peak in tail volume) through day 30. Also, the maximal VEGF-C expression was seen within the hypodermis, where most of the tail swelling was maintained but where lymphatic vessels were scarcer than in the dermis. This VEGF-C upregulation may therefore be a response to the accumulated fluid in the hypodermis.

Lymphatic vessel hyperplasia in the absence of VEGF-C presents a quandary when examining the potential for VEGF-C delivery as a therapy for lymphedema. While VEGF-C treatment has been shown to hasten the resolution of edema in the mouse tail model, this result was accomplished by hastening lymphangiogenesis across the ligation (22) rather than necessarily inducing a change in the local function of lymphatics. Therefore, delivery may only be beneficial in cases where transport insufficiencies are the result of a lack of lymphatic vessels in the tissue by inducing the growth of new lymphatic capillaries (17, 21, 22). Excess VEGF-C has also been shown to cause hyperplasia of lymphatic vessels when no other lymphatic defects were present (24). Therefore, our results, showing that increased VEGF-C and lymphatic hyperplasia is a response to tissue swelling, suggest that VEGF-C therapy may have limited use for treating secondary lymphedema.

In examining functional lymphatic uptake during lymphedema, we found that the disruption in lymphatic transport led to an increase in fluorescent tracer uptake during microlymphangiography in part from the well-established increase in hydraulic conductivity of the interstitium resulting from in the breakdown of the tail matrix (30, 36, 37). We also found that the dilated, hyperplastic lymphatics were less effective at lymph transport and leaked lymph back into the interstitium. It is not known whether or how the decreased lymphatic transport function contributed to the increased lipid accumulation in adipocytes.

In addition to decreased fluid drainage from the interstitium, hyperplastic lymphatics may exacerbate the edematous pathology by decreasing immune cell trafficking. When stimulated, Langerhans dendritic cells normally migrate from the epidermis into the lymphatic capillaries to traffic to lymph nodes for antigen presentation. In edematous skin, Langerhans

cells were not migrating through the dermis until day 14, even though other inflammatory responses like macrophages and massive matrix proteolysis were present earlier in lymphedema. Lack of migration may be due to the absence of migration-directing interstitial flow which only returns once edema is resolving, although it has yet to be demonstrated that interstitial flow specifically guides dendritic cells towards the lymphatics (35). This apparent lack of DC migration to lymphatics during tissue swelling may lead to decreased immune response, which in turn may exacerbate the pathological state of the limb. This notion is consistent with previous work showing that the immune response is compromised in edematous limbs (6), leaving the tissue more prone to infection and further inflammation.

MMP-9, a key MMP in matrix remodeling (31), appeared to play an important role in edema prevention. First, the collagen density in the dermis of MMP-9 null mice was lower than that in wildtype mice, both in normal and edematous states. This reduced matrix density may leave the tissue more susceptible to fluid accumulation and tissue swelling. Indeed, MMP-9 null mice were unable to sufficiently counteract the swelling through responsive remodeling of the matrix; the tail apparently relies on MMP-9 in remodeling the extracellular matrix to counteract the change in volume. Since all other studied factors appeared similar in response to wild type mice, the role of MMP-9 in this pathological state is that of matrix maintenance.

The reproducibility and sustainability of the mouse tail model of lymphedema was demonstrated across two normal strains and for roughly 20-30 days, respectively, although in some mice (for unknown reasons) edema can be sustained indefinitely (29). This time frame is sufficient to observe key features of chronic edema, including collagen breakdown and remodeling, lymphatic hyperplasia, and abnormal lipid accumulation in the skin, consistent with pathological features observed in longer studies in other models (21, 26, 27). Responsive changes in the dermal matrix during swelling – initial degradation followed by compensatory rebuilding – were also temporally correlated to lipid accumulation and macrophage infiltration throughout the tissue, both chronic indicators of lymphedema (4, 5).

In summary, the mouse tail model of lymphedema is reproducible, reliable, and shows many characteristics of chronic lymphedema. We found that sustained tissue swelling due to lymphatic blockage led to marked lymphatic hyperplasia and lipid accumulation, followed by substantial VEGF-C overexpression in the hypodermis. The hyperplastic lymphatic vessels were poorly functional at draining interstitial fluid, and the resulting fluid stagnation may have contributed to decreased Langerhans dendritic cell homing to the lymphatics. These correlations between factors regulating tissue homeostasis and those regulating lymphatic

biology during tissue swelling following lymphatic ligation raise important questions in considering treatment strategies aimed at lymphatic growth for alleviating secondary lymphedema.

ACKNOWLEDGEMENTS

The authors are grateful to Dr. Hugo Schmoekel and Veronique Garea for invaluable assistance with the animals, Miriella Pasquier for sectioning, and Sai T. Reddy and Gabriela Miyazawa for helpful assistance. The authors thank the NIH (RO1-HL075217-01), NSF (BES-0134551), and The Swiss National Science Foundation for funding.

REFERENCES

1. Rockson, S.G. 2001. Lymphedema. *Am J Med* 110:288-295.
2. Witte, M.H., Bernas, M.J., Martin, C.P., and Witte, C.L. 2001. Lymphangiogenesis and lymphangiodysplasia: from molecular to clinical lymphology. *Microsc Res Tech* 55:122-145.
3. Daroczy, J. 1995. Pathology of lymphedema. *Clin Dermatol* 13:433-444.
4. Schirger, A., Harrison, E.G., Jr., and Janes, J.M. 1962. Idiopathic lymphedema. Review of 131 cases. *Jama* 182:14-22.
5. Piller, N.B. 1990. Macrophage and tissue changes in the developmental phases of secondary lymphoedema and during conservative therapy with benzopyrone. *Arch Histol Cytol* 53 Suppl:209-218.
6. Olszewski, W.L., Engeset, A., Romaniuk, A., Grzelak, I., and Ziolkowska, A. 1990. Immune cells in peripheral lymph and skin of patients with obstructive lymphedema. *Lymphology* 23:23-33.
7. Foldi, E. 1998. The treatment of lymphedema. *Cancer* 83:2833-2834.
8. Mortimer, P.S. 1997. Therapy approaches for lymphedema. *Angiology* 48:87-91.
9. Oliver, G., and Alitalo, K. 2005. THE LYMPHATIC VASCULATURE: Recent Progress and Paradigms. *Annu Rev Cell Dev Biol* 21:457-483.
10. Wigle, J.T., and Oliver, G. 1999. Prox1 function is required for the development of the murine lymphatic system. *Cell* 98:769-778.
11. Harvey, N.L., Srinivasan, R.S., Dillard, M.E., Johnson, N.C., Witte, M.H., Boyd, K., Sleeman, M.W., and Oliver, G. 2005. Lymphatic vascular defects promoted by Prox1 haploinsufficiency cause adult-onset obesity. *Nat Genet* 37:1072-1081.
12. Gale, N.W., Thurston, G., Hackett, S.F., Renard, R., Wang, Q., McClain, J., Martin, C., Witte, C., Witte, M.H., Jackson, D., et al. 2002. Angiopoietin-2 is required for postnatal angiogenesis and lymphatic patterning, and only the latter role is rescued by Angiopoietin-1. *Dev Cell* 3:411-423.
13. Dagenais, S.L., Hartsough, R.L., Erickson, R.P., Witte, M.H., Butler, M.G., and Glover, T.W. 2004. Foxc2 is expressed in developing lymphatic vessels and other tissues associated with lymphedema-distichiasis syndrome. *Gene Expr Patterns* 4:611-619.
14. Brice, G., Mansour, S., Bell, R., Collin, J.R., Child, A.H., Brady, A.F., Sarfarazi, M., Burnand, K.G., Jeffery, S., Mortimer, P., et al. 2002. Analysis of the phenotypic abnormalities in lymphoedema-distichiasis syndrome in 74 patients with FOXC2 mutations or linkage to 16q24. *J Med Genet* 39:478-483.
15. Kriederman, B.M., Myloyde, T.L., Witte, M.H., Dagenais, S.L., Witte, C.L., Rennels, M., Bernas, M.J., Lynch, M.T., Erickson, R.P., Caulder, M.S., et al. 2003. FOXC2 haploinsufficient mice are a model for human autosomal dominant lymphedema-distichiasis syndrome. *Hum Mol Genet* 12:1179-1185.
16. Petrova, T.V., Karpanen, T., Norrmen, C., Mellor, R., Tamakoshi, T., Finegold, D., Ferrell, R., Kerjaschki, D., Mortimer, P., Yla-Herttuala, S., et al. 2004. Defective valves and abnormal mural cell recruitment underlie lymphatic vascular failure in lymphedema distichiasis. *Nat Med* 10:974-981.
17. Karkkainen, M.J., Saaristo, A., Jussila, L., Karila, K.A., Lawrence, E.C., Pajusola, K., Bueler, H., Eichmann, A., Kauppinen, R., Kettunen, M.I., et al. 2001. A model for gene therapy of human hereditary lymphedema. *Proc Natl Acad Sci U S A* 98:12677-12682.

18. Kukk, E., Lymboussaki, A., Taira, S., Kaipainen, A., Jeltsch, M., Joukov, V., and Alitalo, K. 1996. VEGF-C receptor binding and pattern of expression with VEGFR-3 suggests a role in lymphatic vascular development. *Development* 122:3829-3837.
19. Oh, S.J., Jeltsch, M.M., Birkenhager, R., McCarthy, J.E., Weich, H.A., Christ, B., Alitalo, K., and Wilting, J. 1997. VEGF and VEGF-C: specific induction of angiogenesis and lymphangiogenesis in the differentiated avian chorioallantoic membrane. *Dev Biol* 188:96-109.
20. Pytowski, B., Goldman, J., Persaud, K., Wu, Y., Witte, L., Hicklin, D.J., Skobe, M., Boardman, K.C., and Swartz, M.A. 2005. Complete and specific inhibition of adult lymphatic regeneration by a novel VEGFR-3 neutralizing antibody. *J Natl Cancer Inst* 97:14-21.
21. Szuba, A., Skobe, M., Karkkainen, M.J., Shin, W.S., Beynet, D.P., Rockson, N.B., Dakhil, N., Spilman, S., Goris, M.L., Strauss, H.W., et al. 2002. Therapeutic lymphangiogenesis with human recombinant VEGF-C. *Faseb J* 16:1985-1987.
22. Yoon, Y.S., Murayama, T., Gravereaux, E., Tkebuchava, T., Silver, M., Curry, C., Wecker, A., Kirchmair, R., Hu, C.S., Kearney, M., et al. 2003. VEGF-C gene therapy augments postnatal lymphangiogenesis and ameliorates secondary lymphedema. *J Clin Invest* 111:717-725.
23. Jeltsch, M., Kaipainen, A., Joukov, V., Meng, X., Lakso, M., Rauvala, H., Swartz, M., Fukumura, D., Jain, R.K., and Alitalo, K. 1997. Hyperplasia of lymphatic vessels in VEGF-C transgenic mice. *Science* 276:1423-1425.
24. Goldman, J., Le, T.X., Skobe, M., and Swartz, M.A. 2005. Overexpression of VEGF-C causes transient lymphatic hyperplasia but not increased lymphangiogenesis in regenerating skin. *Circ Res* 96:1193-1199.
25. Han, L.Y., Chang, T.S., and Hwang, W.Y. 1985. Experimental model of chronic limb lymphedema and determination of lymphatic and venous pressures in normal and lymphedematous limbs. *Ann Plast Surg* 15:303-312.
26. Olszewski, W. 1973. On the pathomechanism of development of postsurgical lymphedema. *Lymphology* 6:35-51.
27. Kanter, M.A., Slavin, S.A., and Kaplan, W. 1990. An experimental model for chronic lymphedema. *Plast Reconstr Surg* 85:573-580.
28. Wang, G.Y., and Zhong, S.Z. 1985. A model of experimental lymphedema in rats' limbs. *Microsurgery* 6:204-210.
29. Slavin, S.A., Van den Abbeele, A.D., Losken, A., Swartz, M.A., and Jain, R.K. 1999. Return of lymphatic function after flap transfer for acute lymphedema. *Ann Surg* 229:421-427.
30. Swartz, M.A., Kaipainen, A., Netti, P.A., Brekken, C., Boucher, Y., Grodzinsky, A.J., and Jain, R.K. 1999. Mechanics of interstitial-lymphatic fluid transport: theoretical foundation and experimental validation. *J Biomech* 32:1297-1307.
31. Stamenkovic, I. 2003. Extracellular matrix remodelling: the role of matrix metalloproteinases. *J Pathol* 200:448-464.
32. Swartz, M.A., Berk, D.A., and Jain, R.K. 1996. Transport in lymphatic capillaries. I. Macroscopic measurements using residence time distribution theory. *Am J Physiol* 270:H324-329.
33. Hagendoorn, J., Padera, T.P., Kashiwagi, S., Isaka, N., Noda, F., Lin, M.I., Huang, P.L., Sessa, W.C., Fukumura, D., and Jain, R.K. 2004. Endothelial nitric oxide synthase regulates microlymphatic flow via collecting lymphatics. *Circ Res* 95:204-209.
34. Boardman, K.C., and Swartz, M.A. 2003. Interstitial flow as a guide for lymphangiogenesis. *Circ Res* 92:801-808.

35. Randolph, G.J., Angeli, V., and Swartz, M.A. 2005. Dendritic-cell trafficking to lymph nodes through lymphatic vessels. *Nat Rev Immunol* 5:617-628.
36. Bert, J.L., and Reed, R.K. 1995. Flow conductivity of rat dermis is determined by hydration. *Biorheology* 32:17-27.
37. Aarli, V., and Aukland, K. 1991. Oedema-preventing mechanisms in a low-compliant tissue: studies on the rat tail. *Acta Physiol Scand* 141:489-495.

FIGURE LEGENDS

Fig. 1. Tail volume changes following lymphatic ligation. Two control strains of mice, FVB/NJ (blue diamonds) and BALB/c (red squares), displayed nearly equivalent swelling and resolution patterns, and both peaked at 15 days. Transgenic mice lacking MMP-9 (green triangles) also displayed maximum volume increase at 15 days, but showed a significantly greater extent of swelling compared to the wild type strains as well as a longer resolution time.

Fig. 2. Extracellular matrix density, lipid accumulation, and macrophage presence in edematous tails. (A) In normal skin, a collagen-dense dermis (gold arrow) and less dense hypodermis (white arrow) was seen. One day following lymphatic ligation, the collagen network was degraded in both the dermis and hypodermis as fluid accumulated. At day 14 when tail volume reaches its peak, the collagen density in the dermis returned to normal (gold arrow) while the architecture of the hypodermis remains severely compromised. At day 30, the collagen architecture throughout the tissue appeared normal. (B) Oil Red O staining showed that the hypodermis dramatically filled with lipids (red) at day 7 and that this accumulation was maintained through 30 days. (C) Macrophages (red) were also present in high numbers at all times during edema. Note the hyperplastic lymphatic (green) vessels at days 7 and 14 (marked by white arrows) as compared to normal vessels (gold arrows). Scale bars = 200 μm.

Fig. 3. Fluorescence microlymphangiography revealed leaky lymphatic capillaries in edematous skin, with higher magnification images shown at right. The normal mouse tail skin possessed a well-defined hexagonal network of dermal lymphatics that transport the fluorescent tracer proximally (left to right) from infusion into the tip of the tail. At 10 days of lymphedema, the tail was swollen and the fluorescent tracer filled both the lymphatic vessels and the interstitial space (back flow indicated by arrows). At 60 days, the lymphatic transport was mostly returned to normal. All images were taken with the same exposure time. Scale bars = 2 mm.

Fig. 4. Lymphatic morphology changes during edema. (A) Normal tissue showed few proliferating cells and small superficial lymphatics (gold arrow heads) with the underlying collecting lymphatic vessels (white arrow heads). PCNA staining indicates that as the tail

volume increased, lymphatic endothelial cells (LECs) proliferated (white arrows). At day 10, LECs in the vessels were proliferating and the vessels were hyperplastic. This LEC proliferation is reduced at 20 days and absent at 30 days. Edema also induced the proliferation of other cells in the tail (gold arrows) (B) Confocal microscopy of the dermal lymphatic vessels forming the hexagonal network in the tail demonstrated the drastic hyperplasia and morphological changes associated with edema at 7 and 14 days, with an abnormal morphology still present at 30 days. Scale bars = 100 μm. (C) The number of LECs per lymphatic structure was greatest at day 7 in both wild type and MMP-9 deficient mice (* indicates $P<0.05$ over control).

Fig. 5. VEGF-C expression in edematous tails. (A) VEGF-C expression (black) was normally quite low and remains so during the onset of edema (through 7 days); orange indicated collagen by orange G staining. At 14 days, however, VEGF-C was greatly increased and remained so during resolution at day 21. Bar = 200 μm (B) The peak of VEGF-C expression (integrated intensity) lagged behind the peak of LEC proliferation and vessel hyperplasia (* indicates $P<0.05$ vs. control).

Fig. 6. Langerhans dendritic cell (DC) trafficking during edema. In normal skin, some DCs were seen between the epidermis and lymphatic vessels (green) in the skin, indicating normal migration. After 7 days of edema, no DCs could be found below the epidermis. At 14, 21, and 30 days, DCs were present in high numbers in the dermis and near the hyperplastic lymphatic vessels, indicating migration. Yellow arrows indicate some DCs in the epidermis, and white arrows indicate migrating DCs. Bar = 200 μm.

Fig. 7. Differences in lymphatic function and morphology and extracellular matrix architecture in MMP-9 null mice vs. wild type controls. (A) In untreated animals, constant-pressure infusion of fluorescent tracer led to 50% more uptake by MMP-9 null mice vs. wildtype controls. The lymphatic vessel networks of the MMP-9 null mice appeared to be much brighter (with equal exposure time) than those of the wildtype controls, indicating a higher uptake rate. Bar = 2 mm. (B) Higher magnification images of the lymphatic structures showed normally functioning vessels with no backflow. Bar = 2 mm. (C) Confocal images of the lymphatic vessels in each type of mouse showed little or no morphological differences between wildtype and MMP-9 null mice; bar = 100 μm. (D) In untreated animals, the collagen matrix (blue) appeared to be less dense in the dermis of the MMP-9 null mice than in that of

the FVB/NJ mice. Bar = 200 μm. (E) After 14 days of edema, the dermal collagen density appeared normal in the wild-type control mice but remained largely degraded in the MMP-9 null mice. Bar = 200 μm.

This page is intentionally left blank.

Figure 1

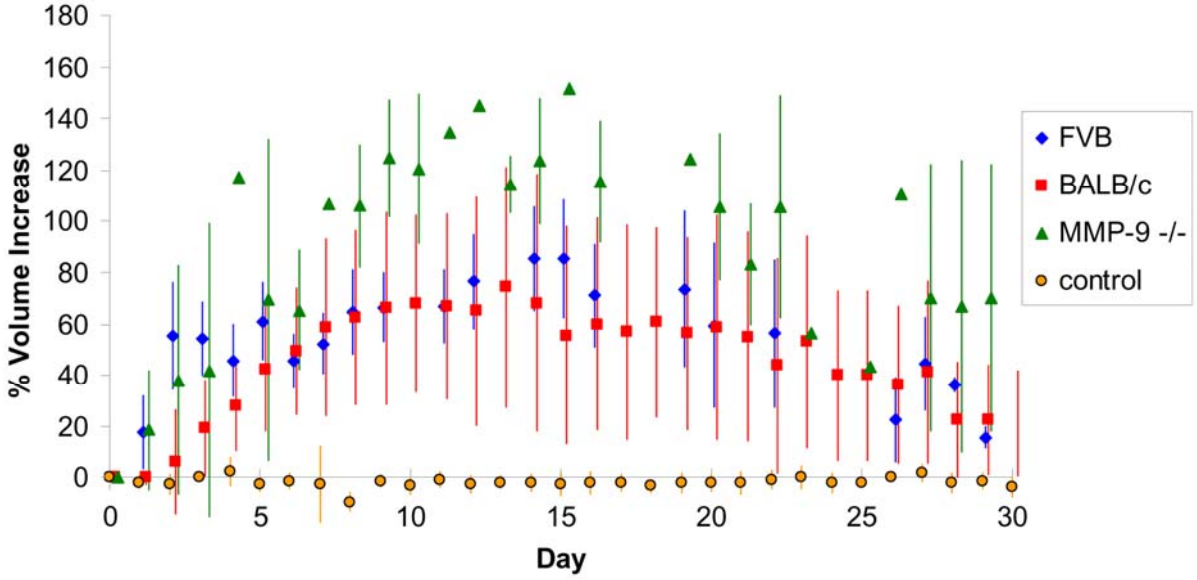
% Volume Increase
180
160
140
120
100
80
60
40
20
0
0
5
10
15
20
25
30
Day
FVB
BALB/c
MMP-9 -/-
control

This page is intentionally left blank.

Figure 2

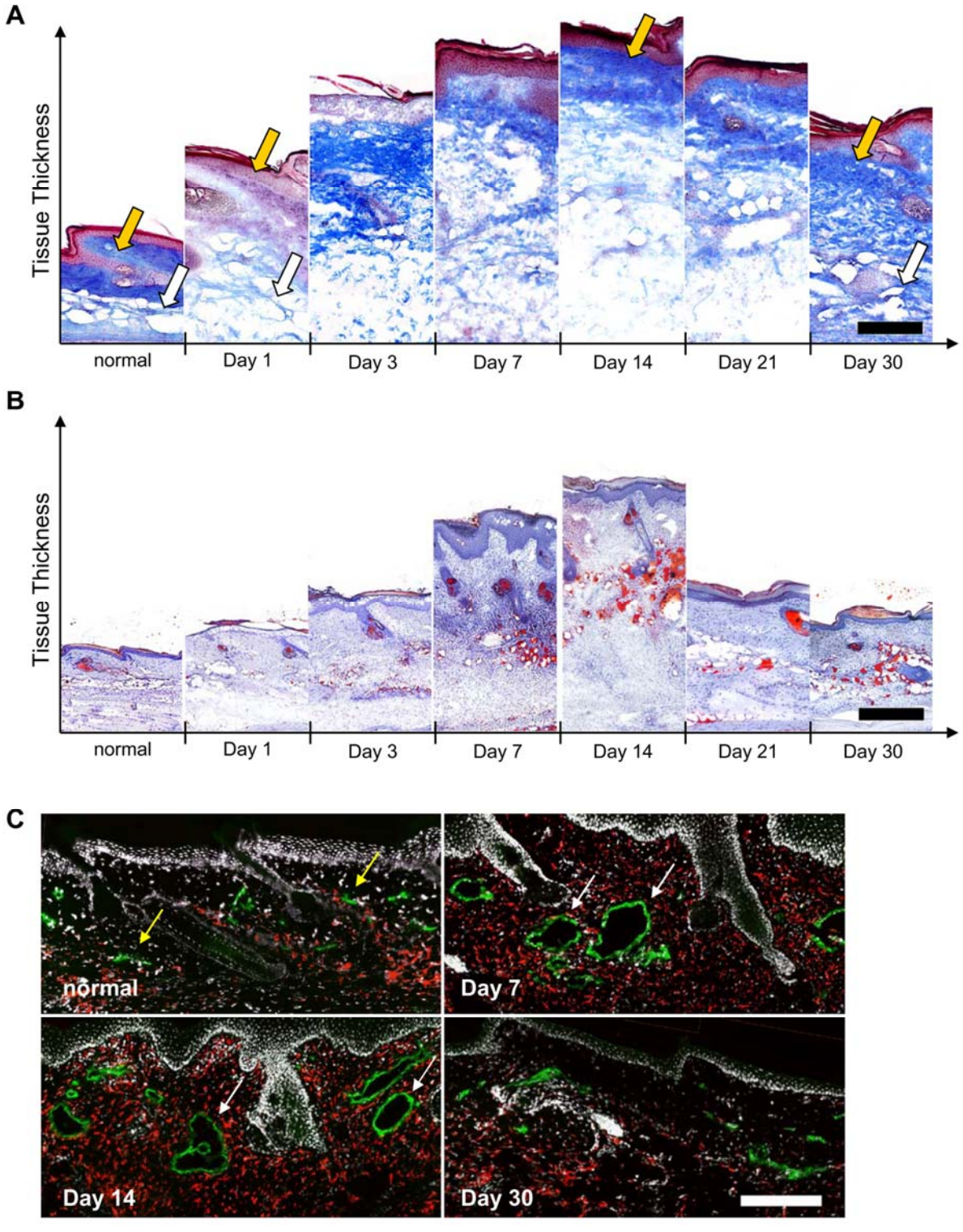
A
Tissue Thickness
normal
Day 1
Day 3
Day 7
Day 14
Day 21
Day 30
B
Tissue Thickness
normal
Day 1
Day 3
Day 7
Day 14
Day 21
Day 30
C
normal
Day 7
Day 14
Day 30

This page is intentionally left blank.

Figure 3

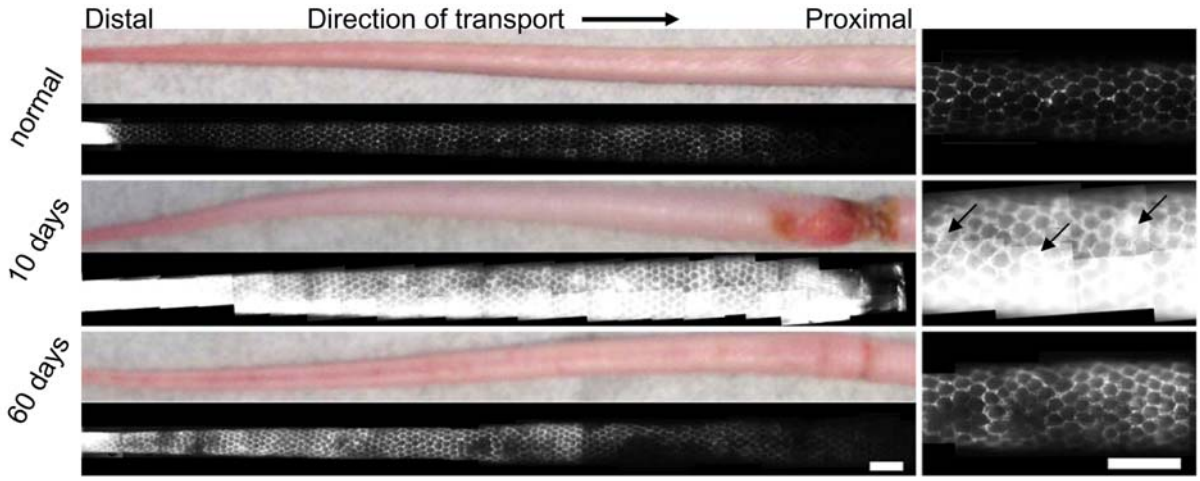
Distal
Direction of transport
Proximal
normal
10 days
60 days

This page is intentionally left blank.

Figure 4

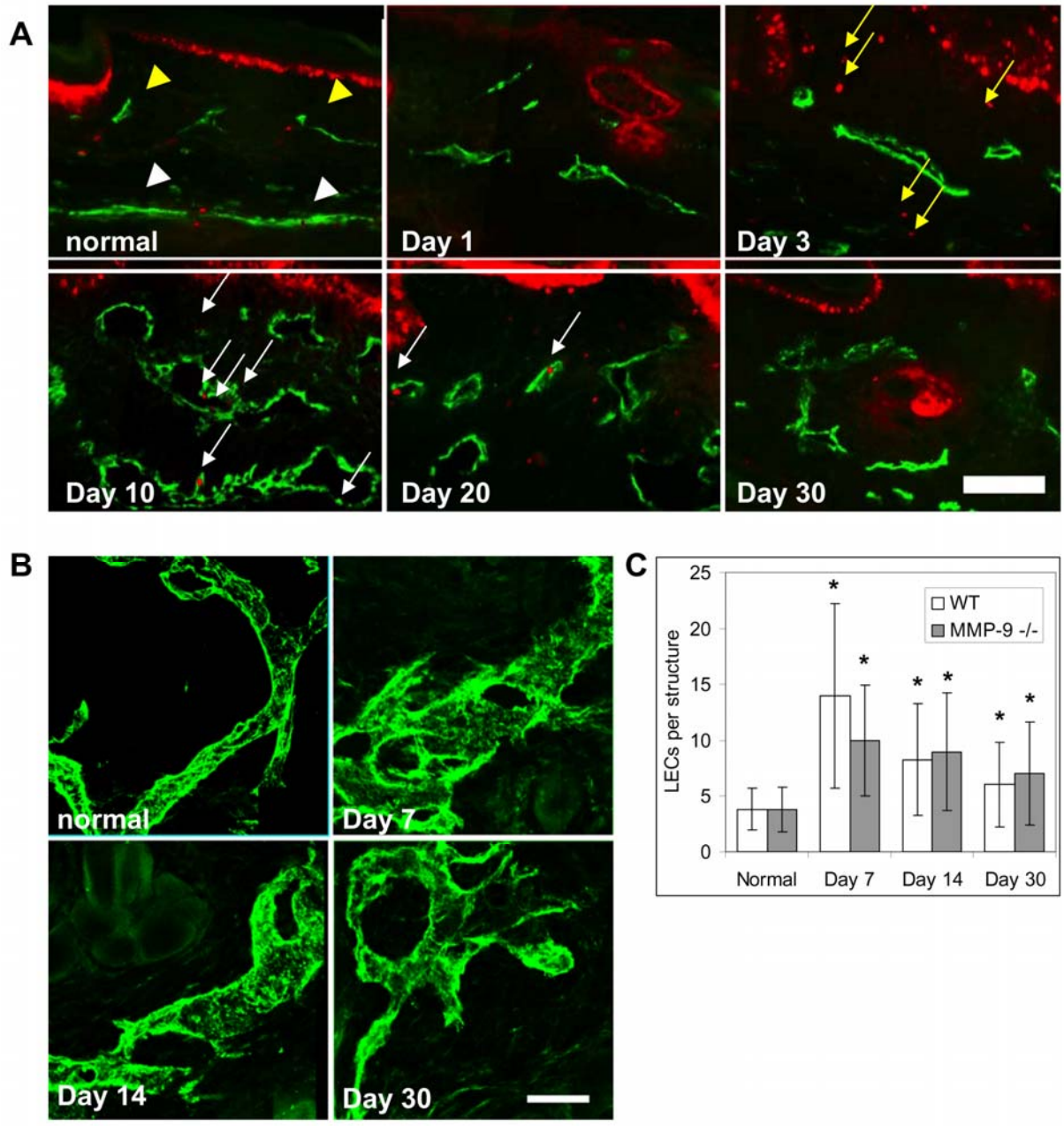
A
normal
Day 1
Day 3
Day 10
Day 20
Day 30
B
normal
Day 7
Day 14
Day 30
C
LECs per structure
25
20
15
10
5
0
WT
MMP-9 -/-
Normal
Day 7
Day 14
Day 30

This page is intentionally left blank.

Figure 5

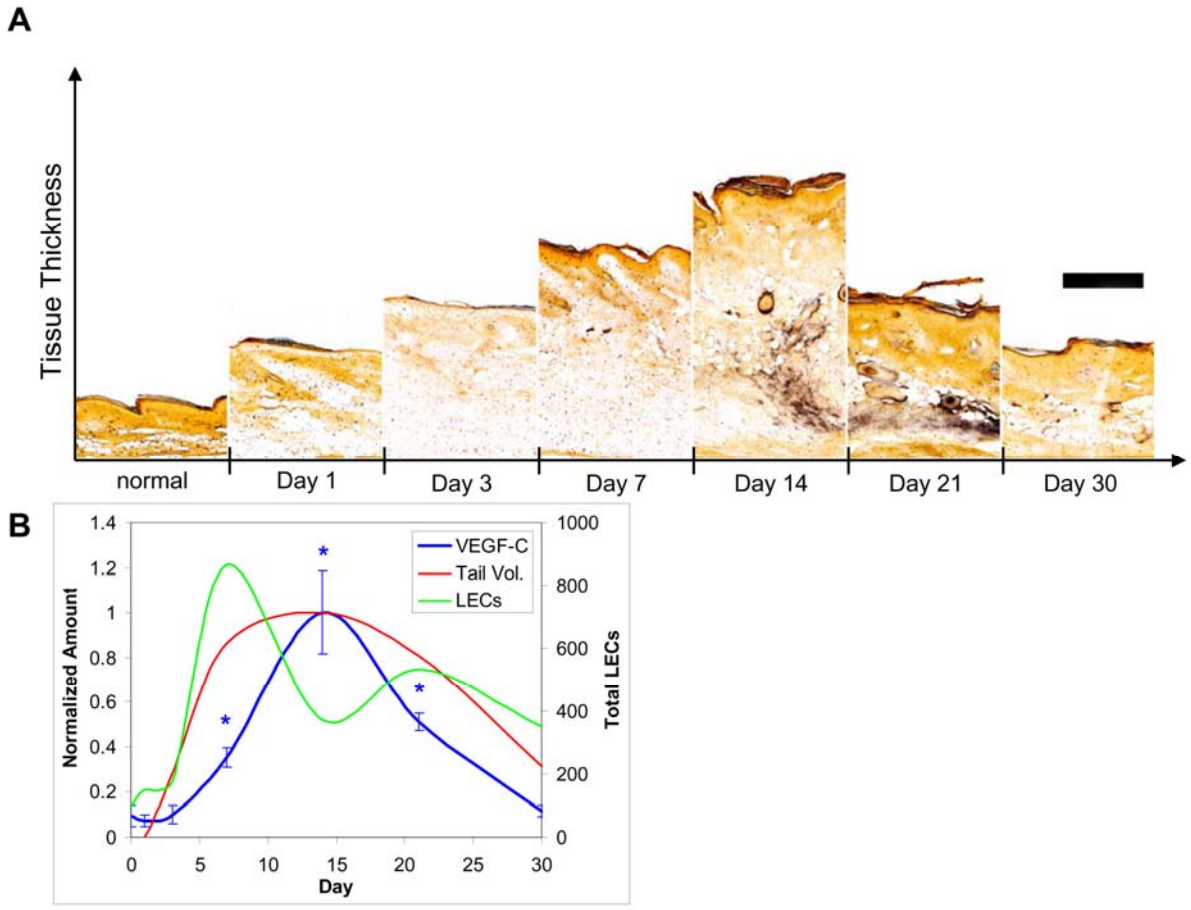
A
Tissue Thickness
normal
Day 1
Day 3
Day 7
Day 14
Day 21
Day 30
B
Normalized Amount
Total LECs
Day
VEGF-C
Tail Vol.
LECs
0
0.2
0.4
0.6
0.8
1
1.2
1.4
0
200
400
600
800
1000
0
5
10
15
20
25
30

This page is intentionally left blank.

Figure 6

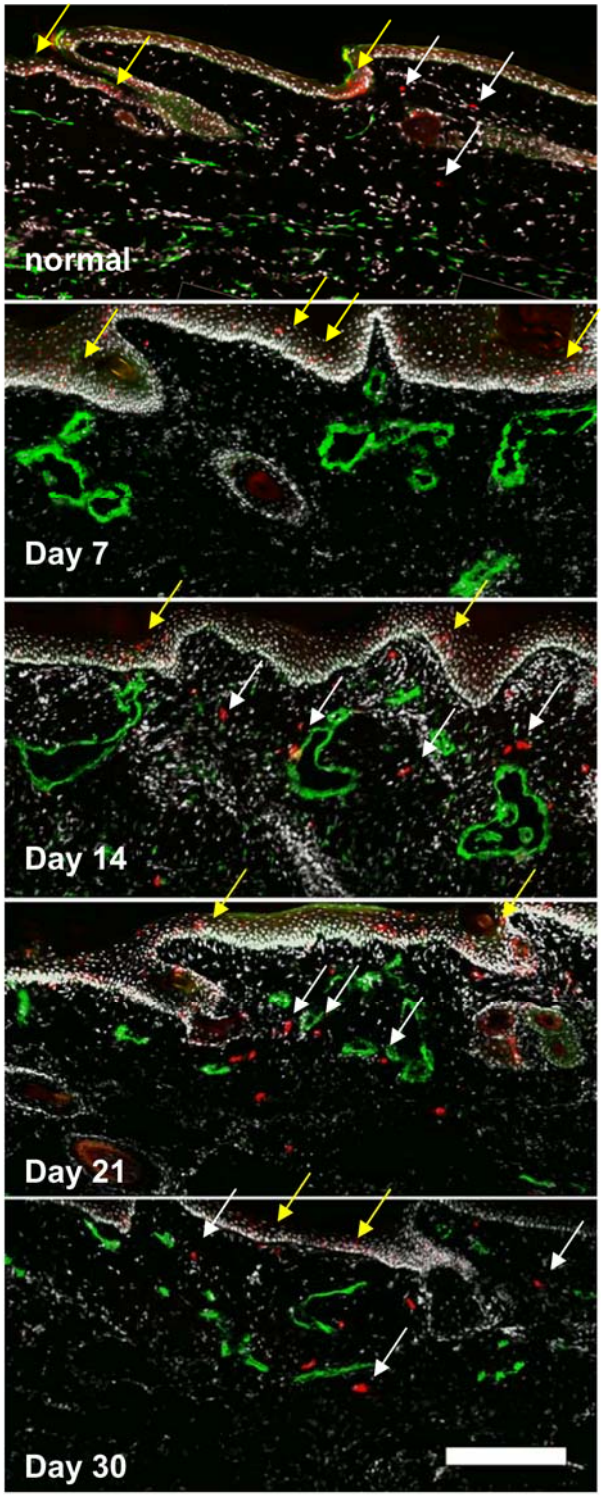

This page is intentionally left blank.

Figure 7

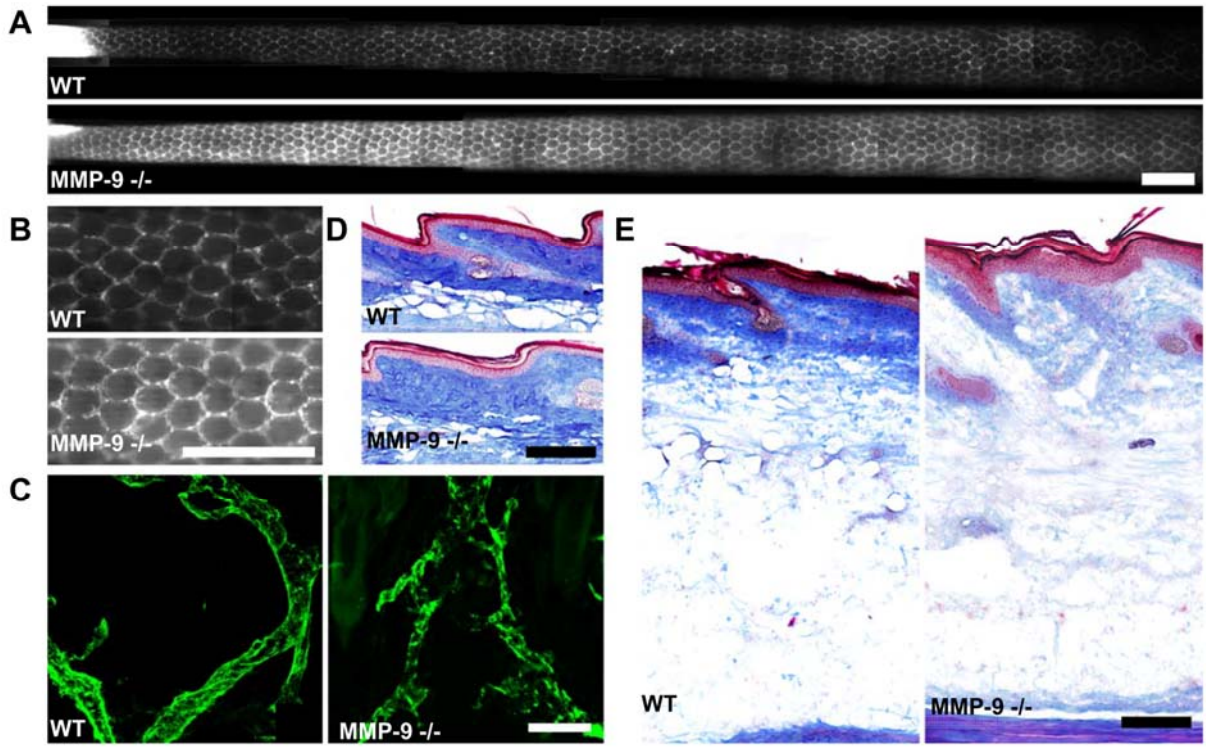

This page is intentionally left blank.

CHAPTER 6:
ORIGINAL MANUSCRIPT 5

A noninvasive, quantitative model for evaluating lymphatic uptake and tissue hydraulic conductivity in the mouse

Joseph M. Rutkowski and Melody A. Swartz

Institute of Bioengineering, École Polytechnique Fédérale de Lausanne (EPFL), Switzerland

Prepared for submission to ***Journal of Applied Physiology***

ABSTRACT

Flow through the interstitium is an important morphogenetic driving force that is present in nearly all tissues. The uptake of interstitial fluid is the primary function of lymphatic capillaries. In this capacity, they are the modulators of interstitial flow: fluid extravasated from blood capillaries is transported across the interstitium to the lower pressure lymphatic capillary. The other chief parameter controlling the ease at which fluid moves through the extracellular matrix is the tissue hydraulic conductivity. Coupled together, lymphatic capillary uptake and tissue hydraulic conductivity dictate interstitial flow rates and, therefore, are important parameters with which to describe the potential morphogenetic impact of flow on cells within the interstitium. Here, we present a simple poroelastic model of interstitial fluid flow and lymphatic capillary uptake that can be used to quantify physiologic *in vivo* lymphatic function and tissue hydraulic conductivity in the mouse tail. The implications of lymphatic dysfunction within tissues are described and the governing equations for tissue hydraulic condictvity are subsequently reformulated in a model of primary lymphedema, the K14-VEGFR-3-Ig mouse. The model is then applied to a mouse model in which we discovered lymphatic hyperplasia, the Apolipoprotein E (ApoE) knockout mouse. In this model, our model's calculations demonstrate a significant reduction in capillary function. Additionally, this provides the first direct experimental evidence linking dyslipidema and lymphatic capillary function. Thus, the quantitative model is sufficiently sensitive to detect changes not only when lymphatics are functional, but also to determine the consequential effects of lymphatic molecular responses. This model is therefore ideal to examine baseline lymphatic function and tissue hydraulic conductivity in transgenic mouse models where these physiologic parameters would be highly influential to the results of inflammation, lymphedema, or immune cell responses.

INTRODUCTION

Lymphatic capillaries reside in nearly all tissues of the body to drain fluid, macromolecules, and cells that have extravasated from the blood circulation (1). In doing so, interstitial flow is directed from the blood capillary to the lymphatic circulation by means of the hydrostatic pressure difference between the two systems (2). Due to the important morphogenetic effects of interstitial flow on cells that reside in and traverse the interstitium (2), understanding flow through the interstitium is important when exploring cell behavior in *in vivo* and in 3-D *in vitro* models.

Due to their critical role in maintaining tissue fluid balance, understanding the uptake and transport of fluid via lymphatic vessels is an important aspect of tissue physiology. Very little, to date, is known about the capacity of normal, healthy lymphatic capillaries to uptake fluid (3); even less is known about pathological states such as lymphedema, where drainage is dramatically reduced or nonexistent (4, 5) or in inflammation, where flows are greatly increased (6). Coupling lymphatic uptake of fluid to interstitial transport is thus a goal in understanding tissue homeostasis.

Tissue exists essentially as a saturated sponge, with fluid flow driven not only by changes in hydrostatic pressure, but flow also being induced by matrix deformation as, for example, in articular cartilage (7); and in turn, flow potentially deforming the matrix. Matrix mechanics are thus a critical component in modulating lymphatic function (1, 8). This makes for potentially complex mathematics if the real-world scenario is modeled. Fortunately, flow through fibrous matrices has been previously modeled to quantify interstitial flow (elegantly reviewed in (9, 10)); the use of a poroelastic model to describe fluid movement through the extracellular matrix has also been performed (11, 12).

Here, we attempt to clarify the mathematics associated with these models and simplify these to parameters readily obtainable through simple experiments for determining tissue hydraulic conductivities and lymphatic uptake *in vivo*. The mathematical models are then applied to transgenic mouse models representing lymphatic dysfunction, lipid metabolic disorder, and inhibited pathological lymphangiogenesis.

METHODOLOGY

Assumptions

These calculations all base themselves in soil mechanics and its subsequent mechanical models. Soil mechanics function as an ideal model for the interstitium, if, for example, an analogy between this tissue and soil is made based on Terzaghi's principles for a matrix of soil. The assumptions:

(a) Homogenous, isotropic matrix
(b) Matrix is 100% saturated
(c) Both solid and liquid phase are incompressible
(d) Solid phase behaves as a linear elastic solid
(e) Strains to the matrix are relatively small
(f) Darcy's Law can be applied for hydrostatic gradients
(g) Permeability and compressibility constants remain constant
(h) There exists a unique relationship between stress and void ratio, dependent on time

With these assumptions in place, a simple mechanical model can be applied using fundamental governing equations for poroelastic theory.

Developing the governing equations

Equation 1 represents a momentum balance for the interstitium as a whole. Stresses are at equilibrium, and inertial effects and body forces are neglected.

(1) $\nabla \bullet \tau = 0$

The constitutive equation for a linear elastic solid is given as:

(2) $\tau = -P\mathbf{I} + \lambda e\mathbf{I} + 2\mu\varepsilon$

where e is the dilatation of the solid matrix, λ and μ are the Lamé parameters (material constants) and ε is the infinitesimal strain tensor. The other governing equation is Darcy's Law for flow through porous medium, Equation 7. First, however, Equations 1 and 2 are combined and simplified by further defining their parameters:

(3) $e = \nabla \bullet \mathbf{u}$

The dilatation of the solid phase is equal to the divergence of **u**, the solid displacement vector.

(4) $\varepsilon = \frac{1}{2}(\nabla \mathbf{u} + \nabla \mathbf{u}^T)$

Equation 4 represents the strain tensor as defined by displacement in a linear elastic solid. If the solid is undergoing purely hydrostatic pressure, there are no shear components and $\mathbf{u}^T$=**u**. Similarly, the strain tensor will thus only have diagonal components; in pure hydrostatic pressure, the divergence of ε equals the gradient of e:

(5) $\nabla e = \nabla \bullet \varepsilon$

These relationships (Eq. 3-5) thereby allow us to combine Eq. 1 and 2 into a more applicable relationship:

(6) $\nabla P = (\lambda + 2\mu)\nabla e$

Equation 6 demonstrates the direct relationship as to how changes in pressure affect matrix dilation, and vice versa. Returning to Darcy's Law of flow through a porous medium; this is defined to obtain the velocity of the interstitial fluid, **v**, relative to the solid network. In this form, the dilatation of the solid phase is coupled:

(7) $\phi\left(\mathbf{v} - \frac{\partial \mathbf{u}}{\partial t}\right) = -K\nabla P$

where Φ is the fluid volume fraction and K is the effective hydraulic conductivity of the tissue. Combining the rate of change of the liquid phase and the rate of change of solid phase, each represented by the divergence of the respective term, and fluid losses, Equation 8 is obtained:

(8) $\nabla \bullet \phi\left(\mathbf{v} - \frac{\partial \mathbf{u}}{\partial t}\right) + \nabla \bullet \frac{\partial \mathbf{u}}{\partial t} + J_v = 0$

where J_v is the fluid input or output, or flux. This equation was previously developed (12) and more elegantly written combined as Equation 9. In this form the flux is written as the resultant changes in the fluid or matrix:

$$(9)\ \nabla \bullet \left(\phi \mathbf{v} + (1-\phi)\frac{\partial \mathbf{u}}{\partial t} \right) = -J_v$$

As a combined continuity equation for flux through the interstitium, the average interstitial fluid velocity and solid matrix displacement vector equal interstitial fluid generation from blood capillary extravastion (11) or interstitial fluid drainage by lymphatic capillaries (12), or a combination of both. Since the governing equation of this model is effectively the conservation of mass, it is perhaps useful to rewrite Eq. 9 in terms of tissue strain, where the form becomes analogous to Fick's second law of diffusion with reaction:

$$(10)\ \frac{\partial e}{\partial t} - K(2\mu + \lambda)\nabla^2 e + J_v = 0$$

Here, dilatation is analogous to the reactive species. Changes in dilatation result in either pseudo-diffusion through the tissue governed by $K(2\mu+\lambda)$ – analogous to the diffusion coefficient D_{ab} – and a pseudo-reaction term represented by the flux term. Flux, or the hydrostatic pressure-driven uptake into lymphatic capillaries, is defined by:

$$(11)\ J_v = \beta(P_i - P_b) = \beta P^*$$

where the newly introduced β is defined as the lymphatic conductance in volume of fluid drained by the vessels per volume of tissue with respect to time and pressure (final units of reciprocal time and pressure) and P* is defined as the hydrostatic pressure driving force between the pressure in the interstitium, P_i, and the baseline physiologic pressure, P_b. Coupling Equations 10 and 11, the final governing equation is achieved:

$$(12)\ \frac{\partial e}{\partial t} - K(2\mu + \lambda)\nabla^2 e + \beta P^* = 0$$

Factors influencing lymphatic uptake

Uptake into lymphatic capillaries is similar to the well-described phenomenon of blood capillary extravasation; a fundamental equation can be used to explore how changes in Starling's Law for transcapillary transport affect the interstitium and vice versa. Starling's Law in its complete form, for blood capillary extravasation:

$$(13)\ J_v = Lp\left(\left(P_{capillary} - P_{\text{int}erstitium}\right) + \sigma\left(\pi_{capillary} - \pi_{\text{int}erstitium}\right)\right)$$

where the flux is related to the hydrostatic driving force, as well as the osmotic pressure driving force, $\Delta\pi$. Lymphatic intravasation is represented by the appropriate directional changes to the driving forces. Physiologically, flux into lymphatic vessels is predominantly intercellular, where lymphatic cell-cell junctions are opened – almost valve-like – to accommodate flow (6, 13). It is therefore reasonable to neglect osmotic differences because interstitial fluid predominantly flows directly into the lymphatic capillary. The filtration coefficient, *Lp*, is dependent on vessel wall area and wall hydraulic conductivity. In blood capillaries, a basement membrane and pericytes affect the wall hydraulic conductivity, but, again, physiologically this is irrelevant for the initial lymphatics. Hence, when *Lp* is redefined as β above (Equation 11), it is essentially the ease at which fluid is taken across the lymphatic capillary wall. Vessel diameter and vessel density will be the contributing physical parameters to lymphatic vessel wall area in any volume of tissue.

Lymphatic endothelial cell-cell junctions, which presumably mediate the open connections through which interstitial fluid enters the capillary, will molecularly contribute to lymphatic flux. Repulsion of cell-cell contacts, for example, by podocalyxin expression, may also inversely contribute (14). Changes in the expression of these molecules (e.g., VE-cadherin) may result in changes in uptake. Indeed, during heightened shear conditions and in inflammation, where flows are increased, molecular expression of cell-cell connections is also altered (6, 13, 15)(Yong, C., et al. unpublished). Equally important in lymphatic drainage during increased flows are cell-matrix interactions. Anchoring filaments that link lymphatic endothelial cells to the matrix permit the capillary to open with increase interstitial fluid pressure in the matrix (Fig. 1). Heightened shear also alters the expression of these molecules in lymphatic endothelial cells (Yong, C., et al. unpublished). While incapable of transporting larger molecules, aquaporin expression may also mediate transcellular water flux across the capillary wall (16). Resultantly, the changes in LEC molecular expression are coupled into β

when calculating lymphatic conductance experimentally. The experimental model should thus be able to detect not only anatomical differences in the lymphatic network, but also the active response of LECs to changes in interstitial flow, molecular agonists, or genetic mutation.

Factors influencing hydraulic conductivity

Hydraulic conductivity is a physical property of the tissue. It will change with changes in matrix composition and density, as well as the tissue saturation. Physiologic tissues are wholly saturated, but the ratio of fluid to solid will affect the overall porosity, or cross-sectional area accessible to fluid flow. Tissues with higher lipid content per volume (e.g., obese or edematious) would have a lower area accessible to flow due to (a) the hydrophobicity of the lipds and (b) the inability of flow to pass directly through cells – in this case adipocytes – that have taken up the lipid. Matrix components such a proteoglycans also posses dense negative charges that inhibit free flow of fluid through the matrix. Further discussion on how the matrix impacts hydraulic conductivities is found in the excellent Levick review (9).

EXPERIMENTAL DESIGN

A fluorescent tracer is slowly infused into the tail tip of an anesthetized mouse beginning at t=0. Flow is driven by a small application of hydrostatic pressure using a water column (Fig. 2) set at 40, 45, 50, and 55 cmH_2O. As the applied pressures are higher than baseline tail pressure, P_b, flow into and through the tissue is created. Very small, constant pressures are essential to maintain the tissue state according to our assumptions (e.g., minimal matrix strain at steady state) and to allow the lymphatic capillary uptake of the infused fluid to reach steady-state with the infusion.

The infusion flowrate, Q, is constantly monitored by tracking a small amount of air drawn into the tubing that separates the water (used to supply the pressure head) from the infused tracer (2% fluorescently-labeled dextran). The distance, x, that fluorescent tracer has traveled through the tail is also monitored by fluorescence microscopy. For each pressure, sufficient time is given for the interstitial transport and lymphatic uptake to reach steady state before the next pressure is applied [This characteristic time can be estimated to be $1/\beta P_0^*$, or approximately 14 minutes based on past measurements of β and K (12)].

Because the physical geometry in the mouse tail is assumed to be purely axial flow, in a symmetric rod geometry, with lymphatic drainage being the outlet of flow, it is easy to recall a symmetric, one-dimensional differential form of the solution in Eq. 6 for the constitutive equation:

$$(14)\ \frac{\partial P^*}{\partial x} = (2\mu + \lambda)\frac{\partial e}{\partial x}$$

Combining Eqs. 12 and 14, strain is directly related to the applied force, pressure, and the governing equation can be re-written in terms of hydrostatic pressure:

$$(15)\ \frac{1}{(2\mu + \lambda)}\frac{\partial P^*}{\partial t} - K\frac{\partial^2 P^*}{\partial x^2} + \beta P^* = 0$$

The distribution of pressure is controlled by the "stress diffusivity" $K(2\mu+\lambda)$, or K^*, and the overall lymphatic conductance $\beta(2\mu+\lambda)$, or β^*. Solving this equation is non-trivial; however, the solution is available in mathematics texts. The boundary conditions are set for P^* as $P^*(0, t)=P^*_0$, $P^*(\infty, t)=0$, and $P^*(x, 0)=0$, where P_0 is the applied pressure ($P_0=P_b$) at the tail tip. Introducing the term $\alpha=\sqrt{(K/\beta)}$ allows for a characteristic penetration length that will govern the steady-state pressure profile, and also permits the final solution for $P^*(x,t)$:

$$(16)\ P^*(x,t) = P^*_0\left(\frac{1}{2}e^{-x/\alpha}\operatorname{erfc}\left(\frac{x}{2\sqrt{K^*t}} - \sqrt{\beta^* t}\right) + \frac{1}{2}e^{x/\alpha}\operatorname{erfc}\left(\frac{x}{2\sqrt{K^*t}} + \sqrt{\beta^* t}\right)\right)$$

Steady-State Approximation

While the complete solution for P^* may appear to be quite complicated, at steady-state ($t\rightarrow\infty$) the equation readily describes the behavior of the pressure profile at to be exponential decay, governed by the ratio α, or the resistance to flow of the tissue versus uptake by the lymphatic capillaries:

$$(17)\ P^*_{ss} = P^*_0\, e^{-x/\alpha}$$

Using this steady-state relationship, the length, L, which is the penetration depth of the infused fluid (Figure 1), can be solved for by applying P^*_{ss} to Darcy's Law for the average fluid velocity.

(18) $\bar{\mathbf{v}} = -K\nabla P = \sqrt{\beta K}\, P^*_0\, \mathrm{e}^{-L/\alpha}$

The penetration length can then be solved in terms of the ratio, α:

(19) $L = -\alpha \ln \frac{P^*_L}{P^*_0} = \alpha \ln \frac{P^*_0}{P^*_L} = \alpha\left(\ln P^*_0 - \ln P^*_L\right)$

In this simple form, it would be possible to readily obtain α by measuring the penetration depth versus the applied pressure P^*_0. The term P^*_L need not be defined. The only necessity is that the ratio P^*_L / P^*_0 be sufficiently small so that convection due to the applied pressure is minimized at L. Also, the measurement of L must be consistently performed at each pressure so as to not to permit any diffusion of the infused solute to skew the necessary length (the time of each measurement period can likewise be shortened so as to eliminate this potential). As the experimental procedure utilizes a fluorescent solute, L can be repeatedly and confidently measured by taking the average fluorescent intensity along the tail length and calculating the distance of the "moving front". Because lymphatic uptake is in equilibrium with axial fluid movement at steady state, after a short time L remains constant at any applied pressure (Fig. 3A). As discussed, at steady-state x becomes the constant L because the infusion flow rate, Q_{ss}, is equivalent to the lymphatic uptake taken over the length, L. If lymphatic uptake were less, continued infusion would result in continued movement of L at he same rate, but this is not the case due to equilibrium (Fig. 3A). Thus, the changes in Q_{ss} with applied pressure can be used to similarly obtain a relationship between lymphatic conductance and hydraulic conductivity:

(20) $Q_{ss} = A\int_0^\infty \beta P^*_{ss}\, \mathrm{d}x = A\sqrt{\beta K}\, P^*_0$

Flow rates into the tail remain constant with homogeneous tissue structure and increase with each applied pressure (Fig. 3B). Therefore, by monitoring the relationship between the

infused flow rate and the penetration length of infusion for each applied pressure, the slopes of these regressions allow for the non-invasive quantification of β and K for any experimental condition.

Non-steady-state: dysfunctional lymphatic drainage

The steady state approximation works well to calculate tissue hydraulic conductivities and lymphatic conductances when lymphatic vessels function and interstitial fluid clearance is normal. However, some experimental conditions with extremely dysfunctional lymphatics – or the complete lack thereof - present a challenge when applying the same governing equations. Primary (hereditary) lymphedema presents just such a case. In two mouse models of primary lymphedema, the "Chy" mouse (17) and "K14" (K14-VEGFR-3-IgG) mouse (18), there are no dermal lymphatics in the tail skin and thus, no lymphatic uptake. If there is no equilibrium state between lymphatic uptake and interstitial fluid movement, then L should never become constant at any pressure. A new solution must be formulated.

A rigorous non-steady state calculation for *K*

The complete solution for $P^*(x,t)$ in the tail is represented in Equation 16. In the Chy or K14 model, the lack of dermal lymphatics should result in $\beta \rightarrow 0$. [As previously mentioned in the model's development, βP^* could technically be taken as the pressure driven flux into lymphatic capillaries, blood capillaries, or post-capillary venuoles according to Starling's Law. Significant flux into the blood capillaries may result when P^*_0 is increased and would be detected as the movement of L would "equilibrate" with capillary reabsorption with increasing P^*_0.] Simply, with $\beta \rightarrow 0$, Equation 16 simplifies to:

$$(21)\quad P^*(x,t) = P^*_0 \operatorname{erfc}\left(\frac{x}{2\sqrt{K^*t}}\right).$$

Equation 21 can be manipulated to solve directly for K^*:

$$(22)\quad K^* = \frac{1}{t}\cdot\left(\frac{x}{2\cdot \operatorname{inverfc}\left(\frac{P^*}{P^*_0}\right)}\right)^2$$

Using a mathematics software package, this can be solved provided the proper data is taken. The recorded times that are taken which were used in the steady-state model to calculate the flowrate into the tail, now enter directly into the calculation as t, and the moving front must be continuously monitored for x from $t=0$, rather than just taking the final L value at 30 minutes.

Problems with this approximation

Whereas in our steady-state calculation P^*, or $P(L,t)$, was mathematically irrelevant, here it is now of critical importance. What is a reasonable approximation of this value? When the infusion pressure is changed, there is an initially fast moving front that eventually slows. In steady-state tissue – that with lymphatic uptake – this decline is rapid. However, if there is no lymphatic uptake, the moving front moves constantly, with no change in rate, through the tissue (Fig. 4). A "steady-state" L cannot, therefore, be applied and x becomes linearly time dependent. The exactness of this model makes it a potential liability for accurate *in vivo* approximations. However, its sensitivity is ideal for detecting flux loss to the vasculature and may thus serve as a guide to at least the correct range of potential hydraulic conductivities.

Other approximate solutions for non-steady state *K*

Some problems presented by the exact solution for non-steady state uptake can be circumvented by taking into consideration a simplification of the governing equation for flow through porous media, Darcy's Law. If the tail is considered merely to be porous media, with all fluid flowing axially through the tail, Darcy's Law represents a reasonable approximation for calculating the hydraulic conductivity in non-steady state tissues.

Instantaneous velocities are a problem in the rigorous, full calculation of K. Thus, if we utilize Darcy's Law with an average moving front velocity over the time of infusion at each pressure, in differential and integrated forms:

$$(23)\quad \frac{\mathrm{d}L}{\mathrm{d}t} = -\frac{KP^*_0}{L}$$

$$(24)\quad L^2 = 2KP^*_0\,\tau$$

where τ represents the time of infusion for each pressure. It should be also be noted that L is the absolute distance that the solute front has moved, not just the distance for each pressure. Unlike the elegant, full calculation for K, this linear approximation will overestimate K. The

deviation from what physically happens can be seen in Table 1 for normal versus edematous mice. The ambiguities of measurable parameters are, however, eliminated. Because monitoring the infusion flowrate is trivial in the experimental setup, Darcy's Law can also be utilized in a form that relates the infused flowrate to the bulk fluid velocity through the tissue:

$$(25)\quad \bar{\mathbf{v}} = \frac{Q}{A} = -\frac{KP^*_0}{L}$$

$$(26)\quad QL = AKP^*_0$$

As with any approximation using a simplified Darcy's Law only, the linear result is an overestimation of the true tissue *K*. However, by coupling two measureable quantities, *Q* and *L*, this approximation maximizes the benefit of the potential experimental inputs for the non-steady state approximation. A comparison of this calculation for normal and edematous mice is seen in Table 1.

How to judge the quality of non-steady-state approximations?

In Table 1, the differences in the three potential approximations of K in mice lacking dermal lymphatic capillaries are visualized. The question of which method yields the most accurate value of K can only be considered if the tissue exhibits true, non-steady-state behavior. Is the approximation of non-steady-state even reasonable? There are three potential ways to test this question:

Method 1: The moving front of solute in the tail is continually monitored for long periods of time to ensure that the interstitial velocity is constant and does not sufficiently decelerate. Deceleration at longer times (i.e., over 20 minutes) indicates flux losses to the vasculature.

Method 2: A comparison of *K* obtained via the non-steady state method can be made to that obtained using the steady-state calculation. Since lymphatic uptake is discounted in the non-steady-state model, the hydraulic conductivity of normal tissue should decrease, while edematous tissue should remain the same or increase in *K*.

Method 3: The infused volume can be directly compared to the volume of tail occupied by the fluorescent tracer at each pressure's infusion. With no loss of solute, the infused volume should be accounted for in the tissue space, as defined by Equation 27:

$$(27)\quad Q_{P^*_0=45} \cdot \tau_{P^*_0=45} = A_{interstitium}\left(L_{P^*_0=45} - L_{P^*_0=40}\right)$$

If these "methods" are used to check the validity of the results obtained in Table 1, the exact solution is the best and should be applied. It demonstrates not only the ability to successfully calculate the tissue hydraulic conductivity, but also the means to sensitively detect flux losses to lymphatic capillaries or blood capillary and post-capillary venuole reabsorption of interstitial fluid at higher pressures. Fortunately, the simple steady-state solution works for all models with functioning lymphatic capillaries – the most likely scenario.

MODEL APPLICATION: Transgenic mouse strains

One of the essential features of a model for lymphatic uptake is that it is sufficiently sensitive to detect changes in lymphatic function when molecular signaling in lymphatic endothelial cells is potentially altered. An ideal application of the model is thus to examine transgenic mouse strains to verify that lymphatic function is normal, as its normalcy – or lack thereof – may dictate the results of other studies of edema, inflammation, or immune cell migration. To both verify the sensitivity of the model and explore some experimental questions, we tested several transgenic mouse strains.

Apolipoprotein E (ApoE) -/-

The apolipoprotein E (ApoE) knockout mouse line has long been used as a model of artherosclerosis and hypercholesterolemia. Gene array analysis on LECs stimulated with VEGF-C and shear stress exhibited significant changes in apolipoprotein expression (19). The potential for lymphatics to be altered in ApoE-/- mice was thus motivated by the potential roles of lymphatics in lipid metabolism (the gene array analysis) and work demonstrating reduced dendritic cell migration (which enter and traffick via lymphatics) in these mice (20).

In ApoE-/- mice aged 16-20 weeks on a high fat diet, dermal edema and increased lymphatic capillary diameter were observed (data not shown). When lymphatic function was measured using the steady-state model, lymphatic conductance was significantly reduced in these mice (Fig. 5A). In young mice that are not yet hypercholesterolemic, no difference in lymphatic function was measured (Fig. 5B). The tissue hydraulic conductivity was identical in all mice. These findings verify not only the sensitivity of the model, but also demonstrate an interplay between lipid metabolism and lymphatic function that has been previously unexplored.

Neural cell adhesion molecule (NCAM) -/-

Neural cell adhesion molecule (NCAM) has been identified as a modulator of tumor lymphangiogenesis (21), and gene array analysis revealed a marked increase in expression by LECs under shear stress (Yong, et al. unpublished). It was thus hypothesized that a lack of NCAM expression in NCAM-/- mice may result in decreased lymphatic capillary function.

NCAM normal, heterozygote, and homozygote -/- mice were tested. Lymphatic capillaries appeared to be normal in these mice, and no significant differences in lymphatic function were detected. Also, no differences were calculated in the tissue hydraulic conductivity. These findings indicate that while NCAM may play a role in lymphatic biology during pathological events (e.g., tumor progression or inflammation), there is little role for LEC NCAM in normal capillary function.

CONCLUSIONS

The results of this work demonstrate an easy to apply, quantitative means to measure lymphatic capillary uptake and tissue hydraulic conductivity *in vivo*. As the two key parameters modulating interstitial flow , understanding lymphatic function and tissue physical properties are essential for understanding the biophysical environment in which cells exist, as well as lending knowledge to proper design of *in vitro* systems that better recapitulate the *in vivo* environment (22, 23). While the need for such an approach has been addressed in the past (12), here we have fully explained the mathematics for a better understanding of the steady-state formulation, and, for the first time, thoroughly discuss the implications of dysfunctional lymphatic uptake on the calculations. These non-steady state governing equations can actually be applied even to steady-state systems as simplified versions that result in reasonable approximations of tissue hydraulic conductivity.

As there is an increasing appreciation of the lymphatic circulation, understanding which molecular signaling pathways affect capillary function is crucial. The sensitivity of our quantitative approach permits the use of transgenic mouse models and antibody and small molecule therapies to determine the relevancy of various molecules and genes to lymphatic capillaries. This is critical to correctly answer questions of dermal physiology, for example, if dendritic cell migration is actually tied to interstitial flowrates and lymphatic function, or if it is wholly independent (15, 24).

By applying the steady-state model to transgenic mouse models, immediately a new finding in lymphatic capillary biology was found. The ApoE-/- mouse was selected as a

model with potentially reduced lymphatic function as indicated by reduced dendritic cell migration to the sentinel lymph node (20). Indeed, we found the lymphatic capillary function was reduced in these mice, despite normal hydraulic conductivity. This makes a strong case for further study on the effect of hypercholesterolemia on lymphatic capillary function. Additionally, as lymphatic capillaries in the intestine play a crucial role in lipid uptake, these results suggest a whole new realm of research on lymphatic function, lipid metabolism, and cardiovascular health.

REFERENCES

1. Swartz, M.A. 2001. The physiology of the lymphatic system. *Adv Drug Deliv Rev* 50:3-20.
2. Rutkowski, J.M., and Swartz, M.A. 2007. A driving force for change: interstitial flow as a morphoregulator. *Trends Cell Biol* 17:44-50.
3. Schmid-Schonbein, G.W. 1990. Microlymphatics and lymph flow. *Physiol Rev* 70:987-1028.
4. Rutkowski, J.M., Moya, M., Johannes, J., Goldman, J., and Swartz, M.A. 2006. Secondary lymphedema in the mouse tail: Lymphatic hyperplasia, VEGF-C upregulation, and the protective role of MMP-9. *Microvasc Res* 72:161-171.
5. Slavin, S.A., Van den Abbeele, A.D., Losken, A., Swartz, M.A., and Jain, R.K. 1999. Return of lymphatic function after flap transfer for acute lymphedema. *Ann Surg* 229:421-427.
6. Lynch, P.M., Delano, F.A., and Schmid-Schonbein, G.W. 2007. The primary valves in the initial lymphatics during inflammation. *Lymphat Res Biol* 5:3-10.
7. Evans, R.C., and Quinn, T.M. 2006. Dynamic compression augments interstitial transport of a glucose-like solute in articular cartilage. *Biophys J*.
8. Wiig, H., Rubin, K., and Reed, R.K. 2003. New and active role of the interstitium in control of interstitial fluid pressure: potential therapeutic consequences. *Acta Anaesthesiol Scand* 47:111-121.
9. Levick, J.R. 1987. Flow through interstitium and other fibrous matrices. *Q J Exp Physiol* 72:409-437.
10. Swartz, M.A., and Fleury, M.E. 2007. Interstitial flow and its effects in soft tissues. *Annu Rev Biomed Eng* 9:229-256.
11. Netti, P.A., Baxter, L.T., Boucher, Y., Skalak, R., and Jain, R.K. 1995. Time-dependent behavior of interstitial fluid pressure in solid tumors: implications for drug delivery. *Cancer Res* 55:5451-5458.
12. Swartz, M.A., Kaipainen, A., Netti, P.A., Brekken, C., Boucher, Y., Grodzinsky, A.J., and Jain, R.K. 1999. Mechanics of interstitial-lymphatic fluid transport: theoretical foundation and experimental validation. *J Biomech* 32:1297-1307.
13. Baluk, P., Fuxe, J., Hashizume, H., Romano, T., Lashnits, E., Butz, S., Vestweber, D., Corada, M., Molendini, C., Dejana, E., et al. 2007. Functionally specialized junctions between endothelial cells of lymphatic vessels. *J Exp Med* 204:2349-2362.
14. Somasiri, A., Nielsen, J.S., Makretsov, N., McCoy, M.L., Prentice, L., Gilks, C.B., Chia, S.K., Gelmon, K.A., Kershaw, D.B., Huntsman, D.G., et al. 2004. Overexpression of the anti-adhesin podocalyxin is an independent predictor of breast cancer progression. *Cancer Res* 64:5068-5073.
15. Johnson, L.A., Clasper, S., Holt, A.P., Lalor, P.F., Baban, D., and Jackson, D.G. 2006. An inflammation-induced mechanism for leukocyte transmigration across lymphatic vessel endothelium. *J Exp Med* 203:2763-2777.
16. Gannon, B.J., and Carati, C.J. 2003. Endothelial distribution of the membrane water channel molecule aquaporin-1: implications for tissue and lymph fluid physiology? *Lymphat Res Biol* 1:55-66.
17. Karkkainen, M.J., Saaristo, A., Jussila, L., Karila, K.A., Lawrence, E.C., Pajusola, K., Bueler, H., Eichmann, A., Kauppinen, R., Kettunen, M.I., et al. 2001. A model for gene therapy of human hereditary lymphedema. *Proc Natl Acad Sci U S A* 98:12677-12682.
18. Makinen, T., Jussila, L., Veikkola, T., Karpanen, T., Kettunen, M.I., Pulkkanen, K.J., Kauppinen, R., Jackson, D.G., Kubo, H., Nishikawa, S., et al. 2001. Inhibition of

lymphangiogenesis with resulting lymphedema in transgenic mice expressing soluble VEGF receptor-3. *Nat Med* 7:199-205.
19. Yong, C., Bridenbaugh, E.A., Zawieja, D.C., and Swartz, M.A. 2005. Microarray analysis of VEGF-C responsive genes in human lymphatic endothelial cells. *Lymphat Res Biol* 3:183-207.
20. Angeli, V., Llodra, J., Rong, J.X., Satoh, K., Ishii, S., Shimizu, T., Fisher, E.A., and Randolph, G.J. 2004. Dyslipidemia associated with atherosclerotic disease systemically alters dendritic cell mobilization. *Immunity* 21:561-574.
21. Crnic, I., Strittmatter, K., Cavallaro, U., Kopfstein, L., Jussila, L., Alitalo, K., and Christofori, G. 2004. Loss of neural cell adhesion molecule induces tumor metastasis by up-regulating lymphangiogenesis. *Cancer Res* 64:8630-8638.
22. Griffith, L.G., and Swartz, M.A. 2006. Capturing complex 3D tissue physiology in vitro. *Nat Rev Mol Cell Biol* 7:211-224.
23. Pedersen, J.A., and Swartz, M.A. 2005. Mechanobiology in the third dimension. *Ann Biomed Eng* 33:1469-1490.
24. Randolph, G.J., Angeli, V., and Swartz, M.A. 2005. Dendritic-cell trafficking to lymph nodes through lymphatic vessels. *Nat Rev Immunol* 5:617-628.

FIGURE LEGENDS

Figure 1: Lymphatic drainage occurs between lymphatic endothelial cells. Increased interstitial fluid pressure (IFP), at right, expands the matrix, and – due to the LEC anchoring filaments – opens the vessel further to promote drainage.

Figure 2. Experimental setup for calculating hydraulic conductivity and lymphatic conductance in the mouse tail. Small increments of 5cmH_2O in hydrostatic pressure are applied (right) and a fluorescent tracer is infused into the tail at flowrate Q. The fluorescent tracer is visualized in the interstitium as the front moves along length x. With lymphatic uptake present, the final value of x, L, is constant at each pressure due to conservation of mass at steady-state. Actual images of fluorescence in the mouse tail after 24 minutes at each applied pressure are shown.

Figure 3: To calculate β and K the change in penetration depth and infusion flowrate with pressure for each pressure step are monitored. A) Plot of the penetration depth of fluorescent dextran for various pressures demonstrates the approximate steady-state values of L: where the curves become level. Steady-state is only possible with lymphatic uptake of infused fluid. B) Increasing, and constant infusion flow rates into the mouse tail are recorded by tracking the small air bubble in the infusion line.

Figure 4: In the K14-VEGFR-3-Ig mouse, there are no dermal lymphatic capillaries and no lymphatic uptake occurs. Thus, the moving front distance continuously increases, with no steady-state L being reached as in wildtype mice.

Figure 5. Lymphatic conductance is reduced with the onset of hypercholesterolemia in aduly ApoE-/- mice. A) Older ApoE-/- mice, which exhibit high cholesterol, artherosclerosis, edematous skin, and enlarged lymphatic capillaries, have significantly reduced lymphatic uptake. B) Young transgenic mice exhibit normal lymphatic function. (from Angeli V, Reddy ST, **Rutkowski JM**, Swartz MA, Randolph GJ. *Impaired lymphatic function in dyslipidemic mice*. Submitted for publication, ***Microcirculation***) mice.

Figure 6. NCAM expression does not significantly affect lymphatic function. In normal wildtype, heterozygote, and knockout mice, the quantified lymphatic conductance was equal.

This page is intentionally left blank.

Figure 1

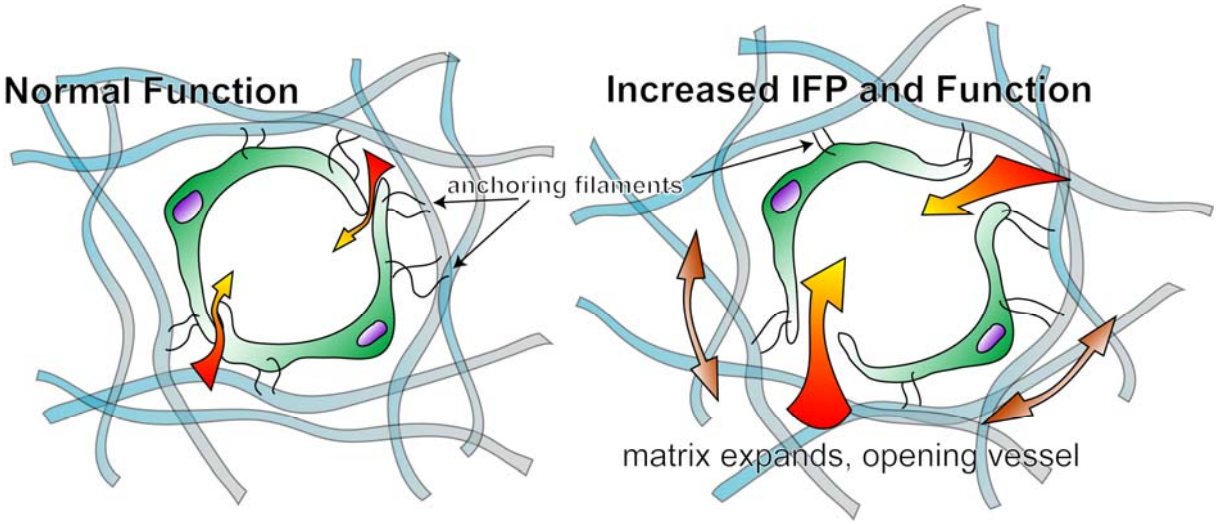
Normal Function
anchoring filaments
Increased IFP and Function
matrix expands, opening vessel

This page is intentionally left blank.

Figure 2

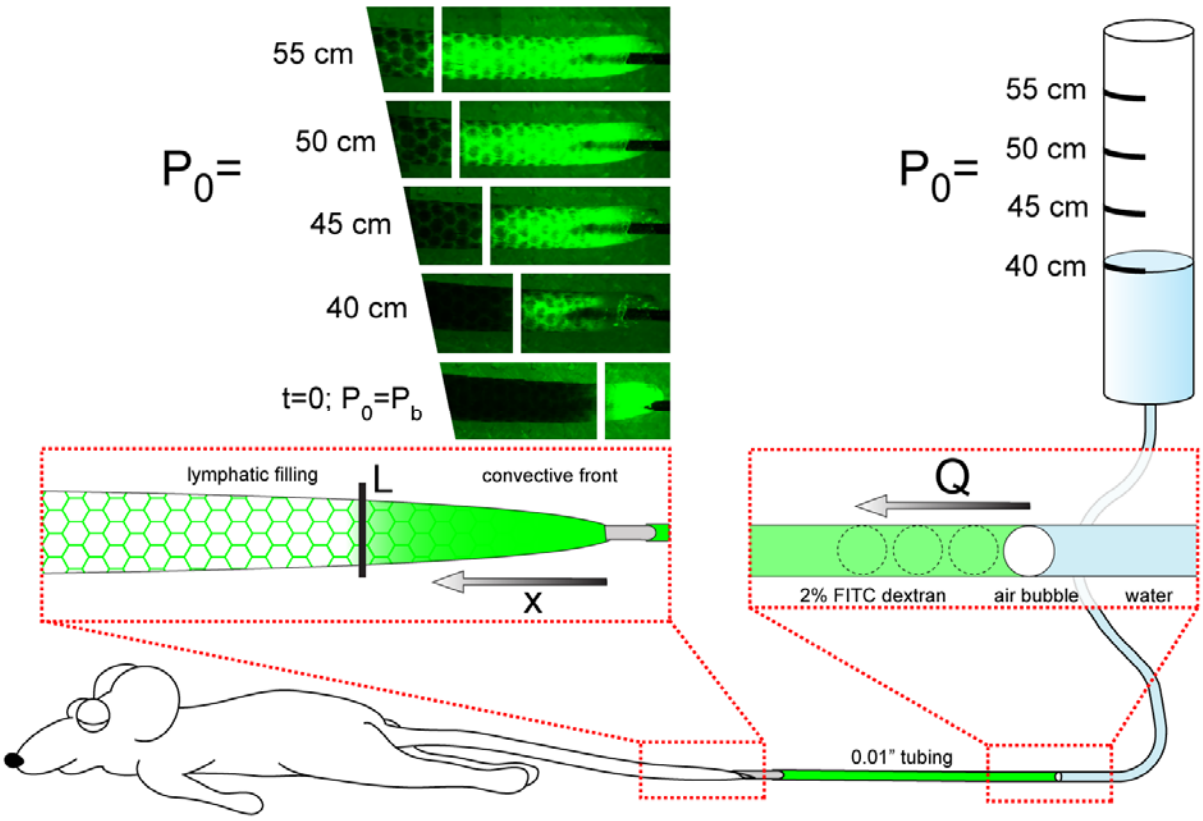
55 cm
50 cm
45 cm
40 cm
t=0; P0=Pb
P0=
lymphatic filling
L
convective front
x
55 cm
50 cm
45 cm
40 cm
P0=
Q
2% FITC dextran
air bubble
water
0.01" tubing

This page is intentionally left blank.

Figure 3

A

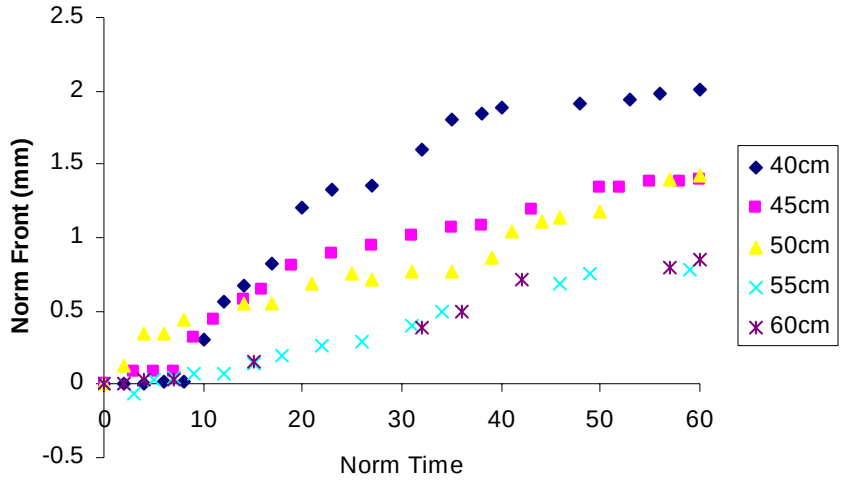
2.5
2
1.5
1
0.5
0
-0.5
Norm Front (mm)
0
10
20
30
40
50
60
Norm Time
40cm
45cm
50cm
55cm
60cm

B

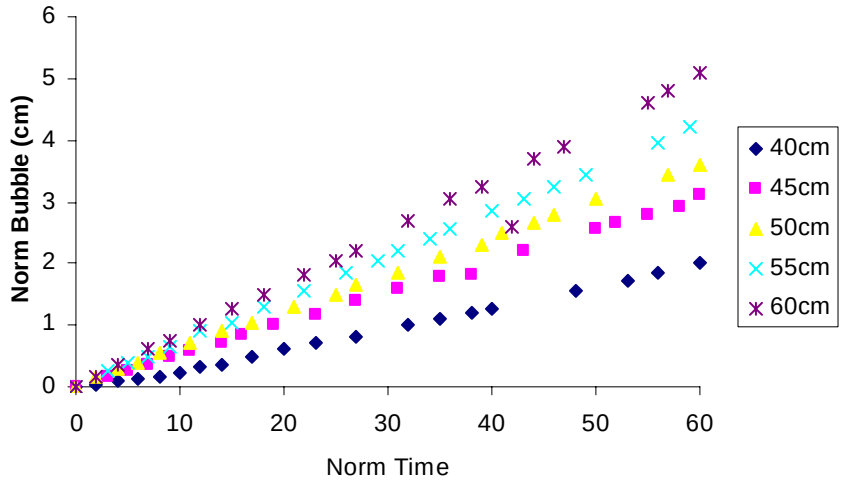
6
5
4
3
2
1
0
Norm Bubble (cm)
0
10
20
30
40
50
60
Norm Time
40cm
45cm
50cm
55cm
60cm

This page is intentionally left blank.

Figure 4

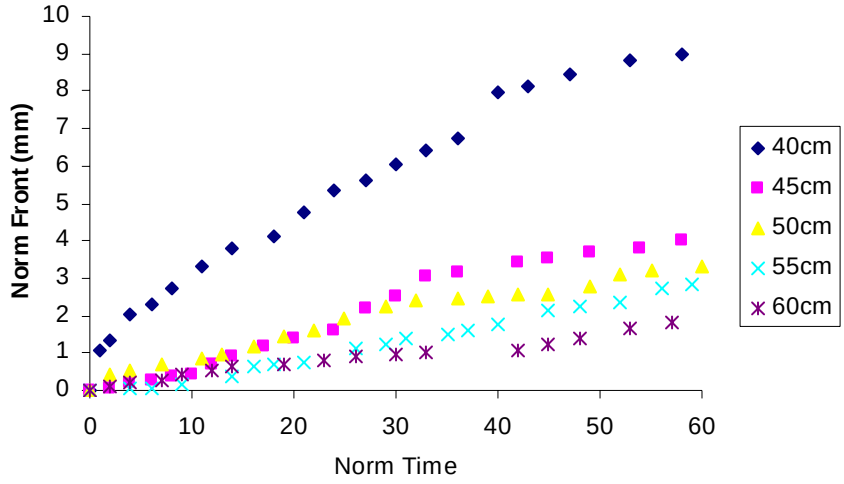
Norm Front (mm)
10
9
8
7
6
5
4
3
2
1
0
0
10
20
30
40
50
60
Norm Time
40cm
45cm
50cm
55cm
60cm

This page is intentionally left blank.

Figure 5

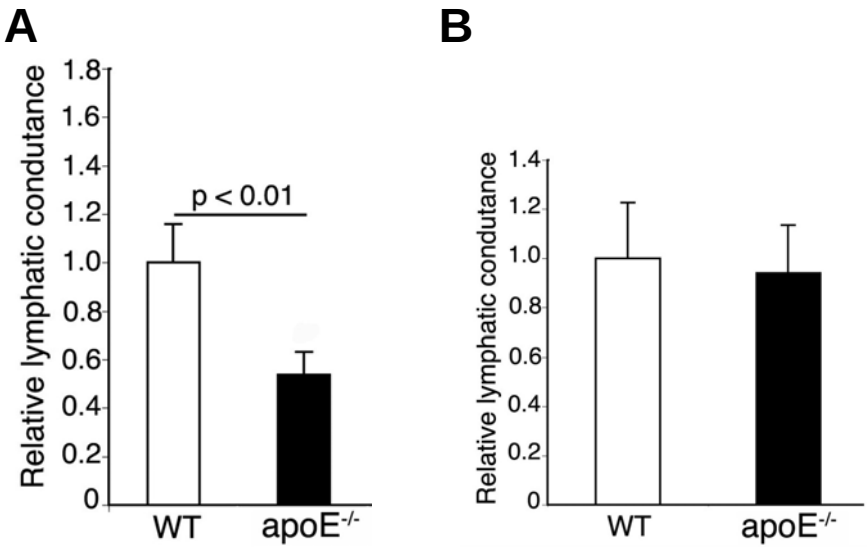
A
B
Relative lymphatic condutance
1.8
1.6
1.4
1.2
1.0
0.8
0.6
0.4
0.2
0
p < 0.01
WT
apoE-/-
Relative lymphatic condutance
1.4
1.2
1.0
0.8
0.6
0.4
0.2
0
WT
apoE-/-

This page is intentionally left blank.

Figure 6

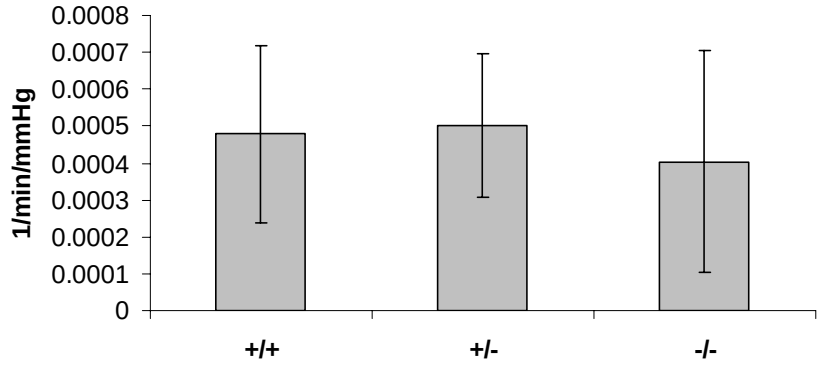

This page is intentionally left blank.

Table 1

	K (mm^2/min/mmHg)	
	Wildtype	K14-VEGFR-3-Ig
Steady-State Approximation	0.0272	0.1185
Non-SS, Exact Solution (P^*_0=29.4mmHg)*	0.0050	0.1345
Non-SS, Exact Solution (P^*_0=40.8mmHg)*	0.0003	0.0050
Non-SS, Approximation #1	0.0307	0.5071
Non-SS, Approximation #2	0.0437	0.3489

* for the exact solution, a P* of 1mmHg was used.

Table 1: Calculated hydraulic conductivities for one example mouse using the various calculations described. Note the variation in change with each technique, particularly the overestimation of the approximate solutions.

This page is intentionally left blank.

CHAPTER 7:
ORIGINAL MANUSCRIPT 6

Differential tissue adaptation in two mouse models of primary congenital lymphedema with defects in VEGFR-3 signaling

Joseph M. Rutkowski[1], Carl Erik Markhus[2], Christina C. Gyenge[2], Kari Alitalo[3], Helge Wiig[2], and Melody A. Swartz[1]

1 : Institute of Bioengineering, École Polytechnique Fédérale de Lausanne (EPFL), Switzerland
2 : Department of Biomedicine, University of Bergen, Norway
3 : Molecular/Cancer Biology Laboratory and Ludwig Institute for Cancer Research, Haartman Institute, University of Helsinki, Finland

Prepared for submission to ***American Journal of Physiology – Heart and Circulatory Physiology***

ABSTRACT

Primary lymphedema is a congenital pathology of dysfunctional lymphatic drainage characterized by swelling of the limbs, thickening of the dermis, and fluid and lipid accumulation in the underlying tissue. Genetic studies in humans and mice have linked mutations in genes of lymphatic endothelial cells to the improper development and function of the lymphatic vasculature in these patients. Two mouse models, the Chy mouse and the K14-VEGFR-3-Ig mouse, target vascular endothelial growth factor receptor (VEGFR) -3 signaling, and exhibit dermal lymphedema symptomatically similar to the human condition. The Chy mouse possesses a genetic mutation in VEGFR-3, while the K14-VEGFR-3-Ig mouse expresses soluble VEGFR-3 that has prevented lymphatic capillary growth; both models lack dermal lymphatic capillaries, and are phenotypically similar. We sought to quantitatively determine both the equivalency of the edematous pathology and the functional interstitial transport implications as a result of the pathology in these models. We found that despite their similarities in increased skin hydration and elevated interstitial fluid pressure, the tissue adaptations to a lack of dermal lymphatics were significantly different. Chy mice skin possessed much higher levels of collagen and fat, while K14-VEGFR-3-Ig mice skin was relatively normal, as compared to their respective wildtype controls. Functionally, this resulted in a normal hydraulic conductivity in Chy mice, and a greatly increased conductivity in K14-VEGFR3-Ig mouse skin. Thus, based on the principles of interstitial flow, the tissue in Chy mice has likely adapted to limit interstitial transport, while the K14-VEGFR3-Ig has adapted to permit interstitial flow over longer distances. These opposing tissue responses to primary lymphedema suggest that tissue remodeling is not simply a consequence, but a purposeful adaption to control the pathology. Thus, successful lymphedema therapy should aim not only restore lymphatic function, but remediate the tissue changes.

Keywords: VEGF-C, lymphatic, hydraulic conductivity, interstitial fluid pressure

INTRODUCTION

Primary or congenital lymphedema is an inherited pathological condition in which excess fluid accumulates in the limb due to dysfunctional lymphatic drainage (1). As a chronic pathology, lymphedema leads to remodeling of the skin and subcutaneous extracellular matrix, accumulation of lipids, and failures in immune response (2-6). These morphological adaptations can worsen the condition and prevent successful resolution – indeed while compression cuffs, massage, and surgical removal of tissue have demonstrated success in minimizing the condition, unfortunately, there is no "cure". In humans, the causes of these conditions have been linked to mutations in genes essential for proper lymphatic vessel development; improper development of lymphatic valve structures or insufficient organization of dermal lymphatic capillaries leads to failed interstitial fluid and lymph clearance (7-9).

To create the pathology of primary lymphedema in mouse models, lymphatic genes have been targeted to disrupt the proper formation of lymphatic vessels during development. Unfortunately, in most cases, homozygote mutations fail to survive beyond the womb as the systemic lymphatic circulation fails to form, and most heterozygote mutations do not truly recapitulate the human condition (7-9). Targeting vascular endothelial growth factor receptor (VEGFR) -3, a critical receptor in lymphangiogenesis, has proven to be reasonably successful in creating an edematous state in two different animal models: the Chy mouse and the K14-VEGFR-3-Ig mouse.

The Chy mutant mouse possesses a heterozygous VEGFR-3 mutation that leads to developmental deficiencies in lymphatic vessels and a complete lack of lymphatic capillaries in the skin. In pups this results in chylous ascites in the gut (the namesake of the strain) and, in the adult, dermal lymphedema. It has been shown that the resulting lymphedema, as well as the location of the gene mutation, mirror the human condition of Milroy's disease (7). The K14-VEGFR-3-Ig mouse is a transgenic mouse strain developed such that a soluble form of the ligand-binding domain of VEGFR-3 is expressed in the epidermis under the keratin-14 (K14) promoter (10). This results in systemically-present soluble VEGFR-3 that prevents proper lymphatic capillary maturation, a lack of dermal lymphatics, and dermal lymphedema much like the Chy mouse model.

Both mouse models exhibit dermal swelling, particularly in the lower limbs, tail, and snout, and tissue histology has revealed a pathological state similar to that of human

lymphedema (i.e., fibrotic thickening of the dermis and swelling and fluid accumulation in the hypodermis). However, despite a lack of dermal lymphatics, in neither case does the extent of the edematous pathology approach that of the human condition. We thus hypothesized that the tissue composition must have adapted to increase the hydraulic conductivity so as to maximize interstitial fluid transport in the absence of dermal lymphatics. Tissue collagen, lipid, and water concentrations were therefore measured to determine the compositional tissue changes in these mice. Interstitial fluid pressures were measured and applied to a quantitative *in vivo* model of tissue hydraulic conductivity. In this way, transport of extravasted fluid and macromolecules within the interstitial space when initial lymphatic capillaries are missing may be better understood. Despite the fact that each of these models exhibits lymphedema by a loss of dermal lymphatic capillaries, we found that the resultant tissue adaptation was quite different between the two strains.

MATERIALS AND METHODS

Animals

Male Chy mice on a C3H background were crossed with wildtype C3H females to obtain heterozygote Chy offspring (7). The Chy mutation was identified by PCR analysis prior to all experiments (11). K14-VEGFR-3-Ig heterozygote mice on a C57Bl6 background were crossed with wildtype C57Bl6 mice. Offspring were genotyped by PCR (10). Heterozygotes and their respective wildtype littermates were used for all studies. Use of the Chy mouse was approved by the Norwegian State Commission for Laboratory Animals while use of the K14-VEGFR-3-Ig mouse was approved by the Veterinary Authorities of the Canton Vaud according to Swiss law (protocol number #1987).

Interstitial Fluid Pressure Measurements

Interstitial fluid pressure (IFP) was measured by micropipettes connected to an automatic counterpressure system (12) inserted into the tail skin of anesthesized mice as previously described in detail (13). After zeroing, measurements were qualified when: (a) the measurement was unaltered with increased feedback gain, (b) suction to the pipette resulted in a resistance change verifying an open capillary, and (c) the zero reference pressure was unchanged (13).

In vivo quantification of tissue hydraulic conductivity

Mice were anesthetized (an intraperitoneal injection of ketamine (65 mg/kg), xylazine (13 mg/kg, followed by subcutaneous additions when necessary) and the functional uptake of the lymphatic vascualture was determined by adapting the technique of fluorescence microlymphangiography (14). Briefly, a 30-gauge needle catheter containing 0.9% NaCl with 2% FITC-conjugated 70kDa dextran (Molecular Probes, Carlsbad, CA) was placed intradermally into the tail tip. The catheter was attached to a low-pressure reservoir that permitted stepwise changes of 5-cm H_2O, from 40-cm H_2O, up to 100-cm H_2O. The low infusion pressure allowed physiologic uptake into the lymphatic capillaries (if present) and minimized the gross swelling or tissue damage that might have resulted from higher pressure injections. The fluorescent dextran, once in the tail, either traveled through the interstitial space (linearly with pressure change) or was taken up and transported by the lymphatic capillaries. The infusion flow rate was continually monitored (via the tracking of a small air bubble introduced into the infusion line); pressures were changed and flow rates monitored for 30 minutes per pressure setting. In K14-VEGFR-3-Ig mice, 40-60 cmH_2O was used; in Chy mice, 40-100 cmH2O was used in 10 cmH_2O steps. By also monitoring the convective front of fluorescence at each infusion pressure, using a fluorescence-equipped Leica MZ16 FA stereomicroscope, the hydraulic conductivity of the matrix was calculated (14). Measured IFPs were applied to the calculations, as well as the quantified cross-sectional areas. Cross-sectional areas were also corrected for lipid content, which, as non-aqueous regions, were considered to be flow impermeable.

Tissue Water and Collagen Composition

Tail skin was excised and the wet weight recorded. The sample was then freeze dried and weighed again. The difference was recorded as the total tissue water. The freeze dried sample was then homogenized for collagen determination.

Tissue collagen was quantified according to the spectrophotometric method described by Woessner (15) based on determination of hydroxyproline content as described in a previous publication (16). The absorbance was read at 557 nm on a Spectramax pluss 384 spectrophotometer (Molecular Devices, Sunnyvale, CA). Hydroxyproline concentration was quantified by comparison to a standard curve of L-4-hydroxyproline (Fluka Chemie GmbH,

Buchs, France) in 1mM HCl. Collagen content was calculated based on a 6.94 to 1 collagen to hydroxyproline ratio (17).

Tissue Lipid Extraction

Lipid content of the tail skin was determined by assessing dry weights before and after fat extraction. Lipid was extracted placing homogenized tail skin samples overnight in 4 mL mixture of chloroform and methanol (2:1). The solvent fraction, containing the lipids, was removed and evaporated before weighing. This was repeated thrice; the total lipid isolated is reported.

Immunofluorescence and Histology

Tail specimens were cut into 10 μm-thick longitudinal cryosections and immunostained. To detect LECs, a rabbit polyclonal antibody against the lymphatic-specific hyaluronan receptor LYVE-1 (Upstate, Charlottesville, VA) was used along with an Alexa Fluor 488 conjugated goat anti-rabbit secondary antibody (Molecular Probes). To detect blood endothelial cells, a rat polyclonal CD31 antibody (BD Pharmingen) was used along with an Alexa Fluor 594 conjugated goat anti-rat secondary antibody (Molecular Probes). Cell nuclei were labeled with DAPI (Vector Labs, Burlingame, CA). Sections were fluorescently imaged with a Zeiss Axiovert 200M fluorescence microscope and Zeiss MRm camera.

For histology, sections were first fixed in 4% PFA. To visualize the matrix, Giemsa staining was used on both tail cross-section and axial sections, which were then dehydrated and mounted with Eukitt (Fluka Chemie AG, Buchs, Switzerland). Oil red O (Sigma-Aldrich, Buchs, Switzerland) was used to stain lipids, with a hematoxylin counterstain, and slides were mounted in Glycergel mounting medium (Dako). Color histological samples were imaged with a Zeiss MRc camera.

Image Analysis

To quantify tissue lipid content from mounted skin sections, Metamorph 6.3 image analysis software (Molecular Devices Corp., Sunnyvale, CA) was used. Five images were captured from each side of the tail of each of five samples. In each, the region between the epidermis and underlying tendon was clearly identified with a freehand tool, and the total oil red O staining of lipids within this region calculated per area analyzed. Interstitial area was similarly quantified on tail cross-sections (taken @ 5mm from the tail tip) with hair follicles, bone, tendon, muscle, etc. excluded from the defined area.

Statistical methods

For all quantifications representing tissue extractions or animal measurements, n is equal to or greater than 6. For quantifications from histochemistry, 5 samples from each of 3 animals were analyzed. Data is presented as mean ± one standard deviation. All *P* values were calculated using a two-sided Student's t-test.

RESULTS

Chy and K14-VEGFR-3-Ig mice lack dermal lymphatic capillaries, but possess deeper collecting vessels

Immunohistochemical analysis of lymphatic and blood capillaries confirmed the absence of lymphatic capillaries in the tail skin with normal blood capillaries in the model strains (Fig. 1A). In the mouse tail, from the perspective of fluid transport, a lack of dermal lymphatic capillaries implies that interstitial fluid must either drain the entire length of the tail, transport the entire depth of the dermis to be taken up by the deeper collecting lymphatic vessel, or be reabsorbed into post-capillary venuoles. Histologically, it appeared that collecting lymphatic vessels were present in both Chy and K14-VEGFR-3-Ig strains, indicating that this route is anatomically possible (Fig. 1A). Functionally, however, direct interstitial fluid uptake by collecting lymphatic vessels has not been previously reported. When fluorescent tracer was infused into the tail of K14-VEGFR-3-Ig mice, no functioning collecting vessels were found (Fig. 1B); tracer moved readily below the dermis.

Chy and K14-VEGFR-3-Ig mice demonstrate significantly increased interstitial fluid pressures, but only K14-VEGFR-3-Ig mice show increased hydraulic conductivity

Interstitial fluid pressure (IFP) is a key parameter of Starling's Law in its complete form, for blood capillary extravasation:

$$J_v = Lp\left(\left(P_{capillary} - P_{\text{int}erstitium}\right) + \sigma\left(\pi_{capillary} - \pi_{\text{int}erstitium}\right)\right)$$

where the flux is related to the hydrostatic driving force, as well as the osmotic pressure driving force, $\Delta\pi$. Lymphatic intravasation is represented by the appropriate directional changes to the driving forces. The filtration coefficient, *Lp*, is dependent on vessel wall area

and wall hydraulic conductivity. During lymphedema, the interstitial fluid pressure is increased (18), which would reduce extravasation from the blood capillaries while increasing the driving force to lymphatic vessels and potentially permitting increased uptake by post-capillary venuoles. Osmotically, there are changes in both the molecular concentrations as well as in σ, the capillary reflection coefficient (19, 20).

Average IFP in the tail skin of Chy mice was measured to be significantly higher than in wildtype (Fig. 2A). Similarly, in K14-VEGFR-3-Ig, the IFP was significantly higher than their wildtype cagemates (both $P<0.01$). The marked increase in IFP exhibited by these mice is another hallmark of their edematous condition. Also, as lymphatic drainage normally provides a low-pressure route for fluid transport, the increased IFP in these mice is likely a consequence of the lack of lymphatic capillaries.

While IFP drives fluid movement through the tissue, the tissue's hydraulic conductivity determines its resistance to flow. Factors influencing tissue hydraulic conductivity include tissue hydration (21) and matrix composition (22). Hydraulic conductivity is also coupled to IFP, as increased IFP leads to swelling of the matrix, which opens "pores" and increases the conduction of fluid (23). We utilized a quantitative *in vivo* model of interstitial transport in the mouse tail to quantify the changes in hydraulic conductivity induced by lymphedema in these mouse strains (Appendix A).

In Chy mice, a higher starting infusion pressure of 50 cmH_2O (typically beginning at 40 cmH_2O) was necessary to visibly induce significant flow through the interstitium. Once flow was established, however, the resultant movement of fluorescent dextran through the matrix was similar to wildtype mice at the same infusion pressure. The calculated hydraulic conductivity of the Chy mice was the same as the wildtype mice examined (Fig. 2B). No uptake and transport by lymphatic vessels was observed ahead of the convective front (Fig. 2C).

K14-VEGFR-3-Ig tissue responded differently in that our standard initial infusion pressure of 40 cmH_2O was sufficient to induce interstitial flow, despite the higher IFP recorded in these mice. Again factoring in the larger flow area and IFP, the hydraulic conductivity of K14-VEGFR-3-Ig was dramatically increased over matching wildtype controls by nearly threefold (Fig. 2D)($P=0.069$). Like in the Chy mouse, no lymphatic uptake was visualized (Fig. 2E).

Chy mice exhibit a greater change in tissue composition than K14-VEGFR-3-Ig mice

Despite the phenotypic appearance of lymphedema, we sought to determine if the underlying tissue structure and composition in Chy and VEGFR-3-Ig mice could suggest adaptations that (a) explain the differences in the measured hydraulic conductivities and (b) could offer clues as to why the extent of the human lymphedema condition is avoided.

Histological analysis of tail skin demonstrated dermal swelling in these strains primarily in the hypodermis (Fig. 3A) and a denser tissue structure in the dermis. The swelling was further demonstrated quantitatively by calculating the cross-sectional area of the interstitium (Fig. 3C). Lipid accumulation, marked by oil red O staining, occurred in the edematous tissue as well (Fig. 3B). Quantification of lipid accumulation by image analysis revealed, however, that while Chy mice exhibit significantly more lipid accumulation (Fig. 3D) than their wildtype littermates ($P=0.039$), K14-VEGFR-3-Ig actually exhibited less, though not significantly ($P=0.25$). These results were applied to the hydraulic conductivity model to ensure maximum accuracy in the calculations.

To complement the histological analyses, we analyzed the skin for total tissue water, collagen, and total lipid concentrations. Total tissue water was significantly higher in both Chy and K14-VEGFR-3-Ig mice ($P<0.01$ for both), indicative of the edematous condition (Fig. 4A). Collagen concentration, on a dry tissue weight basis, was significantly higher in Chy mice as compared to their wildtype controls ($P=0.022$) (Fig. 4B). Conversely, K14-VEGFR-3-Ig mice had a collagen content equivalent to that of their controls ($P=0.87$). Lipid extraction from tail skin confirmed the validity of our histochemical analysis: Chy mice had a significant and marked increase in tissue lipid content, over 25% more ($P=0.013$), while K14-VEGFR-3-Ig mice actually had 10% less lipid content ($P=0.012$) than respective controls (Fig. 4C).

It is quite interesting that the two mouse strains, both without dermal lymphatics, had adapted a very different tissue composition. The Chy mouse adapted a more collagenous dermis, with an increased presence of lipids, while the K14-VEGFR-3-Ig mouse was compositionally quite similar to its wildtype littermates.

DISCUSSION

Though both Chy and K14-VEGFR-3-Ig exhibit lymphedema in the skin resulting from improper VEGFR-3 signaling and the resultant lack of dermal lymphatic capillaries, in neither animal is the extent of lymphedema as severe as the human condition. Despite these

similarities, the lack of lymphatics resulted in different tissue adaptations in the two strains that consequently impacted the hydraulic conductivities of the skin. These differences demonstrate what are, essentially, the ways that tissue might adapt when uptake by the initial lymphatic capillaries is absent.

Blood capillaries are not impermeable to transmural flow and thus form the starting point interstitial flow as fluid and macromolecules extravaste into the interstitium (24). This flux from the blood capillaries is governed by Starling forces. In lymphedema, as exhibited by both Chy and K14-VEGFR-3-Ig mice, the interstitial fluid pressure is increased (18) and interstitial molecule concentrations are altered (11, 19), thus altering the Starling forces not only for blood capillary filtration (20), but likely for lymphatic uptake as well. Increased IFP may also permit reabsoption of interstitial fluid by post-capillary venuoles. One compensatory mechanism by which the tissue may adapt is to reduce flux out of the blood circulation or through the interstitium. Indeed, the Chy mouse tissue may have adapted in this manner. Another study in the Chy mouse demonstrated that skin colloid osmotic pressure was heightened in these mice and that the tissue response to volume loading was exaggerated compared to wildtype mice (11).

Another adaptive mechanism may be for the tissue to remodel such that the hydraulic conductivity is increased. A higher hydraulic conductivity permits flow to pass more easily through the interstitium. As a result, for the same hydrostatic pressure driving force across the interstitium, fluid can travel further. In K14-VEGFR-3-Ig mice, we quantified a significantly higher hydraulic conductivity. Extravasted fluid may, therefore, be more readily transported across the interstitium and taken up by lymphatic vessels outside the dermis.

These results illustrate that while lymphedema may be a sufficient blanket term to describe the pathology resulting from insufficient lymphatic transport, the actual resulting tissue effects may be quite different. The differential response in tissue adaptation demonstrated in the Chy and K14-VEGFR-3-Ig mouse strains exhibit a range of potential adaptations that are possible to not only define qualitatively via pathological methods, but also quantitatively and functionally. The tissue adaptations present in these mice may also explain why mouse models of congenital lymphedema have, thus far, failed to successfully recapitulate the human condition: the tissue adapts too readily to a lack of lymphatic capillary uptake. This suggests that therapies for lymphedema must consider not only the growth of

new lymphatic vessels to restore lymphatic transport in affected tissues, but should also, perhaps more importantly, investigate tissue transformation in any proposed comprehensive curative regimen.

APPENDIX A

Model of Interstitial Transport

For all mice, the tissue hydraulic conductivity was calculated using the model presented by Swartz, et al. (14). As this model includes a term for flux into lymphatic capillaries, and neither the Chy nor the K14-VEGFR-3-Ig mouse has dermal lymphatic capillaries, there was some concern as to the applicability of the steady-state formulation presented. The model can also be applied when no flux is present; thereby changing the final governing equations to solve for *K*, and a comparison between the two solutions reveals the extent of flux losses. Flux in mice without lymphatics would indicate post-capillary venuole reabsorption. The dramatic change in K for wildtype mice (Table A.1) illustrates the unaccounted for flux to lymphatic capillaries, but as there is little difference in *K* for the K14-VEGFR-3-Ig mouse, there is little unaccounted for fluid loss at 29.4mmHg applied infusion pressure. At higher applied pressures, however, some capillary reabsorption may occur.

	K (mm^2/min/mmHg)	
	Wildtype	K14-VEGFR-3-Ig
Steady-State Approximation	0.0272	0.1185
Non-SS, Exact Solution (P^*_0=29.4mmHg)	0.0050	0.1345
Non-SS, Exact Solution (P^*_0=40.8mmHg)	0.0003	0.0050
* for the exact solution, a P* of 1mmHg were used.		

Table A.1. Calculated hydraulic conductivities for one example mouse using the various calculations described. The unsteady state solution fails for mice with lymphatic uptake. Higher infusion pressures potentially force capillary reabsorption, as a flux loss of tracer appears in the unsteady state calculation.

REFERENCES

1. Rockson, S.G. 2001. Lymphedema. *Am J Med* 110:288-295.
2. Daroczy, J. 1995. Pathology of lymphedema. *Clin Dermatol* 13:433-444.
3. Olszewski, W.L., Engeset, A., Romaniuk, A., Grzelak, I., and Ziolkowska, A. 1990. Immune cells in peripheral lymph and skin of patients with obstructive lymphedema. *Lymphology* 23:23-33.
4. Piller, N.B. 1990. Macrophage and tissue changes in the developmental phases of secondary lymphoedema and during conservative therapy with benzopyrone. *Arch Histol Cytol* 53 Suppl:209-218.
5. Rutkowski, J.M., Moya, M., Johannes, J., Goldman, J., and Swartz, M.A. 2006. Secondary lymphedema in the mouse tail: Lymphatic hyperplasia, VEGF-C upregulation, and the protective role of MMP-9. *Microvasc Res* 72:161-171.
6. Schirger, A., Harrison, E.G., Jr., and Janes, J.M. 1962. Idiopathic lymphedema. Review of 131 cases. *Jama* 182:14-22.
7. Karkkainen, M.J., Saaristo, A., Jussila, L., Karila, K.A., Lawrence, E.C., Pajusola, K., Bueler, H., Eichmann, A., Kauppinen, R., Kettunen, M.I., et al. 2001. A model for gene therapy of human hereditary lymphedema. *Proc Natl Acad Sci U S A* 98:12677-12682.
8. Petrova, T.V., Karpanen, T., Norrmen, C., Mellor, R., Tamakoshi, T., Finegold, D., Ferrell, R., Kerjaschki, D., Mortimer, P., Yla-Herttuala, S., et al. 2004. Defective valves and abnormal mural cell recruitment underlie lymphatic vascular failure in lymphedema distichiasis. *Nat Med* 10:974-981.
9. Wigle, J.T., and Oliver, G. 1999. Prox1 function is required for the development of the murine lymphatic system. *Cell* 98:769-778.
10. Makinen, T., Jussila, L., Veikkola, T., Karpanen, T., Kettunen, M.I., Pulkkanen, K.J., Kauppinen, R., Jackson, D.G., Kubo, H., Nishikawa, S., et al. 2001. Inhibition of lymphangiogenesis with resulting lymphedema in transgenic mice expressing soluble VEGF receptor-3. *Nat Med* 7:199-205.
11. Karlsen, T.V., Karkkainen, M.J., Alitalo, K., and Wiig, H. 2006. Transcapillary fluid balance consequences of missing initial lymphatics studied in a mouse model of primary lymphoedema. *J Physiol* 574:583-596.
12. Wiederhielm, C.A., Woodbury, J.W., Kirk, S., and Rushmer, R.F. 1964. Pulsatile Pressures in the Microcirculation of Frog's Mesentery. *Am J Physiol* 207:173-176.
13. Wiig, H., Reed, R.K., and Aukland, K. 1981. Micropuncture measurement of interstitial fluid pressure in rat subcutis and skeletal muscle: comparison to wick-in-needle technique. *Microvasc Res* 21:308-319.
14. Swartz, M.A., Kaipainen, A., Netti, P.A., Brekken, C., Boucher, Y., Grodzinsky, A.J., and Jain, R.K. 1999. Mechanics of interstitial-lymphatic fluid transport: theoretical foundation and experimental validation. *J Biomech* 32:1297-1307.
15. Woessner, J.F., Jr. 1961. The determination of hydroxyproline in tissue and protein samples containing small proportions of this imino acid. *Arch Biochem Biophys* 93:440-447.
16. Reed, R.K., Lepsoe, S., and Wiig, H. 1989. Interstitial exclusion of albumin in rat dermis and subcutis in over- and dehydration. *Am J Physiol* 257:H1819-1827.
17. Jackson, D.S., and Cleary, E.G. 1967. The determination of collagen and elastin. *Methods Biochem Anal* 15:25-76.
18. Bates, D.O., Levick, J.R., and Mortimer, P.S. 1992. Subcutaneous interstitial fluid pressure and arm volume in lymphoedema. *Int J Microcirc Clin Exp* 11:359-373.

19. Bates, D.O., Levick, J.R., and Mortimer, P.S. 1993. Change in macromolecular composition of interstitial fluid from swollen arms after breast cancer treatment, and its implications. *Clin Sci (Lond)* 85:737-746.
20. Bates, D.O., Levick, J.R., and Mortimer, P.S. 1994. Starling pressures in the human arm and their alteration in postmastectomy oedema. *J Physiol* 477 (Pt 2):355-363.
21. Barber, B.J., Babbitt, R.A., Parameswaran, S., and Dutta, S. 1995. Age-related changes in rat interstitial matrix hydration and serum proteins. *J Gerontol A Biol Sci Med Sci* 50:B282-287.
22. Levick, J.R. 1987. Flow through interstitium and other fibrous matrices. *Q J Exp Physiol* 72:409-437.
23. Aukland, K., and Reed, R.K. 1993. Interstitial-lymphatic mechanisms in the control of extracellular fluid volume. *Physiol Rev* 73:1-78.
24. Rutkowski, J.M., and Swartz, M.A. 2007. A driving force for change: interstitial flow as a morphoregulator. *Trends Cell Biol* 17:44-50.

FIGURE LEGENDS

Figure 1: Chy and K14-VEGFR-3-Ig mice lack dermal lymphatic capillaries. As compared to their respective wildtype controls, both Chy mice (left) and K14-VEGFR-3-Ig (right) mice lack dermal lymphatics (arrows)(green, LYVE-1). Subdermal lymphatic vessels (arrowheads) are visible with immunohistochemistry in all mice. The blood vasculature (red, CD31) was normal in the dermis of all strains. Bar=200um. B) Following an infusion of FITC-conjugated dextran, no deeper lymphatic vessels were visible in K14-VEGFR-3-Ig mice. The collecting vessel is visible along the tail vein of wildtype mice. Bar=1mm.

Figure 2: Quantification of interstitial fluid pressure and dermal hydraulic conductivities revealed marked differences in the tissue adaptation to lymphedema. A) In both mouse strains, the measured IFP was significantly higher than their respective wildtype controls ($P<0.01$). B) In Chy mice, the calculated hydraulic conductivity is the same as in wildtype controls, despite the different tissue composition. C) No lymphatic capillary uptake (arrow) was seen downstream of the convective front in Chy mice. D) K14-VEGFR-3-Ig mice exhibit the expected behavior in lymphedema with a significantly increased hydraulic conductivity in the skin. E) Lymphatic capillary uptake (arrow) was not seen in the K14-VEGFR-3-Ig transgenic mouse.

Figure 3: Histologic staining of tail tissue demonstrates that characteristics of lymphedema in Chy and K14-VEGFR-3-Ig mice. A) Giemsa matrix staining reveals the swelling of the hypdermis (arrows) in Chy (left) and K14-VEGFR-3-Ig (right) mice as compared to their respective wildtype controls. Dense thickening of the dermis is also present in each edematous strain (arrowheads). Bar=500um. B) Oil red O staining reveals the lipid accumulation, as compared to normal, in the hypodermis of Chy mice (left). K14-VEGFR-3-Ig mice (right) did not appear to have significant lipid accumulation. Bar=200um. C) The interstitial cross-sectional area is significantly larger in Chy and K14-VEGFR-3-Ig mice at the same distance from the tail tip. D) Quantification of % lipid in the dermis confirmed that Chy mice accumulate significant amounts of lipid, while K14-VEGFR-3-Ig mice may actually have a less fatty hypodermis than normal mice.

Figure 4: Quantifications of tissue water weight, collagen composition, and lipid content reveal marked differences between the skin of Chy and K14-VEGFR-3-Ig mice. A) Total

tissue water, a common symptom in lymphedema, was significantly elevated in each model strain. B) Collagen composition (%, dry weight basis) was significantly increased in Chy mouse skin, but normal in K14-VEGFR-3-Ig mice. C) Lipids extracted (% mass) were significantly increased in Chy skin, but actually decreased in the skin of K14-VEGFR-3-Ig mice. * indicates $P<0.05$.

Figure 1

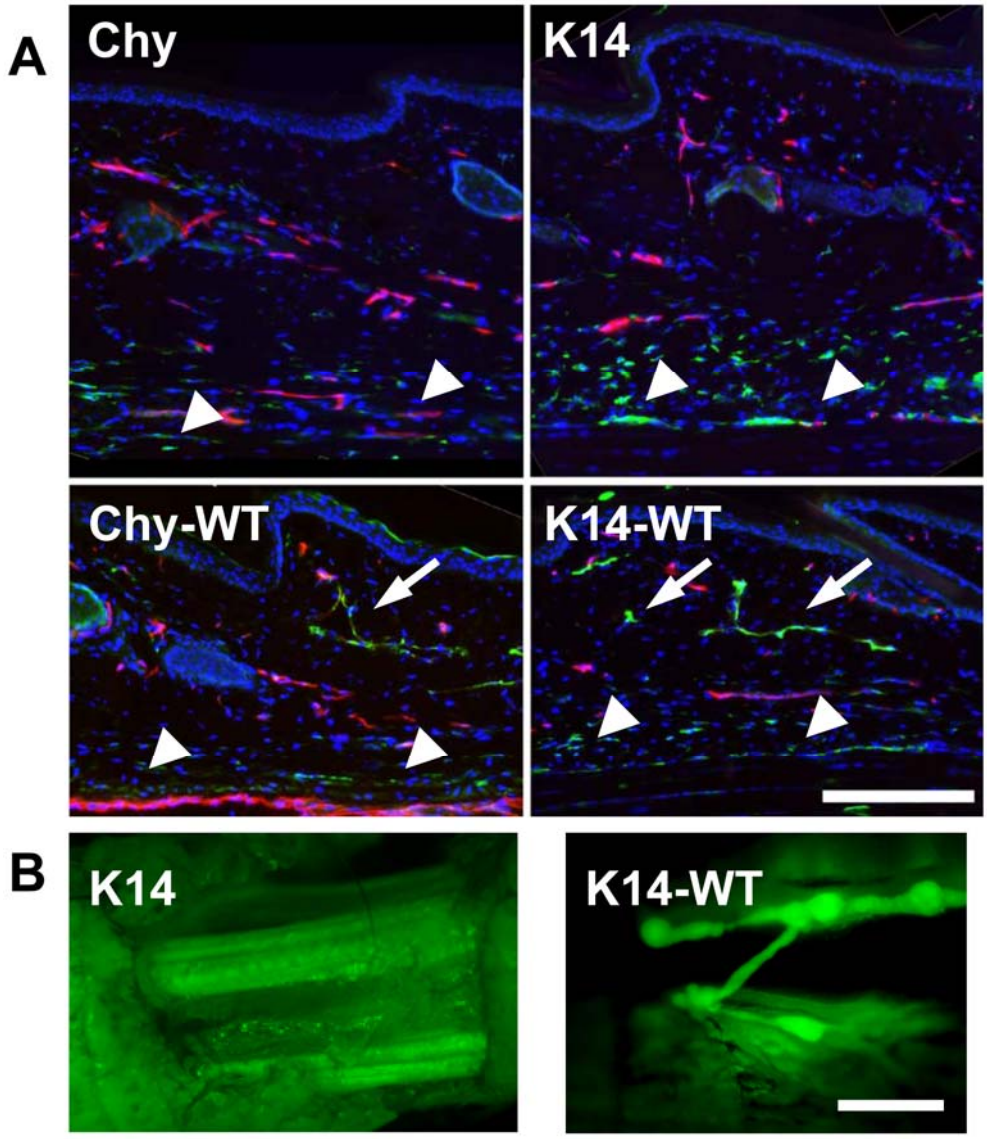

This page is intentionally left blank.

Figure 2

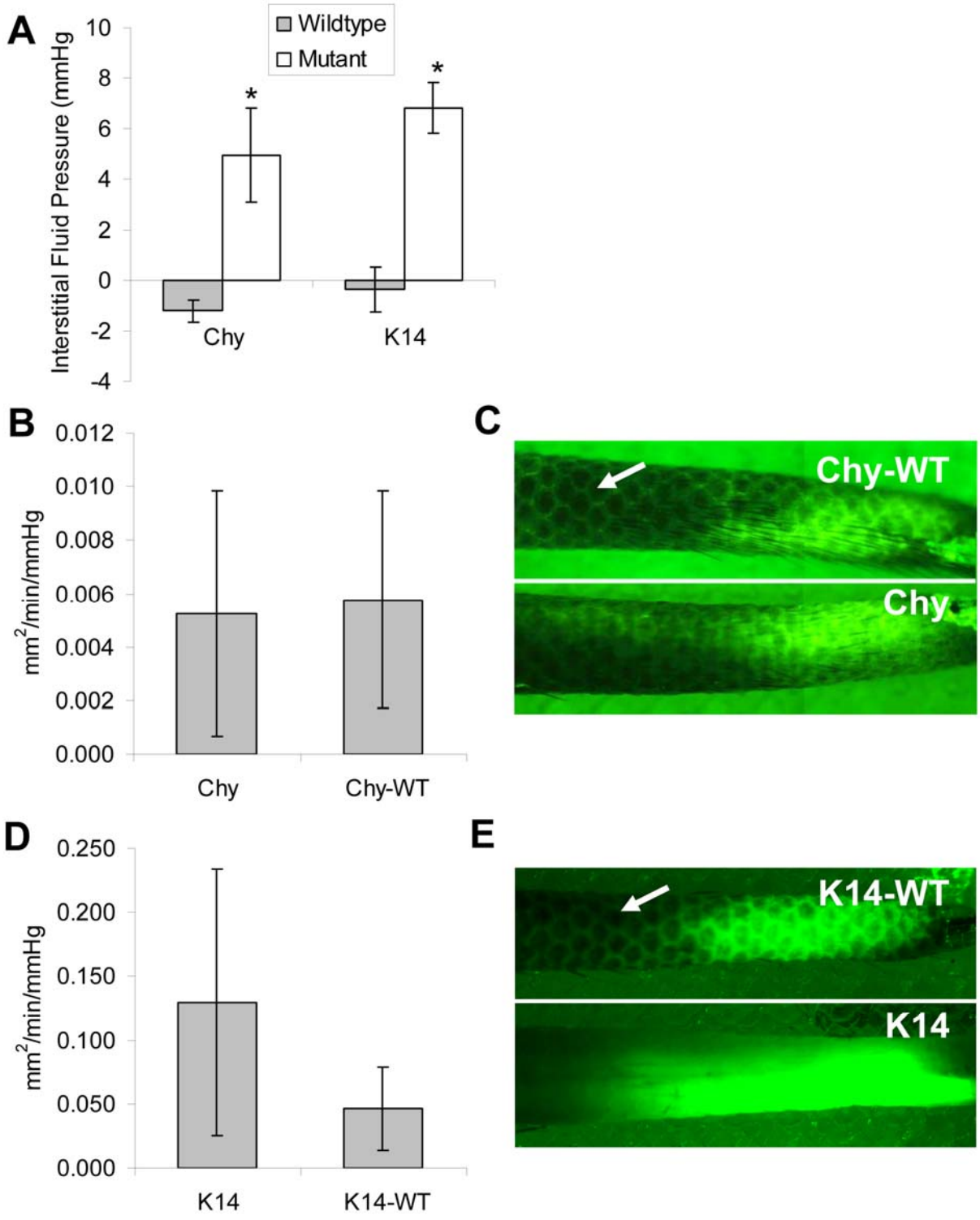
A
Wildtype
Mutant
Interstitial Fluid Pressure (mmHg
10
8
6
4
2
0
-2
-4
*
*
Chy
K14
B
0.012
0.010
0.008
0.006
0.004
0.002
0.000
mm2/min/mmHg
Chy
Chy-WT
C
Chy-WT
Chy
D
0.250
0.200
0.150
0.100
0.050
0.000
mm2/min/mmHg
K14
K14-WT
E
K14-WT
K14

This page is intentionally left blank.

Figure 3

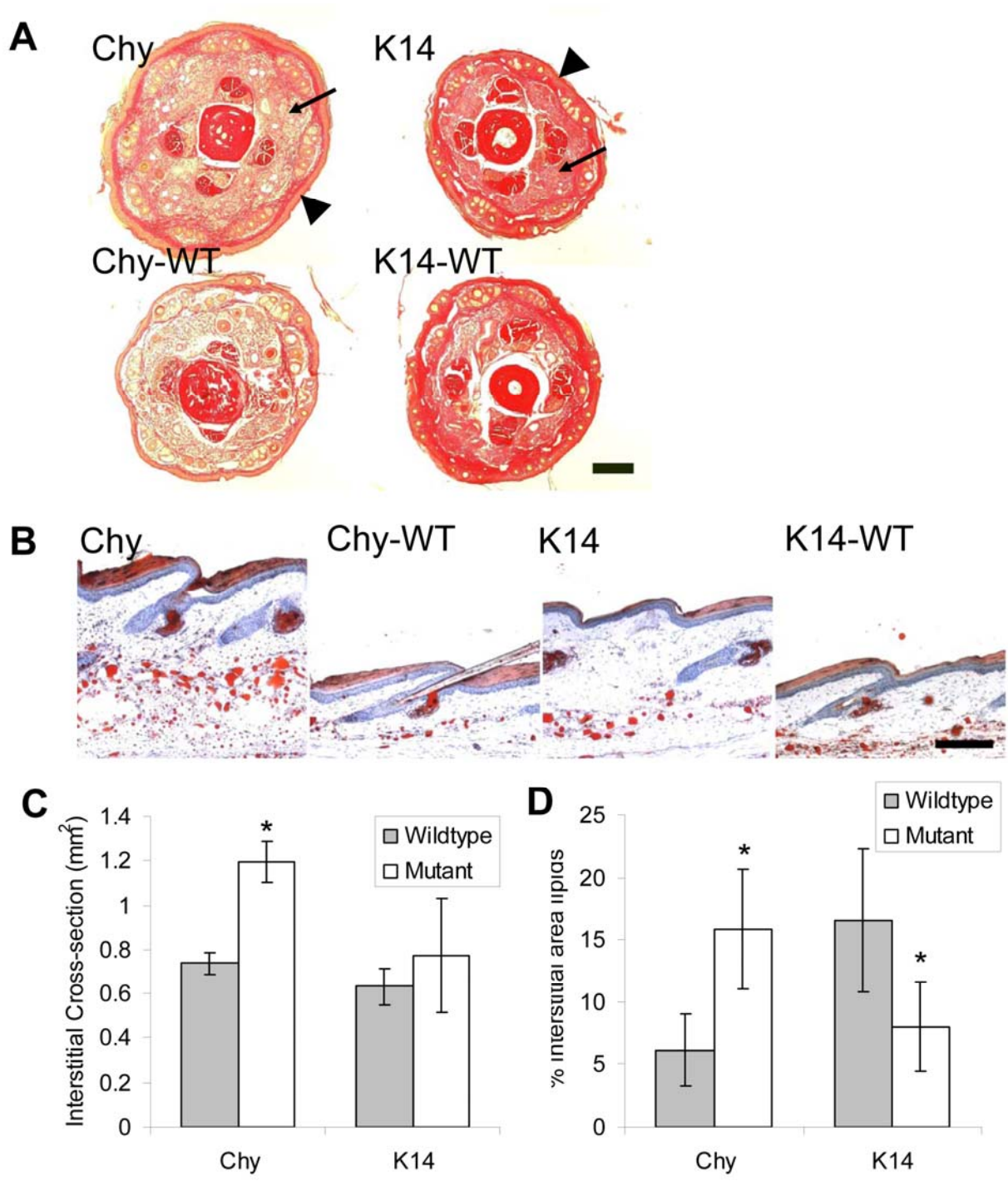
A
Chy
K14
Chy-WT
K14-WT
B
Chy
Chy-WT
K14
K14-WT
C
Interstitial Cross-section (mm²)
1.4
1.2
1
0.8
0.6
0.4
0.2
0
*
Wildtype
Mutant
Chy
K14
D
% Interstitial area lipids
25
20
15
10
5
0
*
*
Wildtype
Mutant
Chy
K14

This page is intentionally left blank.

Figure 4

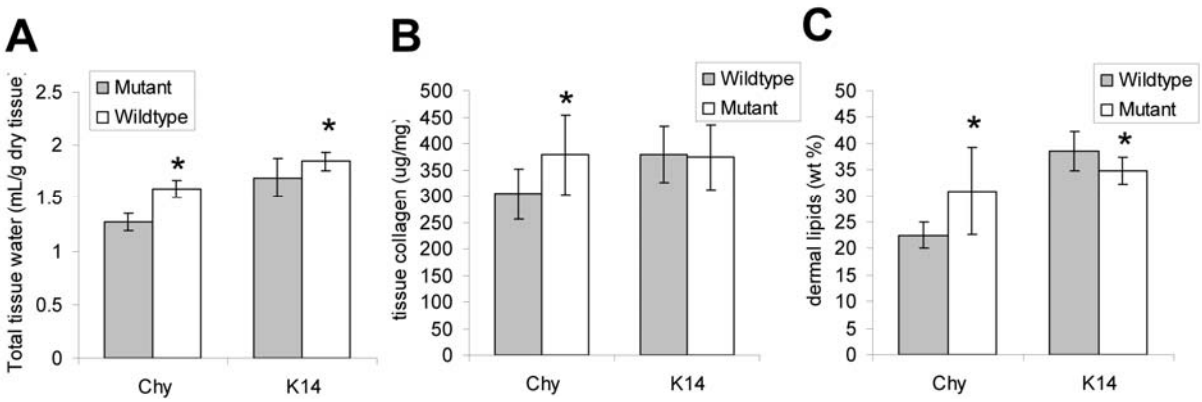
A
Total tissue water (mL/g dry tissue)
2.5
2
1.5
1
0.5
0
Mutant
Wildtype
*
*
Chy
K14
B
tissue collagen (ug/mg)
500
450
400
350
300
250
200
150
100
50
0
Wildtype
Mutant
*
Chy
K14
C
dermal lipids (wt %)
50
45
40
35
30
25
20
15
10
5
0
Wildtype
Mutant
*
*
Chy
K14

This page is intentionally left blank.

CHAPTER 8:
ORIGINAL MANUSCRIPT 7

Ovarian lymphangiogenesis is necessary for hormonal maintenance and fetal development during murine pregnancy

Joseph M. Rutkowski[1]*, Jong Eun Ihm[1]*, Seung Tae Lee[1], Alexandra Liagre-Quazzola[2,3], Veronique I. Greenwood[1], Miriella C. Pasquier[1], Didier Trono[2,3], Jeffrey A. Hubbell[1], and Melody A. Swartz[1]

1: Institute of Bioengineering, School of Life Sciences, École Polytechnique Fédérale de Lausanne (EPFL), Switzerland
2: Global Health Institute, School of Life Sciences, École Polytechnique Fédérale de Lausanne (EPFL), Switzerland
3: "Frontiers in Genetics" National Center for Competence in Research, École Polytechnique Fédérale de Lausanne (EPFL), Switzerland
* These authors contributed equal work

Originally submitted 2 July 2007

Currently in revision with **Journal of Clinical Investigation**

ABSTRACT

Lymphatic vessels surround developing follicles within the ovary, but their roles in follicle maturation and pregnancy, as well as the necessity of lymphangiogenesis in these processes, are undefined. Here we demonstrate a critical role for ovarian lymphatics in murine reproduction by blocking lymphangiogenesis using systemic delivery of mF4-31C1, a specific antagonist antibody to vascular endothelial growth factor receptor (VEGFR)-3. VEGFR-3 neutralization for two weeks prior to mating and pregnancy blocked ovarian lymphangiogenesis in all stages of follicle maturation without limiting blood angiogenesis. While the number of oocytes ovulated and fertilized and embryonic implantations in the uterus were all normal, all pregnancies were unsuccessful due to fetal defects and miscarriage. Preantral follicles isolated directly from treated ovaries, were able to grow and mature normally *in vitro*. When embryos from mF4-31C1 treated mice were isolated and transferred to untreated surrogate mothers, pregnancies were normal and came to term. Conversely, implantation of normal embryos into treated surrogate mothers led to the same fetal deficiencies as observed with pregnancies from mothers treated *in situ*. This suggests the importance of lymphatic capillaries in maintaining an ovarian hormonal environment necessary for fetal development and pregnancy maintenance. Indeed, pregnant mice with limited follicular lymphangiogenesis also exhibited significantly reduced serum progesterone and estradiol, hormones that are sourced from the ovarian corpora lutea during pregnancy. In total, these results demonstrate that lymphangiogenesis is a necessary process for ovarian lymphatic capillaries that transport hormones and thereby critical for successful reproduction.

Keywords: corpus luteum, folliculogenesis, lymphatic, VEGF-C, VEGFR-3, blastocyst

INTRODUCTION

Lymphatic vessels are present within the ovary and surround follicles during maturation (1, 2), but the importance of the lymphatic vasculature and lymphangiogenesis in the ovary is unclear. Consequently, the potential roles of lymphatic vessels in follicle maturation and pregnancy, and the extent or even necessity of lymphangiogenesis in reproduction, are undefined. This contrasts with ovarian blood angiogenesis, whose critical roles in follicular nourishment and maturation as well as the formation and maintenance of the corpus luteum is well appreciated; indeed, oocyte fertilization, embryonic implantation, and pregnancy all require blood angiogenesis (3-5). Lymphangiogenesis, which is often concurrent with blood angiogenesis (6), may play an equally important role in these processes.

Adult blood angiogenesis requires signaling via vascular endothelial growth factor (VEGF) receptor -2 (VEGFR-2), most potently by VEGF ligation (7, 8). In murine ovaries, VEGF expression increases during angiogenic growth phases (9), and blockade of VEGFR-2 signaling effectively prevents angiogenesis, resulting in a marked decrease in ovarian weight, blood vessel density, number of corpora lutea, and infertility (10-12). Since gonadatropin treatment apparently does not correct these deficiencies (13), it is likely that follicle maturation and successful pregnancy are highly dependent on VEGFR-2-mediated neovascularization (3, 14).

VEGFR-3 is expressed primarily on lymphatic endothelial cells (LECs) in adult tissue (15, 16), and its signaling, via ligation by VEGF-C or VEGF-D, is necessary for lymphangiogenesis by inducing LEC proliferation and migration (16-19). Blockade of VEGFR-3 signaling, using a function blocking antibody such as mF4-31C1 (ImClone Systems), completely blocks the initiation of new lymphatic vessels in adult mice without affecting pre-existing lymphatic morphology or function and without apparently affecting blood angiogenesis (17, 18). Here we investigate the roles of lymphatic vessels and lymphangiogenesis in reproductive functions of the ovary. Specifically, we hypothesize that lymphangiogenesis within the ovary parallels blood angiogenesis during reproductive cycles (20-22) and that these new lymphatic capillaries may serve to balance hormones produced within the ovary, transport hormones from the ovary and corpus luteum, and aid in hormonal communication between the uterus and ovaries during pregnancy (23-25). Using combined *in vivo*, *ex vivo*, and *in vitro* methods, we examined which aspects of fertility are influenced by inhibited lymphangiogenesis, including oocyte and follicular development and maturation,

embryonic implantation in the uterus, and embryonic development. We show that blocking ovarian lymphangiogenesis prevents viable, full-term pregnancies due to decreased systemic hormone levels, thereby demonstrating a critical role for the ovarian lymphatic vasculature in reproduction.

MATERIALS AND METHODS

Animal procedures

All protocols were approved by the Veterinary Authorities of the Canton Vaud according to Swiss law (protocols 1687, 1988, and 1988.1). The function-blocking antibody against murine VEGFR-3, mF4-31C1, was kindly provided by ImClone Systems (18). For two weeks prior to mating, 0.25 mL of 2.5 mg/mL mF4-31C1 was injected intraperitoneally every two days. 0.25 mL saline was similarly injected for some control groups with no adverse effects on reproductive potential.

For studies without fertilization, 3 week old female F1 hybrid mice (C57Bl/6JxCBA/caj, Charles River Laboratories, France) were treated for two weeks and then sacrificed. Follicles and ovaries were collected for subsequent *in vitro* culture and histological examination, respectively.

In studies requiring fertilization, 4-6 week old female F1 hybrid (C57Bl/6JxCBA/caj) mice were treated for two weeks before mating (to ensure spanning two full menstrual cycles). At approximately 6-8 weeks of age, mice in estrus were mated and coitus was evaluated by the presence of a vaginal plug 16 hours post-mating. For embryo retrieval, *ex vivo* culture, and transplantation, mice were sacrificed 42 hours post-mating and two-cell embryos collected by oviduct flushing with M2 medium (Sigma-Aldrich, St. Louis, MO).

Embryos were implanted into pseudo-pregnant recipient NMRI mice (Charles River) following standard implantation protocols. Embryos from mF4-31C1 treated and untreated F1 hybrid donors were implanted into treated and untreated recipients. Recipient mice were anesthetized using an intraperitoneal injection of ketamine (100mg/kg) and xylazine (10mg/kg). A small midsagittal incision, over each oviduct, was made and the donor embryos were deposited into each oviduct by mouth pipetting under a stereomicroscope. The incision was then sutured and pregnancies were permitted to continue through day 17. Implantation success was consistently >90%.

For examination of fetal development and uterine implantation, mice were sacrificed at pregnancy day 17 or after birth. Implantation spots were counted in the uterus and fetuses

were graded as either (a) normal, (b) grade i – normal sized but abnormal coloration, (c) grade ii –under-developed fetus (in size or limb development), and (d) grade iii – implanted cell mass or necrotic fetus (refer to Figure 2B for examples).

In vitro follicle culture and maturation

To determine the direct effects of *in vivo* mF4-31C1 treatment on normal follicle maturation potential, ovaries were isolated from 5-week-old mice following two weeks of antibody treatment. *In vitro* maturation of preantral follicles was performed as previously described (26, 27). Briefly, whole ovaries were placed in 3 mL of L-15 Leibovitz-glutamax medium (Gibco, Carlsbad, CA) with 10% FBS (HyClone Laboratories, Logan, UT) and 1% penicillin-streptomycin (Gibco) solution. Preantral follicles with diameters of 100-130 μm were mechanically separated from the ovaries, washed, transferred to individual 10 μL droplets of MEM-alpha-glutamax medium containing 5% FBS, 1% ITS (5 μg/mL, insulin, 5 μg/mL, transferrin, and 5 μg/mL selenium mixture solution; all Gibco), 1% penicillin-streptomycin, and 100 MIU/mL recombinant human follicle stimulating hormone (hFSH) (Organon, Switzerland).

On day 12 of *in vitro* culture, follicle maturation was induced by exposing to medium lacking hFSH, but supplemented with 2.5 IU/mL hCG-Pregnyl (Organon) and 5 ng/mL murine epidermal growth factor (Sigma). After 16 hours, oocytes were retrieved by removing the follicular cumulus cells using 200 IU/mL of hyaluronidase (Sigma). Oocytes were classified by the following maturation states: germinal vesicle (GV), germinal vesicle breakdown (GVBD) and metaphase II (MII).

In groups were VEGFR-3 was neutralized directly on normal follicles, follicles were cultured using the above reagents in a method modified from West, et al. (28). 10 μg/mL mF4-31C1 was added to the culture medium of the test group.

Ex vivo development of 2-cell embryos

To determine the direct effects of VEGFR-3 inhibition on preimplantation embryonic development, two-cell embryos were retrieved from the oviducts and cultured in 4-well dishes containing 400 uL of M16 medium (Sigma). The number of embryos that developed into the 8-cell, morula, and blastocyst stages were quantified and imaged under a Nikon SMZ1000 stereomicroscope with a Nikon DS-5M monochrome camera at 66, 90 and 114 hours after mating, respectively.

Immunofluorescence, immunohistochemistry, and histology

To visualize lymphatic vessels, 6-µm-thick ovary and uterus cryosections were labeled with a primary antibody to the lymphatic-specific marker LYVE-1 (1:500; 07-538; Upstate, Charlottesville, VA). For blood vessels, ovaries were labeled with a FITC-conjugated primary antibody to CD31/PECAM-1 (1:200; 550274; BD Pharmingen, San Jose, CA). Vessels were also co-labeled for VEGFR-3 (1:100; AF743; R&D Systems, Minneapolis, MN). Sections were also labeled for the macrophage-specific surface marker F4/80 (1:50; MCA497; AbD Serotec, Oxford, UK) and collagen IV (1:1000, 10760; MP Biomedicals, Irvine, CA). These antibodies were detected with Alexafluor 488 or 594-conjugated donkey, rabbit, or goat IgG secondary antibodies (1:200, Molecular Probes) and nuclei were labeled with DAPI mounting medium (Vector Labs, Burlingame, CA). Fluorescent labeling was observed and imaged using a Zeiss Axiovert 200M microscope with a Zeiss MRm camera. Slides were then rinsed and counterstained with hematoxylin and eosin, dehydrated, mounted with Eukitt (Fluka Chemie, AG, Buchs, Switzerland), and imaged again using a color Zeiss MRc camera. The corresponding fluorescence and chromogenic images were then compared for identification, and subsequent quantification, of follicular development.

To label apoptotic cells, a fluorescence TUNEL kit was used according to manufacturer's instructions (Roche Diagnositics, Rotkreuz, Switzerland). Oil red O (Sigma-Aldrich, Buchs, Switzerland) was used to stain lipids in ovarian frozen sections. Sections were counterstained with hematoxylin and immediately mounted with Möwiol-based mounting medium for imaging.

Serum Analysis

Serum was collected from all mice when sacrificed and analyzed using ELISA kits for estradiol (Calbiotech, Spring Valley, CA) and progesterone (BioSource, Carlsbad, CA) levels according to manufacturer's instructions. Absorbance was measured using a Tecan Safire2 plate reader (Tecan, Männedorf, Swtizerland).

Image analysis and quantification

To quantify macrophages, Oil red O, and TUNEL labeled slides, images of entire ovaries were assembled, the ovary body was outlined, and the percentage of positive area measured using Metamorph 6.3 (Molecular Devices Corp., Sunnyvale, CA). For lymphatic and blood vessel quantification, we considered each follicular maturation state. Each follicle was outlined using a Wacom CintiQ freehand graphic monitor (Wacom Co., Ltd., Saitama,

Japan) for accuracy. Vessel labeling was defined by fluorescence threshold and the number of positive pixels for each follicle was measured. The average vessel area for each maturation state is reported. Follicle maturation states were scored as follows: (i) preantral follicle (secondary follicle), (ii) antral follicle (small follicle with formed atrium), (iii) Graffian follicle (large follicle with significant atrium), and (iv) corpora lutea (Supplemental Figure 1). These divisions were consistently identified across multiple examiners.

Statistical Methods

For determining statistical significance between treatments in follicle vascularization over the stages of maturation, follicle survival and maturation, and embryo development, ANOVA followed by DUNCAN was used. Students't-tests were used to compare other factors in treated vs. untreated plasma or in ovaries as a whole.

RESULTS

VEGFR-3 neutralization prevents successful murine pregnancy

Female mice were mated at 6-8 weeks of age following 2 weeks of treatment with either (i) anti-VEGFR-3 neutralizing antibody (mF4-31C1), (ii) saline, or (iii) no injection (normal). All treatments were ceased before mating. Mice receiving saline or no injection were equally successful in giving birth to normal and healthy pups. Mice treated with mF4-31C1, however, failed to produce a single live birth in the animals tested. This unexpected response to VEGFR-3 blockade prior to mating led to the hypothesis that lymphangiogenesis within the ovary helps mediate reproductive ability.

Ovarian lymphangiogenesis but not blood angiogenesis is inhibited by VEGFR-3 blockade

First, we examined blood and lymphatic vessels in the ovaries of saline-treated mice using CD31 and LYVE-1 co-labeling, and examined their relative expression of VEGFR-3. While all lymphatic (LYVE-1^{+}) vessels expressed VEGFR-3 (Fig. 1A), limited VEGFR-3 expression was found on follicular blood vessels (Fig. 1B). Lymphatic vessels were observed surrounding nearly every follicle at all maturation states and did not penetrate into the follicular body or thecal layers (Fig. 1A, C). The extent of lymphatic vascularization was dependent on the maturation stage of the follicles, with preantral follicles displaying only a few sparse lymphatics and corpora lutea displaying a significantly higher degree of peripheral lymphatic vessels. In ovaries from mice treated with mF4-31C1, the extent of lymphatic

vascularization was greatly reduced at all stages of follicular maturation, as measured by vessel density (Fig. 1D). There was not, however, a complete lack of lymphatic vessels. This was consistent with our previous studies where VEGFR-3 neutralization prevented lymphangiogenesis but had no morphological effects on pre-existing lymphatic vessels (17, 18).

While mature blood vessels do not express VEGFR-3, angiogenic blood vessels have been observed to express VEGFR-3 during normal development as well as in tumors and healing wounds (29-31), and there is evidence that VEGFR-3 inhibition may limit tumor angiogenesis (32, 33). Since blood angiogenesis in the ovary is necessary for pregnancy (3-5, 13, 34), we examined the blood vessels to assess whether mF4-31C1 had any effects on ovarian blood angiogenesis. We found VEGFR-3 expression primarily limited to lymphatic vessels, with the exception of the blood vasculature within the corpora lutea (Fig. 1B). More importantly, the extent of blood vascularization, as quantified by vessel density, was not significantly affected by VEGFR-3 blockade (Fig. 1E). Therefore, ovarian blood angiogenesis appeared to be unaffected by VEGFR-3 neutralization, consistent with our findings in dermal wound healing and regeneration (17, 18).

VEGFR-3 neutralization pre-fertilization leads to retarded embryonic development

Since pregnancies were not successful in VEGFR-3 neutralized mice, we sought to determine at what stage post-fertilization observable differences could be seen in embryonic and fetal development. Mice were treated for two weeks and then mated, and the uteri examined at pregnancy day 17. We observed no differences in the number of implantation sites in the uteri of treated vs. control mice, but fewer fetuses remained in mF4-31C1-treated mice at pregnancy day 17 (Fig. 2A). More strikingly, those fetuses remaining were dramatically smaller and underdeveloped (Figs. 2A,B), threatening future miscarriage. Combined, these results indicate that multiple abortions had already occurred by day 17, and that the remaining fetuses were likely not viable.

To determine whether the numbers of ovulated oocytes were normal and to examine blastocyst development from VEGFR-3-blocked mice, mice were sacrificed 42 hr after mating and 2-cell embryos were flushed from the oviduct. The numbers of harvested 2-cell embryos per mouse were the same in normal vs treated mice, with an average of 7.1±2.5 and 8.3±1.5 taken from normal and treated mice, respectively. Additionally, all 2-cell embryos were cultured *in vitro* to blastocysts with 100% success, regardless of treatment (Fig. 2C). Thus, although VEGFR-3 neutralization pre-maing dramatically affected embryonic

development, it did not appear to reduce ovulation quantity or fertilization potential of ovulated oocytes.

VEGFR-3 neutralization decreases number of healthy follicles but has no direct effect on their quality

To explore the possible effects of VEGFR-3 signaling and lack of lymphatic vasculature on follicular maturation potential in virgin mice, preantral follicles (100-130 μm in size) were retrieved after 2 weeks of treatment. The numbers of healthy preantral follicles successfully retrieved was lower ($P<0.01$) from mF4-31C1-treated mice than from saline-treated mice (Fig. 3A). This was due to a noted fragile contact between the oocyte and granulosa cells in mF4-31C1 treated mice (noting that preantral follicles require interactions between surrounding granulosa and theca cell layers and the oocyte (26)). These contacts were apparently not, however, due to any loss of integrity of the basal lamina as examined by collagen IV staining (Fig. 3B), since no differences were observed in the granulosa-thecal boundary. While these discrepancies may impact the local hormonal environment *in vivo*, once separated and cultured *in vitro*, both groups of preantral follicles exhibited similar survival rates ($P=0.763$, Fig. 3C). Surviving follicles were able to mature normally, as defined by the method (27), through the GVBD and MII phase with equal success (Fig. 3C).

Finally, to determine whether VEGFR-3 blocking had any direct effects on folliculogenesis, we isolated preantral follicles from untreated mice and cultured them in the presence of 10 μg/mL mF4-31C1 *in vitro*. All follicles survived (Fig. 3D) and grew to similar sizes ($P=0.299$, Fig. 3E). Thus, VEGFR-3 blocking had no direct effect on *in vitro* growth and maturation of secondary follicles.

Loss of lymphatic capillaries does not alter macrophage recruitment, lipid accumulation, or apoptosis within the ovary

Our combined *in vivo* and *in vitro* results suggest that failed pregnancies derive from alterations in the follicular environment due to the lack of lymphatic vessels. Since immune function may be important in mediating the balance between hormone accumulation (35) and follicle maturation and ovulation within the ovary (36, 37), and since lymphatic capillaries may be important in ovarian immune cell trafficking (20, 21), we examined macrophage populations in the ovaries (Fig. 4A). We found no significant differences in macrophage numbers within the ovaries ($P=0.362$; Fig. 4B). Therefore, the lack of lymphatic capillaries did not visibly alter overall macrophage recruitment in the ovary.

Furthermore, lymphatic insufficiencies have been linked to excessive tissue lipid accumulation in skin (38, 39). Since lipids are necessary for hormone synthesis by granulosa and luteal cells in the ovary (40, 41), we examined gross lipid content in the ovaries via oil red O staining (Fig. 4C), but no differences were observed between mF4-31C1-treated and control animals (P=0.532; Fig. 4D).

Finally, we sought to determine whether blocking VEGFR-3 would affect cellular apoptosis, which normally occurs within certain bodies of the ovary throughout the menstrual cycle (42). Analysis of apoptotic cells revealed a similar distribution and number of TUNEL-positive cells within the ovary (Fig. 4F) in both groups. Consistent with earlier findings (42, 43), apoptotic cells were confined primarily to the interior layer granulosum of regressing antral follicles, regressing corpora lutea, and post-ovulatory cells at the ovarian wall in both groups (Fig. 4E). Thus, neither the direct blockade of VEGFR-3 nor the resultant lack of a significant lymphatic vasculature led to abnormal cell apoptosis in the ovary.

Loss of ovarian lymphatics results in significantly reduced hormone levels during pregnancy

With few other differences between ovaries from treated and untreated mice noted, we sought to determine whether the lack of ovarian lymphatics altered hormone levels during pregnancy. Serum collected from systemic circulation 42 hours after mating revealed no change in progesterone levels (Fig. 5A), but a significant decrease in estradiol levels (Fig. 5B). As estradiol is sourced from the granulosa/luteal cells in the corpus luteum during pregnancy, and since mF4-31C1 treatment had the greatest effect on decreasing follicle-associated lymphatic capillaries around the corpora lutea (Fig. 1D), these data suggest that ovarian lymphangiogenesis is critical for hormone transport and that decreased follicular lymphatics lead to decreased progesterone and estrogen transport, critical for maintaining pregnancy, from the ovary. These findings also support the hypothesis that intraovarian lymphatic capillaries are the entry point of ovarian sourced hormones to the systemic circulation (25).

As hormone secretion by the murine corpora lutea has also been linked to proper blood angiogenesis, we verified the blood vasculature of pregnant mouse ovaries at day 17. In both untreated and treated mice, the blood vasculature of the corpora lutea appeared normal (Fig. 5C) while the lymphatic vasculature surrounding these bodies in mF4-31C1 treated ovaries was notably deficient.

Reduced ovarian hormone production by recipient mothers results in poor fetal development and miscarriage of transplanted normal embryos

Finally, to demonstrate an ovarian, and not uterine, cause to pregnancy failures, we isolated two-cell embryos from normal and treated mothers and implanted them into normal and treated pseudo-pregnant recipient mothers. Regardless of the treatment of the donor mother, transplantation of embryos into normal mothers resulted in normal implantation and fetal development with only normal, viable fetuses found in the uterus at day 17 (Fig. 6A). Conversely, the deficient ovarian hormone signaling demonstrated in treated recipient mothers led to retarded fetal development of implanted embryos (Fig. 6A). In fact, the developmental deficiencies observed (Fig. 6B) were nearly identical to those found during *in situ* pregnancies (Fig. 2A,B). This supports the hypothesis of early ovarian lymphangiogenesis being necessary for subsequent pregnancy success.

Further verification of an ovarian source to failed pregnancies was found upon examination of the uterine blood and lymphatic vasculature from normal and treated mothers. No changes in the blood or lymphatic vessel network of the ovarian wall were noted in early pregnancy (Fig. 6D). This lack of differences in the uterine vasculature supported the findings of normal implantation rates, and reinforced that ovarian lymphangiogenesis is the likely process affecting hormone maintenance.

DISCUSSION

Taken in total, these results demonstrate that ovarian lymphatics, particularly those that develop during folliculogenesis, are necessary for maintaining pregnancy by providing a conduit for hormone transport. We saw that blockade of VEGFR-3 effectively halted lymphangiogenesis of maturing follicles within the ovary while not visibly affecting blood angiogenesis, macrophage recruitment, lipid accumulation, or overall cell apoptosis. In the absence of lymphangiogenesis, there were fewer patent secondary follicles, but those that were patent could mature normally, were ovulated, and could be fertilized. Embryonic masses naturally implanted in the uterus and partially developed, but all eventually miscarried; there were no successful births despite a normal number of uterine implantation spots. The absence of new lymphatics in the ovary appears mainly to disturb progesterone and estradiol levels during pregnancy. As these hormones are sourced from the copora lutea, it is likely the follicular lymphatic capillaries are necessary in regulating a hormonal environment conducive to normal pregnancy maintenance.

The ovarian microvasculature is critical in regulating hormonal transport during pregnancy. Normally, as follicles mature, the theca layers become vascularized by blood vessels (44) and support follicles by synthesizing estrogen (45); abnormalities in the theca cell layers can result in infertility (46). Post-implantation, proper blood vascularization is necessary for successful pregnancy (3) and blocking blood vessel formation in the corpus luteum leads to pregnancy failures (5). The developing blood vasculature of the corpus luteum permits this pseudo-organ to function properly, supplying increased progesterone and estrogen to the uterus to maintain pregnancy (5, 34, 47). New lymphatic capillaries must supply a route by which hormones produced within the ovary enter systemic circulation (25). Additionally, it has also been suggested that retrograde transfer of prostaglandin E2 – involved in many crucial processes of pregnancy, including maintenance of the corpora lutea - from the uterus to the ovary may occur via lymphatic transport (24, 34). Indeed, our data demonstrates that ovarian lymphatic vessels and lymphangiogenesis are essential for reproduction. The poorly connected granulose of isolated follicles and lower levels of progesterone and estradiol during pregnancy are likely related (48). The blocked growth of lymphatic capillaries during folliculogenesis disturbs the hormonal balance, as evidenced by reduced estardiol with VEGFR-3 neutralization. The lymphatic vasculature of these follicles is then insufficient to modulate the copora lutea and their hormone secretions during pregnancy. As VEGFR-3 signaling, and therefore, lymphangiogenesis, was only blocked prior to mating, oocytes are ovulated and fertilized and embryos implant normally in the uterus, we have isolated a developmental period in which lymphangiogenesis appears to most critically occur.

Another important role of lymphatic vasculature is to maintain fluid balance and interstitial fluid pressure (IFP). Throughout the body, these roles are inherently tied to lymphatic function. In the ovary, follicles become increasingly vascularized as they grow and a fluid-filled antrum is formed. The IFP in antra of developing follicles is approximately 15 mmHg regardless of size and drops rapidly to 5mm Hg immediately preceding ovulation (49). Post-ovulation, the IFP in the highly vascularized corpus luteum has been reported at a very high 50 mmHg (49). Ovarian lymphatics clearly must play a role in modulating fluid pressures. Furthermore, concurrent lymphangiogenesis is likely necessary to drain extravasated fluid from the newly formed blood capillaries (21) and may help to regulate morphogenetic processes and signaling on the luteal cells by controlling interstitial flow, an important morphoregulator for many cell types (50).

Lack of ovarian lymphatics have also been reported in ADAMTS-1 knockout mice (1) and Frizzled4 knockout mice exhibit low levels of ovarian VEGF-C, the primary ligand to VEGFR-3 (51). Both of these strains are infertile, despite normal mating behavior; infertility in these mice was concluded to be the result of failed hormone transport, intrafollicular pressure modulation, or maintenance of the corpus luteum. Mice possessing mutations in VEGFR-3 such that their lymphatic capillaries are present but poorly functional can reproduce, albeit at a lower success rate than wildtype mice (52, 53).

In conclusion, our data demonstrate that VEGFR-3-mediated lymphangiogenesis in the ovary is necessary for pregnancy by modulating levels of progesterone and estrogen from the corpora lutea. With anti-lymphangiogenic therapies aimed at preventing tumor metastases proposed as a cancer therapy (32, 33, 54) and pro-lymphangiogenic therapies proposed for treating lymphedema (52, 55, 56), it is critical to understand the role of lymphangiogenesis in the ovary and the role of lymphatics in fertility. Moreover, an increased knowledge of the physiologic role of lymphangiogenesis in the ovaries may provide insight into causes of infertility (and potential therapeutic strategies) and permit a more careful examination of angiogenesis and lymphangiogenesis inherent with ovarian cancers.

ACKNOWLEDGEMENTS

The authors are very grateful to Bronislaw Pytowski for helpful comments and discussion, and to ImClone Systems for the VEGFR-3 neutralizing antibody, mF4-31C1. We would also like to thank Veronique Borel and Sonia Verp for their assistance with the animals during this study. This work was funded in part by grants from the NIH (HL075217) and the Swiss National Science Foundation (107602).

REFERENCES

1. Brown, H.M., Dunning, K.R., Robker, R.L., Pritchard, M., and Russell, D.L. 2006. Requirement for ADAMTS-1 in extracellular matrix remodeling during ovarian folliculogenesis and lymphangiogenesis. *Dev Biol*.
2. Gaytan, F., Tarradas, E., Bellido, C., Morales, C., and Sanchez-Criado, J.E. 2002. Prostaglandin E(1) inhibits abnormal follicle rupture and restores ovulation in indomethacin-treated rats. *Biol Reprod* 67:1140-1147.
3. Fraser, H.M. 2006. Regulation of the ovarian follicular vasculature. *Reprod Biol Endocrinol* 4:18.
4. Kaczmarek, M.M., Schams, D., and Ziecik, A.J. 2005. Role of vascular endothelial growth factor in ovarian physiology - an overview. *Reprod Biol* 5:111-136.
5. Pauli, S.A., Tang, H., Wang, J., Bohlen, P., Posser, R., Hartman, T., Sauer, M.V., Kitajewski, J., and Zimmermann, R.C. 2005. The vascular endothelial growth factor (VEGF)/VEGF receptor 2 pathway is critical for blood vessel survival in corpora lutea of pregnancy in the rodent. *Endocrinology* 146:1301-1311.
6. Skobe, M., Hamberg, L.M., Hawighorst, T., Schirner, M., Wolf, G.L., Alitalo, K., and Detmar, M. 2001. Concurrent induction of lymphangiogenesis, angiogenesis, and macrophage recruitment by vascular endothelial growth factor-C in melanoma. *Am J Pathol* 159:893-903.
7. Ferrara, N. 2004. Vascular endothelial growth factor: basic science and clinical progress. *Endocr Rev* 25:581-611.
8. Shibuya, M. 2006. Differential roles of vascular endothelial growth factor receptor-1 and receptor-2 in angiogenesis. *J Biochem Mol Biol* 39:469-478.
9. Iijima, K., Jiang, J.Y., Shimizu, T., Sasada, H., and Sato, E. 2005. Acceleration of follicular development by administration of vascular endothelial growth factor in cycling female rats. *J Reprod Dev* 51:161-168.
10. Gomez, R., Simon, C., Remohi, J., and Pellicer, A. 2002. Vascular endothelial growth factor receptor-2 activation induces vascular permeability in hyperstimulated rats, and this effect is prevented by receptor blockade. *Endocrinology* 143:4339-4348.
11. Hazzard, T.M., Rohan, R.M., Molskness, T.A., Fanton, J.W., D'Amato, R.J., and Stouffer, R.L. 2002. Injection of antiangiogenic agents into the macaque preovulatory follicle: disruption of corpus luteum development and function. *Endocrine* 17:199-206.
12. Zimmermann, R.C., Hartman, T., Bohlen, P., Sauer, M.V., and Kitajewski, J. 2001. Preovulatory treatment of mice with anti-VEGF receptor 2 antibody inhibits angiogenesis in corpora lutea. *Microvasc Res* 62:15-25.
13. Zimmermann, R.C., Hartman, T., Kavic, S., Pauli, S.A., Bohlen, P., Sauer, M.V., and Kitajewski, J. 2003. Vascular endothelial growth factor receptor 2-mediated angiogenesis is essential for gonadotropin-dependent follicle development. *J Clin Invest* 112:659-669.
14. Stouffer, R.L., Xu, F., and Duffy, D.M. 2007. Molecular control of ovulation and luteinization in the primate follicle. *Front Biosci* 12:297-307.
15. Adams, R.H., and Alitalo, K. 2007. Molecular regulation of angiogenesis and lymphangiogenesis. *Nat Rev Mol Cell Biol* 8:464-478.
16. Alitalo, K., Tammela, T., and Petrova, T.V. 2005. Lymphangiogenesis in development and human disease. *Nature* 438:946-953.
17. Goldman, J., Rutkowski, J.M., Shields, J.D., Pasquier, M.C., Cui, Y., Schmokel, H.G., Willey, S., Hicklin, D.J., Pytowski, B., and Swartz, M.A. 2007. Cooperative and

redundant roles of VEGFR-2 and VEGFR-3 signaling in adult lymphangiogenesis. *Faseb J* 21:1003-1012.
18. Pytowski, B., Goldman, J., Persaud, K., Wu, Y., Witte, L., Hicklin, D.J., Skobe, M., Boardman, K.C., and Swartz, M.A. 2005. Complete and specific inhibition of adult lymphatic regeneration by a novel VEGFR-3 neutralizing antibody. *J Natl Cancer Inst* 97:14-21.
19. Tammela, T., Enholm, B., Alitalo, K., and Paavonen, K. 2005. The biology of vascular endothelial growth factors. *Cardiovasc Res* 65:550-563.
20. Otsuki, Y., Magari, S., and Sugimoto, O. 1986. Lymphatic capillaries in rabbit ovaries during ovulation: an ultrastructural study. *Lymphology* 19:55-64.
21. Otsuki, Y., Magari, S., and Sugimoto, O. 1987. Fine structure and morphometric analysis of lymphatic capillaries in the developing corpus luteum of the rabbit. *Lymphology* 20:64-72.
22. Ichikawa, S., Uchino, S., and Hirata, Y. 1987. Lymphatic and blood vasculature of the forming corpus luteum. *Lymphology* 20:73-83.
23. Heap, R.B., Fleet, I.R., Davis, A.J., Goode, J.A., Hamon, M.H., Walters, D.E., and Flint, A.P. 1989. Neurotransmitters and lymphatic-vascular transfer of prostaglandin F2 alpha stimulate ovarian oxytocin output in sheep. *J Endocrinol* 122:147-159.
24. Stefanczyk-Krzymowska, S., Chlopek, J., Grzegorzewski, W., and Radomski, M. 2005. Local transfer of prostaglandin E2 into the ovary and its retrograde transfer into the uterus in early pregnant sows. *Exp Physiol* 90:807-814.
25. Stefanczyk-Krzymowska, S., and Krzymowski, T. 2002. Local adjustment of blood and lymph circulation in the hormonal regulation of reproduction in female pigs--facts, conclusions and suggestions for future research. *Reprod Biol* 2:115-132.
26. Demeestere, I., Delbaere, A., Gervy, C., Van Den Bergh, M., Devreker, F., and Englert, Y. 2002. Effect of preantral follicle isolation technique on in-vitro follicular growth, oocyte maturation and embryo development in mice. *Hum Reprod* 17:2152-2159.
27. Liu, J., Van Der Elst, J., Van Den Broecke, R., Dumortier, F., and Dhont, M. 2000. Maturation of mouse primordial follicles by combination of grafting and in vitro culture. *Biol Reprod* 62:1218-1223.
28. West, E.R., Xu, M., Woodruff, T.K., and Shea, L.D. 2007. Physical properties of alginate hydrogels and their effects on in vitro follicle development. *Biomaterials* 28:4439-4448.
29. Inai, T., Mancuso, M., Hashizume, H., Baffert, F., Haskell, A., Baluk, P., Hu-Lowe, D.D., Shalinsky, D.R., Thurston, G., Yancopoulos, G.D., et al. 2004. Inhibition of vascular endothelial growth factor (VEGF) signaling in cancer causes loss of endothelial fenestrations, regression of tumor vessels, and appearance of basement membrane ghosts. *Am J Pathol* 165:35-52.
30. Partanen, T.A., and Paavonen, K. 2001. Lymphatic versus blood vascular endothelial growth factors and receptors in humans. *Microsc Res Tech* 55:108-121.
31. Witmer, A.N., van Blijswijk, B.C., Dai, J., Hofman, P., Partanen, T.A., Vrensen, G.F., and Schlingemann, R.O. 2001. VEGFR-3 in adult angiogenesis. *J Pathol* 195:490-497.
32. Laakkonen, P., Waltari, M., Holopainen, T., Takahashi, T., Pytowski, B., Steiner, P., Hicklin, D., Persaud, K., Tonra, J.R., Witte, L., et al. 2007. Vascular endothelial growth factor receptor 3 is involved in tumor angiogenesis and growth. *Cancer Res* 67:593-599.
33. Roberts, N., Kloos, B., Cassella, M., Podgrabinska, S., Persaud, K., Wu, Y., Pytowski, B., and Skobe, M. 2006. Inhibition of VEGFR-3 activation with the antagonistic

antibody more potently suppresses lymph node and distant metastases than inactivation of VEGFR-2. *Cancer Res* 66:2650-2657.
34. Reynolds, L.P., Grazul-Bilska, A.T., and Redmer, D.A. 2000. Angiogenesis in the corpus luteum. *Endocrine* 12:1-9.
35. Pate, J.L., and Landis Keyes, P. 2001. Immune cells in the corpus luteum: friends or foes? *Reproduction* 122:665-676.
36. Hedger, M.P., Qin, J.X., Robertson, D.M., and de Kretser, D.M. 1990. Intragonadal regulation of immune system functions. *Reprod Fertil Dev* 2:263-280.
37. Shakil, T., and Whitehead, S.A. 1994. Inhibitory action of peritoneal macrophages on progesterone secretion from co-cultured rat granulosa cells. *Biol Reprod* 50:1183-1189.
38. Rockson, S.G. 2001. Lymphedema. *Am J Med* 110:288-295.
39. Rutkowski, J.M., Moya, M., Johannes, J., Goldman, J., and Swartz, M.A. 2006. Secondary lymphedema in the mouse tail: Lymphatic hyperplasia, VEGF-C upregulation, and the protective role of MMP-9. *Microvasc Res*.
40. Skarzynski, D., Mlynarczuk, J., and Kotwica, J. 2003. Involvement of high-density lipoprotein in stimulatory effect of hormones supporting function of the bovine corpus luteum. *Acta Vet Hung* 51:111-120.
41. Veldhuis, J.D. 1988. Follicle-stimulating hormone regulates low density lipoprotein metabolism by swine granulosa cells. *Endocrinology* 123:1660-1667.
42. Rolaki, A., Drakakis, P., Millingos, S., Loutradis, D., and Makrigiannakis, A. 2005. Novel trends in follicular development, atresia and corpus luteum regression: a role for apoptosis. *Reprod Biomed Online* 11:93-103.
43. Nourani, M.R., Owada, Y., Kitanaka, N., Sakagami, H., Hoshi, H., Iwasa, H., Spener, F., and Kondo, H. 2005. Occurrence of immunoreactivity for adipocyte-type fatty acid binding protein in degenerating granulosa cells in atretic antral follicles of mouse ovary. *J Mol Histol* 36:491-497.
44. Vollmar, B., Laschke, M.W., Rohan, R., Koenig, J., and Menger, M.D. 2001. In vivo imaging of physiological angiogenesis from immature to preovulatory ovarian follicles. *Am J Pathol* 159:1661-1670.
45. Acosta, T.J., and Miyamoto, A. 2004. Vascular control of ovarian function: ovulation, corpus luteum formation and regression. *Anim Reprod Sci* 82-83:127-140.
46. Magoffin, D.A. 2005. Ovarian theca cell. *Int J Biochem Cell Biol* 37:1344-1349.
47. Jabbour, H.N., Kelly, R.W., Fraser, H.M., and Critchley, H.O. 2006. Endocrine regulation of menstruation. *Endocr Rev* 27:17-46.
48. Drummond, A.E., and Findlay, J.K. 1999. The role of estrogen in folliculogenesis. *Mol Cell Endocrinol* 151:57-64.
49. Espey, L.L., and Lipner, H. 1963. Measurements Of Intrafollicular Pressures In The Rabbit Ovary. *Am J Physiol* 205:1067-1072.
50. Rutkowski, J.M., and Swartz, M.A. 2007. A driving force for change: interstitial flow as a morphoregulator. *Trends Cell Biol* 17:44-50.
51. Hsieh, M., Boerboom, D., Shimada, M., Lo, Y., Parlow, A.F., Luhmann, U.F., Berger, W., and Richards, J.S. 2005. Mice null for Frizzled4 (Fzd4-/-) are infertile and exhibit impaired corpora lutea formation and function. *Biol Reprod* 73:1135-1146.
52. Karkkainen, M.J., Saaristo, A., Jussila, L., Karila, K.A., Lawrence, E.C., Pajusola, K., Bueler, H., Eichmann, A., Kauppinen, R., Kettunen, M.I., et al. 2001. A model for gene therapy of human hereditary lymphedema. *Proc Natl Acad Sci U S A* 98:12677-12682.
53. Makinen, T., Jussila, L., Veikkola, T., Karpanen, T., Kettunen, M.I., Pulkkanen, K.J., Kauppinen, R., Jackson, D.G., Kubo, H., Nishikawa, S., et al. 2001. Inhibition of

lymphangiogenesis with resulting lymphedema in transgenic mice expressing soluble VEGF receptor-3. *Nat Med* 7:199-205.
54. Achen, M.G., Mann, G.B., and Stacker, S.A. 2006. Targeting lymphangiogenesis to prevent tumour metastasis. *Br J Cancer* 94:1355-1360.
55. Szuba, A., Skobe, M., Karkkainen, M.J., Shin, W.S., Beynet, D.P., Rockson, N.B., Dakhil, N., Spilman, S., Goris, M.L., Strauss, H.W., et al. 2002. Therapeutic lymphangiogenesis with human recombinant VEGF-C. *Faseb J* 16:1985-1987.
56. Yoon, Y.S., Murayama, T., Gravereaux, E., Tkebuchava, T., Silver, M., Curry, C., Wecker, A., Kirchmair, R., Hu, C.S., Kearney, M., et al. 2003. VEGF-C gene therapy augments postnatal lymphangiogenesis and ameliorates secondary lymphedema. *J Clin Invest* 111:717-725.

FIGURE LEGENDS

Fig. 1. Ovarian and follicular lymphangiogenesis, but not blood angiogenesis, was inhibited by VEGFR-3 blockade in the ovary, preventing successful pregnancy. A) Ovarian lymphatic vessels (green, LYVE-1) are VEGFR-3 (red) positive (arrowheads). Some non-lymphatic associated VEGFR-3 is found on the vessels within the copora lutea (arrows) B) Blood vessels (green, CD31) are mostly negative for VEGFR-3 (red), with the exception of those within the corpora lutea (arrow). As lymphatic vessels also express CD31, the strong VEGFR-3 colocalization is likely marking lymphatics (yellow arrows). C) The extent of lymphatic vasculature (green, LYVE-1) normally developing within the ovary, left, was reduced in VEGFR-3 blocked ovaries, right; the blood vasculature and blood angiogenesis (red, CD31) were unaffected by the treatment. Bars=200μm. D) Quantification of lymphatic vessel coverage in (i) preantral follicles, (ii) small follicles with formed atrium, (iii) large follicles with significant atrium and (iv) corpora lutea (Supplemental Figure 1) demonstrated the significant reduction in lymphatic vessels at each maturation state with VEGFR-3 blockade. E) Blood vessel coverage was not statistically affected by VEGFR-3 blockade, despite some vessels expressing VEGFR-3. Notice the normal increase in vascularization of the follicles with maturation for both lymphatic and blood vessels. *$P<0.05$ between treatments.

Fig. 2. Pregnancies occurred after lymphangiogenesis was blocked, but embryonic development was severely impaired in the womb. A) In mice treated with mF4-31C1 prior to fertilization, few bodies remained within the uterus at pregnancy day 17, and they were scored as normal, (i) normal sized but discolored, (ii) deficient size and underdeveloped and (iii) identifiable cell masses. B) Fetuses extracted at pregnancy day 17 from treated animals displayed a marked deficiency from control animals. Grid=4mm. C) 2-cell embryos were extracted from fertilized VEGFR-3 treated mice and culture in vitro. The appearance of both 2-cell embryos and blastomeres appeared identical to those taken from control animals. Scale bar=100μm.

Fig. 3. Secondary follicles, once retrieved from the ovaries of treated mice, matured normally in vitro. A) Fewer patent follicles were successfully separated from collected ovaries in treated mice. B) Patency was not determined by basal lamina quality, as collagen IV staining (green) displayed intact basement membranes in both control and treated follicles (arrows). Bar=100μm. C) Follicles and their oocytes separated from ovaries of VEGFR-3 treated mice

survive normally in vitro. Surviving germinal vesicle (GV) oocytes from treated and control mice mature to germinal vesicle breakdown (GVBD) and metaphase II (MII) stages using the in vitro drop culture technique at equal rates. D) Survival of secondary follicles directly treated with the VEGFR-3 blocking antibody in vitro was unihibited. E) Maturation potential, as determined by follicle size, was also unaffected by direct VEGFR-3 treatment on the follicles.

Fig. 4. Macrophage recruitment, lipid accumulation, and cell apoptosis in the ovary appeared to be unaffected by VEGFR-3 blockade. A) Macrophages (red, F4/80) present in the ovary was limited to follicular peripheries in both control and treated ovaries. Bar=100μm. B) The total number quantified within the ovary was unchanged. C) The ovaries contain large amount of lipids (red, Oil Red O), particularly in the copora lutea (arrowheads). Bar=300μm. D) Lipid accumulation in the ovary was not significantly different without lymphatics. E) Apoptotic cells (green, TUNEL) were limited to interior granulosa cells (arrows) of regressing follicles and regular apoptosis of regressing corpora lutea and corpus hemorrhagicum (arrowheads) in both treatments. Bar=100μm. F) No difference was measured in the number of apoptotic cells within the ovary with mF4-31C1 treatment.

Fig. 5. Blockade of lymphangiogenesis led to reduced systemic estradiol levels in mice following fertilization and decreases in both eastradiol and progesterone during pregnancy. A) Serum progesterone levels in control and mF4-31C1 treated mice were normal at pregnancy day 2, but significantly reduced at pregnancy day 17. Since treatment was halted before mating, and since no difference was seen in serum levels at day 2, the mF4-31C1 treatment did not directly affect these hormones. B) Estradiol levels were significantly reduced during pregnancy when ovarian lymphangiogenesis was blocked. *$P<0.05$ between treatments. C) The blood vasculature (red, CD31) corpora lutea in the ovaries of pregnant mothers at day 17 was normal in mice when lymphangiogenesis was blocked prior to mating. In normal mothers, lymphatic vessels (arrows) (green, LYVE-1) surround the corpus luteum and other follicles. Bar=200μm.

Fig. 6. All embryos – normal and treated – implanted into treated recipient mothers were insufficiently developed despite normal uterine vasculature. A) Both normal and treated embryos implanted into normal, pseudo-pregnant recipient mothers developed into normal, viable fetuses by day 17. In pseudo-pregnant mothers pre-treated with mF4-31C1, no embryos

developed into normal fetuses, despite normal implantations. Grid=4mm. B) The distribution of fetal quality at day 17 following normal embryo transfer to mF4-31C1 treated recipients closely replicated that of in situ fetal development, as reported in Figure 2. C) Blood (red, CD31) and lymphatic (green, LYVE-1) capillaries in the uterine wall appeared normal in both mF4-31C1 treated and untreated mothers, further supporting an ovarian cause. Bar=200μm.

Supplemental Figure 1. Follicular vasculature was calculated for four stages of follicle maturation. A) Follicles exist in various maturation states within the murine follicle with increasing vasculature with maturation. Follicles that had reached preantral status were identified for quantifying their surrounding vasculature. B) Each follicle was first identified and numbered on hematoxylin labeled sections, where follicular structure was easier to recognize. C) On the corresponding fluorescence image, each follicle was then outlined in Metamorph software (white lines indicate the concept) and the percent area of lymphatic and blood vessel coverage within each region of interest was quantified. Bars=200μm.

Figure 1

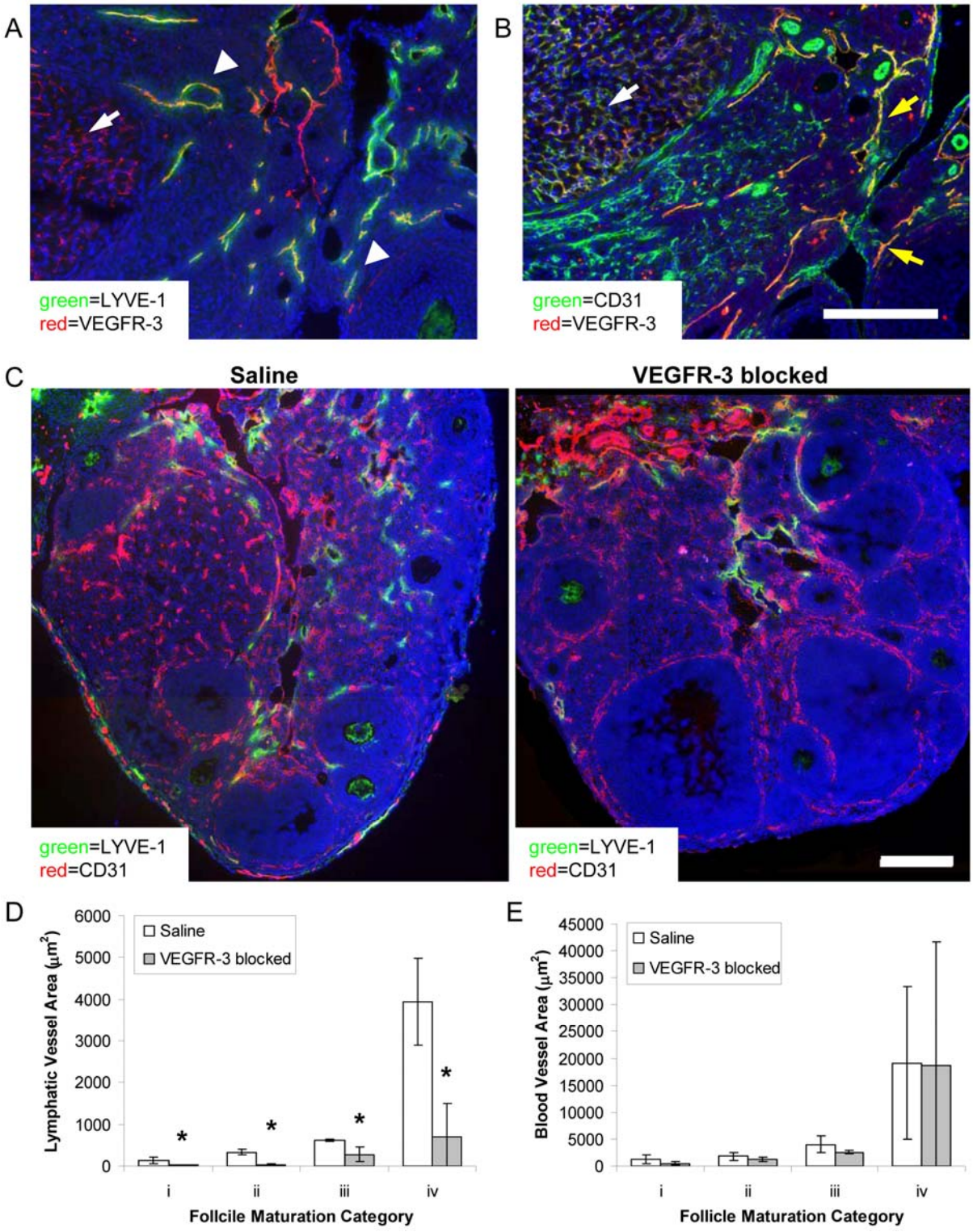
A
green=LYVE-1
red=VEGFR-3
B
green=CD31
red=VEGFR-3
C
Saline
VEGFR-3 blocked
green=LYVE-1
red=CD31
green=LYVE-1
red=CD31
D
Lymphatic Vessel Area (μm²)
6000
5000
4000
3000
2000
1000
0
Saline
VEGFR-3 blocked
*
*
*
*
i
ii
iii
iv
Follcile Maturation Category
E
Blood Vessel Area (μm²)
45000
40000
35000
30000
25000
20000
15000
10000
5000
0
Saline
VEGFR-3 blocked
i
ii
iii
iv
Follicle Maturation Category

This page is intentionally left blank.

Figure 2

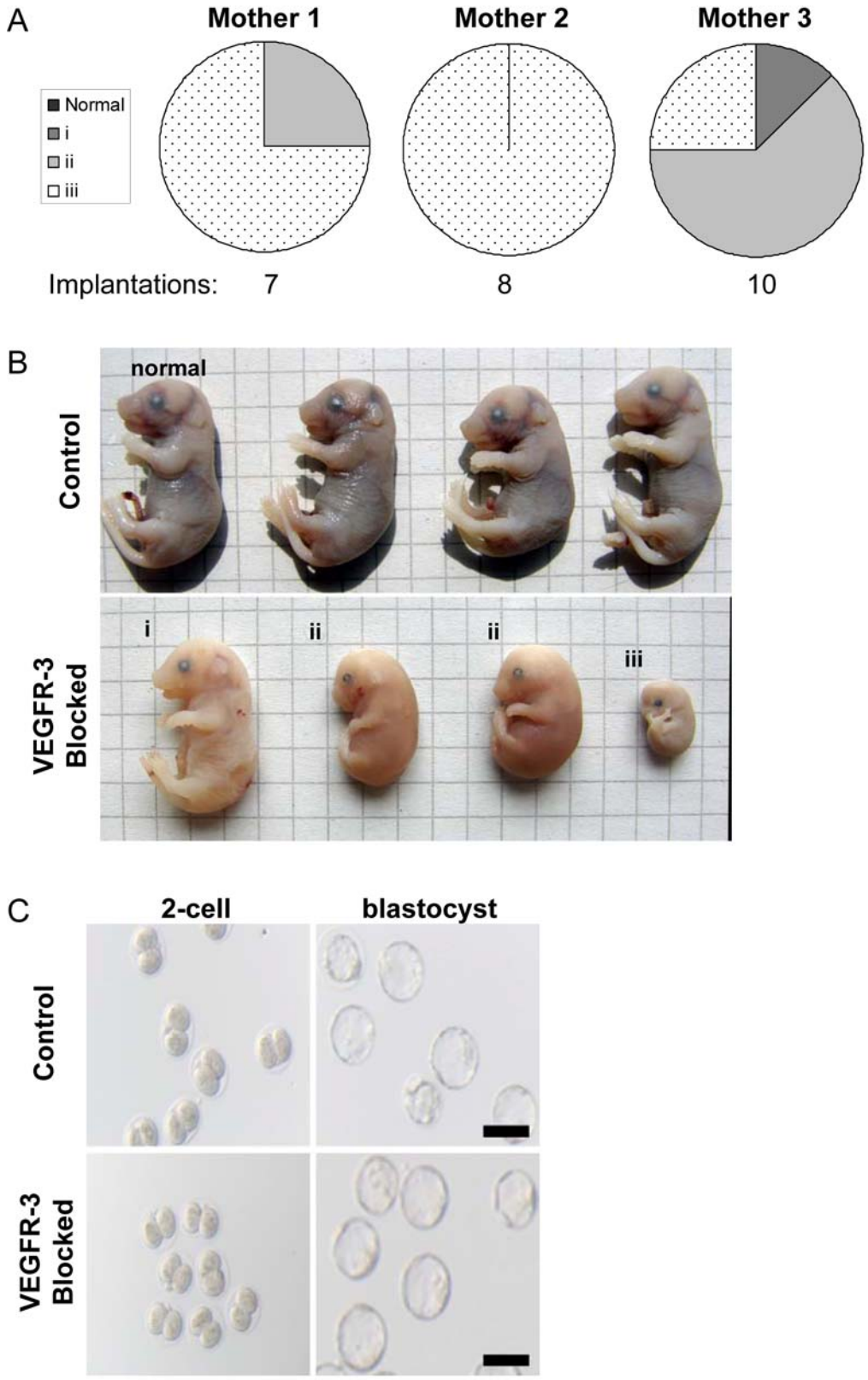
A
Mother 1
Mother 2
Mother 3
Normal
i
ii
iii
Implantations: 7 8 10
B
normal
Control
VEGFR-3 Blocked
i
ii
ii
iii
C
2-cell
blastocyst
Control
VEGFR-3 Blocked

This page is intentionally left blank.

Figure 3

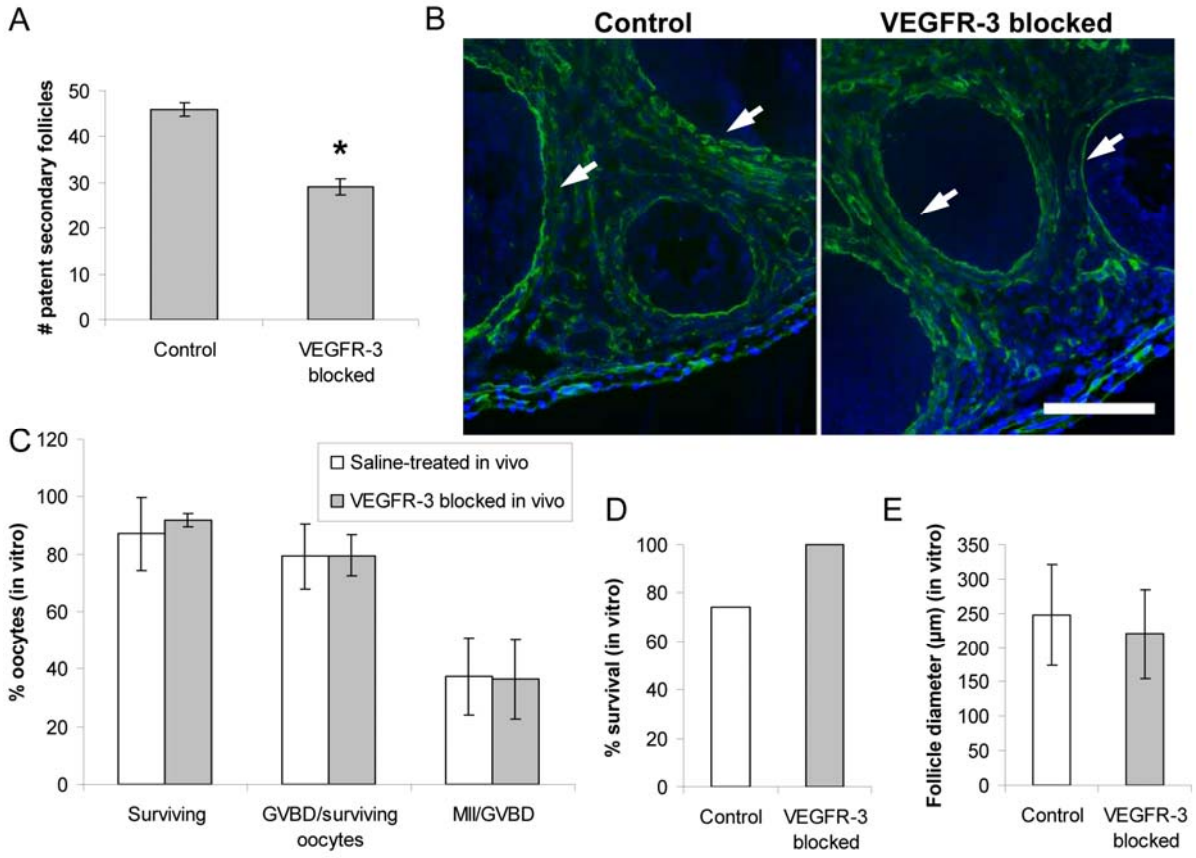
A
patent secondary follicles
50
40
30
20
10
0
*
Control
VEGFR-3 blocked
B
Control
VEGFR-3 blocked
C
% oocytes (in vitro)
120
100
80
60
40
20
0
Saline-treated in vivo
VEGFR-3 blocked in vivo
Surviving
GVBD/surviving oocytes
MII/GVBD
D
% survival (in vitro)
100
80
60
40
20
0
Control
VEGFR-3 blocked
E
Follicle diameter (µm) (in vitro)
350
300
250
200
150
100
50
0
Control
VEGFR-3 blocked

This page is intentionally left blank.

Figure 4

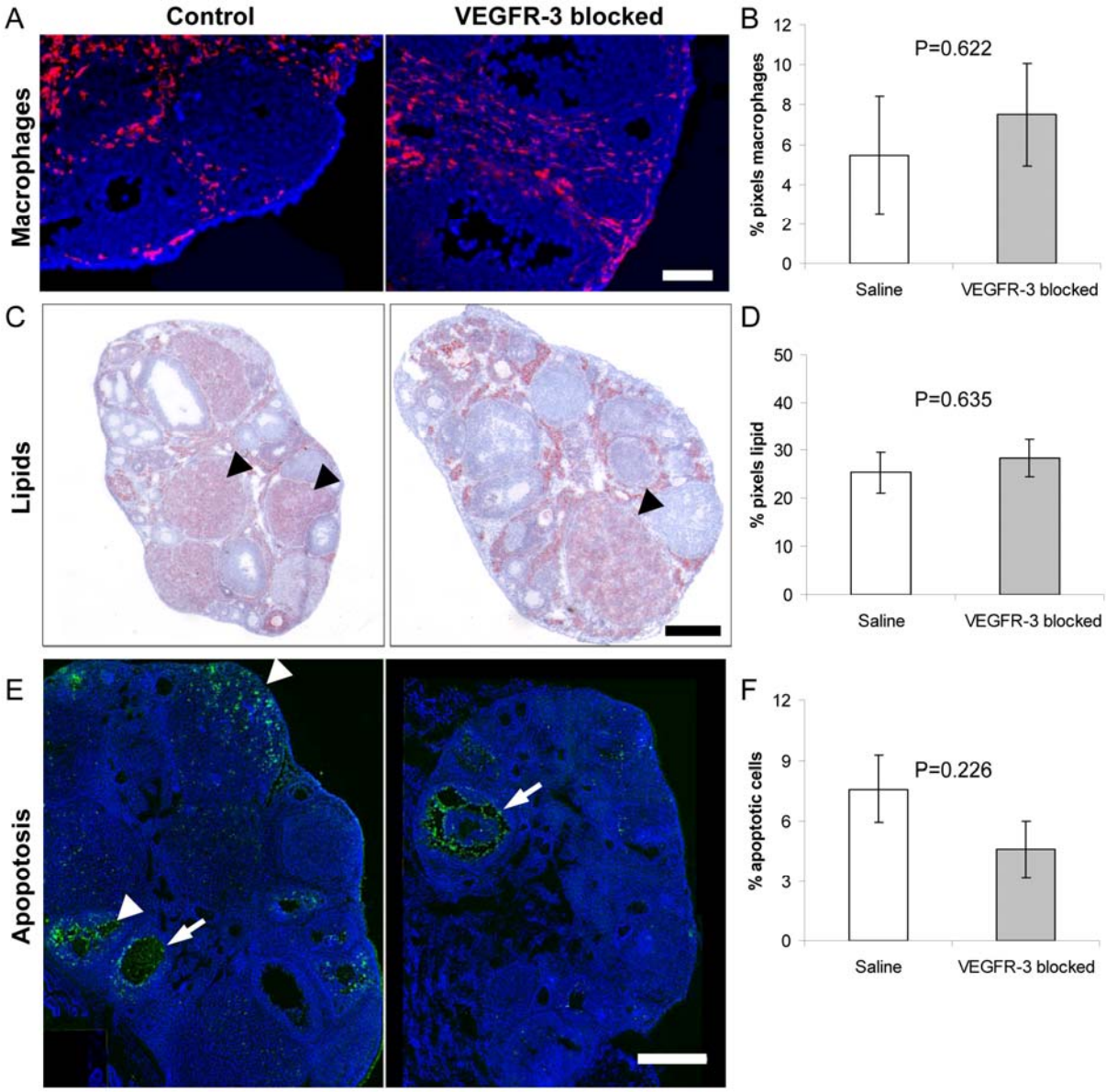
A
Control
VEGFR-3 blocked
Macrophages
B
P=0.622
% pixels macrophages
12
10
8
6
4
2
0
Saline
VEGFR-3 blocked
C
Lipids
D
P=0.635
% pixels lipid
50
40
30
20
10
0
Saline
VEGFR-3 blocked
E
Apopotosis
F
P=0.226
% apoptotic cells
12
9
6
3
0
Saline
VEGFR-3 blocked

This page is intentionally left blank.

Figure 5

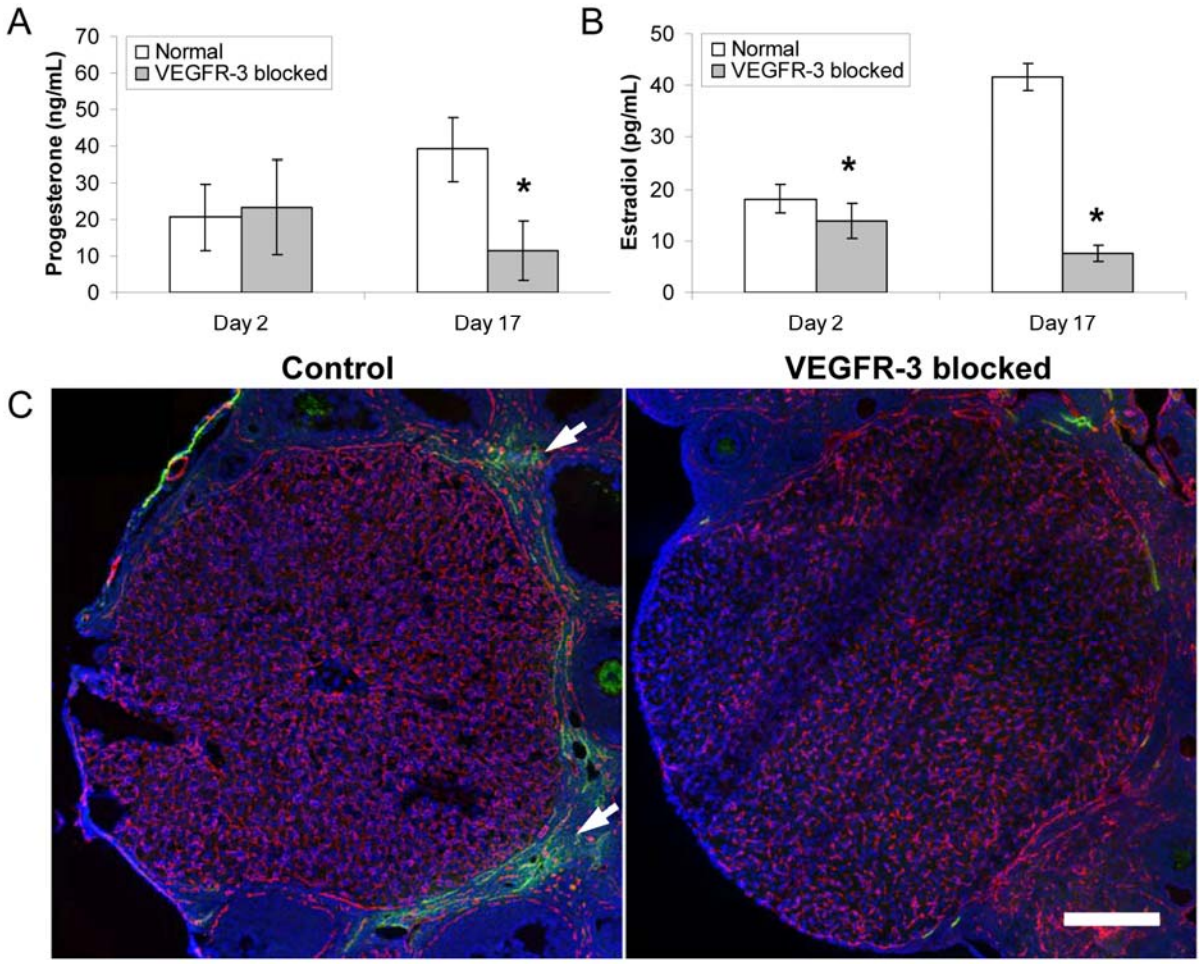
A
Progesterone (ng/mL)
70
60
50
40
30
20
10
0
Normal
VEGFR-3 blocked
*
Day 2
Day 17
B
Estradiol (pg/mL)
50
40
30
20
10
0
Normal
VEGFR-3 blocked
*
*
Day 2
Day 17
C
Control
VEGFR-3 blocked

This page is intentionally left blank.

Figure 6

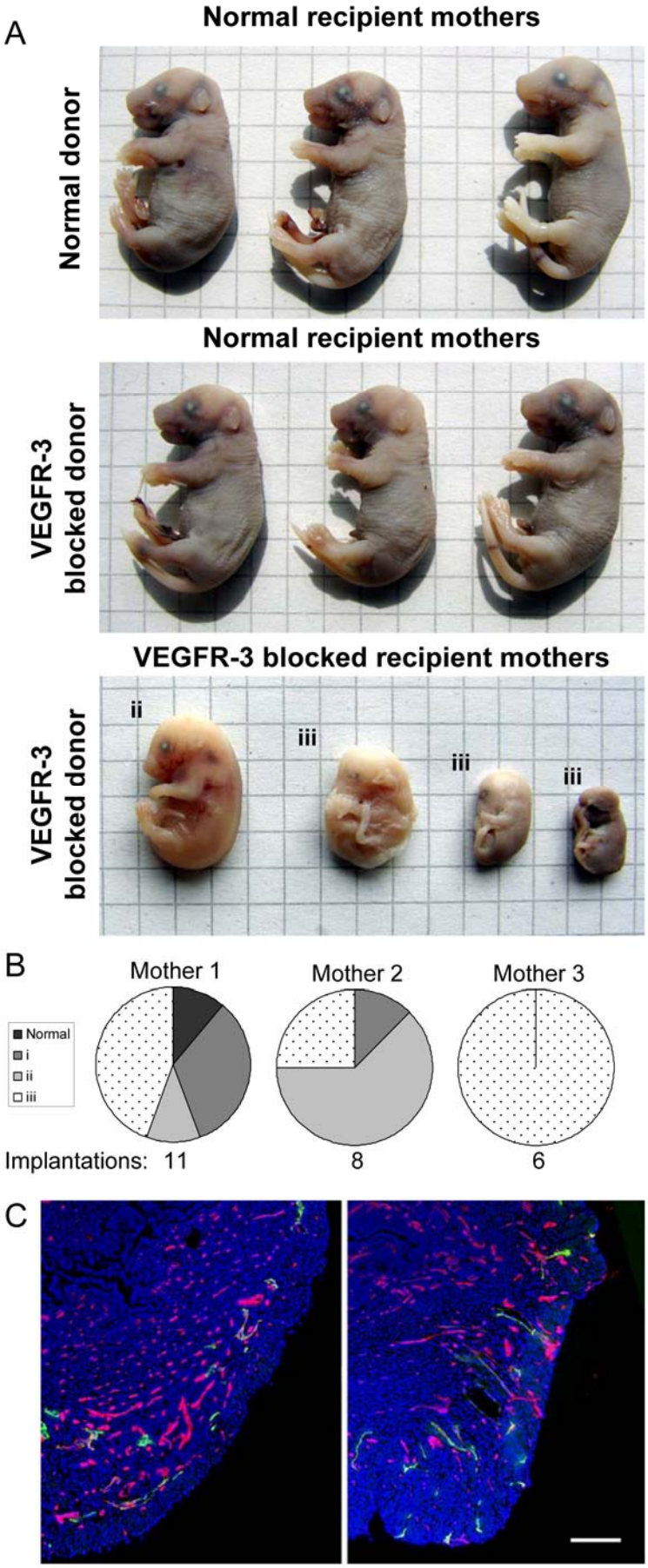
A
Normal recipient mothers
Normal donor
Normal recipient mothers
VEGFR-3 blocked donor
VEGFR-3 blocked recipient mothers
VEGFR-3 blocked donor
ii
iii
iii
iii
B
Mother 1
Mother 2
Mother 3
Normal
i
ii
iii
Implantations: 11
8
6
C

This page is intentionally left blank.

Supplemental Figure 1

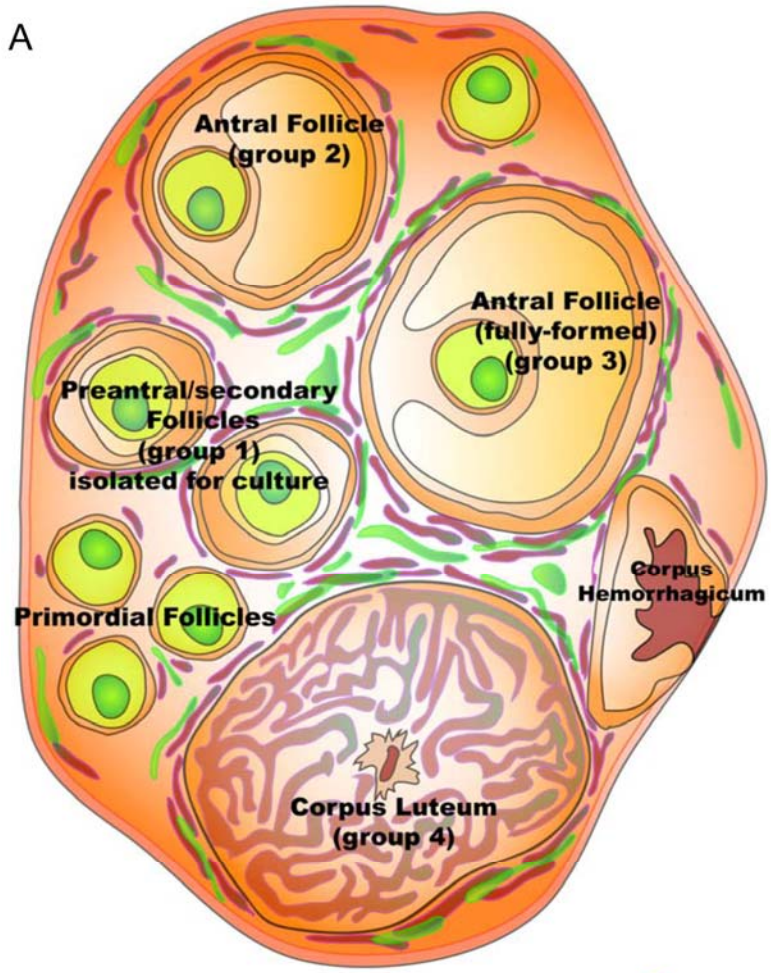

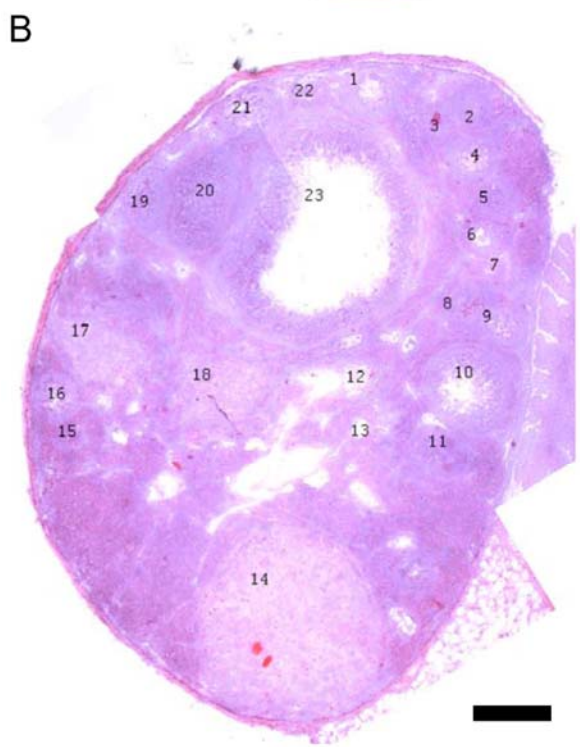

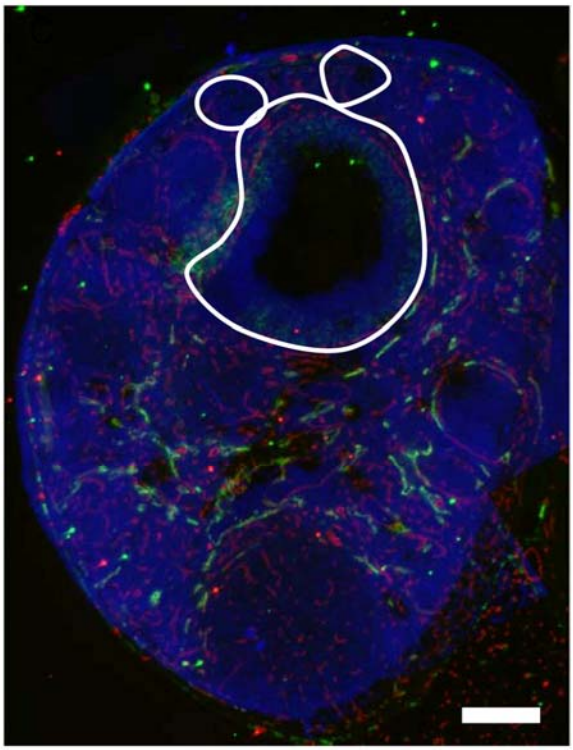

This page is intentionally left blank.

CHAPTER 9:
CONCLUSIONS & FUTURE DIRECTIONS

Research in lymphatic biology has been rapidly growing as the importance of the lymphatic circulation is increasingly appreciated. Fundamental work in lymphatic development, interstitial fluid balance, lymphatic vessel pumping, and tumor lymphangiogenesis has laid the critical groundwork, but more research is necessary to elucidate the role played by lymphatic capillaries. These vessels act as the entry point of interstitial fluid, immune cells, and lipids into the lymphatic system, thus placing lymphatic capillary biology at the intersection of many essential physiologic processes and diverse fields of study. It is therefore an important step in understanding lymphatic biology to explore the interactions between potential molecular and mechanical regulators of lymphatic capillary function. The overall aim of this thesis was to do just that, specifically: identifying contributing factors to lymphangiogenesis during wound healing, determining the lymphatic capillary and tissue response to lymphedema, developing a model to quantify lymphatic capillary fluid uptake and tissue hydraulic conductivity, and defining a role for lymphatic capillaries in reproduction. In accomplishing these aims, this thesis contributes a significant body of original and important knowledge towards furthering our understanding of lymphatic capillary biology.

By taking an integrative biomedical engineering approach to studying lymphatic capillary biology *in vivo*, novel mechanisms of lymphatic capillary biology were elucidated. We believe that this approach has allowed us to place our results in a more physiologically relevant context than what would have been possible *in vitro*; indeed, there is no *in vitro* technique that can recapitulate a functional lymphatic capillary. In lymphangiogenesis, our model of skin regeneration in the mouse tail provided a unique platform in which to study not only the growth factors and proteases essential for the growth of new lymphatic capillaries, but also the importance of interstitial flow as an organizational guiding force. Interstitial flow is absolutely essential for LEC organization into functional lymphatic capillaries and the tail model, as a virtue of its reproducibility and resultant well-defined stepwise lymphatic regeneration was able to elegantly illustrate that VEGF-C signaling only initiates lymphangiogenesis. These key findings – the first to demonstrate that a biomechanical force guides lymphangiogenesis - have several immediate implications. Firstly, as described in this thesis, we now know why, in lymphedema, lymphatic capillaries become hyperplastic and highly dysfunctional despite the presence of high concentrations of growth factor: there is no

flow to guide proper cellular organization. Hence, VEGF-C to VEGFR-3 signaling initiates an exaggerated proliferative response, but without interstitial flow LECs remain in situ and generate tortuous hyperplastic vessels. Secondly, we demonstrate that growth factor therapies to cure diseases of lymphatic dysfunction (e.g., lymphedema) will have limited success due to the lack of flow necessary to organize a functional vasculature. Our additional findings in lymphedema – the massive breakdown and remodeling of the ECM – have identified another roadblock to successful remediation of edematous tissue: lymphatic dysfunctionality is further worsened by connective tissue destruction and the resultant loss of intimate connections between LECs and ECM that permit drainage. In primary lymphedema, where lymphatic capillaries were never present in the dermis, we found that different animal models exhibit different tissue adaptations to modulate capillary extravasation and interstitial transport. The combined findings in our integrative models of lymphangiogenesis and lymphedema demand that any future approach to therapies for lymphatic pathologies must seek to (a) restore interstitial flow and (b) remediate the matrix morphology; growth factor therapy alone will be insufficient. One potential means to grow new lymphatics, restore flow, and remodel the matrix might be to purposefully target antigen-presenting cells (APCs) in the tissue (i.e., dendritic cells and macrophages) to stimulate migration by alternative activation (anti-inflammatory activation) and the secretion of pro-lymphangiogenic factors. Therefore, utilizing immunobiomaterials to target APCs in the tissue that normally migrate via the lymphatics might simultaneously provide sufficient proteolytic remodeling of the matrix and lymphatic capillary growth.

Our model of dermal interstitial transport and lymphatic capillary uptake provides a starting point for future studies that question which molecules play a role in LEC biology and lymphatic function. Studies utilizing either transgenic mouse models or the delivery of agonistic or antagonistic molecules can now readily determine not only a yes-or-no as to which molecules are important to lymphatic capillary function, but also the quantitative extent to their functional modulation. In the ApoE-/- mouse, for example, we found the dyslipidemia or hypercholesterolemia resulted in significantly decreased uptake by lymphatic capillaries. Not only did this verify the applicability and functionality of the model, but also opened a whole new realm of research in lymphatic-lipid interplay. If dyslipidemia alters lymphatic vessel function, the opposite might also be true: lymphatic dysfunction leads to lipid metabolic disorders. Currently, we are beginning to explore more deeply this interplay. One approach is to quantify if correction of the lipid metabolic disorder (e.g., via delivery of cholesterol medication) improves lymphatic function. Another is to determine if lymphatic

dysfunction, as in the Chy or K14-VEGFR-3-Ig mouse, leads to dyslipidemia. The exciting potential of these interactions has significant implications ranging from lymphatic therapies to obesity.

Finally, we have identified a new role for the lymphatic circulation: modulation of hormone levels during pregnancy. With this work, we are only just beginning to scratch the surface of lymphatics in reproduction. We have successfully demonstrated that lymphangiogenesis occurs within the ovary during folliculogenesis, that this is essential for pregnancy, and that this is likely the cause of a systemic decrease in estrogen; just how the lymphatic circulation modulates this is still unknown. Also, as lymphatic vessels are critical in inflammation and fluid balance, there is even more potential for reproductive lymphatic circulation to control the complex processes of folliculogenesis, ovulation, and pregnancy. Some researchers describe ovulation as a massive inflammatory event: the modulation of pressures within the antrum of developing follicles, the massive secretion of hormones, and the eventual rupture of the ovarian capsule should present an almost insustainable inflammatory environment. Clearly, lymphatic vessels have the potential to modulate these factors as would occur in other tissues. Further examination of intrafollicular pressures, granulose cell molecular expression and hormone secretion, and hormonal rescue therapy may elucidate the roles of ovarian lymphatic capillaries more sufficiently.

In summary, this thesis has produced a series of significant and unique contributions to our understanding of the dynamism of lymphatic capillary biology and the complex biochemical and biomechanical environments in which they reside. Specifically, we demonstrated, for the first time, that:

- Lymphangiogenesis requires interstitial flow as an organizational guiding force
- VEGFR-3 signaling is only required for LEC proliferation and migration in the initial stages of lymphangiogenesis
- Lymphedema therapy requires an integrative approach targeting both the restoration of interstitial flow and matrix remediation for success
- Matrix remodeling, lymphedema, and dyslipidemia reduce lymphatic capillary function
- Lymphangiogenesis within the ovary is an essential process in reproduction

Within various realms of biological research, the lymphatic circulation has become increasingly appreciated. As the initial component of the lymphatic circulation and a critical mediator of the interstitial environment, the functional behavior of lymphatic capillaries demands further attention, and has implications not only to the lymphatic research

community, but also to those interested in inflammation, immunology, lipid metabolism, and reproduction.

CURRICULUM VITAE

Joseph M. Rutkowski

Institute of Bioengineering, École Polytechnique Fédérale de Lausanne (EPFL), Lausanne, Switzerland

Education

PhD in Bioengineering, July 2008
École Polytechnique Fédérale de Lausanne (EPFL), Lausanne, Switzerland
PhD advisor: Prof. Melody A. Swartz
Thesis: "Molecular and Mechanical Regulators of Lymphatic Biology"

MS in Chemical Engineering, December 2003
Northwestern University, McCormick School of Engineering and Applied Science, Evanston, IL

BS in Chemical Engineering, December 2001
Penn State University, Schreyer Honors College , University Park, PA
Advisor: Prof. James S. Ultman
Honors Thesis: "The Antioxidant Capacity of Biological Substrates With Respect to Ozone"

Peer-Reviewed Publications

Goldman JG*, **Rutkowski JM***, Shields JD*, Pasquier M, Cui Y, Schmökel HG, Pytowski B, Swartz MA. Co-operative and redundant roles of VEGFR-2 and VEGFR-3 signaling in adult lymphangiogenesis. *FASEB J.* **2007** Apr;21(4):1003-12. (* equal contribution)

Goldman J, Conley KA, Raehl A, Bondy DM, Pytowski B, Swartz MA, **Rutkowski JM**, Jaroch DB, Ongstad EL. Regulation of VEGF-C by interstitial flow. *Am J Physiol Heart Circ Physiol.* **2007** May;292(5):H2176-83.

Rutkowski JM and Swartz MA. A driving force for change: Interstitial flow as a morphoregulator. *Trends Cell Biol.* **2007** Jan;17(1):44-50.

Rutkowski JM, Moya M, Johannes J, Goldman J, Swartz MA. Secondary lymphedema in the mouse tail: lymphatic hyperplasia, VEGF-C upregulation, and the protective role of MMP-9. *Microvasc Res.* **2006** Nov;72(3):161-71.

Rutkowski JM, Boardman KC, Swartz MA. Characterization of lymphangiogenesis in a model of adult skin regeneration. *Am J Physiol Heart Circ Physiol.* **2006** Sep;291(3):H1402-10.

Rutkowski JM, Santiago LY, Ben-Jebria, Ultman JS. Development of an assay for ozone-specific antioxidant capacity. Inhal Toxicol. **2003** Nov;15(13):1369-85.

Publications in preparation or submitted

Rutkowski JM, Markhus CE, Gyenge CC, Alitalo K, Wiig H, Swartz MA. Differential tissue adaptation in two mouse models of primary congenital lymphedema with defects in VEGFR-3 signaling. (in preparation)

Rutkowski JM, Swartz MA. A noninvasive, quantitative model for evaluating lymphatic uptake and tissue hydraulic conductivity in the mouse. (in preparation)

Rutkowski JM*, Ihm JE*, Lee ST, Greenwood VI, Pasquier MC, Quazolla A, Trono D, Hubbell JA, Swartz MA. Ovarian lymphangiogenesis is necessary for hormonal maintenance and fetal development during murine pregnancy. (* equal contribution) (submitted)

Angeli V, Reddy ST, **Rutkowski JM**, Swartz MA, Randolph GJ, Impaired lymphatic function in hypercholesterolemic mice. (in review)

Conference Presentations

Rutkowski JM, Ihm JE, Lee ST, Greenwood VI, Hubbell JA, Swartz MA. "VEGFR-3 mediated lymphangiogenesis in the murine ovary is necessary for follicle maturation and pregnancy", Gordon Research Conference: Molecular Mechanisms in Lymphatic Function & Disease, Mar 2008 (poster)

Rutkowski JM, Yong C, Swartz MA. "Molecular and biophysical regulators of lymphatic transport", AIChE Annual Meeting, Nov 2007 (podium)

Rutkowski JM, Yong C, Angeli V, Swartz MA. "Molecular and biophysical regulators of lymphatic transport", BMES Annual Meeting, Oct 2007 (podium)

Rutkowski JM, Yong C, Swartz MA. "Active and differential responses of the lymphatic endothelium to acute inflammation versus chronic lymphedema: in vivo and in vitro studies", 8th World Congress on Microcirculation, Aug 2007 (poster)

Rutkowski JM, Ihm JE, Lee ST, Greenwood VI, Hubbell JA, Swartz MA. "VEGFR-3 mediated lymphangiogenesis in the ovary is necessary for follicle maturation and murine pregnancy", 8th World Congress on Microcirculation, Aug 2007 (poster)

Rutkowski JM, Yong C, Swartz MA. "Active response of the lymphatic endothelium to acute inflammation vs. chronic lymphedema: in vivo and in vitro studies", Experimental Biology Annual Meeting, Apr 2007 (poster)

Rutkowski JM, Swartz MA. "Tissue response to secondary lymphedema", BMES Annual Meeting, Oct 2006 (podium)

Rutkowski JM, Swartz MA. "Secondary lymphedema in the mouse tail: Lymphatic hyperplasia, VEGF-C upregulation, and the protective role of MMP-9", Gordon Research Conference: Molecular Mechanisms in Lymphatic Function & Disease, Sept 2006 (Oral presentation as winner of the Moisoff Award)

Rutkowski JM, Shields JD, Goldman J, Swartz MA. "VEGF receptor signaling in lymphangiogenesis: co-operative and redundant roles", 24th European Conference on Microcirculation, Sept 2006 (poster)

Rutkowski JM, Shields JD, Goldman J, Swartz MA. "Effects of VEGFR-3 and VEGFR-2 Blocking on Lymphatic Regeneration: Co-operative and Redundant Roles" Joint US/UK Microcirculatory Society Meeting, Sept 2005 (podium)

Rutkowski JM, Ultman JS. "Determination of the Antioxidant Capacity of Biological Fluids During Ozone Exposure" National Conference of Undergraduate Research, Mar 2001 (podium)

Honors and Awards

German Society for Microcirculation and Vascular Biology – Travel Award "Active and differential responses of the lymphatic endothelium to acute inflammation versus chronic lymphedema: in vivo and in vitro studies", 8th World Congress on Microcirculation, August 2007.

Ed Yellin "Integrative Cardiovascular Physiology Award" (best manuscript) "Co-operative and redundant roles of VEGFR-2 and VEGFR-3 signaling in adult lymphangiogenesis", Cardiovascular System Dynamics Society (CSDS) 17th Annual Meeting. September 2006.

Lymphatic Research Foundation - Andrew Moisoff Young Investigator Award "Secondary lymphedema in the mouse tail: Lymphatic hyperplasia, VEGF-C upregulation, and the protective role of MMP-9", Gordon Research Conference: Molecular Mechanisms in Lymphatic Function and Disease. September 2006.

Meetings Attended

- Gordon Research Conference: Molecular Mechanisms in Lymphatic Function & Disease, Ventura, California, Mar 2008
- AIChE Annual Meeting, Salt Lake City, Utah, Nov 2007
- 8th World Congress on Microcirculation, Milwaukee, Wisconsin, Aug 2007
- Experimental Biology 2007, Washington D.C., Apr 2007
- Biomedical Engineering Society Annual Fall Meeting, Chicago, Illinois, Oct 2006
- Gordon Research Conference: Molecular Mechanisms in Lymphatic Function & Disease, Les Diablerets, Switzerland, Sept 2006
- 24th European Conference on Microcirculation, Amsterdam, The Netherlands, Sept 2006
- Swiss Society of Bioengineering Annual Meeting, Lausanne, Switzerland, Sept 2005
- Joint US/UK Microcirculatory Society Meeting, Durham, New Hampshire, Sept 2005
- Biomedical Engineering Society Annual Fall Meeting, Philadelphia, Pennsylvania, Oct 2004
- Tissue Engineering Society International Meeting, Lausanne, Switzerland, Oct 2004
- Biomedical Engineering Society Annual Fall Meeting, Nashville, Tennessee, Oct 2003
- ASME Summer Bioengineering Conference, Biscayne Bay, Florida, Aug 2003
- National Conference of Undergraduate Research, Lexington, Kentucky, Mar 2001

Society Membership

- European Society for Microcirculation, 2007
- The American Physiological Society (APS), 2006
- The Microcirculatory Society, 2005
- Swiss Society for Biomedical Engineering (SSBE), 2005
- Biomedical Engineering Society (BMES), 2003
- American Institute of Chemical Engineers (AIChE), 1999

Skills

- Microscopy
  - Fluorescence and brightfield microscopy systems (Zeiss, Leica, and Olympus systems)
  - Single-photon confocal microscopy (Zeiss and Leica systems)
  - Extensive knowledge of image analysis and editing software (Metamorph and Photoshop)

- Animal Work
  - Currently certified for animal research in mice, rats, and rabbits within Switzerland
  - Combined 6 years of animal study research, handling, and breeding
  - Skilled in gross and micro surgical techniques
  - In vivo fluorescence imaging
- Cell & Molecular Techniques
  - Cell isolation from human and murine tissues
  - Flow cytometry
  - Immunohistochemistry and immunofluorescence
  - ELISA
  - Tissue and cell culture
  - PCR for genotyping

Research and Teaching Experience

Research Assistant, December 2002-present

Dr. Melody Swartz Laboratory in the Institute of Bioengineering, EPFL, Lausanne, Switzerland (Jan 2004-present); formerly the Department of Chemical Engineering, Northwestern University (Dec 2002-Dec 2004)

- Examined the impact of lymphatic dysfunction on peripheral dendritic cell migration and lipid clearance
- Defined a role for lymphatic transport in follicle development and reproduction
- Determined that lymphatic ligation leads to irreversible matrix remodeling – of which MMP-9 is a key contributor – that prevents successful resolution of lymphedema
- Correlated lymphatic hyperplasia in secondary lymphedema temporally with endogenous VEGF-C
- Characterized interstitial flow guided lymphangiogenesis in the mouse tail with respect to MMP expression, immune cell infiltration, and growth factor secretion
- Managed animal colonies and protocols and microscopy and computer equipment for lab users

Teaching assistantships

- EPFL, Dept. Chemical Engineering, "Advanced Transport Phenomena" (2007)
- EPFL, Dept. Chemical Engineering, "Practical Training in Chemical & Biological Engineering" (2006)
- Northwestern University, Dept. of Chemical Engineering, "Mass Transfer" (2004)

Lab Technician, January 2002 - September 2002
Research Assistant, September 1998 - December 2001

Dr. James Ultman Laboratory in the Department of Chemical Engineering

- Conceived assay and constructed equipment capable of determining reductive capacity of respiratory mucus
- Analyzed solutions using fluorometric and spectrophotometric techniques
- Developed reverse-phase HPLC protocols for analysis of human mucus and blood samples
- Certified in human subject research and human sample collection and handling
- Responsible for laboratory ordering and inventory, safety, and equipment and computer maintenance

Research Assistant, August 1997 - May 1998

Dr. Daniel R. Deaver Laboratory in the Department Dairy & Animal Science

- Investigated drug delivery and absorption in mucus membranes via hormonal analysis
  - Handled animals (mice, rats, pigs, and sheep)
  - Collected and analyzed murine and ovine plasma luteinizing hormone levels
- Quantified the effect of a GnRH receptor-agonist on nitric oxide production in the rat testes